UNIVERSITY OF SOUTHAMPTON

Faculty of Science

Department of Oceanography

Permanent subduction and ventilation of the thermocline: a model study

by

Ian Michael Udall

This thesis was submitted for examination for the award of
Doctor of Philosophy

July, 1995

UNIVERSITY OF SOUTHAMPTON

ABSTRACT

FACULTY OF SCIENCE

OCEANOGRAPHY

Doctor of Philosophy

Permanent subduction and ventilation of the thermocline: a model study

by Ian Michael Udall

The permanent subduction of mode waters into the permanent thermocline and the subsequent ventilation of the permanent thermocline by these water masses is climatically important. First, mode waters determine the structure and circulation of the permanent thermocline. Secondly, the mode waters sequestrate heat and dissolved gases in the permanent thermocline for extended periods.

The processes of permanent subduction and ventilation are studied in an isopycnic ocean general circulation model, with particular emphasis on the production of subtropical mode waters. It is demonstrated in a 2-degree resolution model that the diffusion of isopycnic layer thickness plays an important role in determining the character of the thermocline circulation. For a low value of the diffusion coefficient, ventilation tongues develop which are associated with strong southward velocities on their eastern flanks. For high values of the diffusion coefficient the ventilation tongues are smoothed and the southward 'jet' is made broader and slower.

The importance of isopycnic tracer diffusion to the permanent subduction rate is found to depend on the thermocline flow. For the fast flows, associated with a low thickness diffusion coefficient, the contribution of isopycnic tracer diffusion is smaller than found for an ocean basin with a high value of the thickness diffusion coefficient.

A large perturbation to the meteorological forcing is imposed on a high thickness diffusion isopycnic model for one year. It is found that the permanent subduction rate increases during the year of the perturbation but returns to the control values over a period of 2-3 years. No change in the circulation of the permanent thermocline is observed. This is thought to arise from the slow thermocline circulation.

A 1-degree resolution isopycnic model of the northern and equatorial Atlantic (AIM) is studied. It is found that permanent subduction in this model is predominantly by advection, with the transport of water by isopycnic diffusion making an insignificant contribution to the total mass flux into the permanent thermocline.

It is also demonstrated that the evolution of the buoyancy content of the upper thermocline for a Lagrangian water column in AIM is dominated by the net surface buoyancy flux (Ekman plus surface fluxes). This is in contrast to the simple geometry isopycnic model where the divergence of the mass fluxes in the upper thermocline makes an important contribution to the evolution of the upper thermocline. The qualitative difference in the importance of the net surface heat flux is thought to arise from the different thickness diffusion coefficients used in the two models.

CONTENTS

List of figures

Chapter One

Chapter Two

Chapter Three

Chapter Four

Chapter Five

Chapter Six

List of tables

Glossary

α The reference volume of sea water, $\frac{1}{\rho}$.

α_E The thermal expansion coefficient of sea water.

β The meridional gradient in the Coriolis parameter, $\partial f/\partial\phi$.

δ_{ij} The Kronecker delta, $\delta_{ij} = 1$ if $i=j$, otherwise $\delta_{ij} = 0$.

ε The rate of TKE dissipation.

κ_I The isopycnic tracer diffusion coefficient in units of cm^2s^{-1}.

κ_T The isopycnic layer thickness diffusion coefficient in units of cm^2s^{-1}.

ρ The potential density of water, the density of sea water if it was raised adiabatically to the sea surface.

ρ_k The potential density of the *k*-th layer of the model.

$\bar{\rho}$ The reference density of sea water, taken to be $1.02525 g/cm^3$.

σ Dimensionless density quantity, $\frac{\rho - \bar{\rho}}{\bar{\rho}}$

$\Delta\sigma$ The difference in sigma values between isopycnic layers. In AIM and Box3 $\Delta\sigma$=0.15 while in Box1 and Box2 $\Delta\sigma$ varies from 0.10-0.45.

τ A general tracer quantity, *e.g.* temperature, salinity or ventilation tracer.

τ The wind stress vector at the ocean surface.

υ The eddy viscosity.

ζ The relative vorticity of the fluid; $\zeta = \nabla \times \mathbf{u}$.

AIM Atlantic Isopycnic Model

B_{conv} The buoyancy flux associated with the convergence of mean mass flux.

B_{difn} The buoyancy flux associated with the diffusion of density in the mixed layer.

B_{Ekman} The buoyancy flux associated with the Ekman drift.

B_0 The surface buoyancy flux, the sum of radiative, latent and sensible heat fluxes and net evaporation fluxes.

B_{pump} The buoyancy flux associated with Ekman pumping.

B_{shear} The buoyancy flux arising from vertical shear of the mean velocity (*i.e.* not including Ekman drift).

B_{thk} The buoyancy flux associated with the thickness diffusion mass flux.

b_k The buoyancy of the *k*-th layer, $b_k = -g\sigma_k$.

c_D The drag coefficient for the ocean surface.

c_w The specific heat capacity of sea water.

E Total energy required to lift the thermocline layers by the mixed layer

f The Coriolis parameter, $2\Omega\sin\phi$.

f_{ijk} The fraction of layer *k* at grid point (*i,j*) lying within the permanent thermocline.

GCM General Circulation Model.

H_i The mixed layer depth in metres at the start of the mixed layer entrainment and detrainment phase experiments.

H_{max} The depth of the seasonal thermocline, the maximum depth to which the mixed layer extends over the annual cycle.

H_{net} The net surface heating fluxes, the sum of surface heating fluxes, H_0, and the heat fluxes associated with Ekman drift.

H_0 The surface heat fluxes arising from radiation and latent and sensible heat fluxes.

H_W The length scale of wind-driven mixing in metres.

h The thickness of an isopycnic layer in metres.

h_k The thickness of the *k*-th isopycnic layer in metres.

I_0 The penetrating component of the surface radiative heat flux.

k The unit vertical coordinate vector.

L Horizontal scale length, used in Péclet number calculation.

LSW Labrador Sea Water

M The Montgomery potential on an isopycnic layer; $M = gz + p\alpha$.

MICOM Miami Isopycnic Coordinate Ocean Model

m The efficiency parameter for the generation of TKE from surface wind stress.

n The efficiency parameter for the generation of TKE from convection.

p The pressure coordinate; $p = \int_z^0 -g\rho\,dz$.

Δp The thickness of an isopycnic layer in pressure coordinates; $\Delta p = g\bar{\rho}h$.

Q The potential vorticity, $\frac{f}{\rho}\frac{\partial\rho}{\partial z}$.

Q_B The potential vorticity at the base of the mixed layer.

R The radiative heat flux at the ocean surface.

S Instantaneous subduction rate, the rate at which water is passed from the mixed layer into the thermocline.

S_{ann} The annual permanent subduction rate, the rate at which water previously mixed by the winter mixed layer are transported into the permanent thermocline for the following winter.

S_{ijk} The instantaneous permanent subduction rate at the model grid point (i,j) on or from model layer *k*.

Sverdrups Units of volume flux; 1 Sv = $10^6 m^3 s^{-1}$.

TKE Turbulent kinetic energy.

T Potential temperature.

T^* The surface relaxation temperature used in the Haney heat flux.

T The permanent subduction period, the period over which waters detrained from the mixed layer will enter the permanent thermocline over the course of the annual cycle rather than be entrained during the following winter.

T_i Initial mixed layer temperature in the entrainment and detrainment phase experiments.

Δt The length of one model time step.

U Horizontal scale velocity, used in Péclet number calculations.

U_{ijk} The mean mass flux ($uh\Delta y$) in the x-direction (eastward) at the model grid point (*i,j*) on layer *k*.

U^*_{ijk} The eddy mass flux (due to thickness diffusion) in the x-direction (eastward) at the model grid point (*i,j*) on layer *k*.

U_{10} The wind speed at an altitude of 10 metres.

u The zonal component of the mean horizontal velocity.

u The horizontal velocity vector (u,v) representing the sense and magnitude of the 'mean' circulation (total velocity less the eddy component).

$\mathbf{u_B}$ The mean horizontal velocity at the base of the mixed layer.

$\mathbf{u_{Ek}}$ The Ekman drift velocity.

U_* The friction speed of the wind.

v The mean horizontal velocity vector.

V_{ijk} The mean mass flux ($vh\Delta x$) in the y-direction (northward) at the model grid point (*i,j*) on layer *k*.

V^*_{ijk} The eddy mass flux (due to thickness diffusion) in the y-direction (northward) at the model grid point (i,j) on layer k.

v The meridional component of the mean horizontal velocity.

w The upward vertical velocity.

w_E Ekman pumping velocity, the vertical velocity associated with the divergence in the Ekman drift, defined such that a positive velocity is upwards.

x The horizontal position vector, (x,y)

Δx The model grid point separation in the x-direction (eastward).

Δy The model grid point separation in the y-direction (northward).

Detrainment The transfer of water across the base of the mixed layer, from the mixed layer into the ocean interior. Detrainment can occur either through the shallowing of the mixed layer, *e.g.* in Spring when the surface buoyancy flux changes sign, or through vertical motion of water parcels, *e.g.* Ekman pumping.

Entrainment The transfer of water across the base of the mixed layer from the stratified interior of the ocean into the mixed layer. Entrainment can occur through turbulent kinetic energy being used to lift underlying water or through vertical motion of water through the base of the mixed layer, *e.g.* Ekman suction.

Permanent entrainment The entrainment of water from the thermocline where the water entrained remained in the thermocline for the duration of the previous winter, *i.e.* the water has passed from the permanent thermocline to the seasonal thermocline during the course of the year.

Permanent entrainment period The period over which permanent entrainment occurs.

Permanent entrainment rate The volume of water entrained by the mixed layer during the course of the permanent entrainment period. This is the volume that is transferred into the seasonal thermocline and then exposed to the atmosphere in a year. This volume is described as a mean annual rate, either for a density class, where the units are of volume flux (Sverdrups), or per unit horizontal area, where the units are metres per year.

Permanent subduction The subduction of water into the thermocline where the detrained water is destined not to be entrained by the mixed layer during the following winter, *i.e.* where the water enters the permanent thermocline during the course of the year, also termed 'effective subduction' by Marshall, *et al.* (1993).

Permanent subduction period The period over which permanent subduction occurs, also termed 'effective subduction period' by Marshall, *et al.* (1993).

Permanent subduction rate The volume of water subducted by the mixed layer during the permanent subduction period. This is the volume that is transferred from the seasonal thermocline to the permanent thermocline during a year having been exposed to the atmosphere. This volume is described as an annual mean rate, either for a density class, where the units are of volume flux (Sverdrups), or per unit horizontal area, where the units are of velocity, metres per year.

Renewal period The ratio of the permanent subduction rate (in Sverdrups) for a particular density class to the volume of water of that density in the permanent thermocline. This gives a period which indicates the turn-over of water in the permanent thermocline, assuming a simple pipe-flow model.

Subduction The passage of water of one density beneath a lighter water mass (*c.f.* geological subduction in plate tectonics). During the Spring detrainment season the mixed layer is simultaneously detraining and heating and so during this period the processes of detrainment and subduction are identical.

Acknowledgements

I would like to thank my supervisor Dr Kelvin Richards for his thorough reading of this manuscript during its long gestation and for suffering my all too frequent lapses of style and grammar; and the wilful exoticism of my punctuation. Without his intercession this thesis would have been rather less readable.

I would also like to extend my sincere thanks to Dr George Nurser whose experience and ideas have made an invaluable contribution to the shape of this thesis. Much of what I have learnt about the practise of science has come from our discussions of this work; my lapses from this ideal are of my own introduction.

I would like to thank the AIM group for their hospitality during my many visits to the James Rennell Centre. Drs Adrian New and Yanli Jia, and Sally Barnard & Bob Marsh have been generous in both the provision of a CASE award and of Cray CPU time, and with their advice and expertise whilst I ran amok through the JRC computer network and Epoch (sorry Sally!).

Much of the work on the final draft of this thesis was undertaken while I was employed at the Centre for Global Atmospheric Modelling, Reading. My thanks are extended to Prof. Alan O'Neill and other members of CGAM for allowing me to continue the preparation of this thesis while under their employ.

And finally, I would like to thank all of those people who have made my stay in Southampton so enjoyable. In no particular order; Steve K. & Wessex Films, Bablu, Lisa, Steve B., Jason, Duncan, Nigel, Simon & Andy and many other too numerous to mention. I would especially like to thank Mai Mai for her readily available shoulder, ice cream, *etc.* that went to make this thesis possible.

Lastly, to PMF goes my love as ever.

CHAPTER ONE

Introduction and historical review

"Surely Divine Providence did not make the vast body of the Sea for no other use, than for Fishes to disport themselves therein, or (as some do conceit) only for to quench and qualifie the drought and heat of the Sun."

Thomas Fuller (1608-1661),
"The Worthies of England"

1.1 Introduction

The standard view of the role of the ocean in the climate system is that of a flywheel coupled to an atmospheric heat engine (*e.g.* Niiler, 1992). The ocean's regulatory role occurs through two properties. First, the specific heat capacity of water is far greater than that of air, thus a column of sea water 2.5 metres deep has the same heat capacity as the entire column of atmosphere above it. With a mean depth of ~4 km, the oceans represent a potentially large thermal buffer. Secondly, the ocean is thought to play an important role in the global budget of gases, such as carbon dioxide (Broecker, *et al.* 1979). Through the sequestration of these gases, the ocean is thought to moderate changes in the balance of radiative heat fluxes in the atmosphere. The role of more complex oceanic systems, especially the role of marine biology, is unclear at present and they could provide either a positive or negative feedback to climate change.

Although the potential buffer the ocean provides is large, the buffer available over decadal time scales is much less. The oceanic mixed layer is intimately coupled to the atmosphere. However, the thermocline beneath the mixed layer receives little direct forcing from the atmosphere other than equatorial insolation (Woods, *et al.*, 1984) which is limited to the upper few tens of metres of the total thermocline depth (~1km). The mixed layer mediates between the atmosphere and the ocean interior, and it is the efficiency with which this mediation occurs that dictates the proportion of the ocean available as a climatic buffer over decadal time scales; over longer periods, ~100-1000's years, the slow conveyor belt circulation becomes important. If the mixed layer and

thermocline were to decouple then only 1/80th of the total ocean volume would be accessible (Kraus, 1988). In addition, the intimate coupling between the mixed layer and the atmosphere permits heat and gases to remain close to equilibrium with the atmosphere. Once in the thermocline, heat and gases remain sequestered regardless of the state of the atmosphere (Sarmiento & Toggweiler, 1984) until the thermocline water masses have completed their circuit of the subtropical gyre and re-enter the western boundary current.

The coupling of the mixed layer to the thermocline occurs through the process of 'subduction' (Cushman-Roisin, 1987). Subduction occurs when water in the thermocline passes beneath lighter water, this can either occur by Ekman pumping through the base of the mixed layer (Stommel, 1979) or as a result of the seasonal cycle in the depth of the mixed layer (Woods, 1985). This second process is otherwise known as 'lateral induction'. The term 'ventilation' has also been used to denote subduction (Huang, 1991), but throughout this thesis the term 'subduction' will be used exclusively; 'ventilation' will be used to denote the subsequent circulation of the subducted water in the thermocline. The process of 'detrainment' is the transfer of water from the mixed layer to the thermocline. This process can be equated with subduction; the choice of term depends on whether the transfer of water is being considered in relation to the mixed layer or the thermocline. The process of 'entrainment' is the transfer of water previously in the thermocline into the mixed layer.

The mixed layer undergoes strong cycles in its depth and density over annual time-scales. Driven by atmospheric forcing through this cycle, the mixed layer periodically entrains then detrains part of the thermocline, denoted the 'seasonal thermocline'; that part of the thermocline beyond the reach of the mixed layer is the 'permanent thermocline'. Obviously, water in the seasonal thermocline is exposed to the atmosphere over part of the annual cycle whereas water remaining in the permanent thermocline is not exposed to the atmosphere until it circulates back into the seasonal thermocline. The entry of water into the permanent thermocline ('permanent subduction') is of primary interest for this thesis, this water is removed from the zone of atmospheric influence for periods of greater than one year. It is this water which plays the most important role in the climate

for time scales of greater than the annual (Broecker, 1991). Permanent subduction is balanced by 'permanent entrainment', the entrainment of waters into the mixed layer which were previously in the permanent thermocline.

Associated with the subduction of water into the permanent thermocline are the mode waters (Woods & Barkmann, 1986a). These water masses are found in most subpolar and subtropical basins (McCartney, 1982) and they are characterised by their weak vertical property gradients, high oxygen content and low potential vorticity (McCartney & Talley, 1982). The most widely known of these mode waters are the 18°C waters in the Sargasso Sea and the Labrador Sea Water. This thesis will focus on the study of the subtropical mode waters of which the 18°C waters are representative, although occasional reference is given to the Labrador Sea Water where appropriate.

Through the production of mode waters, the process of permanent subduction also determines the structure and circulation of the thermocline. In an adiabatic ocean, both the potential density and the potential vorticity of the water are conserved by fluid parcels. Thus trajectories in the thermocline are constrained to follow the intersections of isopycnic surfaces and the surfaces of constant potential vorticity. Both of these quantities are related to the structure of the thermocline and they are both selected through the process of permanent subduction. The relation between subduction and circulation has been explored by numerous authors, *e.g.* Williams, 1989 and Luyten, *et al.* (1983). It is expected, therefore, that changes in the surface forcing should elicit a dynamical response in the ocean through the interaction of the mixed layer and thermocline.

The work presented in this thesis examines the process of permanent subduction and the subsequent ventilation of the thermocline. In particular, the work will use the Miami Isopycnic Coordinate Ocean Model (MICOM) to examine the interaction of surface forcing, mixed layer and large-scale circulation in determining the permanent subduction rate and the patterns of thermocline ventilation.

In the rest of this chapter a brief overview of research conducted into permanent subduction and the ventilation of the thermocline will be given. In the following section observational evidence for the presence and variability of the subtropical mode waters will be presented. In the third section the formation of the mode waters and the process of permanent subduction will be reviewed. A very brief description of the role of the mixed layer, its internal processes and its representation in general circulation models (GCMs) will be given in section four. Section five will discuss the mean circulation of the thermocline and will be followed by a section discussing the role of eddies. Section seven will give a short description of the Miami Isopycnic Ocean Model (MICOM). The final section of this chapter will describe the aims of this research and give an outline of the experiments undertaken.

1.2 Observational evidence of the mode waters and their variability

The relative abundance of 18°C water in the North Atlantic was first noted by Wyville-Thomas in the report on the Challenger expedition of 1872-1875 (Worthington, 1976). Temperature sections of the leg of the voyage from New York to St.Thomas via Bermuda clearly show a thermostad at 18°C, extending southward across the Sargasso Sea and tapering in thickness towards the south. More recent transects of the North Atlantic (*e.g.* Fugilister, 1963) clearly show thermostads and associated pycnostads at 18°C in the subtropical North Atlantic Ocean. It is now recognised that the waters observed by Wyville-Thomas are at the lighter end of a spectrum of 'mode waters' generated in the subtropical North Atlantic, $26.4<\sigma<27.1$ (McCartney, 1982). The 18°C water remains the most consistently observed mode water through their circulation past the Bermuda sounding station '*Panulirus*'.

The presence of 18°C water has been shown to be remarkably persistent over long periods (1873-1958, Schroeder, *et al.*, 1959). Analyses of series of soundings taken before 1954 show that the properties of the thermostad had little variance, 17.9±0.03°C and 36.5±0.10$^{0}/_{00}$, over 1,993 measurements (Worthington, 1959). More recent time

series from Bermuda reveal that in recent decades significant variability in the 18°C water has occurred. Frankignoul (1981) found temporal variability on the scale O(100 days), but without spatial information he could not distinguish between the seasonal cycle and the mesoscale eddy field as the source of this variance. On longer time scales dramatic variations were found by both Jenkins (1982) and Talley & Raymer (1982) using ^{3}H and potential vorticity measurements as tracers for their studies.

It was found that 18°C water potential vorticity was uniform between 1954-'71 with a sudden increase in potential vorticity in 1971 lasting until 1977, whereon 18°C properties reverted to their 1954 values. Over the period 1954-'64 the T, S and ρ characteristics were constant, but between 1964 and 1971 the mode water cooled and became more saline, increasing its density (Talley & Raymer, 1982). Between 1971 and 1977 little 18°C water was generated (indicated by the high potential vorticity) (Worthington, 1977 and Talley & Raymer, 1982). The winter of 1976-'77 was exceptionally severe on the eastern coast of the United States and it was observed to generate ~500m of 18°C water at the surface, south of the Gulf Stream (Leetmaa, 1977). It is probable that it also resulted in the observed changes to the helium-3 and tritium concentrations in 18°C water (Jenkins, 1982) through de-gassing.

Jenkins (1982) suggested that changes in the characteristics of the Sargasso Sea mode waters indicated a change in the circulation. This was refuted by Talley & Raymer (1982) who assumed that it could be described by a shift in the density of the mode waters produced. This phenomenon is observed in GCMs subject to anomalous cooling (R.Marsh, personal communication). A shift in the position of surface isopycnals results in a shift in the sites of mode water production.

The cause of the period of 18°C water variability (1964-1977) is not established. However, before 1954 significant decadal scale variability in the sea surface temperature was observed (see Pocklington, 1972) with no corresponding change in the properties of the mode waters over the same period. However, 1964-1977 covers the period of the Great Salinity Anomaly (Sarmiento, *et al.*, 1992). The coincidence is suggestive but the northern salinity anomaly and the Sargasso variability may be unrelated. The salinity

anomaly was largely contained within the subpolar gyre (Lazier, 1988), thus the freshening could not directly influence the Sargasso Sea. However, the two phenomena may have a common cause through the North Atlantic Oscillation (Dickson, *et al.*, 1989).

Warren (1972) hypothesised that the invariance of 18°C water properties (before 1964) was a result of the extent of the mode water mass. The mode water layer is 200-400 metres thick and it is only exposed for a brief period. This model is, however, inadequate. The Bermuda soundings indicate that Sargasso SSTs are always greater than 18°C (Iselin, 1939). Furthermore, Bermuda lies in the recirculation zone of the Gulf Stream (Worthington, 1976); mode waters would quickly be advected back into the Gulf Stream and do not remain in the Sargasso Sea for exposure to successive winters. Therefore, 18°C mode waters must be generated in relatively large quantities to balance this advection. Dewar (1986) has suggested that eddies in this region act to mix subducted water with a reservoir accumulated over previous years thus guaranteeing the stability of water mass properties.

1.3 The formation of mode waters

The modification of water mass properties can either occur through diapycnic mixing or through exposure to direct atmospheric forcing in the mixed layer (Csanady, 1984). As indicated above, exposure to atmospheric forcing for Sargasso mode waters *in situ* is not possible (Iselin, 1939) whilst diapycnal diffusivities are $\sim 10^6$ times smaller than isopycnic diffusivities (Montgomery, 1938). Montgomery suggested that in the adiabatic ocean interior flow lies predominantly along isopycnic surfaces. Thus the properties of the thermocline are those of the sea surface where the isopycnic trajectory intersects the mixed layer.

Worthington (1959) proposed that the cooling of the surface layers produced a convergence and subsequent sinking of the surface waters into the interior. Masuzawa (1969) extended this idea and balanced the convergence with a diapycnic flux in the southern subtropics and a northward flux in the surface layers. The northward flow

required by the model is not supported by the dynamic topography of the Sargasso Sea (Warren, 1972).

The properties of the thermocline are predominantly those of the upstream winter mixed layer (Worthington, 1959). In a simple model Stommel (1979) showed that the properties driven by Ekman pumping down isopycnic surfaces could be selected by the mixed layer cycle (see figure 1.1). Only waters pumped through the base of the mixed layer in late winter/early spring would move from the seasonal to the permanent thermocline over the year. Thus the 'Ekman demon' selects the properties of the permanent thermocline. The action of the 'Ekman demon' depends on the brevity of the period over which water leaving the mixed layer enters the permanent thermocline during the course of following year. A brief period will ensure that only the winter mixed layer properties are selected. Attempts to deduce this period, the 'permanent subduction period', from hydrography (Marshall, *et al.*, 1993) give estimates of 1-2 months, whilst the CME model produces shorter periods, ~1 month (Williams, *et al.*, 1995). The length of the permanent subduction period will be examined later (Chapter 4) for the Atlantic Isopycnic Model (AIM).

Stommel's model uses Ekman pumping to transfer water from the mixed layer to the thermocline with the detrainment/entrainment cycle of the mixed layer imposed only to censor the waters. Estimates of the permanent subduction rate for the North Atlantic from the distribution of tritium (Sarmiento, 1983b) produced permanent subduction rates in excess of those possible from Ekman pumping alone. Evidently Ekman pumping is augmented by at least one process. Woods (1985) proposed a simple mechanism, 'lateral induction' (see figure 1.2). The annual mixed layer cycle does not descend to the same depth at all points in the North Atlantic. In the Gulf Stream and the North Atlantic Drift Current the winter air-sea temperature difference generates deep winter mixed layers (~400 metres). To the south of this area of deep winter mixing the winter air-sea temperature difference is not as great and so the winter mixed layer depth is shallower. In this region the mean meridional flow is southward and so the geostrophic flow will carry fluid through the sloping base of the mixed layer. Thus the full, instantaneous subduction rate, S, (Cushman-Roisin, 1987) is;

$$S = -w_b - \frac{\partial h}{\partial t} - \mathbf{u}_b \cdot \nabla h, \qquad \text{Eq. 1.1}$$

where w_b is the vertical velocity at the base of the mixed layer, h is the instantaneous mixed layer depth and $\mathbf{u}_b$ is the horizontal velocity at the base of mixed layer. Over the annual cycle the permanent subduction rate is given by the passage of fluid through the base of the seasonal thermocline (*i.e.* the local maximum in the depth of the mixed layer over the annual cycle, h_{max}) and it is given by Marshall, *et al.* (1993) as;

$$S_{ann} = \overline{-w_E} - \overline{\mathbf{u}_H} \cdot \nabla H + \frac{\beta}{f} \int_{-h}^{0-} \overline{v} dz, \qquad \text{Eq. 1.2}$$

where the over-bar represents the annual mean, w_E is the Ekman velocity, H is the maximum depth of the mixed layer over the annual cycle. The third term on the RHS is a vertical velocity induced by the linear vorticity balance; f is the Coriolis parameter, β is the meridional gradient of f and v is the meridional component of the velocity. In the Gulf Stream the vertical velocity is dominated by the vorticity balance (McWilliams, 1983), however it is doubtful that the linear vorticity balance used in the Marshall, *et al.* (1993) calculations will hold in the region of the Gulf Stream where the high velocities imply a strongly non-linear flow regime. On the southern flank of the Gulf Stream the $\overline{\mathbf{u}_H} \cdot \nabla H$ term dominates (Rooth & Ostlund, 1972), although it has been found to make an important contribution over most of the rest of the gyre (Williams, *et al.*, 1995) for the creation of central waters (Woods & Barkmann, 1986a).

The convection of the winter mixed layer removes vertical gradients of tracer properties and restores the gaseous content to values in equilibrium with the atmosphere (high oxygen, and contemporary helium-3 concentrations and CFC ratios). The low potential vorticity (Q) of the resultant mode waters arises during subduction (Williams, 1991) through the density change in the mixed layer (ρ_1) through advection and buoyancy fluxes (B_0) as the water column is formed by fluid passing out of the mixed layer of depth h by Ekman pumping and advection;

$$Q = f \frac{B_0 + \mathbf{u}_b \cdot \nabla \rho_1}{\rho_0 (w_E + \mathbf{u}_b \cdot \nabla h)}, \qquad \text{Eq. 1.3}$$

ρ_0 represents a reference density. For typical subtropical values of w_E (~50m/year) it is clear that low potential vorticity water masses cannot be generated through the Ekman-driven subduction model (Woods, 1985).

The connection between water mass formation and surface heat loss is mentioned above. Worthington (1972) indicated that mode water formation in the Gulf Stream and Kuroshio were determined by surface heat fluxes. Woods & Barkmann (1986a) associated the main site of lateral induction with the zero net buoyancy flux line. A more detailed study by Nurser & Marshall (1991) related the subduction rate in an idealised thermocline model (Marshall & Nurser, 1991) to surface forcing by considering the evolution of the thermocline density gradient, and thus the potential vorticity, of a one-dimensional water column including a mixed layer and thermocline. The relation derived by Nurser & Marshall is;

$$S = \frac{\alpha_E f H_{net}}{\rho_0 h c_w Q_b}, \qquad \text{Eq. 1.4}$$

where H_{net} is the total heat flux arising from Ekman drift and surface heat fluxes, α_E is the expansion coefficient of water, c_w is the specific heat capacity of water and Q_b is the potential vorticity at the base of the mixed layer. Integration of S over the permanent subduction period for a Lagrangian column derives the permanent subduction rate. It has been demonstrated by Marshall, *et al.* (1993) that this integral is equal to the integral of S along the Lagrangian trajectory over an annual cycle minus the contribution of Ekman pumping over the year. The relation used above can be extended to include the influence of fresh water forcing on thebuoyancy of the water column.

Heat fluxes at the surface enable cross-isopycnic flow in the mixed layer, and thus the transformation of water masses. This approach was used by Walin (1982) to estimate the meridional overturning of the North Atlantic as 10 Sverdrups. More detailed studies of the transformation between the North Atlantic density classes have been undertaken by Speer & Tziperman (1992) and Wright (1972). Speer & Tziperman (1992) analysed density classes $\sigma \geq 26.2$, and deduced the presence of distinct classes of mode water, the subtropical modes and the subpolar modes. Wright used annual mean heat fluxes to derive an estimate of the formation rate of Labrador Sea Water; the rate he derived was

3.2 Sverdrups, close to the value estimated from field studies by Clarke & Gascard (1983).

Labrador Sea Water (LSW) is formed in the Labrador basin by deep convection down to 1km. The characteristic properties of LSW are a temperature of 3.5°C and a potential density of σ=27.75. The potential vorticity of the LSW is the lowest of any water mass in the world ocean (McCartney & Talley, 1982). Estimates of the production of LSW lie between 3.2 Sverdrups and 8.5 Sverdrups. This water is largely exported south by the Deep Western Boundary Current, but some is modified by mixing at the Greenland-Shetland ridge and at the interface with Mediterranean outflow water (Talley & McCartney, 1982).

The use of passive tracers in the examination of permanent subduction has been invaluable, in particular the bomb-tritium released by the above ground bomb tests of the late 1950's and early 1960's. The input of tritium into the environment over this period dwarfed the input from natural sources. The entry of tritium into the ocean has allowed information to be gathered on the rates of permanent subduction (Sarmiento, 1983b) and on the dispersion of mode waters in the thermocline (Sarmiento, 1983a). The decay of tritium into helium-3 also allows the estimation of ventilation ages (the time elapsed since the water was last exposed to the atmosphere). It should be noted, however, that tracer ventilation ages have associated errors through isopycnic tracer mixing and the 'inelasticity' of tritium compared to helium-3 in the event of exposure to the atmosphere; helium-3 will readily de-gas whilst tritium will remain in the ocean, altering the ventilation age (Doney & Jenkins, 1988). Tracers are increasingly used in model calibration and validation (*e.g.* Sarmiento, 1983b and Jia & Richards, 1995).

A more traditional passive tracer, oxygen, can also be used to examine mode waters (Worthington, 1959); however, the interpretation of measurements can be obscured by biological processes acting on O_2 concentration. The use of CFC concentrations and, in particular, the use of ratios of CFC-types (CFC-111, CFC-112 and CFC-113) promises better estimates of subduction and thermocline ventilation.

1.4 The oceanic mixed layer

The role of the mixed layer as the intermediary in the interaction of the atmosphere with the ocean interior (see section 1.1 and 1.3) implies that in order to understand permanent subduction, an understanding of the mixed layer is necessary, at least over seasonal time scales. In the extra-tropics, the diurnal cycle of the mixed layer is assumed to be of limited importance over long periods (Woods & Barkmann, 1986b). The focus of this study is therefore placed on the seasonal cycle. The diurnal cycle is not included.

For the purposes of this thesis the mixed layer will be assumed to be a well-defined layer upper-most in the ocean column. Temperature, salinity and other tracers within the mixed layer are homogenised by 3-D turbulence (Phillips, 1966). The homogenisation of the above tracers and of momentum in the mixed layer is assumed to be complete in the representation used here (Kraus & Turner, 1967). The turbulent processes in the mixed layer are driven by numerous sources; convection, breaking internal and surface waves, Langmuir circulation and shear instabilities at the base of the mixed layer (Niiler & Kraus, 1977). The explicit representation of these processes in models is generally too time-consuming to be permissible.

Naturally the Kraus-Turner representation of the mixed layer is not an exact portrayal of surface mixing processes. The definition of the base of the mixed layer from field data is problematic since T and S profiles also indicate fossil mixed layers (detrained, low stability waters). These problems can be overcome by defining the base of the mixed layer by the turbocline (sharp gradient in the turbulent kinetic energy) (Woods & Barkmann, 1986b), but this requires *in situ* measurements not routinely taken on deep sea hydrographic surveys. In addition, the assumption that mixing is directly surface-induced does not hold in the Equatorial wave-guide and in regions of strong shear. In these regions shear instabilities play an important role in determining the stratification beneath the surface mixed layer (Pacanowski & Philander, 1981).

The representation of mixing processes has been subject to intense research, and numerous models have been developed (see the review by Large, *et al.*, 1994). These

models can be broadly divided into three types; bulk models, transilient models and turbulence closure models (Niiler & Kraus, 1977). The most complex of these models are the turbulence closure schemes, such as Mellor & Yamada (1982). These solve the equations for Reynolds stresses and turbulent kinetic energy explicitly with some parametrisation of turbulent quantities to close the scheme at some order (usually second order). Turbulence closure models require closure conditions that are uncertain, furthermore the results generated by turbulence closure models in the extratropics are relatively poor despite the extra computational expense in their operation compared to other schemes.

Eddy coefficient schemes, such as that of Pacanowski & Philander (1981), are extensively used in GCM ocean simulations. These models parametrise the upper ocean turbulence through the use of the diffusion equation with the diffusion coefficients determined from the gradient Richardson number. These schemes have been found to operate reasonably well in equatorial simulations, but they under-represent the effects of wind-induced mixing.

Bulk mixed layer models (*e.g.* Kraus & Turner, 1967 and Price, *et al.*, 1986) are commonly used in GCMs. They are mathematically simple and therefore do not require large amounts of computer time. Despite their simplicity, Kraus-Turner models produce reasonable results in the extratropics whilst the Richardson number relaxation scheme of Price, *et al.* (1986) has been successfully applied to the Equatorial ocean. The hybrid scheme of Chen, *et al.* (1994) appears to have addressed the deficiencies of both models by a combination of the Kraus-Turner bulk mixed layer with a Richardson number-dependent scheme in the thermocline below.

1.5 The mean circulation of the subtropical thermocline

The circulation of water in the thermocline is classically viewed as conservative in both the potential density and the potential vorticity of the fluid. At depth there are no diabatic heat sources or sinks (disregarding hydrothermal vents), little mechanical forcing and the roles of dissipative and diffusive processes are assumed to be weak. The conservation of

potential density can be shown to hold through the presence of distinct water masses, such as Labrador Sea Water, over much of the world ocean. The conservation of potential vorticity is assumed to hold away from the surface layers and frictional boundary layers.

The conservation of potential density by water parcels implies that circulation and mixing in the thermocline occurs predominantly along isopycnic surfaces, thus isopycnic surfaces are the natural framework within which to view water mass properties. As a result many layer models have been developed to examine the thermocline (*e.g.* Huang, 1987, *et seq.*). These models are being augmented by isopycnic general circulation models (Bleck, *et al.*, 1992 and Oberhuber, 1993a&b), the use of which is becoming more widespread.

Our understanding of the subtropical thermocline has developed from two complementary models. The models are the 'ventilated thermocline' model of Luyten, Pedlosky & Stommel (1983) (henceforward LPS) and the 'unventilated thermocline' model of Rhines & Young (1982). Subsequent investigations of the dynamics of the thermocline have sought to unify these two descriptions and to address some of the questions raised by their solutions.

Rhines & Young examined an isopycnic layer at depth, isolated from the wind-induced surface currents, using a quasi-geostrophic layer model with interfacial friction between isopycnic layers. They demonstrated that circulation at depth could occur for a sufficiently strong wind stress. The wind-forcing deforms the layer interfaces and in doing so distorts the potential vorticity contours from their initial conditions. Given a sufficiently strong wind stress potential vorticity contours develop into closed loops, allowing circulation to occur. In addition, Rhines & Young also derived a β-plane version of Batchelor's potential vorticity homogenisation theory (Batchelor, 1956) and demonstrated that for weak dissipation the potential vorticity within the closed contours becomes homogenised, forming a 'pool' zone. Potential vorticity contours that intersect the eastern boundary are blocked and so no motion occurs along these contours, forming a 'shadow' zone.

Luyten, Pedlosky & Stommel considered the circulation on layers which outcrop in the subtropical gyre. Their model consisted of a series of isopycnic layers with geostrophic flow on each. The circulation was driven by Ekman pumping through the surface of the model and the Sverdrup relation. The circulation derived from their model produced three regions in the thermocline (see figure 1.3). At the eastern boundary a shadow zone with zero thermocline depth was produced. In the centre of the gyre potential vorticity contours lead from the isopycnic outcrop into the interior, denoting the flow of water from a notional mixed layer into the interior. This is called the 'ventilated' zone. To the western extreme of the gyre lies a region where water circulates without reaching the outcrop. The potential vorticity in this region could not be described by the LPS model. This region was identified with the pool zone of Rhines & Young.

The tripartite division of the thermocline into shadow, pool and ventilated zones is partly supported by observational evidence. Maps of potential vorticity (e.g. McDowell, *et al.*, 1982 and Keffer, 1985) show plateaux of potential vorticity at depth, consistent with the potential vorticity homogenisation theory of Rhines & Young. However, further studies have indicated that homogeneous potential vorticity could occur through other processes. Young (1984) showed that a weakly diffusive western boundary current would produce potential vorticity plateaux, although Ierley & Young (1983) showed that potential vorticity homogenisation could not occur for strong dissipative western boundary currents. Williams (1991) indicated that solutions of the ventilated thermocline model producing plateaux of potential vorticity could be derived if the latitude of the outcrop lines was allowed to vary with longitude. A study by Liu, *et al.* (1993) has also indicated that the division of the Sverdrup transport between layers in the pool zone would also act to produce low potential vorticity gradients. Numerical studies at eddy-resolution indicate that eddies can quickly homogenise the potential vorticity, much faster the time scale predicted by Rhines & Young's theory (Cox, 1985).

Studies of the ^{3}H distribution in the thermocline (Sarmiento, 1983a) indicate a low tracer concentration region in the eastern North Atlantic, suggesting a shadow zone. However, these surveys do not indicate a low ^{3}H concentration region in the western basin which would be expected from the unventilated thermocline model. This is thought to be due to

the energetic eddy field near the western boundary current mixing tracer across streamlines (Cox, 1985).

The combination of the Rhines & Young and LPS models has shown that the pool zone is smaller and the circulation is weaker than that of the Rhines & Young study (Pedlosky & Young, 1983). Dewar (1986) successfully framed the ventilated thermocline model in a quasi-geostrophic model with weak dissipation, akin to the Rhines & Young model. It was found that the eddies played an important role in communicating with the low potential vorticity pool zone, thus providing access to a buffer for mode water properties.

The majority of the models cited above address the problem of a purely wind-driven gyre. The role of the mixed layer cycle in the circulation has been addressed for idealised conditions and in numerical models Huang & Bryan (1987) indicate a conversion of high potential vorticity waters into low potential vorticity waters in the western boundary current. This may play an important role in the potential vorticity field and in a weakly dissipative thermocline. This would allow inter-annual meteorological variations to influence the circulation of the thermocline (Williams, 1991). Liu & Pedlosky (1994) showed that for a ideal thermocline model the variability of the ventilated thermocline was driven primarily by the surface buoyancy forcing with a maximal response on the decadal time scale. The variability of the surface wind stress was not found to generate a baroclinic response in the ventilated thermocline in an idealised model (Liu, 1993a&b).

A detailed description of the dynamics of the western boundary current is beyond the scope of this study (see Ierley, 1990 for a recent review), however Ierley & Young (1983) have indicated that the western boundary current plays an important role in the structure of the thermocline. The faithful representation of the western boundary current remains a difficult problem. A measure of this difficulty is the separation point, which is observed to lie off Cape Hatteras in the North Atlantic. With one exception (Sawdey, *et al.*, 1995), models of all resolutions and types fail to position the separation point correctly. The determination of the separation point is unclear, it could be determined by the inertial recirculation (Fofonoff, 1954), the influence of bottom topography (Hogg &

Stommel, 1985), the outcropping of isopycnic surfaces (Parsons, 1969) or a combination of all three processes.

The presence and structure of the shadow zone at the eastern boundary has been discussed by Pedlosky (1983). He demonstrated that finite isopycnic layer thickness and thermocline depth could occur if a zonal flow at the eastern boundary was permitted. Pedlosky invoked an eastern boundary current to satisfy the continuity equation. Cessi (1992) has shown that the inclusion of meridional wind stresses could generate such a current. Cessi cited the pressure gradient along the Pacific coast of the United States as evidence of such a current, while Schopp & Arhan (1986) have found a similar meridional current in the north eastern Atlantic.

1.6 The role of eddies in the permanent thermocline

The low frequency variability of the ocean, the ocean eddy field, is far more energetic than the mean circulation (Robinson, 1983). However, the small characteristic size of these phenomena (of the order of the Rossby radius) places their spatial scale beneath the resolution of basin-scale hydrographic data and most GCMs, while few ocean eddy-resolving GCMs resolve the higher baroclinic Rossby modes. Limited domain field studies, *e.g.* POLYMODE, have gathered much information concerning eddy dynamics, however, much remains to be done.

In non-eddy resolving GCMs it is necessary to parametrise the effects of eddies, if only to produce numerical stability. Eddies are presumed to transport quantities down-gradient, most notably momentum, but also tracers and potential vorticity. To parametrise this transport the use of Laplacian and biharmonic diffusion terms in numerical models has become widespread, although the deficiencies of such schemes are widely acknowledged. More advanced schemes have been developed in order to relate the diffusion coefficients to the observed eddy kinetic energy distribution (Armi, 1979), *e.g.* Smagorinsky (1963) introduced a deformation dependence for eddy viscosity. Smagorinsky's scheme gives an enhanced viscosity in the western boundary current

where viscosity keeps the width of the boundary current within the resolution of the model.

The role of eddies in the circulation of the thermocline has been mentioned briefly above. Rhines & Young (1982) invoked a weak potential vorticity diffusion to create the homogenised pool zone while Dewar (1986) has indicated that the stability of mode water properties may result from eddy transports and a reservoir of mode water in the pool zone. Sarmiento (1983a,b) argued that tracer distributions were heavily influenced by the thermocline eddy field. Musgrave (1990) has also suggested that eddies play an important part in the transfer of water from the seasonal thermocline to the permanent thermocline, thus augmenting the permanent subduction rates due to Ekman pumping and lateral induction.

The orientation of eddy-driven mixing is predominantly isopycnic (Jenkins, 1980 and McDougall & Church, 1986) and many Bryan-Cox GCMs now use isopycnic diffusion tensors (Redi, 1982). Gent, *et al.* (1995) examined the continuity and tracer conservation equations in an isopycnic framework. Through the decomposition of the fields into mean and eddy components they derived an alternative expression for the tracer conservation equation,

$$\frac{\partial \bar{\tau}}{\partial t} + \frac{1}{\bar{h}}\frac{\partial}{\partial t}\left(\overline{h'\tau'}\right) + \left[\bar{\mathbf{u}} + \frac{\overline{h'\mathbf{u}'}}{\bar{h}}\right]\cdot\nabla\bar{\tau} = -\frac{\overline{\nabla\cdot(h\mathbf{u})'\tau'}}{\bar{h}} \qquad \text{Eq.1.5}$$

where τ is the tracer concentration, h is the isopycnic layer thickness and $\mathbf{u}$ is the velocity on the isopycnic layer. The over bar denotes a time/space mean (over suitable scales) and the prime denotes the time dependent variation of the quantity from that mean, the eddy component. It is generally assumed that anomalies inb the tracer and thickness are uncorrelated in the mean (*i.e.* $\overline{h'\tau'}=0$) removing the second term on the LHS. The resulting equation can be interpreted as stating that the evolution of the mean tracer field is determined by advection across gradients of τ (third term on LHS of Eq.1.5) and by the divergence of the addy tracer flux (term on RHS of Eq.1.5). This last term is usually represented as a down-gradient Fickian diffusion of the mean tracer field, *i.e.* $\left[\nabla\cdot\left(\kappa_I\, h\nabla\tau\right)\right]h^{-1}$.

It will be noted that the advection term in Eq.1.5 can b divided into two components. The first component Is the familiar advection be the mean circulation. The additional component is associated with the eddy flux of mass along an isopycnic surface, $\overline{h'\mathbf{u}'}$, and the velocity which is associated with this mass flux is termed the 'eddy-induced transport velocity', $\mathbf{u}^* = \frac{\overline{\mathbf{u}'h'}}{\overline{h}}$ (Gent, *et al.*, 1995). In atmospheric modelling it has long been recognised that the transport of tracer in the stratosphere occurs through both the mean circulation and through the eddy mass fluxes.

Gent & McWilliams (1990) proposed that the turbulent flux of layer thickness ($\overline{h'\mathbf{u}'}$) along isopycnic surfaces could be represented by a Fickian diffusion of layer thickness. This parametrisation was chosen to give a sign-definite sink of domain-averaged potential energy, and in this way the parametrisation is thought to mimic the large-scale effects of baroclinic instabilities which draw on the mean potential energy of the ocean (McDougall & Church, 1986).

The use of thickness diffusion schemes in isopycnic GCMs is mandatory to maintain numerical stability (Bleck, *et al.*, 1992) while the use of the Gent & McWilliams scheme in Bryan-Cox GCMs has improved the representation of the thermocline (Danabasoglu, *et al.* 1995 and Gent, *et al.*, 1995). Small-scale variations in the potential vorticity field in the ocean (*e.g.* Pollard & Regier, 1990 and Armi & Stommel, 1983) superimposed on the large-scale homogenised potential vorticity field could be interpreted as a signature of the eddy transport of potential vorticity. McDowell, *et al.* (1982) found that baroclinic instabilities are probable over most of the subtropical North Atlantic.

Studies of passive tracers in ocean gyres have been undertaken as an aid to the interpretation of both model and field data, and to aid the calibration of the model diffusion coefficients. Jia & Richards (1994) and Musgrave (1990) examined the tracer dispersion in idealised gyres and the dependence of this dispersion on the Péclet number (Pé=UL/κ). Jia & Richards found that gyres where Pé≥20 produced tongues of tracer, indicating the dominance of advection over diffusion in the transport of tracer in the gyre interior.

The eddy-resolving model of Böning & Cox (1988) was used to study the eddy-dispersal of particles in the North Atlantic. Their model did not produce ventilation tongues or a boundary between the pool and ventilated zone in the thermocline. The diffusivities derived from the dispersion of particles indicated that the process was anisotropic; dispersion was faster in the zonal direction than in the meridional direction. For a model Péclet number of 3-4, Böning & Cox derived a zonal diffusion coefficient of $7-8\times10^{7}\ \mathrm{cm^{2}s^{-1}}$ and in the meridional direction $\sim 3\times10^{7}\ \mathrm{cm^{2}s^{-1}}$.

Isopycnic diffusion coefficients derived from mid-ocean experiments and observations (e.g. sofar floats, tracers, etc.) indicate values from as low as $0.7\times10^{7}\ \mathrm{cm^{2}s^{-1}}$ in the deep thermocline (Freeland, *et al.*, 1975) to $2.5\times10^{7}\ \mathrm{cm^{2}s^{-1}}$ in the upper thermocline (Thiele, *et al.*, 1986). More recent observations of buoys drogued to 100 metres in the South Atlantic (Schäfer & Krauss, 1995) show that values of up to $10.2\times10^{7}\mathrm{cm^{2}s^{-1}}$ can occur. Estimates of isopycnic thickness diffusion coefficients are not currently available. In the field studies mentioned above it is not clear to what extent the process of thickness diffusion was aliased as isopycnic tracer diffusion. Furthermore, it is not clear what relation (if any) should exist between the isopycnic tracer diffusivity and the thickness diffusivity.

1.7 The Miami Isopycnic Coordinate Ocean Model

Isopycnic ocean models differ from the more usual Bryan-Cox depth coordinate models in that they use depth-varying constant density layers to describe the vertical structure of the ocean rather than constant depth, variable density levels. The isopycnic description of the ocean explicitly describes the water masses and diapycnic mixing is entirely prescribed. Thus isopycnic coordinates are the most 'natural' framework within which to examine the formation and distribution of water masses. The isopycnic general circulation model used in this thesis is the Miami Isopycnic Coordinate Ocean Model (MICOM) developed by Bleck and others since the late 1970's. Two versions of this model are examined; these two versions are described in the following sub-sections.

1.7.1 The Atlantic Isopycnic Model

The Atlantic Isopycnic Model (AIM) is a 1° resolution C-grid model of the northern and equatorial Atlantic Ocean based on the work of Bleck & Smith (1990) and run by the James Rennell Centre for Ocean Circulation. The model is composed of a Kraus-Turner mixed layer (Bleck, *et al.*, 1989) and nineteen isopycnic layers with densities of between 25.65 and 28.15 sigma-units. The model domain extends from approximately 20° South to 80° North and includes the main Atlantic basin, the Gulf of Mexico, the Caribbean, Labrador and Greenland Seas. It does not include the Mediterranean or its outflow, or the European shelf seas. The model topography (figure 1.4) is taken directly from the 1° Scripps data set and includes the Greenland-Iceland-Scotland (GIS) ridge system. In order to give as uniform a grid mesh as possible over the main body of the North Atlantic, the model grid is constructed to be regular on a rotated Mercator projection whereby the geometric pole lies in the Equatorial Pacific. This rotation gives precisely 1° resolution at 40°W falling off to both the east and west to approximately 0.5° resolution at 100°W. Temperature and salinity are advected and diffused independently on all layers. The eddy viscosity and diffusivity parameters used in AIM are given in Table 1.1.

AIM is forced using climatological data sets composed of monthly mean fluxes; Ebensen & Kushnir (1981) heat fluxes, Hellerman & Rosenstein (1983) wind speeds and stresses, Jaeger (1976) precipitation and Ebensen & Kushnir (1981) evaporation. In addition, a Haney (1971) term for both temperature and salinity are added to relax the surface temperature and salinity back to the Levitus (1982) values over a time scale of four months for a 100 metre water column. A description of the model is given in Appendix A and a description of the Kraus-Turner mixed layer is given in Appendix B.

Results of the spin-up of AIM and its predecessors are presented in numerous papers, but most notably for the purposes of this thesis in New, *et al.* (1995) and New & Bleck (1995). These papers present the results of a thirty year integration of AIM from Levitus (1982) initial conditions. The barotropic streamfunction for the summer of the thirtieth year of this integration is shown in figure 1.5. It is clear that the gyre has developed a circulation pattern similar to that observed, a strong westward equatorial current with a strong poleward flow along the western edge of the basin with a separation point at

about the latitude of Cape Cod. This is somewhat to the north of the Cape Hatteras separation point, but this failing is typical of models at this resolution. The circulation of the basin is divided into four gyres; the familiar subpolar and subtropical gyres and a pair of tropical gyres on opposite sides of the Equator with each gyre centred on 10° North and 10° South respectively. The transport of the subtropical gyre varies seasonally between 26 Sverdrups in summer to 44 Sverdrups in January (New & Bleck, 1995), slightly higher than the transport expected from the Sverdrup relation.

The production of mode waters in AIM was examined by New, *et al.* (1995) who found from the layer thickness field that the subtropical thermocline is ventilated by a series of tongues on isopycnic layers in the density range σ=26.40-27.15, with progressively denser layers ventilated further east. The response of the subtropical thermocline to the excessive cooling of the Gulf Stream (arising from the incorrect position of the separation point) has been noted by New & Bleck (1995). They indicate that the changes in AIM's subtropical temperature, salinity and potential vorticity fields are similar to those observed in the North Atlantic during the period between the early 1950's and 1980's. The subtropical gyre of AIM and the UKMO Hadley Centre Bryan-Cox model were compared in the paper by Marsh & Roberts (1995). The patterns of permanent subduction found by the kinematic method are similar in these models; estimates of the rates of permanent subduction for both of these models are given in Chapter Four.

In the subpolar region the model is found to produce large amounts of σ=27.75 water in the Labrador Sea and the Irminger basin, as observed in the North Atlantic (Talley & McCartney, 1982). This water mass was found to spread southwards along the North American coastline in a slow, broad Deep Western Boundary Current (DWBC) and along the eastern flank of the mid-Atlantic ridge. This is in agreement with the observed distribution of potential vorticity at this density, although the width of the DWBC is found to be narrower in the observations. The comparison of the AIM subpolar gyre and the UKMO Hadley Centre model's subpolar gyre with hydrography by Roberts, *et al.* (1995) found that the representation of the GIS overflow in AIM was more accurate. In particular, it was found that the Hadley Centre model produced strong diapycnic mixing at the ridge and so little North Atlantic Deep Water was exported from the Greenland

basin, most of it was mixed with lighter waters to produce an intermediate water mass. The modified water mass in the Hadley Centre model was thought to be responsible for the deflection of the North Atlantic Drift Current along a more southern course.

1.7.2 The simple geometry version of MICOM, Boxmix

The second version of MICOM used in this thesis is called Boxmix for brevity throughout the rest of this thesis. This version of MICOM was developed by Bleck, *et al.* (1989) from the fully-isopycnic model of Bleck & Boudra (1986). The Boxmix domain extends from 10°N to 60°N and across 64° longitude, bounded by lines of constant latitude and longitude. The model's B-grid mesh is regular in the standard Mercator projection and gives a longitudinal resolution of 2° at the Equator. The salinity of Boxmix is constant, thus removing the need to advect or diffuse temperature in the isopycnic interior. The model has a flat bottom at a depth of 5000 metres. The model equations differ from those of AIM largely through the use of a rigid lid to remove the barotropic divergence. A description of the model is given in Appendix A and a description of the Kraus-Turner mixed layer model is given in Appendix B.

The model is forced by seasonally varying zonally-averaged functions for the radiative heat flux, wind stress, pseudo-air temperature and the wind speed at 10 metres altitude. The pseudo-air temperature is used in a Haney term to represent the turbulent heat fluxes (latent and sensible). These functions are given in Table A.1 of Appendix A.

Three configurations of Boxmix are examined in Chapters Three, Five and Six of this thesis. The circulations generated by these three configurations are examined in Chapter Five. The first version, taken as the standard version, is called Box1 in order to differentiate it from the two other versions used in Chapter Five. As will be noted in Chapter Five, various runs of this configuration of Boxmix will be undertaken with various isopycnic tracer diffusivities. The dynamics of these runs are identical since isopycnic diffusion does not influence the ocean stratification, thus the model version used in these runs is referred to as Box1 and the individual tracer runs are called Run 1a, etc. Box1 has nine isopycnic layers and a Kraus-Turner mixed layer. The values of the eddy viscosity and diffusivity parameters are given in Table 1.1 as viscous and diffusive

'velocities'. These 'velocities' are used to scale the local diffusivity of the model to the local grid resolution. The eddy viscosity and eddy diffusivity are derived thus,

$$\nu = v_v \Delta x \qquad \text{Eq. 1.6}$$

where ν is the eddy viscosity or diffusivity, v_V is the viscous or diffusive 'velocity' and Δx is the local grid size.

Boxmix version Box2 is similar to Box1 in that it has nine isopycnic layers and a Kraus-Turner mixed layer model. The eddy viscosity and diffusivity parameters given in Table 1.1 are the same as for Box1 apart from the layer thickness diffusion velocity which has a value of 0.45cm/s in Box2 compared to 1.5 cm/s in Box1. As will be noted in Chapter Five, this influences the model dynamics.

A third version of Boxmix, used in both Chapters Five and Six, is called Box3. This version uses the same parameter values as Box1 and the same isopycnic tracer diffusion as Run 1a (see Table 1.1). Only one value of the tracer diffusivity is used in Chapters Five and Six. In common with Box1 and Box2, Box3 has a Kraus-Turner mixed layer. Run 3 differs from Boxmix versions Box1 and Box2 in that it has seventeen isopycnic layer with the same densities as the lightest seventeen isopycnic layers of AIM. The increase in the number of isopycnic layers increases the density resolution of the model in the subtropics.

The dynamics of these three versions of Boxmix are discussed in detail in Chapter Five.

Model, Run	Resolution	Viscous velocity[1]	Thickness diffusion velocity[1]	Tracer diffusion velocity[1]	Number of isopycnic layers
AIM	1°	2.0	1.0	1.0	19
Box1, Run 1a	2°	1.5	1.5	2.0	9
Box1, Run 1b	2°	1.5	1.5	1.0	9
Box1, Run 1c	2°	1.5	1.5	0.0	9
Box2, Run 2a	2°	1.5	0.45	2.0	9
Box2, Run 2b	2°	1.5	0.45	0.0	9
Box3, Run 3	2°	1.5	1.5	2.0	17
Units	degrees	cm/s	cm/s	cm/s	n/a

Table 1.1: A summary of the model parameters used in AIM and Boxmix in this thesis

1.8 Aims and methodology

The objectives of the research presented in this thesis are;

i) to measure and understand the process of subduction as represented in an ocean general circulation model (GCM),

ii) to use the insight gained here to infer the nature of the process as it occurs in the North Atlantic,

iii) to examine the dependence of the permanent subduction rate and the ventilation pattern on the parametrised eddy fluxes of tracer and mass, and

iv) to examine the influence of inter-annual meteorological variability on the permanent subduction rate and the ventilation of the thermocline.

An outline of the experiments undertaken in Chapters Two-Six is given below.

[1] Note: the eddy viscosity and diffusivity parameters are given as viscous and diffusive 'velocities', to derive the eddy viscosities and diffusivities these 'velocities' are multiplied by the length of side of the local grid square. This gives viscosities and diffusivities which depend upon the local grid resolution.

The mixed layer parametrisation is systematically examined in Chapter 2 for the entrainment and detrainment phases of the mixed layer cycle with the SST, winter mixed layer depth and spring stratification taken as measures of the response. The problems of coupling a variable density mixed layer to an isopycnic thermocline are identified.

The application of one-dimensional models of the upper ocean to the examination of subduction is studied in Chapter 3. Lagrangian mixed layer simulations (after Woods & Barkmann, 1986a) are examined and found to diverge rapidly from the results of a fully-three dimensional GCM after one year. The appropriateness of the one-dimensional approximation made in these simulations and in other models (*e.g.* Marshall, *et al.*, 1993) is studied in the Atlantic Isopycnic Model (AIM) and in a simple geometry version of MICOM ('Boxmix') through buoyancy budgets of one-dimensional columns advected around the model ocean gyres. It is demonstrated that in AIM the one-dimensional approximation holds well in the regions of water mass formation. In Boxmix, however, the 'residual' terms that cannot be accommodated in a one-dimensional model are found to be significant.

In Chapter 4 the permanent subduction rate and the permanent subduction period in AIM are derived using particle trajectories. The subduction rates are compared to the results of tracer and kinematic studies for AIM. The tracer results are presumed to be the most accurate method and are taken as 'truth' for the study (the effects of vertical truncation are found to be minor in Chapter 5). The permanent subduction rate in AIM is then compared to the permanent subduction rate in the North Atlantic derived from various field measurements and other ocean models.

The role of eddies as means of transporting water from the seasonal thermocline into the permanent thermocline (Musgrave, 1990) is supported by the results presented in Chapter 5. The permanent subduction rate is found to be sensitively dependent on the isopycnic diffusivity. The influence of isopycnic layer thickness diffusion on the permanent subduction rate is found to be less significant over the parameter range explored. However, the thickness diffusion coefficient is found to control the definition

of soliton-like structures (Dewar, 1990) in the seasonal thermocline and their associated ventilation tongues.

In the sixth chapter the influence of inter-annual meteorological variability is examined in a simple experiment. It is found that the permanent subduction rates are reasonably stable to cooling events in the long term, but exhibit significant inter-annual variability. The dynamics of the permanent thermocline are found to be stable, contrary to the expectation described above. It is suggested that the anomalous potential vorticity signal generated by the change in the surface forcing conditions does not enter the permanent thermocline because the time scale for the advection of the anomaly through the seasonal thermocline into the permanent thermocline is longer than the scale imposed by the seasonal cycle. Thus the anomaly is removed by the mixed layer in the following winter.

The final chapter, Chapter 7, summarises the findings of the preceding five chapters and suggests work to extend the conclusions drawn. In particular, an exploration of the influence of thickness diffusion on the propagation of thermocline potential vorticity anomalies is suggested.

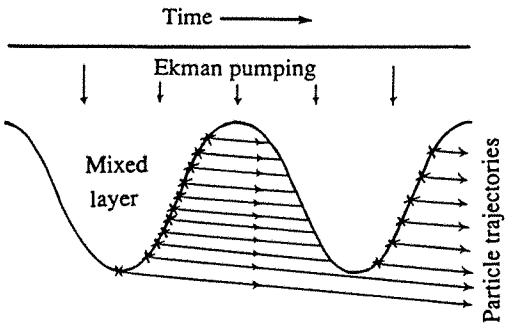

Figure 1.1: A schematic diagram of Stommel's 'Ekman demon'; it shows the mixed layer cycle over two years in a region of Ekman pumping. Particles are detrained from the mixed layer (at points x) and they are driven downwards by Ekman pumping. Only those particles that are detrained in late winter/early spring escape into the permanent thermocline over the year.

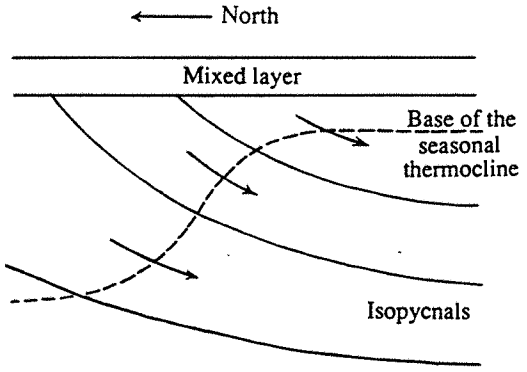

Figure 1.2: A schematic diagram of lateral induction; it shows an idealised meridional section through a subtropical gyre in summer. The dotted line indicates the base of the seasonal thermocline, that is the greatest depth to which the mixed layer descends over the annual cycle. The arrows indicate the sense of the total net flux of fluid in the thermocline.

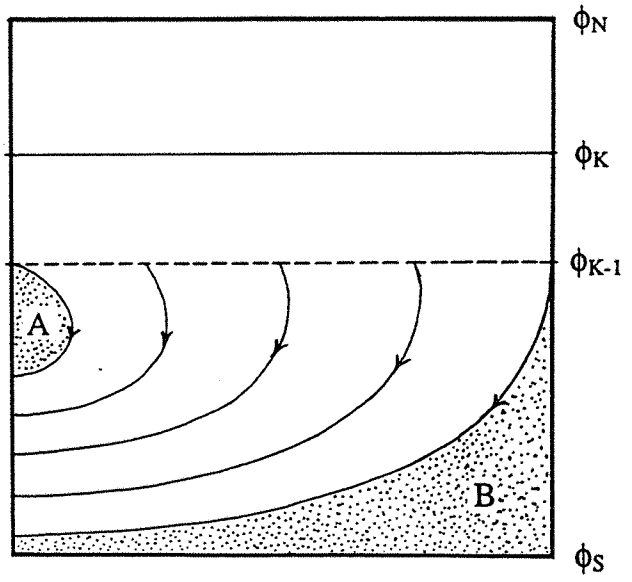

Figure 1.3: A schematic diagram of the circulation on an isopycnic layer in a basin where the western boundary current is not included. The layer outcrops between ϕ_{K-1} and ϕ_K. To the north of ϕ_K water of this density does not exist. To the south of ϕ_{K-1} this isopycnic layer is isolated from the surface forcing and geostrophic dynamics prevail. The trajectories of particles in the ventilated thermocline are illustrated by arrows. In the stippled region A the circulation is not defined by this model, this area is identified with the 'pool' zone of Rhines & Young (1982). The stippled region B is identified with the 'shadow' zone of Rhines & Young.

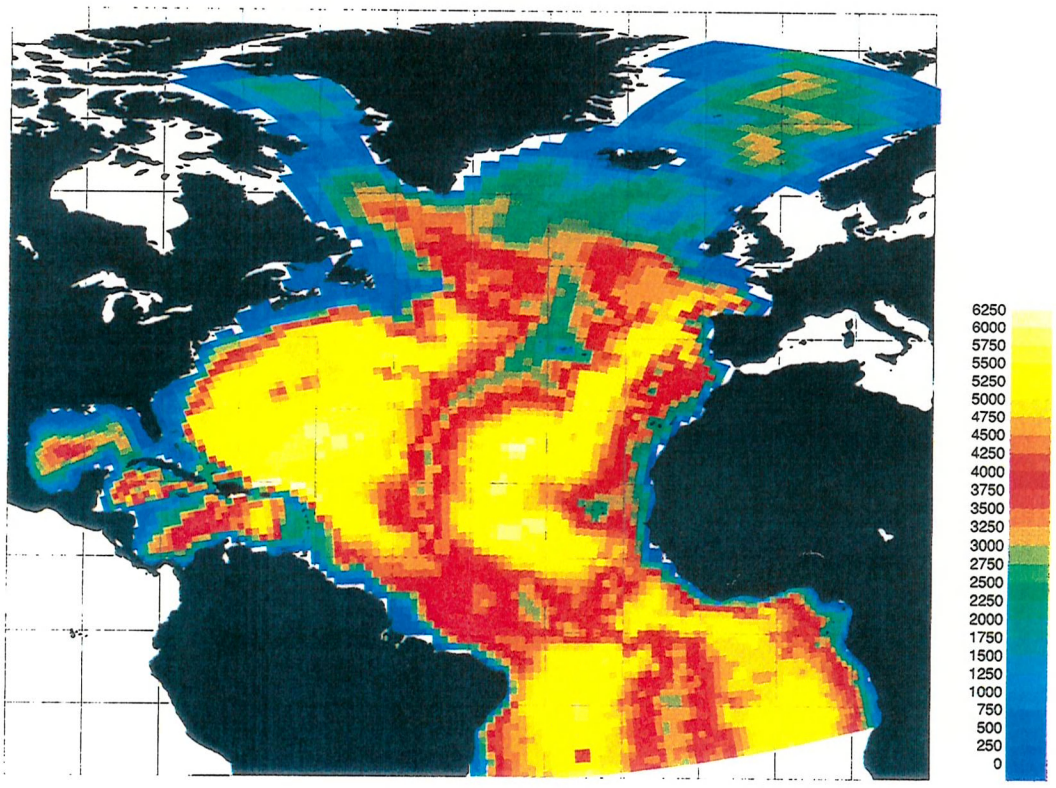

Figure 1.4: The bathymetry of the Atlantic Isopycnic Model (AIM) basin in metres. The depth of the ocean floor is plotted in the Mercator projection for each of the model grid boxes, clearly showing the distortion of the model grid relative to the standard Mercator projection. It will be noted that the plot includes the mid-Atlantic ridge system, the Greenland-Iceland-Scotland ridge and the rim of the Caribbean basin accurately but excludes the North Sea and the Mediterranean.

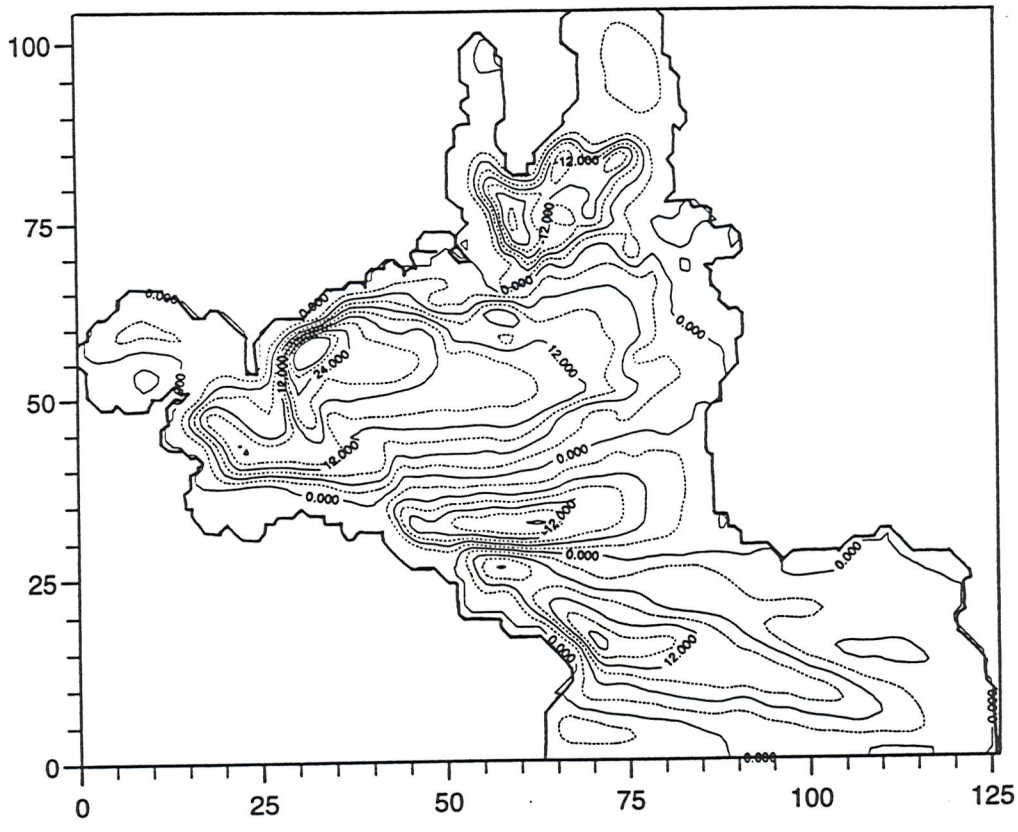

Figure 1.5: The barotropic streamfunction for the Atlantic Isopycnic Model (AIM) in September of year 30 of a standard spin-up. The streamfunction is plotted on the model's grid with the outline of the continents superimposed (compare with figure 1.4). The streamfunction is given in Sverdrups with contours at intervals of 3 Sverdrups and with a positive streamfunction value indicating anti-cyclonic circulation. From this plot it is clear that the AIM basin is divided between four gyres; the sub-polar and sub-tropical gyres, and a pair of tropical gyres either side of the Equator.

CHAPTER TWO

The sensitivity of the mixed layer to surface forcing and parametrisation

2.1 Introduction

The description of lateral induction given by Woods (1985), repeated in the previous chapter, emphasises the role of the mixed layer in the transfer of water and tracer species from the mixed layer to the thermocline. Before examining subduction in a fully three-dimensional general circulation model (GCM) it is first necessary to understand the mixed layer as represented by the mixed layer model. The GCM used in later chapters to examine subduction and ventilation is an isopycnic coordinate GCM developed by Bleck and others, called the Miami Isopycnic Coordinate Ocean Model (MICOM). This model has several implementations and is described in more detail in Appendix A. Most versions of MICOM employ a simple bulk mixed layer model of the type first developed by Kraus & Turner (1967) with certain modifications made to the detrainment algorithm to enable it to couple to an isopycnic thermocline.

In the following section a brief description of the Kraus-Turner mixed layer model will be presented. In the third section a series of simple parametrisation tests will be described. The studies are separated into two series, one to examine the entrainment phase of the mixed layer evolution and another to examine the detrainment phase. A description of the experiments and the results from the two series of studies will be presented separately; the entrainment studies are presented in section four and the detrainment phase studies are presented in section five. A sixth section will give a brief discussion of the results of these studies.

2.2 The Kraus-Turner mixed layer model

The mixed layer model used in MICOM is based on the model of Kraus & Turner (1967). Only a brief description is given here, a more detailed description of the model and a list of papers detailing the development of the model are given in Appendix B. The

Kraus-Turner mixed layer model is a 'slab' model, that is, it assumes *a priori* that a well-mixed layer exists at the surface of the ocean. This allows the properties of the layer to considered in bulk and simplifies the equations governing the evolution of the mixed layer. The turbulent kinetic energy is calculated from the surface wind stress and the input from convection. This input of energy is balanced by dissipation, which is assumed to be local to the point of generation, and through changes in the potential energy of the water column, *i.e.* through entrainment of underlying, heavier water masses.

During periods of mixed layer shallowing the mixed layer depth is determined by a complex set of criteria. In the limit of infinite-density resolution, the mixed layer model used in MICOM would give a mixed layer depth equal to the Monin-Obukhov length-scale (the depth at which the stirring influence of the wind is balanced by the restratifying influence of an influx of buoyancy into the ocean). However, the coupling of a finite resolution isopycnic thermocline to a variable density mixed layer requires that water detrained from the mixed layer to the thermocline should be of a limited number of density classes. To fulfil this requirement and to moderate the sea surface temperature changes the model reduces the rate at which the excess mixed layer water is detrained and redistributes the excess heat from the detrained water through the water column. This will be shown to have a significant influence on the stratification left by the mixed layer model in Spring.

2.3 Outline of the experiments

For the studies of the influence of surface forcing on permanent subduction and for the studies of the sensitivity of the model to the parameters used, a pair of idealised forcing functions were used. The heat flux was assumed to be sinusoidal, with an amplitude of 50W/m^2 and a zero net annual heat flux (positive upwards),

$$H_0 = 50\sin\left(2\pi\frac{\mathrm{DAY}}{360}\right)\mathrm{Wm}^{-2} \qquad \text{Eq.2.1}$$

The wind stress was given by,

$$\tau = 5 + 9e^{-5\sin^2\left(2\pi\frac{\mathrm{DAY}}{360}+0.1\right)}\mathrm{Nm}^{-2} \qquad \text{Eq.2.2}$$

The calendar is such that day 0 is the spring equinox and day 180 the autumnal equinox. These forcing functions are an approximation to the conditions thought to be prevalent at ~40°N in the North Atlantic, but the simulations presented here do not represent an attempt to accurately model the mixed layer at this location.

The neglect of the evaporation minus precipitation flux of fresh water (Q_o) is not significant for this study of the model. The Kraus-Turner model determines the mixed layer depth using the buoyancy flux rather than distinct heat and fresh water fluxes, thus the source of the buoyancy flux is not relevant. Furthermore, in the subtropical North Atlantic, the area of most interest for the study of subduction, the surface buoyancy flux is dominated by the heat fluxes; the fresh water flux takes a subsidiary role. A constant salinity of 35.0 $^{0}/_{00}$ was used.

The entrainment and detrainment regimes are examined separately in recognition of the differences in their mode of operation in the Kraus-Turner model. The brevity of the model runs (180 days for the entrainment experiments and 100 days for the detrainment experiments) means that the model has not entered a limit cycle, but is still adjusting to the initial stratification to the surface forcing. For the greater part of the ocean, circulation adjusts the thermocline structure so it is inappropriate to examine the mixed layer model behaviour in isolation beyond the period it takes to respond to one season. The two sets of experiments are described in the following sections.

2.4 The entrainment experiments

The standard initial conditions for the entrainment experiments consist of a 20m deep mixed layer with a temperature of 17°C. Below the mixed layer lies a seasonal thermocline with an arrangement of isopycnic layers giving a mean temperature gradient of 5×10^{-2} °C/m with a temperature of 17°C defined at the mixed layer base. The standard forcing functions are applied so that the runs began at mid-summer (day 180 of the model year described by the forcing functions) and are continued for 360 days (until day 540).

The two variables of most interest are the mid-winter values (day 360) of mixed layer temperature and depth. The standard values of the parameters n, m and H_w are taken to be 0.15, 0.8 and 50m respectively, these values are those used in the Boxmix version, Box1 of MICOM and they have been found to give a reasonable seasonal response. The isopycnic layers are set to the density values used in the Atlantic Isopycnic Model (AIM) for the standard run; these are increments of 0.15 (σ units) over nineteen isopycnic layers with the first isopycnic layer set to 25.65 (σ units).

For brevity the experiments conducted are summarised in Table 2.1.

Variable	Symbol	Units	Range	Wind stress	Heat flux	Stratification
Buoyancy-driven mixing efficiency	n	-	0.1-1.0	none	standard	standard
Wind-driven mixing efficiency	m	non-dim.	0.1-1.2	standard	none	standard
Wind mixing length scale	H_W	metres	10m-150m	standard	none	standard
Initial mixed layer temperature	T_i	°C	17-23 °C	standard	standard	standard
Initial mixed layer depth	H_i	metres	10m-100m	standard	standard	standard
Initial thermocline stratification	$\frac{\partial T}{\partial z}\|_{t=0}$	$°Cm^{-1}$	0.5-5.0 $x10^{-2}$	standard	standard	-
Model density resolution	$\Delta\sigma$	-	0.05-0.40	standard	standard	standard & weak ($0.5x10^{-2}$ $°Cm^{-1}$)
Surface heat flux	H_o	Wm^{-2}	10- 100	none	-	standard
Wind stress	τ	Nm^{-2}	0.02-0.3	-	none	standard
Ekman pumping	w_{Ek}	m/year	-50.0- 50.0	standard	standard	standard

Table 2.1: Summary of the entrainment experiments

For clarity, only one source of TKE was applied to the model where appropriate. Thus the heat flux is not applied when the wind mixing parametrisation is studied and the wind stress is not applied when the buoyancy-driven mixing parametrisation is studied.

2.4.1 The standard entrainment experiment

Results from the standard model run are shown in figures 2.1a and 2.1b. The standard model run produces a mixed layer depth of 109.1m and a mixed layer temperature of 14.03°C on day 360 (180th day of the run). Over the preceding period the mixed layer had eroded the upper ten isopycnic layers with sigma values of between 25.65 and 26.85, and had entrained the upper 2.8m of the σ=27.00 isopycnic layer. The mixed layer sigma value implied by the temperature is 26.21 giving a density jump at the mixed layer base greater than the density difference between isopycnic layers.

The rate of descent of the mixed layer base was greatest in the first five days of the run with a mean entrainment velocity of $3.81 \times 10^{-5} ms^{-1}$. The mean entrainment velocity fell to $5.72 \times 10^{-6} ms^{-1}$ between day 25 and day 50. A velocity of approximately $5 \times 10^{-6} ms^{-1}$ was then maintained by the model over days 230-330 to give a linear descent of the mixed layer base. Over the final thirty days of the 180 day period the mean entrainment velocity fell to $1.82 \times 10^{-6} ms^{-1}$ with a mean of $6.02 \times 10^{-7} ms^{-1}$ over the final five days.

The mixed layer temperature followed the broad pattern of the mixed layer depth. The most rapid fall in mixed layer temperature occurred over the first five days, but the rate of cooling continued to drop as the mixed layer deepened. However, over the interval between days 205 and 330 the deviation from the mean rate was slight when compared with the initial rate of cooling.

2.4.2 The sensitivity of entrainment to the parametrisation of mixing

The study of the influence of the buoyancy dissipation parameter, n, gave an approximately linear dependence of the spring mixed layer temperature (day 360) on n with slight deviations from the linear at n=0.7 and at n=0.1 (Fig.2.2). The spring mixed layer depth followed a shallow curve, the gradient of the variation of mixed layer depth with n flattened off for higher values of n.

The variation of the wind mixing parameter, m, showed the marked influence of m on both the mixed layer depth and the mixed layer temperature (Fig.2.3). An increased

wind-mixing efficiency deepened the mixed layer, and the water entrained lowered the mixed layer temperature. For higher values of m the gradient of mixed layer depth against m was shallower than for lower values of m. Similarly, the decrease in mixed layer temperature occurred more gradually at higher values of m. For the standard value, m=0.8, the mixed layer depth and temperature on day 360 appeared to be moderately sensitive to m.

The study of the variation of the wind-mixing length scale, H_w, produced a similar result to the study of the parameter m; for larger values of H_w the variation in mixed layer depth and temperature was less (Fig.2.4). For values close to the standard value, H_w, the mixed layer depth and temperature were sensitive to H_w.

2.4.3 The sensitivity of entrainment to the initial conditions

The study of the variation of the initial mixed layer depth showed that the mixed layer depth on day 360 does increase with the initial depth (Fig.2.5). However, the eventual spring maximum depth (day 360) increased by less than the increase in the initial depth; that is, as the initial layer thickness was increased, the amount of the underlying thermocline that was entrained was reduced, from 97.7m to 53.7m for initial depths of 10m and 100m respectively. Similarly, the mixed layer temperature on day 360 did not change as much for deeper initial mixed layers, the mixed layer temperature dropped by 3.38°C for an initial depth of 10m whereas it dropped by 1.29°C for an initial depth of 100m.

The effect of a higher mixed layer temperature was to reduce the spring mixed layer depth and raise the mid-winter mixed layer temperature (Fig.2.6). The results show an approximately linear response for both mid-winter temperature and depth.

The study of the influence of thermocline stratification on the spring mixed layer state showed that there was a marked influence on both mixed layer depth and temperature (Fig.2.7). The spring mixed layer depth was particularly sensitive to the stratification for very weak thermocline stratifications, the spring mixed layer depth increased rapidly for stratifications weaker than 1×10^{-2} °Cm^{-1}. The sensitivity of the spring mixed layer

temperature to the stratification was less pronounced but over the range of stratifications investigated still showed a variation of almost 2°C.

2.4.4 The sensitivity of entrainment to the resolution of the thermocline

The influence of the isopycnic resolution on the mixed layer on day 360 depended on the stratification of the thermocline (compare Fig.s 2.8 and 2.9). The more strongly stratified thermocline permitted less variation in mixed layer depth and temperature on day 360. The lower variation was especially so for finer resolutions ($\Delta\sigma$=0.05,0.075 & 0.1). The mixed layer temperature showed less variation than the mixed layer depth with resolution.

2.4.5 The sensitivity of entrainment to surface heating

The rate of heat loss at the surface was found to strongly control the spring mixed layer depth and temperature (Fig.2.10). With increasing heat loss the mixed layer becomes both deeper and cooler. Mixed layer depth and temperature display shallow curves when plotted against heat loss; the gradients of the mixed layer depth and temperature curves with heat flux are reduced for stronger surface cooler.

2.4.6 The sensitivity of entrainment to wind stress

The spring mixed layer depth and temperature are most sensitive to the magnitude of the wind stress for lower values of the wind stress (Fig.2.11). For greater wind stresses, the spring mixed layer is deeper and cooler but the depth and temperature of the mixed layer becomes less sensitive to the magnitude of the wind stress.

2.4.7 The sensitivity of entrainment to Ekman pumping

Ekman pumping (w_{EK}<0) increases the spring mixed layer depth and increases the temperature of the mid-winter mixed layer, while Ekman suction (w_{EK}>0) reduces the spring mixed layer depth and temperature (Fig.2.12). The gradients of both spring mixed layer temperature and depth are approximately linear about the zero Ekman velocity. There does not appear to be an asymmetry between Ekman suction and Ekman pumping.

2.4.8 Conclusion

The entrainment experiments have shown that the mixed layer depth and temperature observed after a 180 day model run depend on most of the parameters used and on most of the conditions imposed. A deeper, cooler spring mixed layer (day 360) will be brought about by increasing the parameters n, m or H_w, or increasing the surface heat flux, the wind stress or the density increments between the isopycnic layers. An increase in the initial mixed layer temperature will bring about a warmer, shallower spring mixed layer. Increased Ekman pumping and a deeper mid-summer mixed layer both bring about deeper, warmer spring mixed layers, whereas an increase in the thermocline stratification causes a shallower, cooler spring mixed layer.

The results summarised above can be understood from the consideration of the equation governing the depth of the mixed layer during entrainment. A re-arrangement of equation B.12 gives a rate of mixed layer deepening,

$$\frac{\partial h_1}{\partial t} = \frac{2E}{h_1(\rho_2 - \rho_1)}, \qquad \text{Eq.2.3}$$

where E is the total tubulent kinetic energy input into the mixed layer. The depth and density of the mixed layer are respectively h_1 and ρ_1, while the density of the underlying layer is ρ_2. Equation 2.3 illustrates that for steady forcing the rate of mixed layer deepening will decrease as the model run progresses. This is the result of the combined effects of the deeper mixed layer (it involves more energy to raise the thermocline water) and the increase in the value of ρ_2 with depth (the water being raised is denser). The increase in thermocline density with depth is partly offset by the cooling of the mixed layer through the entrainment of cooler underlying waters and through the surface heat loss. This can be observed in stratification versus time plots where the initial isopycnic layers thicknesses are large; the rate of entrainment from a particular isopycnic layer increases with time as the mixed layer cools and its density approaches that of the underlying layer. The strong thermocline at the mixed layer base in the standard entrainment run indicates, however, that this buoyancy loss during mixed layer deepening is not usually sufficient to offset the thermocline density gradient.

The values of the mixing parameters n and m influence the mixed layer by controlling the fraction of the TKE available for entrainment. In this way an increase in the value of these parameters is analogous to an increase in the surface forcing functions; more energy is available resulting in a deeper mixed layer. The exponential component of the parameter m means that the amount of wind-generated TKE available for entrainment will be reduced, making the rate of entrainment more dependent on buoyancy-driven mixing. It will be noted, however, that for the model runs used here the mixed layer depth and temperature on day 360 still have a dependence on the wind stress.

The presence of a density jump at the mixed layer will result in a shallower and warmer mixed layer because the mixed layer entrainment rate will be reduced (ρ_2-ρ_1 will be greater) thus the cooling of the mixed layer through entrainment will be less, and although the heat loss through the surface is drawn from a shallower depth, the higher initial temperature will still result in a warmer mixed layer. A deeper summer mixed layer, however, will result in a warmer spring mixed layer through the increased bulk of the mixed layer; the mixed layer density will not drop as quickly for the same rates of entrainment and heat loss. Additionally, the mixed layer is initially deeper so the initial rate of entrainment will be lower. The mean rate of entrainment over the the run will be lower since the density jump at the mixed layer base will not drop as rapidly.

The thermocline stratification further illustrates the controlling influence of the density jump at the mixed layer base. For weaker stratifications the mixed layer density, ρ_1, approaches the density of the underlying layer as it cools. This increases the rate at which water is entrained from that layer and so the eventual depth of the mixed layer will be greater. The spring mixed layer temperature, however, will be higher because the deeper mixed layer reduces the rate at which the mixed layer temperature drops and because the average temperature of the layers from which the mixed layer entrains is greater. A similar result is found with reduced isopycnic resolution; lower resolution results in thick isopycnic layers, especially in a weakly stratified thermocline.

The Ekman pumping results in a deeper and warmer spring mixed layer since the mixed layer is deepened with no change in its temperature. The greater depth reduces the rate

at which the mixed layer cools and maintains a greater density jump at the mixed layer base. This in turn results in less of the thermocline being entrained, but this reduction in entrainment rate is offset by the Ekman pumping. Similarly, Ekman suction increases the entrainment rate by reducing the depth of the mixed layer, thereby increasing the rate of mixed layer cooling. However, the increased entrainment rate is offset by the action of Ekman suction which results in a shallower mixed layer. It should be borne in mind that the Ekman drift currents implied by the Ekman pumping velocities are assumed to be bearing waters of exactly the same temperature as the mixed layer at all times, that is there was no temperature change associated with the Ekman drift.

2.5 The detrainment experiments

The initial conditions chosen as standard for the detrainment regime experiments consist of a 400m deep mixed layer with a temperature of 10°C. These conditions are considered a reasonable approximation to the conditions prevalent in the Atlantic at 40°N in late-winter/spring. The thermocline stratification below the mixed layer was set to $5x10^{-3}$ $°Cm^{-1}$, but it should be noted the interior stratification is irrelevant to the process of re-stratification.

The standard surface heat flux and wind stress functions given above (Section 2.3) were used to force the model for 100 days starting at day 0 (spring equinox); one hundred days was found to be enough time for the mixed layer to recede completely under most conditions. In studying the re-stratification, the variables of most interest are the densities of the isopycnic layers on to which the mixed layer detrains and the quantity of water that the mixed layer places on each layer: these are sampled on day 100 of the run. The formulation of the Kraus-Turner mixed layer model used with an isopycnic thermocline requires that for detrainment to occur there must be an input of buoyancy into the ocean. Therefore, when the influence of the parametrisation of wind-driven mixing was examined, the standard heat flux was applied.

The standard values of m and H_w were taken to be 0.8 and 50m as above. However, the value of n during detrainment is defined to be 1.0 in the Kraus-Turner model, this was

not altered. The isopycnic layers were set to the values used in AIM: increments of 0.15 (σ units) with the first layer set to 25.65 (σ units).

For brevity the experiments conducted are summarised in Table 2.2, below.

Variable	Symbol	Units	Range	Wind stress	Heat flux
Wind-mixing efficiency	m	non-dim.	0.1-1.2	standard	standard
Wind mixing length-scale	H_W	metres	10-150	standard	standard
Initial mixed layer temperature	T_i	°C	9.8-10.7	standard	standard
Initial mixed layer depth	H_i	metres	50-600	standard	standard
Model density resolution	$\Delta\sigma$	non-dim.	0.05-0.4	standard	standard
Surface heat flux	H_o	Wm^{-2}	-10- -100	none	-
Wind stress	τ	Nm^{-2}	0.02-0.3	-	standard
Ekman pumping	w_{Ek}	m/year	-50- 50	standard	standard

Table 2.2: Summary of the detrainment experiments

For all experiments other than that studying the influence of the surface heat flux the standard heat flux is employed; a net heat gain is necessary to bring about detrainment. The heat fluxes and wind stresses used in their respective studies are steady for the duration of the model run with the other forcing function taking its standard value. For the study of the influence of the initial mixed layer temperature the range of values is that necessary to span the density difference between two bracketing isopycnic layer densities; the temperature of the mixed layer relative to the isopycnic resolution is of greater importance than the absolute temperature.

2.5.1 The standard detrainment experiment

The mixed layer shallowed from the initial depth of 400m to 22.9m over the first 50 days of the standard run, while the mixed layer temperature rose from 10°C to 10.92°C (Fig.2.13). The detrained water was divided between two isopycnic layers; σ=26.85 and σ=27.00. The σ=27.00 layer inflated first receiving the water detrained over the first 40 days of the run; after this period water was detrained into the σ=26.85 isopycnic layer. By day 65 a very small amount of water was being detrained into the σ=26.70 isopycnic layer as the mixed layer approached the 20m mixed layer depth limit.

Over the main detrainment period, days 0-50, the rate of detrainment showed a remarkable degree of variation from the mean value over the same period. The mixed layer depth and temperature are plotted in figure 2.13 and five day averages of the detrainment rate are plotted in figure 2.14 These show that for the first two days of the detrainment period the mixed layer depth did not change. The mixed layer begins to detrain very suddenly on the third day of the run and the rate of detrainment continues to increase until day 10. Over the interval day 5 to day 10 the mean detrainment rate reaches $1.64 \times 10^{-4} ms^{-1}$. After day 10 the detrainment rate begins to drop rapidly at first, becoming more gradual for shallower mixed layer depths. On day 40 the mixed layer shallows very suddenly, detraining 51.4m into the σ=26.85 isopycnic layer in one day. This corresponds to a detrainment rate of $5.95 \times 10^{-4} ms^{-1}$. After this peak the five-day mean detrainment rate returns to the general trend observed before day 40; the detrainment rate becomes insignificant by day 60.

The five day mean rate of mixed layer temperature rise shows that over the first 40 days of the detrainment period the rate rises in a roughly linear manner from 2.6×10^{-3} °C/day to 3.34×10^{-2} °C/day. This implies an approximate t^2 relation for the mixed layer temperature. The deviations from this linear increase in the five-day mean rate of mixed layer temperature rise occur during the interval days 20-25 and days 40-45.

2.5.2 The sensitivity of detrainment to wind mixing parametrisation

The variation of the wind-mixing parameter m showed a weak dependence of the spring stratification on m (Fig.2.15). For values of m in the range 0.0-0.8 the mixed layer was

deepened by only 0.1m. The σ=26.85 isopycnic layer lost 0.4m of which 0.3m were lost to the σ=26.70 isopycnic layer. For values of m above 0.8 the mixed layer depth increased with a corresponding reduction in the depth of the σ=26.85 isopycnic layer. The σ=26.70 isopycnic layer was thickest for m=1.0 (2.6m), for values of m above 1.0 this isopycnic layer also became thinner. The σ=27.00 isopycnic layer remained the same thickness over the range of m examined.

The variation of the wind-mixing length scale, H_w, showed (Fig.2.16) that for values of H_w below 90m the variation in the mixed layer depth and in the thickness of the σ=26.85 isopycnic layer is slight; less than 0.5m for the mixed layer and 3.4m for the σ=26.85 isopycnic layer. For longer scale lengths the mixed layer becomes marginally deeper, reaching 23.4m for H_w=150m, while the σ=26.85 isopycnic layer becomes slightly thinner for values of H_w in the range 100m-130m, but thickens again for H_w>130m. The σ=27.00 isopycnic layer remains unchanged for H_w<100m, but becomes slightly thinner for longer scale lengths reaching a thickness of 315.5m for H_w=150m.

2.5.3 The sensitivity of detrainment to the initial conditions

The initial mixed layer temperature was found to have a significant effect on the post-detrainment stratification (Fig.2.17). The initial temperatures spanned the temperature difference between the σ=26.85 and σ=27.00 layers. Over this interval the variation of the thickness of both the σ=26.85 and σ=27.00 layers changed linearly, as the initial temperature was raised more water was detrained into σ=26.85 while less was detrained into σ=27.00. The increase and decrease in the layer thicknesses were complimentary. No significant change was observed in the mixed layer depth.

The initial mixed layer depth had a significant influence on the quantity of σ=26.85 and σ=27.00 water produced (Fig.2.18). The post-detrainment stratification showed a linear increase in the thickness of both of these isopycnic layers. The mixed layer depth remained approximately unchanged.

2.5.4 The sensitivity of detrainment to the resolution of the thermocline

The variation in the increments between isopycnic layers showed that the bulk of the detrained water was received by the two isopycnic layers with sigma values that bracketed the initial mixed layer value of σ=26.97. Isopycnic layers lighter than the bracketing pair received detrained water when the sigma increments between layers was fine but the amount of water detrained on to these upper layers was much less than the quantity detrained over the whole detrainment period. The results are summarised in Table 2.3 (below), where a particular layer was not present for the given resolution a dash (-) is given.

Layer density	$\Delta\sigma$ 0.05	$\Delta\sigma$ 0.075	$\Delta\sigma$ 0.15	$\Delta\sigma$ 0.3	$\Delta\sigma$ 0.4
26.70	-	-	-	**31.0**	**121.8**
26.85	2.2	3.77	**59.5**	-	-
26.90	7.1	-	-	-	-
26.92	-	**115.1**	-	-	-
26.95	**168.1**	-	-	-	-
27.00	**199.1**	**258.0**	**317.9**	**348.0**	-
27.10	-	-		-	**256.7**

Table 2.3: Summary of the thickness of isopycnic layers in metres after restratification

2.5.5 The sensitivity of detrainment to the surface heat flux

The surface forcing imposed on the model during the detrainment period was found to have no discernible influence on the eventual stratification for heat fluxes above 40Wm^{-2} (Fig.2.19). However, the greater heat fluxes did reduce the time taken for re-stratification to occur; for heat fluxes below 40Wm^{-2} the re-stratification took up to 75 days (H_o=10Wm^{-2}). The inclusion of a wind stress during the model runs also meant that the spring equilibrium mixed layer depth became deeper as the surface heat flux became weaker reaching a depth of 64.0m for a flux of 10Wm^{-2}. The deepening of the mixed layer was met with a corresponding reduction in the thickness of the σ=26.85 isopycnic layer; for a flux of 10Wm^{-2} the thickness of this layer fell to 18.5m. The σ=27.00 isopycnic layer remained unchanged over the range of heat fluxes examined.

2.5.6 The sensitivity of detrainment to the wind stress

The examination of the influence of the wind stress on the post-detrainment stratification showed that for wind stresses below $0.06Nm^{-2}$ the mixed layer depth and thermocline stratification remained largely unchanged (Fig.2.20). The mixed layer became deeper for wind stresses above $0.06Nm^{-2}$ reducing the thickness of the σ=26.85 layer. For wind stress slightly higher than $0.06Nm^{-2}$ the σ=26.70 isopycnic layer received up to 3.1m of detrained water. However, as the wind stress was increased further this layer received less water. The σ=27.00 isopycnic layer remained unchanged for wind stresses below $0.1Nm^{-2}$, above this value the layer thickness began to be reduced.

2.5.7 The sensitivity of detrainment to Ekman pumping

The influence of Ekman pumping was found to be slight over the detrainment period. The mixed layer depth on day 50 did appear to deepen with increased Ekman pumping and to shallow with Ekman suction. The same general trend was observed for both the σ=26.85 and σ=27.00 isopycnic layers.

Layer density	25.0 m/year	0 m/year	-25 m/year	-50m/year
Mixed layer	22.8	22.9	23.3	23.6
26.85	57.4	59.2	60.8	62.5
27.00	316.7	318.2	319.7	321.2

Table 2.4: Layer thickness in metres after restratification with various constant Ekman pumping velocities

2.5.8 Conclusion

The detrainment experiments have shown that the stratification of the spring thermocline is insensitive to the value of the wind parameters and, over a broad range of values, on the magnitude of the wind stress. The surface heat flux does not appear to control the stratification of the deep thermocline other than by determining the length of the detrainment period. Weak heat fluxes in spring can influence the stratification of the upper thermocline if the heat flux is not sufficient to lower the Monin-Obukhov length scale to less than 20m, the minimum mixed layer depth.

The most important determinants of the stratification of the spring thermocline appear to be the state of the mixed layer at the start of detrainment and, to a lesser degree, the resolution of the model isopycnic layers. Of especial interest is the tendency of the model to place the bulk of the detrained water on two isopycnic layers. The layers selected depend on the initial mixed layer density and are the isopycnic layers which have densities that bracket the initial mixed layer density. The initial mixed layer depth simply determines the quantity of water that is detrained into each layer. The proportion of the detrained water placed in each isopycnic layer is controlled by the initial density of the mixed layer. The water will be divided in a proportion that will preserve the heat content of the total quantity of detrained water.

An increase in the resolution of the model isopycnic layers will result in a less stratified thermocline; there will be less of a density difference between the layers selected to receive the detrained water. If the resolution of the isopycnic layers is made fine enough then the detrainment algorithm will cease to divide the water between two layers and give more structure to the thermocline. However the resolution necessary to do this must be able to resolve changes in the mixed layer density over the very brief detrainment period and, as the above results show, this resolution is far higher than those which have been examined here.

From the time series of the thermocline stratification it will be seen that the rate of detrainment varies considerably throughout the detrainment period. It is of particular interest that the rate of detrainment peaks briefly as the mixed layer temperature reaches the value of the upper-most of the two layers selected to receive the detrained water (for the preceding thirty days the rate of detrainment decreased). This is due to the dependence of the detrainment algorithm on the surface heat flux and the mixed layer density.

The surface heat flux determines the Monin-Obukhov length scale; greater surface heating will result in a smaller length scale. This length scale together with the surface heat flux then determine the maximum permissible mixed layer temperature. For a continuous thermocline the mixed layer depth compatible with this maximum

temperature would have a depth equal to the Monin-Obukhov length scale. However in an isopycnic model the finite resolution of the thermocline and the condition that the model conserves heat require an additional heat flux into the mixed layer from the detrained fluid. This internal heat flux is greater for the same detrainment rate if the density difference between the first hydrostatically stable layer and the mixed layer is large. As the mixed layer temperature shallows and heats, therefore, the detrainment rate will drop. Once the mixed layer density has risen above the density of the next isopycnic layer that layer will receive the detrained water. The slight density difference between the mixed layer and the thermocline at this moment permits a rapid detrainment of the excess mixed layer water, manifesting itself as a sudden peak in the detrainment rate.

The conservation of the original heat content by the detrained fluid arises naturally out of the detrainment algorithm. Below the base of the Monin-Obukhov layer all heating is due to the internal heat flux and therefore is only a re-adjustment of the heat content of the detrained water. Over most of the detrainment period the internal heat flux is much larger than the surface heat flux so the variation in the Monin-Obukhov depth will have only a slight heating influence on the thermocline.

The stratification produced by the detrainment algorithm will be artificially high because of the conservation of heat during detrainment. The interface between the two isopycnic layers inflated by detrainment must be deeper than the Monin-Obukhov length; the mixed layer depth is greater than the Monin-Obukhov length when the mixed layer reaches the temperature of the upper isopycnic layer, thus the upper layer is inflated from deeper in the water column. This problem is reduced as the isopycnic resolution increases, but will only be resolved if the isopycnic resolution is fine enough to allow the mixed layer depth to follow the Monin-Obukhov length scale. This can only occur if the isopycnic layers resolve the mixed layer density changes between successive time steps during the detrainment phase which for the standard detrainment run is of the order of 0.01 sigma-units or less.

2.6 Summary

The above results have shown that in the Kraus-Turner model developed for an isopycnic thermocline the spring stratification depends on the mixed layer conditions at the start of the detrainment period. The surface forcing appears to have no influence, contrary to the theoretical work by Williams(1989). Thus the influence of surface forcing on the thermocline circulation, studied later in this thesis, can only occur through changes in the mixed layer depth and density before the start of the detrainment phase. This finding is a result of the model formulation; the requirement that the model conserves heat during detrainment leads to a re-distribution of heat within the water column and it is this redistribution that dominates the thermocline structure. The effect can be removed by increasing the resolution of the isopycnic layers to capture the density changes that occur during detrainment. However, the resolution required is too high to be feasible in a GCM. In examining the mixed layer response in an isopycnic GCM, therefore, one must be aware that the potential vorticity of the fluid entering the permanent thermocline will generally be higher in a low density-resolution isopycnic GCM than would be expected from a mixed layer behaving as the Monin-Obukhov equation predicts. The isopycnic surfaces in the seasonal thermocline immediately after the spring detrainment will be tilted over to a far greater extent that would be expected to occur in a continuous fluid. The influence of surface forcing, examined later in this thesis, cannot occur through the mechanism proposed by Williams (1991) but can only be conveyed through changes in the mixed layer depth and density fields at the start of the detrainment phase.

The conditions at the start of detrainment have been shown to be under a complex set of influences. The stratification underneath the mixed layer and the mid-summer mixed layer depth and temperature influence the winter mixed layer and are themselves influenced by the previous winter mixed layer. Wind forcing has a greater influence for shallower mixed layers and so its influence will be stronger in summer and early autumn.

Figure 2.1: (a) A time series of the mixed layer temperature during the 360 days of its run for the standard entrainment run. The abscissa is the day of the run, the starting time (first day of the run) is day 180 of the model year.

(b) A time series of the stratification of the mixed layer model over the same period as (a). The uppermost layer is the mixed layer beneath which lie the isopycnic layers of the thermocline.

The arrow indicates the time at which the mixed layer depth and temperature were measured.

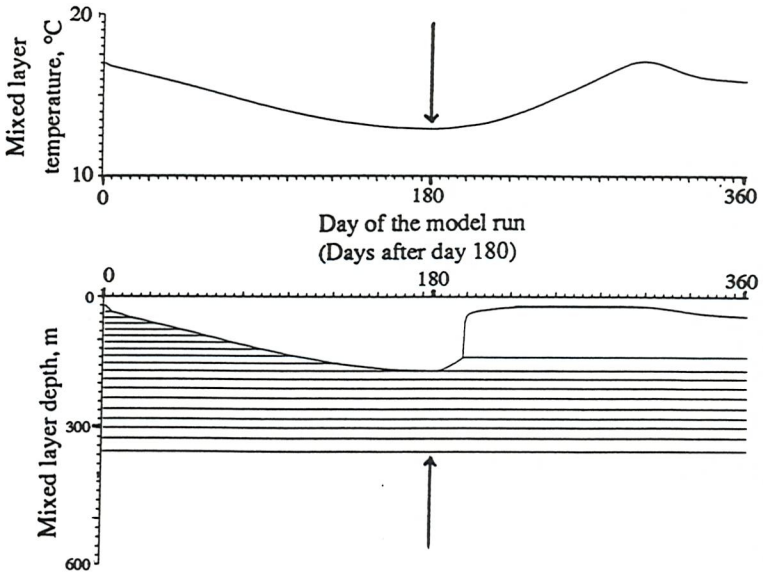

Figure 2.2: A graph showing the variation in the mixed layer depth and temperature on the 180th day of the entrainment run (day 360 of the model year) for various values of the buoyancy - driven mixing parameter, n.

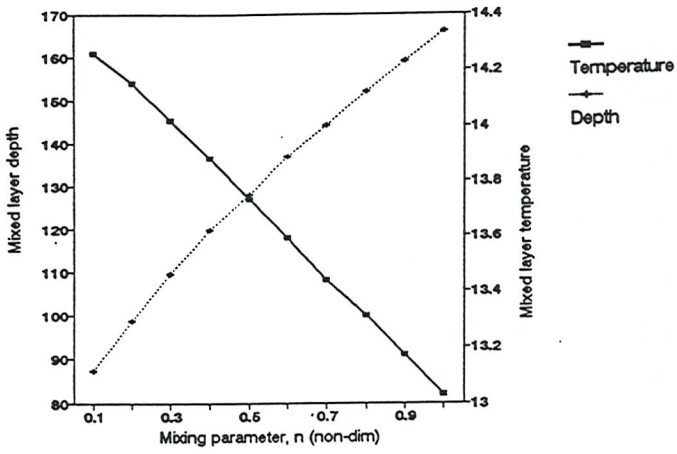

Figure 2.3: A graph showing the variation in the mixed layer depth and temperature on the 180th day of the entrainment run (day 360 of the model year) for various values of the wind - driven mixing parameter, m.

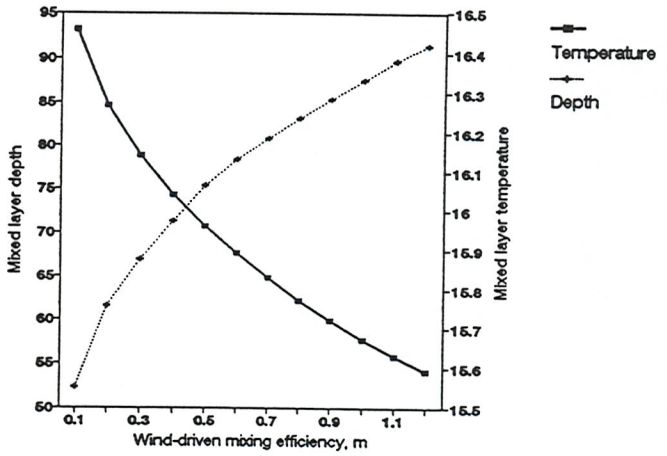

Figure 2.4: A graph showing the variation in the mixed layer depth and temperature on the 180th day of the entrainment run (day 360 of the model year) for various values of the wind - driven mixing length scale, H_W.

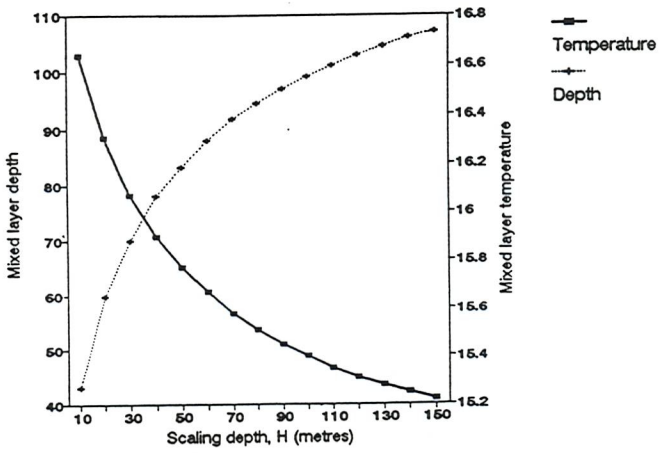

Figure 2.5: A graph showing the variation in the mixed layer depth and temperature on the 180th day of the entrainment run (day 360 of the model year) for various values of the initial mixed layer depth.

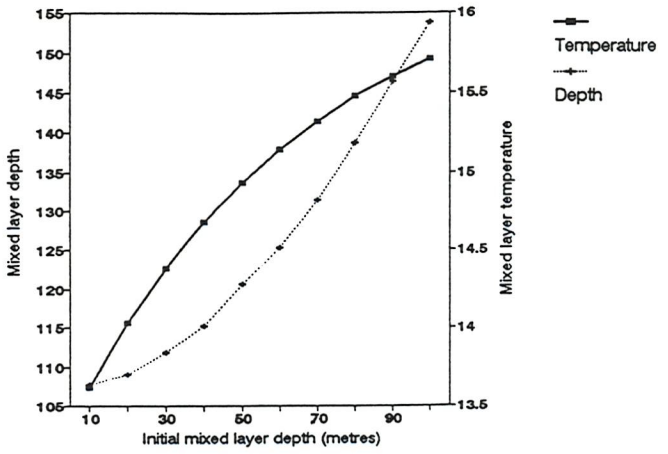

Figure 2.6: A graph showing the variation in the mixed layer depth and temperature on the 180th day of the entrainment run (day 360 of the model year) for various values of the initial mixed layer temperature.

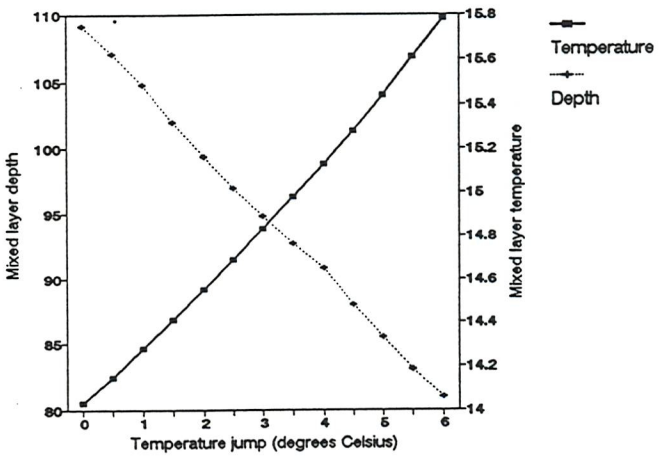

Figure 2.7: A graph showing the variation in the mixed layer depth and temperature on the 180th day of the entrainment run (day 360 of the model year) for various vales of the thermocline temperature gradient.

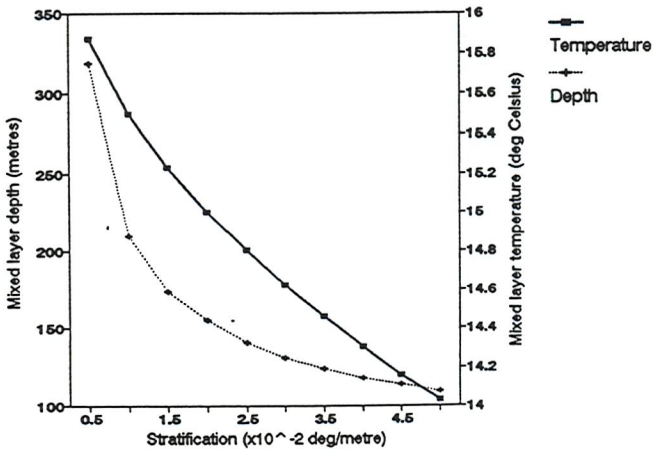

Figure 2.8: A graph showing the variation in the mixed layer depth and temperature on the 180th day of the entrainment run (day 360 of the model year) for various values of the density increments between isopycnic layers with a 'weak' thermocline stratification.

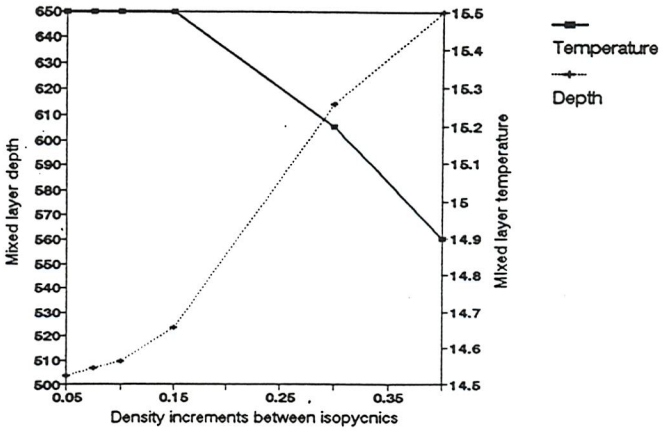

Figure 2.9: A graph showing the variation in the mixed layer depth and temperature on the 180th day of the entrainment run (day 360 of the model year) for various values of the density increments between isopycnic layers with a 'strong' thermocline stratification.

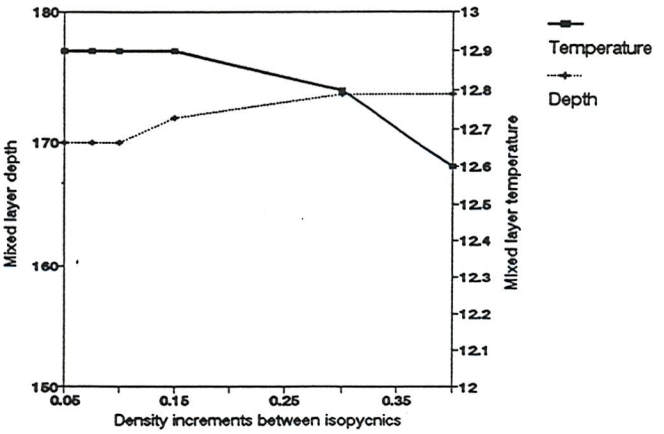

Figure 2.10: A graph showing the variation in the mixed layer depth and temperature on the 180th day of the entrainment run (day 360 of the model year) for various values of the constant surface heat flux (positive upwards).

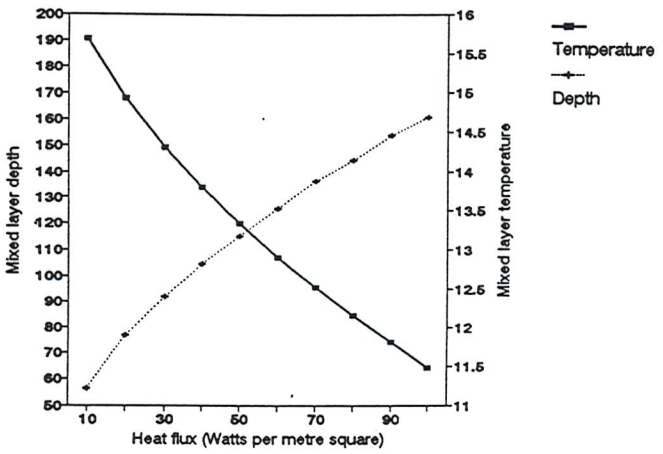

Figure 2.11: A graph showing the variation in the mixed layer depth and temperature on the 180th day of the entrainment run (day 360 of the model year) for various values of a constant wind stress.

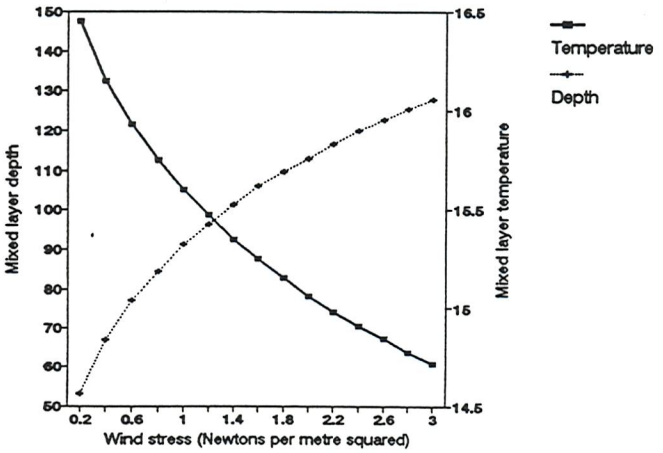

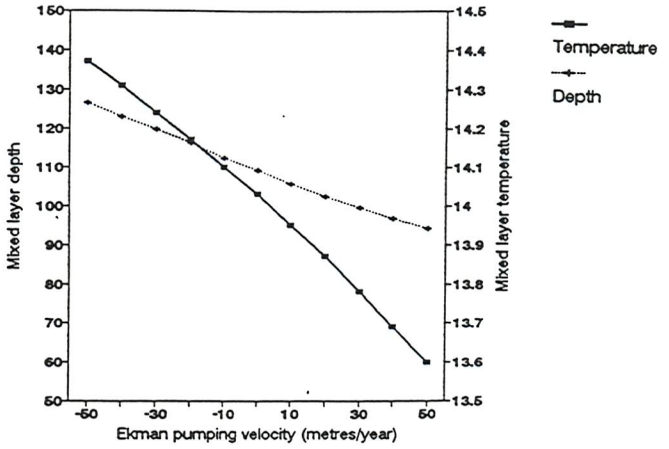

Figure 2.12: A graph showing the variation in the mixed layer depth and temperature on the 180th day of the entrainment run (day 360 of the model year) for various values of the Ekman pumping velocity (positive downwards).

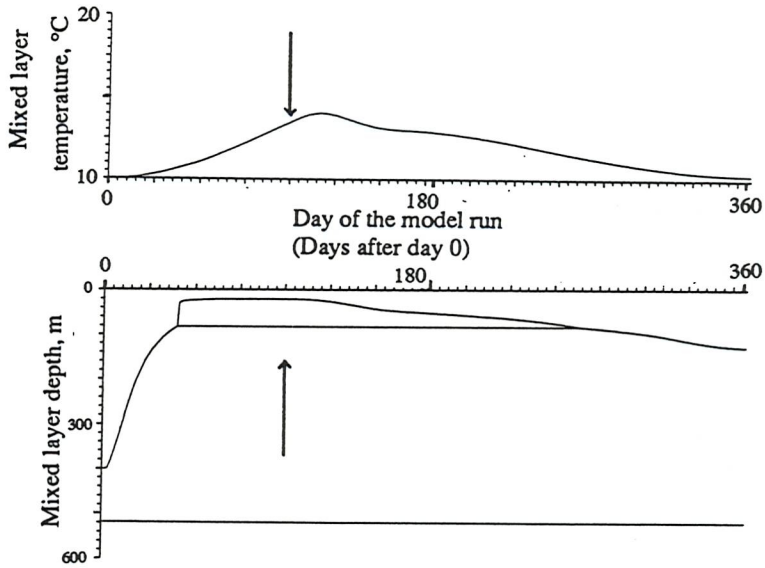

Figure 2.13: (a) A time series of the mixed layer temperature during the 360 days of its run for the standard detrainment run. The abscissa is the day of the run, the starting time (first day of the run) is day 0 of the model year.

(b) A time series of the stratification of the mixed layer model during the same period as (a). The upper-most layer is the mixed layer beneath which lie the isopycnic layers of the thermocline.

The arrow indicates the time at which the mixed layer depth and temperature were measured.

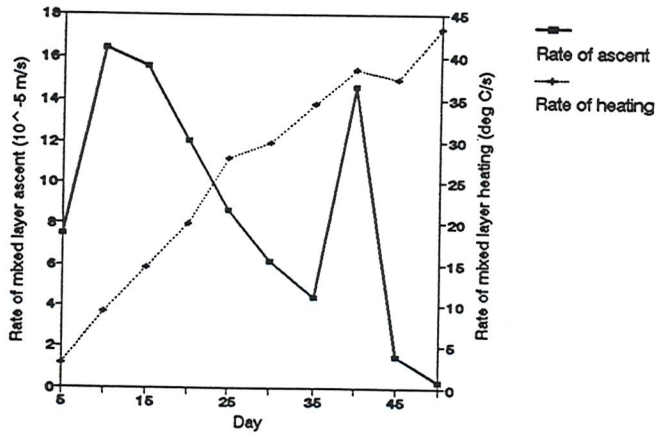

Figure 2.14: The five-day mean detrainment rate and rate of temperature change for the mixed layer during the standard detrainment run. Each value is plotted at the end of the five day period over which the mean was taken.

Figure 2.15: A graph showing the variation in the mixed layer depth and temperature on the 100th day of the detrainment run (day 100 of the model year) for various values of the wind - driven mixing parameter, m.

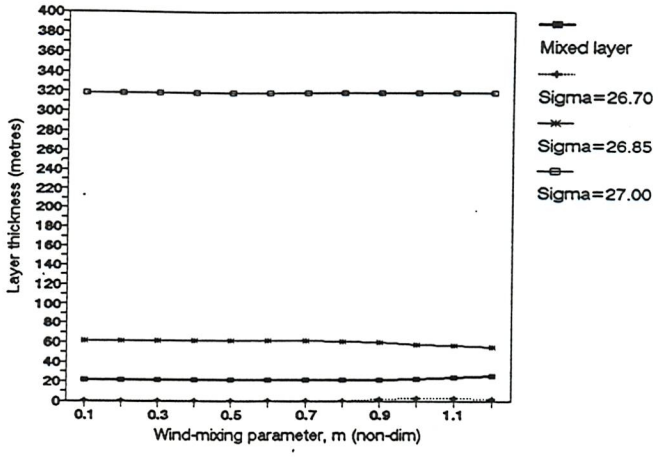

Figure 2.16: A graph showing the variation in the mixed layer depth and temperature on the 100th day of the detrainment run (day 100 of the model year) for various values of the wind - driven mixing length scale, H_W.

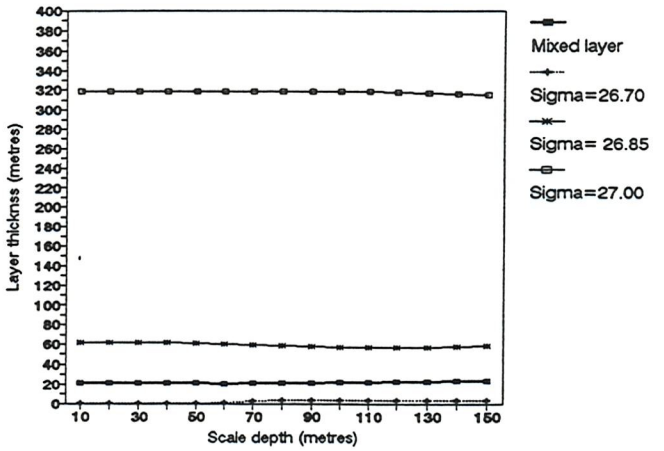

Figure 2.17: A graph showing the variation in the mixed layer depth and temperature on the 100th day of the detrainment run (day 100 of the model year) for various values of the initial mixed layer temperature.

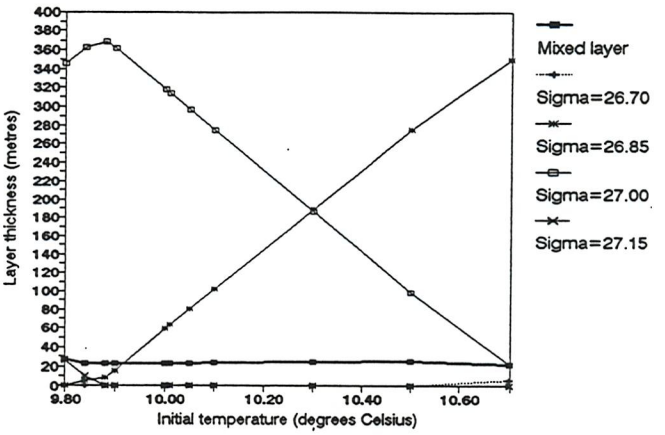

Figure 2.18: A graph showing the variation in the mixed layer depth and temperature on the 100th day of the detrainment run (day 100 of the model year) for various values of the initial mixed layer depth.

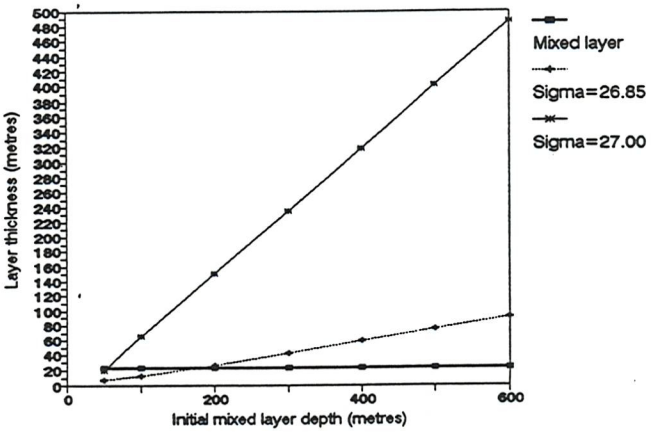

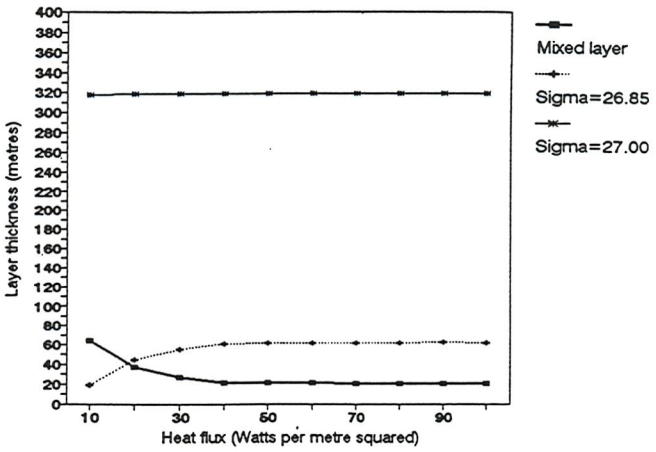

Figure 2.19: A graph showing the variation in the mixed layer depth and temperature on the 100th day of the detrainment run (day 100 of the model year) for various values of a constant surface heat fluxes (positive downward).

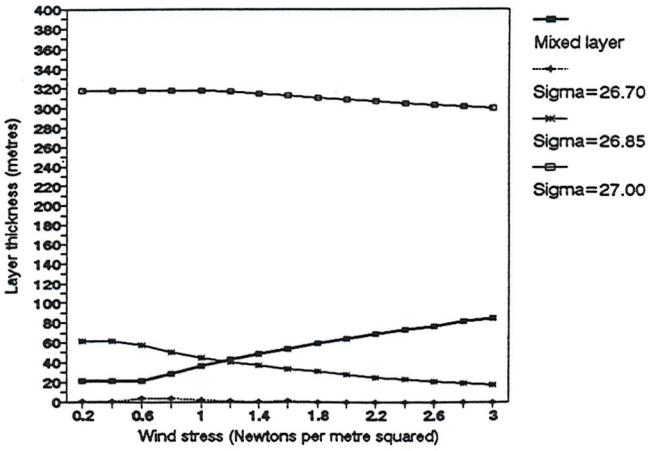

Figure 2.20: A graph showing the variation in the mixed layer depth and temperature on the 100th day of the detrainment run (day 100 of the model year) for various values of a constant surface wind stress.

CHAPTER THREE

Buoyancy budgets in an isopycnic ocean model

3.1 Introduction

The role of the mixed layer in permanent subduction in the North Atlantic has been emphasised by Stommel (1979), Cushmann-Roisin (1984) and Woods (1985). The seasonal variation in the depth of the mixed layer is the means by which the properties of the permanent thermocline are selected (the operation of the 'Ekman demon'), and it is the spatial variation in the depth of the mixed layer that produces lateral induction. This last process augments the contribution of Ekman pumping to the permanent subduction rates in the North Pacific (Huang, 1990), while in the North Atlantic it is thought to be the dominant process (Sarmiento, 1983b). In addition, the response of the mixed layer in spring determines the subsequent circulation in the thermocline of the subducted water masses through the potential vorticity left behind as it recedes (Williams, 1991).

The process of lateral induction combines the mixed layer seasonal cycle with the southward Sverdrup drift of the sub-tropical gyre. This drift affects the buoyancy at a stationary point which in turn plays an important role in the evolution of the upper layers of the ocean. It is therefore necessary for models of permanent subduction to combine the mixed layer cycle with advection. This can be done through the use of a fully three-dimensional ocean model, as presented in later chapters of this thesis, but simpler one-dimensional approaches have the advantage of clarity. This chapter aims to explore the validity of the one-dimensional approach to the examination of the upper thermocline and to examine the components of the buoyancy tendency in the upper thermocline in two versions of MICOM.

Where vertical shear in the thermocline is slight and the contributions of diffusive eddy processes to the evolution of the mixed layer and thermocline are minimal, a one-dimensional mixed layer model can be used to simulate the upper ocean. The mean velocities of a gyre are used to form trajectories and the surface forcing along each trajectory is interpolated to form a time series of heat and fresh water fluxes and wind

stresses. The one-dimensional mixed layer model can then be forced with these fluxes to simulate the evolution of the mixed layer and upper thermocline as a water column is advected southward over the zero net buoyancy flux line. This approach was first used by Woods & Barkmann (1986a).

The approach of Woods & Barkmann (referred to here as a Lagrangian mixed layer model) was used to simulate the evolution of a number of water columns as they were advected through the idealised domain of the Box1 general circulation model (GCM). A representative example of these experiments is presented in the following section. It will be demonstrated that the surface forcing alone does not reproduce the evolution of the GCM thermocline, taken as truth for these experiments. In the third section of this chapter a budget for the buoyancy changes observed in a Lagrangian upper thermocline water column will be presented and the problems of closing this budget will be discussed. In the fourth section a second approach to the buoyancy budget of a GCM will be undertaken and the results presented. In the final section the results of this chapter will be reviewed.

3.2 Lagrangian mixed layer simulations

In this section a Lagrangian mixed layer model is used to simulate the evolution of the upper thermocline and mixed layer. This one-dimensional mixed layer model is identical in many respects to the one-dimensional models examined in Chapter Two. However, rather than forcing the model with the annual cycle of surface forcing at one point in the basin the mixed layer model is forced using the forcing functions that would be encountered if the water column had been advected around the GCM basin. In this way the Lagrangian mixed layer model includes the effects of the advection of buoyancy. However, Lagrangian mixed layer simulations neglect certain processes; the horizontal diffusion of buoyancy in the mixed layer, vertical shear and the transport of mass by thickness diffusion.

3.2.1 The calculation of water column trajectories

The flow field for these experiments was generated by the simple geometry version of MICOM, Box1, which is described in Chapter One. From the model data sets, which are composed of velocity points arranged on the model's B-grid, a trajectory is constructed. This requires some method of converting the data sets into a spatially and temporally continuous field, and then solving the advection equation,

$$\frac{d}{dt}\mathbf{x}(t) = \mathbf{u}(\mathbf{x}(t), t) \qquad \text{Eq. 3.1}$$

The interpolation scheme used to create the continuous velocity fields is a simple linear scheme in both space and time. This scheme is more economical than higher order schemes. The benefits of using a higher order scheme for spatial interpolation are slight since the mixed layer model was found to be insensitive to the precise trajectory outside the western boundary current. The use of a higher order scheme for the temporal component would also be inappropriate since model forcing is constructed from a linear interpolation of monthly data sets. The B-grid staggers the velocity and mass points so the interpolation scheme uses two grids for the interpolation of velocity and the surface flux properties, each grid staggered appropriately.

The differential equation Eq. 3.1 is solved using a simple midpoint Runge-Kutta scheme. This involves two stages; the first is to establish a mid-time position; the second is to use the velocity at the mid-time position to advance the particle over the time step from its original position. To do this the velocity field is interpolated to the particle's original position ($\mathbf{x}_i$) to give the instantaneous velocity, $\mathbf{v}_i$. A simple Euler step is then taken to advance the particle half a time-step to a new, temporary position, $\mathbf{x}_{i+1/2}$ ($= \mathbf{x}_i + \mathbf{v}_i.\Delta t/2$). At this new position and time the velocity is interpolated to find a second displacement vector. This second vector is used to complete a whole step by moving the particle position from $\mathbf{x}_i$ to $\mathbf{x}_{i+1}$, where $\mathbf{x}_{i+1} = \mathbf{x}_i + (\mathbf{v}_{i+1/2}.\Delta t)$ and Δt is the length of the time step between iterations i and i+1.

The scheme was tested in a circular flow field and it was found that the trajectories generated by this combination of linear interpolation and Runge-Kutta advection scheme were accurate for the conditions encountered in the GCM basin for a time step of 1/30th

of a day. Further tests showed that in the main sub-tropical gyre trajectories of up to two years duration were reversible with the particle returning to a position much closer to the original position than the grid spacing could resolve (≤0.2 grid spaces, increasing in the western boundary current and its extension). This further validates the Runge-Kutta scheme. The use of linear interpolation in constructing the velocity field, however, cannot be validated, as will be discussed later in this chapter.

3.2.2 Description of the experiments

A number of trajectories were calculated for the sub-tropical gyre of the MICOM implementation, Box1 (see Chapter One). These trajectories start at the time of the maximum winter mixed layer depth and continue for two years. For each starting point two trajectories were calculated; one for a particle advected in the mixed layer using the total mixed layer velocities (i.e. including the Ekman drift velocity), and a second using the mean velocity (i.e. not including the thickness diffusion velocity) of the layer immediately beneath the mixed layer at the start of the trajectory. Examples of the trajectories over two years for particles advected in the mixed layer and on an interior isopycnic layer are given in figures 3.1a&b.

The surface forcing appropriate to these trajectories is then reconstructed in order to ensure that the one-dimensional mixed layer model receives the same forcing as a water mass advected along the trajectory in Box1. The wind stress and the radiative heat fluxes used by Box1 are analytic functions and so they are calculated directly from the particles' positions. The turbulent heat fluxes (latent and sensible) in Box1 are calculated from the model SST using an analytic air temperature. The SST for Box1 along the particles' trajectories are calculated from the data produced at 30 day intervals and linearly interpolated in both space and time to the particles' positions. The interpolated Box1 SST is then substituted for the mixed layer model's SST in the calculation of the turbulent heat flux along the trajectories.

The series of surface forcing functions are then used to drive a one-dimensional model of the mixed layer and thermocline. The mixed layer model is identical to that used by Box1 and the initial values of the isopycnic layer depths and the mixed layer temperature are

set at the Box1 values appropriate to the starting point and time of the trajectory. The mixed layer models are then run for two years.

The evolution of the model stratifications is compared to the stratification of Box1 along the same trajectory. This stratification is constructed using linear interpolation from the model data sets, reconstructing the Box1 stratification and the mixed layer temperature.

3.2.3 Results of the Lagrangian mixed layer simulations

The results (shown in figures 3.3a&b) for the mixed layer model forced with the surface forcing functions appropriate to mixed layer trajectories in the subtropical gyre indicate that the model successfully simulates the sea surface temperature in summer but in winter it is generally too cool (by ~1.5°C), especially on the northern rim of the subtropical gyre. This is through the shallower mixed layer developed by the mixed layer model in comparison to the GCM. An example of the stratification of the model Box1 (figures 3.2a&b) shows that over the first year of the trajectories there are marked changes in the stratification of the thermocline. As water columns are advected southward into the heart of the gyre isopycnic surfaces in the thermocline are seen to deepen. In the mixed layer model simulations (*e.g.* figure 3.3a&b) the stratification of the thermocline remains in its initial state. Thus in the mixed layer model simulation denser water is nearer the surface and this acts to prevent the creation of winter mixed layers as deep as those observed in the GCM. The shallower mixed layer is still cooled by the same surface heat flux and so the mixed layer model produces a cooler winter SST. The divergence between the results of the GCM and the one-dimensional mixed layer model arise from the strong southward Ekman drift in the mixed layer velocity fields. In the GCM the Ekman drift results in a strong shear at the base of the mixed layer which the one-dimensional model cannot simulate.

As outlined in the previous chapter, the detrainment process is sensitive to the winter mixed layer temperature. Thus the stratification of the seasonal thermocline in the mixed layer model simulations diverges rapidly from that of the GCM in the second year of the simulation. This would appear to represent a serious weakness in the intercomparison of

a mixed layer model and an isopycnic GCM, and limits the ability of a one-dimensional mixed layer model of this type to reproduce the GCM stratification to one year.

The mixed layer model simulations (see figure 3.5a&b for an example) using the trajectories in the thermocline were more successful at reproducing the thermocline stratification. It was found that the stratification of the GCM along trajectories in the thermocline varied much less than the stratification observed along the mixed layer trajectories (*e.g.* figure 3.4a&b). The thickness of the layer for which the trajectory was calculated was found to be largely constant, consistent with potential vorticity conservation. For shallower layers there is evidence of thinning of deep mode water layers produced by the spring detrainment, presumably through isopycnic thickness diffusion in the GCM.

The mixed layer temperatures produced by the mixed layer models remain slightly cooler than those from the GCM in winter, the slight differences in the stratification of the mixed layer models still influence the mixed layer temperature. Consequently, the second spring restratification produces a seasonal thermocline that does not necessarily correspond to that of the GCM.

3.2.4 Discussion of the results of the Lagrangian mixed layer simulation

The examples given above, together with the results of Chapter Two, indicate that the simulation of the evolution of the seasonal thermocline in an isopycnic model over periods of more than one year requires a much improved simulation of the late winter SST. This problem becomes more acute as the density resolution of the thermocline is increased. By following trajectories in the thermocline, the evolution of the thermocline is partly accounted for, but the mass convergence due to the Ekman drift would appear to make a significant contribution to the structure of the upper thermocline. Including this term in the mixed layer model should increase the accuracy of the mixed layer model simulation. The inclusion of the Ekman heat flux into the mixed layer was of limited importance in the example presented, but it is of greater importance in other regions of the basin and should also be included in the forcing terms.

3.3 A buoyancy budget for an ensemble of water columns in the Atlantic isopycnic Model

The results of the previous section for Lagrangian mixed layer models indicate that the divergence between the mixed layer model and the GCM increases as time progresses. The surface forcing used in the mixed layer simulation was identical to that found along the trajectory in the GCM within the bounds of the interpolation scheme, while the trajectory itself was calculated from the GCM velocity. The differences between the results of the two models arise from the processes that are not represented in the Lagrangian mixed layer model. The differences are also magnified by the spring restratification through the sensitivity of the spring stratification to the mixed layer state at the start of detrainment (see Chapter Two). The features which cannot easily be incorporated into a one-dimensional model are thickness diffusion, shear motions, and the diffusion of buoyancy into the water column in the mixed layer. The buoyancy fluxes due to the Ekman drift and pumping terms, however, have been incorporated into a one-dimensional model of the thermocline (Marshall, Nurser & Williams, 1993). The validity of a Lagrangian approach will, therefore, depend upon the net contribution of the excluded processes to the evolution of the mixed layer and the thermocline compared to the barotropic advection of the water column and the surface forcing.

To evaluate the contribution of the above fluxes to the evolution of the upper ocean it is necessary to have some measure of their relative influence. The thermocline stratification and the state of the mixed layer are indicated by the buoyancy content of the water column, and the processes listed above will all influence the buoyancy content of the water column. The relative importance of these fluxes should therefore be gauged by their respective contributions to the change in the buoyancy content of the water column. The buoyancy budget was first examined for a realistic geometry isopycnic model of the northern and equatorial Atlantic, the Atlantic Isopycnic Model (AIM), described in Chapter One.

In the following sub-section an outline of the method of calculating a buoyancy budget for an ensemble of water columns in the AIM basin will be outlined. In the second sub-

section the results of the calculation will be presented and in the final sub-section a brief discussion of the result will be given.

3.3.1 Calculation of the buoyancy budget in AIM

The change in the total buoyancy content of a water column occurs through surface heating, vertical shear, mass convergence, mixed layer diffusion and isopycnic layer thickness diffusion. The influence of vertical shear can be further sub-divided into shear due to Ekman drift and that due to the geostrophic shear. Thus the flux of buoyancy can be written as,

$$\frac{d}{dt}\sum_{i=1}^{k}\left(h_i\left(b_i - b_k\right)\right) = B_0 + B_{Ekman} + B_{shear} + B_{conv} + B_{thk} + B_{difn} \qquad \text{Eq. 3.2}$$

Buoyancy here is taken as $b_i = -g\sigma_i$. It will be noted that all buoyancies in the above and following equations are referenced to the buoyancy of the k-th layer, the layer immediately beneath the mixed layer at the start of the water column's trajectory. The expression for surface forcing, B_0, is given by equation B.7. The other terms are,

$$B_{Ekman} = h_1 \mathbf{u}_{Ek} \cdot \nabla b_1 \qquad \text{Eq. 3.3a}$$

$$B_{pump} = -\left(b_1 - b_k\right)\nabla \cdot \left(\mathbf{u}_{Ek} h_1\right) \qquad \text{Eq. 3.3b}$$

$$B_{shear} = h_1\left(\mathbf{u}_1 - \mathbf{u}_k - \mathbf{u}_{Ek}\right) \cdot \nabla b_1 \qquad \text{Eq. 3.4}$$

$$B_{convergence} = \sum_{i=1}^{k-1}\left(b_i - b_k\right)\nabla \cdot h_i\left(\mathbf{u}_i - \delta_{1i}\mathbf{u}_{Ek}\right) \qquad \text{Eq. 3.5}$$

$$B_{thk} = \sum_{i=1}^{k-1}\nabla \cdot \left(\kappa_T\left(b_i - b_k\right)\nabla h_i\right) \qquad \text{Eq. 3.6}$$

$$B_{difn} = -h_1 \kappa_I \nabla^2 b_1 \qquad \text{Eq. 3.7}$$

where,

$$\mathbf{u}_{Ek} = \frac{-\mathbf{k} \times \tau}{\overline{\rho} f h_1}$$

These terms can be calculated from the model data sets to produce a series of fields for each monthly data set produced by the model.

The buoyancy budget was calculated for water columns advected over one year. The start of each column trajectory was at a grid point in the model between 10°N and 60°N at the local time of the mixed layer's maximum depth. The trajectories were then

calculated from these grid points using the velocities of the layer immediately beneath the mixed layer (layer k in equations 3.3-3.6). An example of the trajectories is given in figure 3.6. Where the layer followed (k) became massless along the trajectory, the grid point was removed from the calculation; under these conditions buoyancy could be exchanged between the mixed layers and the deeper isopycnic layers, invalidating the restriction of the budget to the upper k layers.

During the evolution of the trajectory, the buoyancy fluxes, $B_0+B_{\text{Ekman}}+B_{\text{pump}}$, (calculated by R.Marsh) were interpolated to the particle's position and integrated over time. The net buoyancy change of the water column was found by integrating the buoyancy content over the upper k layers in AIM at the start time and position of the grid point and comparing this with the same integral over the upper k layers in AIM at the position of the water column at the end of the year.

3.3.2 Results of the buoyancy budget for AIM

The results of the buoyancy budget are shown in figures 3.7 to 3.9. The first figure shows the net change in the buoyancy content of each water column plotted at its initial grid point on the model grid. This shows that the zero net buoyancy line runs from Bermuda to the Bay of Biscay. To the north of this line the k-th layer is seen to disappear over the annual cycle, indicated by the deep blue region over the Gulf Stream extension. Net buoyancy loss implies that the seasonal thermocline of a one dimensional water column is deepening over the year. Thus the layer that was immediately below the base of the seasonal thermocline in the first year will lie within it in the second. There is a narrow band of buoyancy loss where this does not occur, presumably because the deepening of the seasonal thermocline over the year does not completely engulf the layer followed (layer k).

To the south of the Gulf Stream region lies the region of net buoyancy gain. The area of strongest buoyancy gain lies to the south, in the region of the return flow. This is to the south of the zonal axis of the sub-tropical gyre, in this region the Ekman drift velocity is down the gradient of SST.

The second figure (Fig.3.8) shows the net buoyancy flux (the sum of the surface buoyancy flux B_0, Ekman drift buoyancy flux, B_{ekman} and the Ekman pumping flux, B_{pump}) integrated along the trajectories of the water columns over one year with the sum plotted at the starting position of the water column. It will be noted that figure 3.8 is very similar to figure 3.7, a zero net buoyancy flux line from Bermuda to Biscay and strong heating in the southern portion of the sub-tropical gyre. In both figures the eastern basin is an area of little buoyancy gain by Lagrangian water column over the year. The third figure (Fig.3.9) shows the differences between the net change in total buoyancy content and the combined integrals of surface buoyancy and Ekman drift fluxes. The largest differences are found where the surface flux and observed change are large while the residual is much smaller.

3.3.3 Discussion of the buoyancy budget for AIM

The above plots show that the agreement between the net change in buoyancy of a water column and the net input of buoyancy through the surface are reasonably good in AIM. The net residual is generally <20% of the combined input by the surface forcing and the Ekman terms, although much higher proportions are observed in regions where the net surface and Ekman fluxes are near-zero. This implies that mixed layer simulations of the AIM mixed layer and thermocline that include the Ekman drift term in their surface forcing should produce reasonably similar results to the actual evolution of the AIM thermocline. It also implies that the relation described by Marshall & Nurser (1989) (Eq.1.4) for the permanent subduction rates should hold reasonably well for the AIM basin away from the region of the return flow. By extension, it could be suggested that the results also imply that the evaluation of the permanent subduction rate by Woods & Barkmann (1986a) for the North Atlantic from atlas data should be reasonable to within the accuracy of the climatological data sets used for forcing and trajectories. However, further evidence would be required to substantiate this assertion. This will be discussed later in this chapter.

For a closed buoyancy budget it is necessary that the residual shown in figure 3.9 is divided between the processes that are described by equations 3.4-3.7; attempts to do this have not been successful. Budgets of the heat content for a region in the AIM sub-

polar gyre and an attempted budget for the buoyancy content of static water columns (not shown) have demonstrated that the truncation error introduced by AIM's data handling routines is too great to allow a budget to balance over time scales of a year or more (S. Barnard, personal communication). In a Lagrangian framework this problem is exacerbated by the positioning of the water column away from grid points over most of its trajectory. This introduces the need for an interpolation scheme which was chosen to be linear in these calculations. However, the assumption that the construction of a continuous field can be made from the model's discrete output, a line integral performed over this field and a favourable comparison made with the model's output is uncertain, as has been indicated by Böning & Cox (1988). It is not clear whether model-generated fields should be treated as a series of plateaux with discontinuities at the boundaries of grid-squares or as interpolated fields. This problem is inherent to all Lagrangian interpretations of GCM data.

Given the problems encountered in a derivation of a buoyancy budget from data produced after a model run, a second approach was taken with a simple geometry model. The buoyancy budget is described in the next section.

3.4 A buoyancy budget for a simple geometry GCM

The failure of the buoyancy budget in the previous section brought about a second attempt where by the budget was performed as the GCM ran. This was undertaken using the simple geometry version of MICOM, Box1, described in Chapter One and referred to earlier in this chapter. The circulation of this model is descibed in detail in Chapter Five, but an example of the circulation pattern of the model interior is given in figure 3.1b. A brief description of the method used is given in the following sub-section, followed by a demonstration of the results. The final sub-section discussed the results of the buoyancy budget for the model.

3.4.1 A method for calculating Lagrangian budgets in GCMs

The code of the simple geometry GCM, Box1, is constructed as a series of modules each of which enacts one process such as the diffusion of layer thickness or

entrainment/detrainment by the mixed layer. This modular structure allows the model code to be easily comprehended and for each of the processes enacted in the model to be identified.

The contribution of each process to the net change in the buoyancy of a grid column can be found by measuring the buoyancy content of that water column before and after that process takes place. By doing this continuously as the model runs for the two time levels (old/new and centre) of the leapfrog scheme and summing the changes found after each process, an exact budget for the buoyancy change observed in the model can be constructed. This approach to the calculation of buoyancy changes can be extended to cover water columns moving in a Lagrangian framework by adding a simple linear interpolation scheme to the process, interpolating the new buoyancy content to the particle's position after each process and comparing this interpolated buoyancy content with the previous content. The advection scheme used for the water column trajectories is a simple Euler forward scheme in this study.

The interpolation of buoyancy content and differencing between the values before and after a process can generate the contribution of each subroutine to the buoyancy change, but where a subroutine contains several processes implicitly, separation of the contribution of these processes is not possible as the model runs. This is especially problematic with the Ekman pumping and drift terms which are implicit in the formulation for the momentum and continuity equations. For this study these terms are calculated explicitly during the model run using the model's mixed layer fields and the imposed wind stress to derive a buoyancy flux for the equilibrium Ekman drift. This calculation is independent of any mixed layer momentum calculation made in the model. After the model run the Ekman pumping buoyancy flux, B_{pump}, is subtracted from the total mass convergence flux to give $B_{convergence}$ and the Ekman drift flux, B_{Ekman}, is subtracted from the total mixed layer advection flux to give B_{shear}. This method is not entirely satisfactory, but it is unavoidable in a primitive equation model.

The problems raised by Böning & Cox (1988) have been largely circumvented by this approach. By calculating the same quantity, in this case column buoyancy content,

repeatedly the budget is constrained to close. The errors in the trajectory of the Lagrangian particle arising from aliased non-linear terms and from the choice of interpolation fields will be included in the relative advection term. It is difficult to see how these errors could be estimated, but it is assumed that in the main body of the gyre, away from the strong shears of the western boundary current, the errors in the trajectory are not of any great importance, while the AIM model is in a largely linear flow regime, making the non-linear terms of limited importance.

3.4.2 The results of the buoyancy budget for the simple geometry GCM

The results of the simple geometry GCM buoyancy budget are shown in figures 3.10 to 3.16. The first figure shows the net total buoyancy content change for the upper k layers of the model, where k is as defined in section 3.3. Where the plot is blank the layer on which the particle was tracked through the Box1 gyre became completely entrained by the mixed layer at some time through the course of the year. The division of the net heating and net cooling regimes in the model runs diagonally across the sub-tropical gyre, as was found in AIM. To the north the Lagrangian columns that experience the greatest buoyancy loss are those starting their trajectory in spring in the western boundary current extension, as would be expected from the relatively fast northward flowing waters found in this region. In the sub-polar gyre the buoyancy loss is less and in the southward flowing portion of the gyre water columns gain buoyancy over the year.

Figure 3.11 shows the net buoyancy flux into the water columns due to the surface heat fluxes and the Ekman terms ($B_0+B_{Ekman}+B_0$). This indicates that the zero net buoyancy loss line due to surface forcing and Ekman fluxes lies further to the south than the observed change in buoyancy, especially in the eastern part of the basin where very strong buoyancy loss is observed. Buoyancy gain due to surface forcing and the Ekman terms is strong in the return flow of the sub-tropical gyre where the northward Ekman drift drives warm surface waters down the SST gradient, and in the southward flowing part of the sub-polar gyre.

Figure 3.12 shows the residual of the above, derived from an explicit calculation of the component terms rather than from the subtraction of the net surface and Ekman fluxes

from the observed change in column buoyancy. The component terms in this plot are shear advection of buoyancy other than by Ekman drift $[h_1(\mathbf{u}_1 - \mathbf{u}_k - \mathbf{u}_{Ekman}) \cdot \nabla b_1]$, divergence of the mean mass fluxes other than the Ekman fluxes $[\sum_{i=1}^{k-1}(b_i - b_k)\nabla \cdot (h_i(\mathbf{u}_i - \delta_{1i}\mathbf{u}_{Ekman}))]$, the transport of buoyancy by thickness diffusion $[\sum_{i=1}^{k-1}\nabla \cdot (\kappa_T(b_i - b_k)\nabla h_i)]$ and the diffusion of buoyancy in the mixed layer $[h_1 \kappa_I \nabla^2 b_1]$, where $b_i = -g\sigma_i$. The figure indicates that there is extensive buoyancy gain in the separated western boundary current, over most of the sub-polar gyre and along the eastern boundary current. Areas of buoyancy loss coincide with the areas of buoyancy gain in figure 3.11, the southward flowing portion of the sub-polar gyre and the return flow of the sub-polar gyre.

The relative importance of the components of the residual is shown in figures 3.13 to 3.16. From this it is clear that the influence of mixed layer diffusion on the buoyancy budget is slight (figure 3.13), as would be expected. The residual advection of buoyancy in the mixed layer relative to the water column once the Ekman flux is subtracted produces a strong net loss of buoyancy for water columns starting from the separated western boundary current (figure 3.14). Residual buoyancy advection produces a net loss for columns advected from the tropical and most of the sub-tropical gyres. In the southern half of the sub-tropical gyre and along the eastern boundary residual advection makes a net contribution to the buoyancy content of water columns. The strongest contribution lies along the eastern boundary where the southward velocities in the thermocline are stronger than in the gyre interior.

Thickness diffusion (figure 3.15) reduces the buoyancy content of the upper ocean in the model, except in the tropical gyre where it produces a slight gain. The largest contribution to the buoyancy content of the water columns is in the western end of the sub-polar gyre. In the separated western boundary current thickness diffusion is of secondary importance in the west, but becomes relatively more important in the east where the contribution of residual advection is slight. Experiments presented in Chapter Five will imply that this flux of buoyancy is northwards into the subpolar gyre.

The residual of the mass divergence (figure 3.16) makes a large net contribution to the buoyancy content of columns starting in the separated western boundary current. In this region this is the dominant term, 50% greater than the magnitude of the buoyancy loss due to residual advection. Towards the eastern half of the basin the contributions of thickness diffusion and residual mass divergence are approximately equal. Outside a band stretching from ~30°N to ~49°N (grid points j=11-17) the residual mass divergence removes buoyancy from the water columns. The buoyancy loss is strongest near the southern boundary.

3.4.3 Discussion of the results of the buoyancy budget

The most important note to make of the buoyancy budget for the simple geometry isopycnic model Box1 is that, unlike the budget for AIM, the contribution of the residual terms to the observed change in water column buoyancy is significant. This is particularly the case in the eastern basin.

In the separated western boundary current the greatest positive contribution to the buoyancy content is made by the residual mass divergence with a secondary contribution from thickness diffusion. This is opposed by a net buoyancy loss due to residual buoyancy advection. The large buoyancy gain in the eastern basin is due to a large contribution from the residual mass divergence with contributions from both thickness diffusion and residual buoyancy advection. The contribution of thickness diffusion increases with latitude while that of advection remains reasonably constant along the eastern boundary.

The use of one-dimensional Lagrangian methods of evaluating the evolution of the mixed layer and thermocline and the permanent subduction rates would not appear to be valid in Box1. The contributions made by three-dimensional processes to the evolution of the water column, implied by the large contribution made to the change in buoyancy content, are too large to be ignored.

The significant contribution of the residual buoyancy flux terms (Eq.3.3-3.7) to the Lagrangian buoyancy budget indicates a difference between the dynamics of Box1 and

AIM. The mathematical formulations of the two models are substantially the same (see Appendix A) which would suggest that differences in the character of the solutions generated by the two models must lie in the different areas of parameter space occupied by the two models. The parameters of greatest interest are the eddy viscosity and the thickness diffusivity. Both of these coefficients are lower in AIM, indicating a less diffusive simulated ocean than Box1. Experiments reported in Chapter Five show that the thickness diffusion coefficient has a strong influence on the character of the thermocline circulation. In AIM the low thickness diffusion coefficient permits the creation of ventilation tongues and mode water boluses, it also produces steeper isopycnal outcropping. This last produces stronger southward geostrophic flow, and reduces the vertical shear through the thermal wind equation. The ventilation tongues also reduce the divergence of the upper water column and it also increases the proportion of the upper water column occupied by the k-th layer at the expense of lighter layers, again reducing the vertical shear. Thus a reduced thickness diffusion coefficient would be expected to improve the accuracy of a one-dimensional description of the mixed layer and upper thermocline.

Comparisons of the circulation patterns and tracer distributions from AIM and Box1 with those derived from tracer studies of the North Atlantic (*e.g.* Sarmiento, 1983a) indicate that the North Atlantic is a more diffusive ocean than its representation in AIM would suggest and that Box1 is, perhaps, a better approximation to the North Atlantic. This implies that the one-dimensional approach to the study of the evolution of the mixed layer and upper thermocline of the North Atlantic is not appropriate.

3.5 Summary

In this chapter it has been demonstrated that the use of simple surface forcing along a Lagrangian trajectory does not re-produce the evolution of a one-dimensional water column as it is advected through a GCM basin. The cause of this difference is largely the Ekman fluxes in the mixed layer, both the Ekman advection of water and the convergence of water in the mixed layer through Ekman pumping. In re-producing the evolution of the mixed layer and thermocline of AIM in the sub-tropics the inclusion of

these Ekman terms would appear to be sufficient to ensure accuracy. However, in Box1 there are large contributions from thickness diffusion, the non-Ekman convergence of mass and non-Ekman advection of mixed layer buoyancy, especially in the eastern part of the sub-tropical gyre. This implies that one-dimensional methods will not re-produce the upper thermocline of Box1.

It should be recognised that AIM and Box1 are essentially similar models, the most important differences in their formulation lie in the differences in the grid-mesh resolution (1° and 2° respectively) and type (C-grid and B-grid), the solution of the problem of barotropic divergence (split-explicit and rigid lid methods) and in the parameters used to represent sub-gridscale processes (see Table 1.1, Chapter One). However, despite the similarities in the models' formulations, the results of the above buoyancy budgets indicate a qualitative difference in the importance of the various processes in determining the ocean stratification and, thereby, the circulation. The qualities of the oceanic circulation are, most probably, independent of the model grid and of the treatment of the barotropic divergence. It would, therefore be reasonable to assume that the differences in between the two models arise from the different eddy viscosity and diffusivity parameters used.

In the main body of the North Atlantic, the eddy kinetic energy is higher than the kinetic energy of the mean circulation, indicating the importance of eddy processes to the circulation of the North Atlantic. It would therefore be expected that the conditions prevalent in the North Atlantic are more comparable to those in Box1 than in AIM; Box1 has a Péclet number comparable to that estimated for the North Atlantic (Thiel, *et al.* (1986) estimate Pé≈2 in the upper thermocline compared to 1.46 in Box1 using the same definitions as Thiel, *et al.*) and higher diffusivities than in AIM (Pé≈4.2 for AIM). Thus, if we assume that the diffusive representation of eddy processes is sufficiently accurate for our purposes, then we can conclude that estimates of the evolution of the upper thermocline of the North Atlantic derived from one-dimensional methods will not be accurate.

Figure 3.1: (a) A plot of the trajectories of particles advected in the mixed layer of the simple geometry GCM, Boxmix. The plot is presented on the model grid which is a regular Cartesian mesh in the Mercator projection. Latitudes are given on the extreme right. The dots show the start of each trajectory.

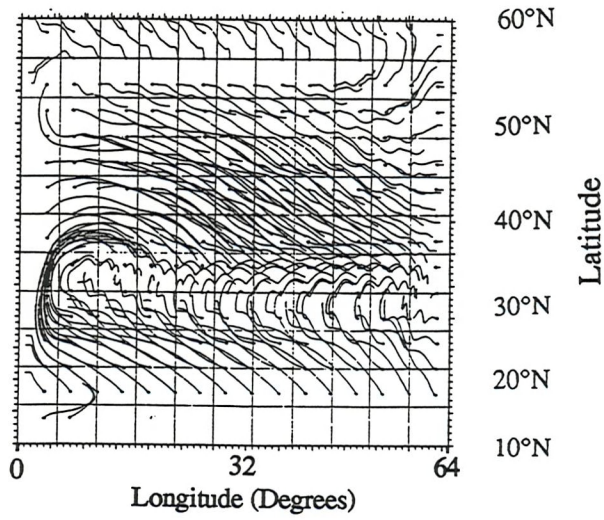

(b) A plot of the trajectories of particles advected over a two year period on the isopycnic layer σ=27.00 in Boxmix. The plot is presented on the model grid with latitudes given on the extreme right. The trajectories begin on the dots.

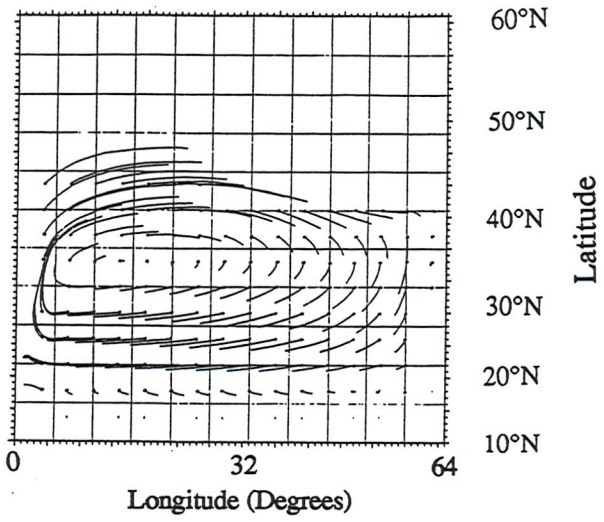

Figure 3.2: (a) The SST of the Boxmix GCM along the trajectory of a particle advected over two years in the mixed layer from a point on the northern rim of the subtropical gyre.

(b) The stratification of the upper 500m of Boxmix along the trajectory of a particle advected over two years in the mixed layer of the Boxmix GCM, starting at a point on the northern rim of the subtropical gyre.

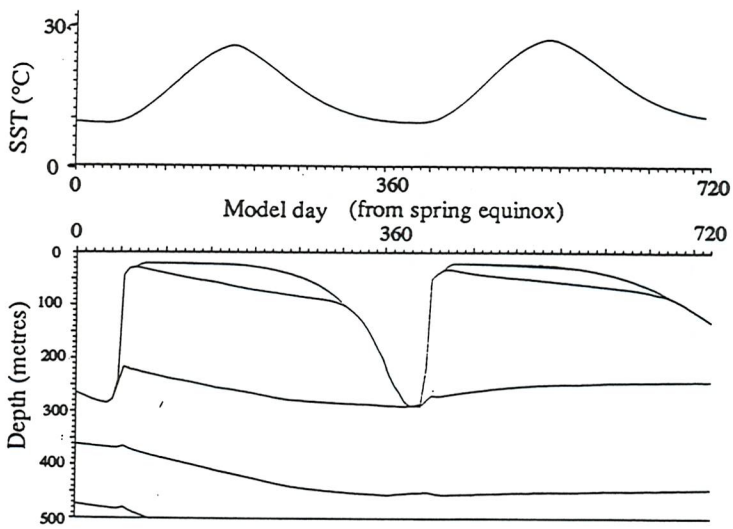

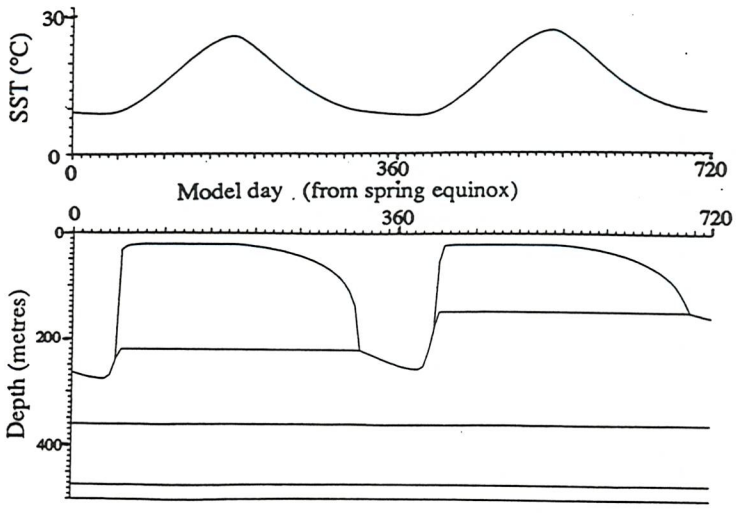

Figure 3.3: (a) The SST of a mixed layer model forced by the surface forcing encountered by a particle advected in the mixed layer of the Boxmix GCM for a period of two years.

(b) The stratification of the upper 500m of a mixed layer model forced by the surface forcing encountered by a particle advected in the mixed layer of the Boxmix GCM for a period of two years.

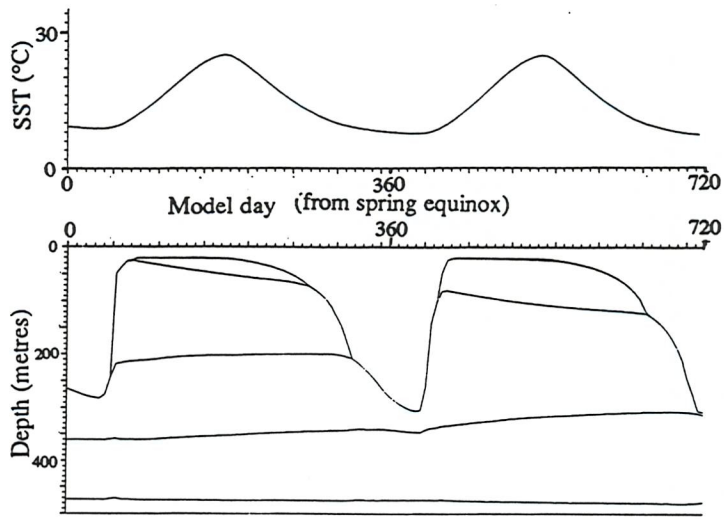

Figure 3.4: (a) The SST of the Boxmix GCM along the trajectory of a particle advected over two years on the layer σ=27.00 from a point on the northern rim of the subtropical gyre.

(b) The stratification of the upper 500m of Boxmix along the trajectory of a particle advected over two years on the layer σ=27.00 of the Boxmix GCM, starting at a point on the northern rim of the subtropical gyre.

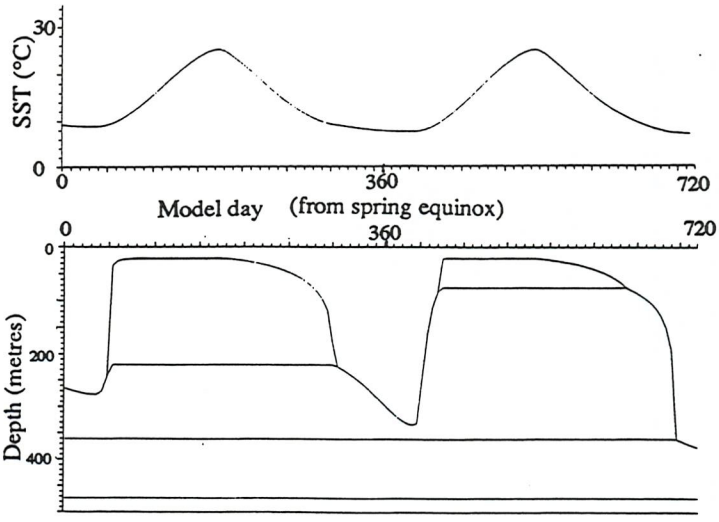

Figure 3.5: (a) The SST of a mixed layer model forced by the surface forcing encountered by a particle advected on the layer σ=27.00 of the Boxmix GCM for a period of two years.

(b) The stratification of the upper 500m of a mixed layer model forced by the surface forcing encountered by a particle advected on the layer σ=27.00 of the Boxmix GCM for a period of two years.

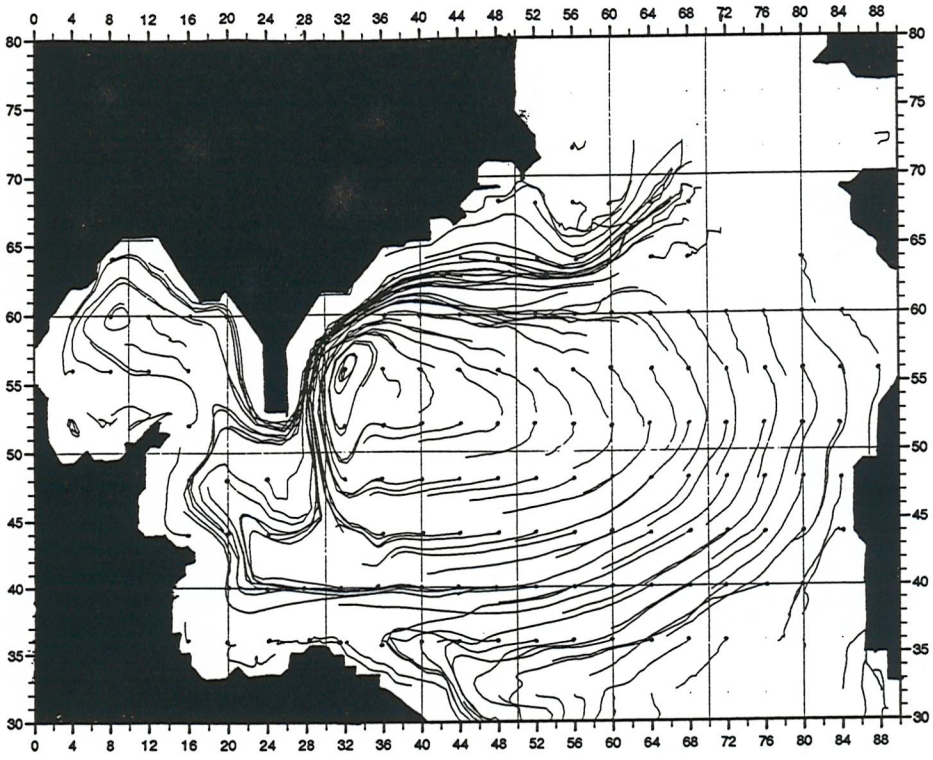

Figure 3.6: A plot of the particle trajectories for particles advected over a two year period on isopycnic layer σ=26.70 in the Atlantic Isopycnic Model (AIM) on the model grid. The particles start at a model grid point at the time of the mixed layer's deepest mixing. The model trajectories begin at the dot.

Figure 3.7: A plot of the change in the total buoyancy content of the upper k layers of the ocean for an ensemble of water columns advected over a period of one year. The change in water column buoyancy content is plotted at the grid point at the start of each column's trajectory. The k-th layer is locally determined as the first massive isopycnic layer beneath the mixed layer at the time of the mixed layer's local maximum depth (the start of the period over which the water column is advected). The trajectory of the water column is determined by the velocity field of the k-th layer. The blue regions are where the k-th layer is totally entrained at some point over the course of the year. The change in buoyancy is plotted in units of kg/m^2 (see overleaf).

Figure 3.8: A plot of the net surface buoyancy flux (sum of the Ekman buoyancy flux, B_{Ekman}, the surface buoyancy flux, B_0 and the Ekman pumping term, B_{pump}) integrated along the trajectories of an ensemble of water columns advected by the velocity fields in the k-th layer, where k is defined above. The integral is plotted at the start of the trajectory. The blue regions are where the k-th layer becomes massless over the course of the trajectory. The integral of the net buoyancy flux is expressed as ρgz in units of kg/m^2 (see overleaf).

Figure 3.9: A plot of the difference between the change in buoyancy content of the upper k layers of a water column and the integral of the net buoyancy flux into the same water column over the course of one year. Where the plot is yellow the k-th layer became massless over the course of the year. The difference is expressed as ρgz in units of kg/m^2 (see overleaf).

Figure 3.7

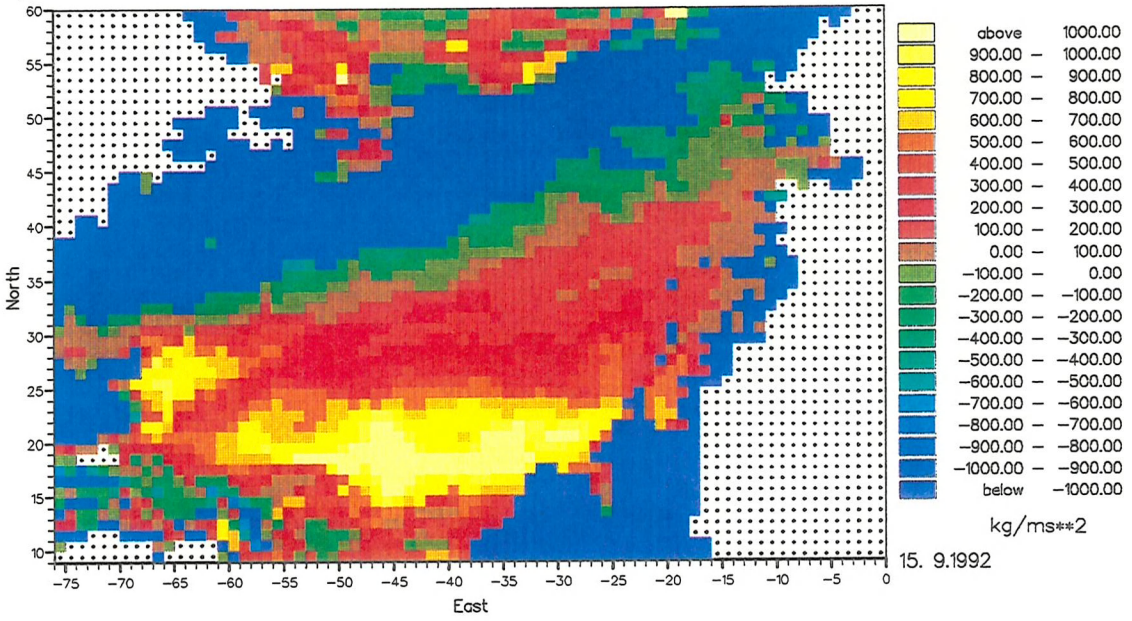

Figure 3.8

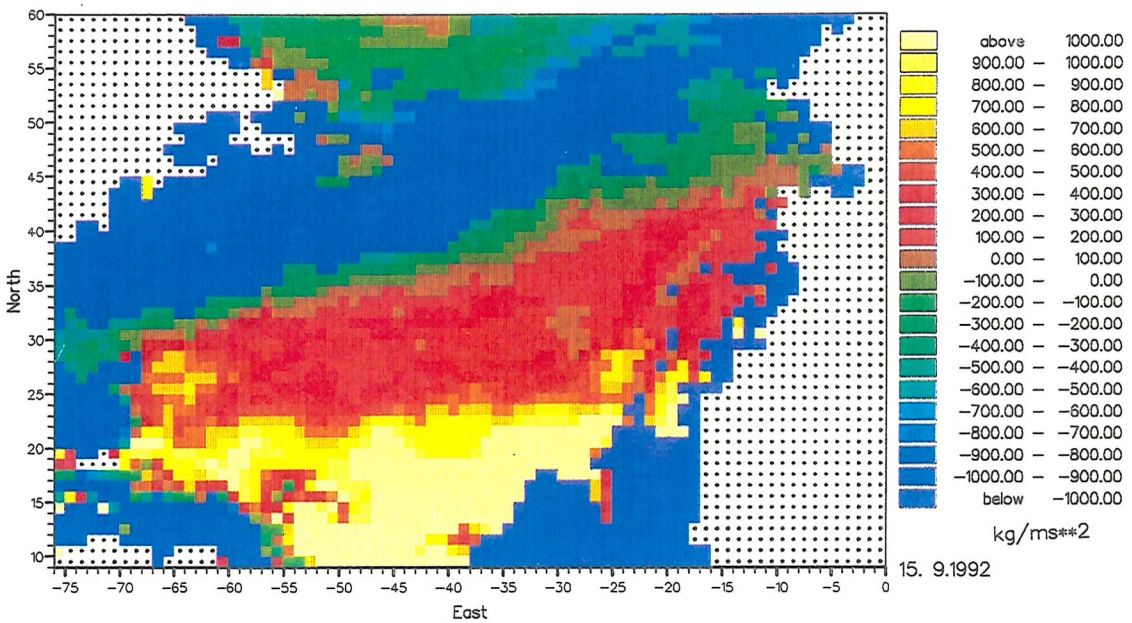

Figure 3.9

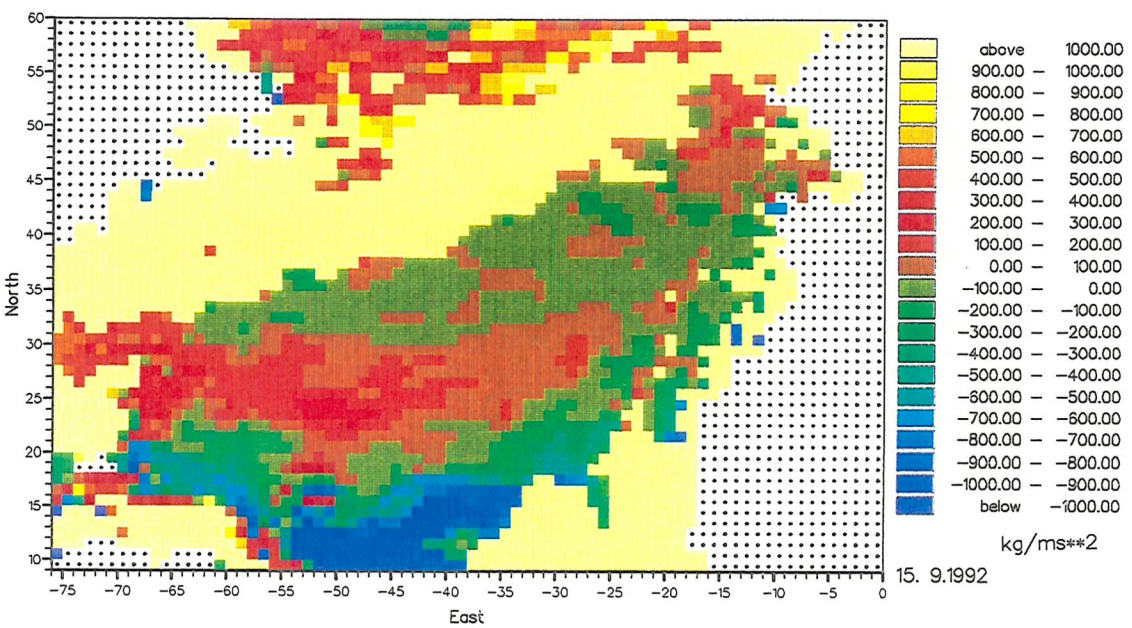

Figure 3.10: A plot of the change in the total buoyancy content of the upper k layers of an ocean model for an ensemble of Lagrangian water columns advected for one year with the velocities of the k-th layer. The change is plotted at the starting point of the trajectory in kg/ms^2 and where the plot is blank the k-th layer becomes massless during the course of the year. The plot is presented on the model grid.

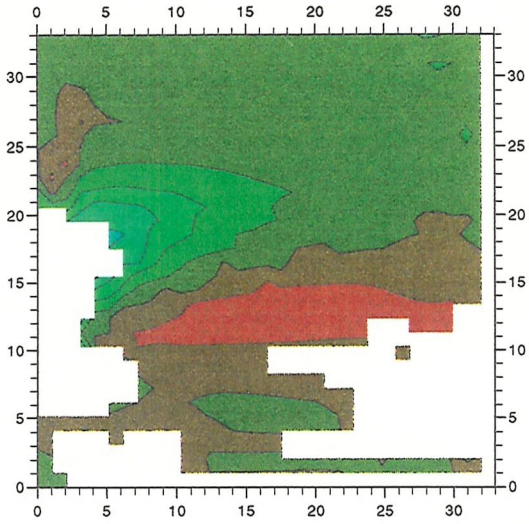

Figure 3.11: A plot of the integral of the net surface buoyancy flux (Ekman plus surface fluxes) for an ensemble of Lagrangian water columns advected for one year. The integral is plotted in units of kg/ms^2 at the starting point of the trajectory. Where the plot is blank the k-th layer has becomes massless during the course of the year. The plot is presented on the model grid.

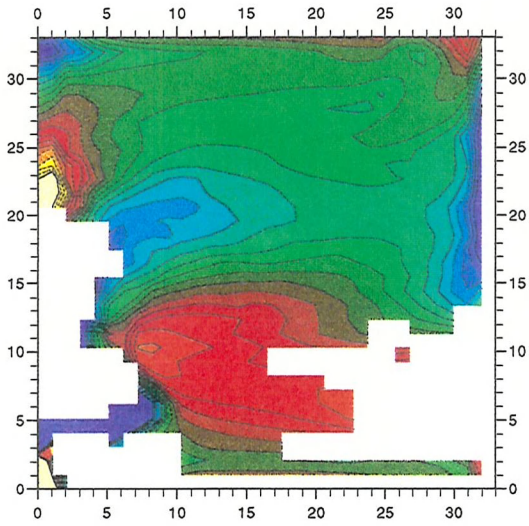

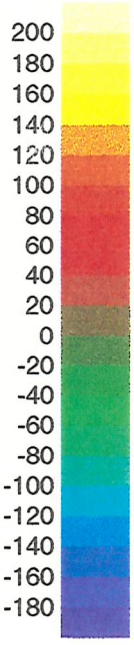

Figure 3.12: A plot of the integral of the net buoyancy flux due to the residual terms (Eq.3.4-3.7) along an ensemble of water column trajectories. The integral is plotted at the start of the trajectory in units of kg/ms^2. Where the plot is blank the k-th layer is massless at some point along the trajectory.

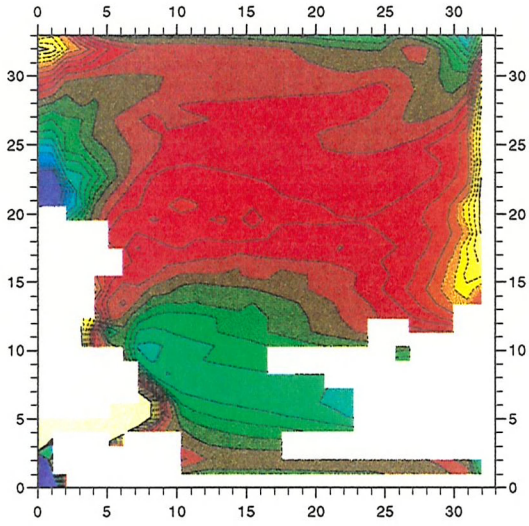

Figure 3.13: A plot of the integral of the buoyancy flux due to buoyancy diffusion in the mixed layer for an ensemble of water columns advected over one year in an isopycnic GCM. The integral is plotted at the starting point of the trajectory in units of kg/ms^2. The plot is presented on the model grid and where the plot is blank the k-th layer becomes massless during the course of the year.

Figure 3.14: A plot of the integral of the buoyancy flux due to vertical shear between the mixed layer and the k-th layer for an ensemble of water columns advected over one year in an isopycnic GCM. The integral is plotted at the starting point of the trajectory in units of kg/ms^2. The plot is presented on the model grid and where the plot is blank the k-th layer becomes massless during the course of the year.

Figure 3.15: A plot of the integral of the buoyancy flux due to thickness diffusion for an ensemble of water columns advected over one year in an isopycnic GCM. The integral is plotted at the starting point of the trajectory in units of kg/ms^2. The plot is presented on the model grid and where the plot is blank the k-th layer becomes massless during the course of the year.

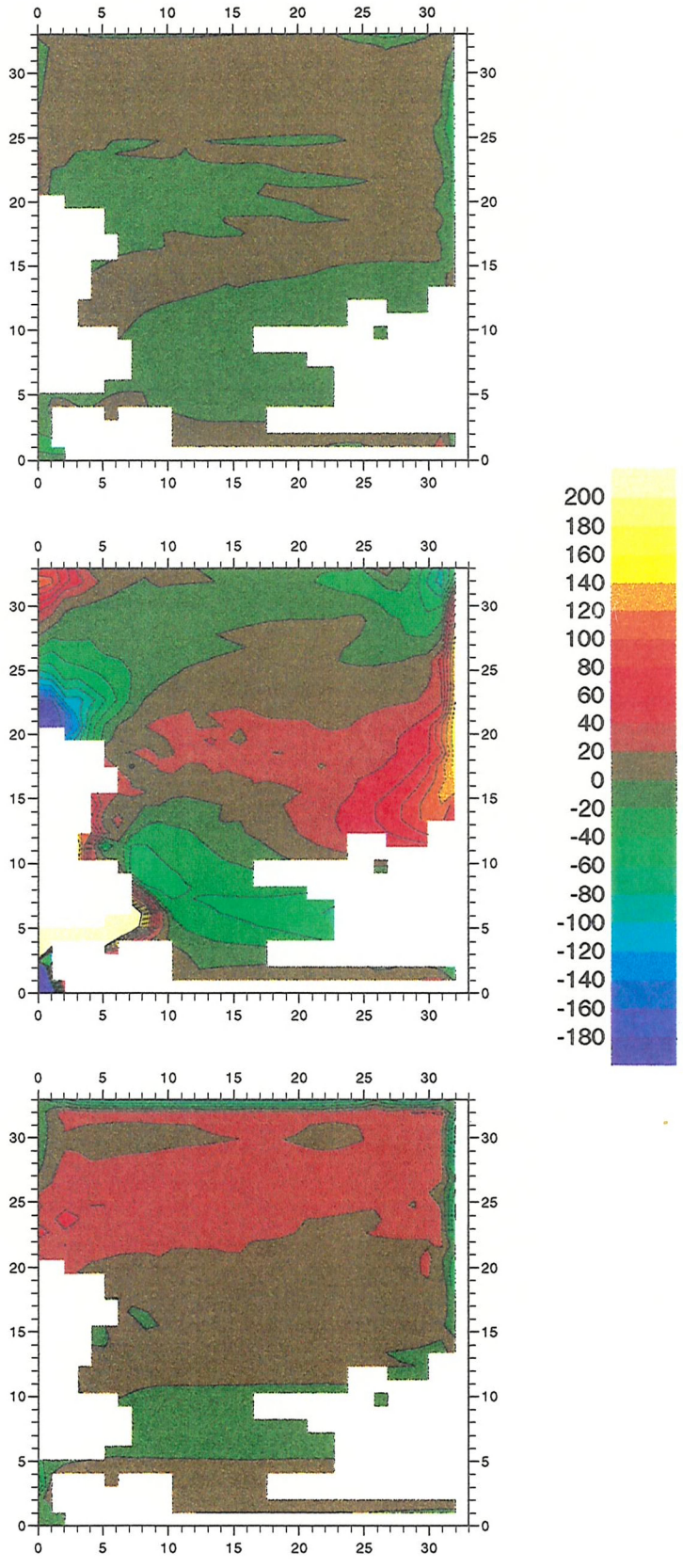

Figure 3.16: A plot of the integral of the buoyancy flux due to non-Ekman mass divergence for an ensemble of water columns advected over one year in an isopycnic GCM. The integral is plotted at the starting point of the trajectory in units of kg/ms^2. The plot is presented on the model grid and where the plot is blank the k-th layer becomes massless during the course of the year.

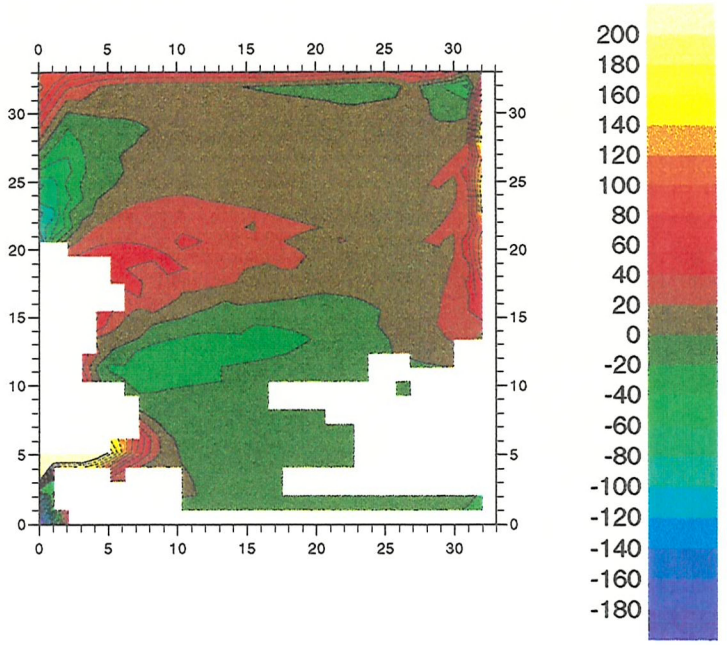

CHAPTER FOUR

Estimates of the rates of permanent subduction and entrainment in an isopycnic model of the North Atlantic

4.1 Introduction

The role of the North Atlantic in closing the thermohaline circulation has been emphasised by Broecker (1991). The slow overturning of the world ocean produces a net northward transport of ~10 Sverdrups of warm surface waters (McCartney & Talley, 1984), balanced by a similar outflow at depth. Associated with the northward surface mass flux, there is also a northward heat flux of ~1 petaWatts ($1PW=10^{15}W$) at 25°N (Bryden & Hall, 1980). This heat is exhausted to the atmosphere over the North Atlantic; resulting in the clement European climate and in the creation of subtropical and subpolar water masses (Worthington, 1972). The rate at which the North Atlantic mode water masses are produced determines, with the deep water production rate in the Weddell Sea, the rate of the thermohaline circulation and the extent to which the upper layers of the ocean are coupled to the intermediate and deep layers.

In this chapter the rate at which a model ocean introduces mode waters into the permanent thermocline will be studied. A number of methods will be outlined and their relative merits discussed; a new method of determining the rates of both subduction and entrainment from particle trajectories will be described and the results of this method for an Atlantic circulation model (AIM) will be presented. These results will be compared with the results of three other methods; the kinematic method, a second particle approach (after Williams, Spall & Marshall, 1995, henceforward referred to as the WSM method) and from tracer studies. The subduction rates for AIM will be compared with the results derived by other authors from tracer measurements in the North Atlantic, considerations of the water mass transformation rates implied by climatological data, and from the results of other North Atlantic models.

4.2 Methods of determining the rates of permanent entrainment and permanent subduction

The definition of the permanent subduction rate used throughout this thesis is the volume transferred over one year from the seasonal thermocline (the volume swept out by the mixed layer over the annual cycle) to the permanent thermocline (that part of the thermocline beyond the reach of the winter mixed layer. Figure 4.1 shows a schematic diagram of the two processes of permanent entrainment and subduction. The permanent entrainment and subduction rates are expressed as annual means in Sverdrups when considering water mass renewal. When the geographical distribution of the two processes are considered the annual volume transferred per unit area per annum is considered (the permanent entrainment/subduction depth).

A number of methods have been used to determine the permanent subduction rate in the North Atlantic and in ocean models. Four methods are used in this chapter; the kinematic method, the method of Williams, *et al.* (1995), a ventilation tracer method and a method described later in this chapter which will be referred to as the particle method. These four methods are described in more detail in the relevant sections below.

In addition to these four methods, others have been employed to diagnose the permanent subduction rate in the North Atlantic. Woods & Barkmann (1986a) used an ensemble of Lagrangian one-dimensional mixed layer models advected through the subtropical North Atlantic gyre to estimate the rate at which subtropical mode waters are generated. Their forcing data and velocity fields were taken from climatological values and the mixed layer models were run for four years to reproduce the southward shoaling of the base of the seasonal thermocline, thereby producing an estimate of the mode water production rate.

A second Lagrangian approach is that of Marshall & Nurser (1991). They analysed the thermal requirements of subduction and found that if the influences of shear and diffusion are of minimal importance in the evolution of the upper thermocline then the instantaneous subduction rate could be related to the net buoyancy flux (surface and

Ekman buoyancy fluxes) into the ocean. By integrating the instantaneous subduction rate in a Lagrangian frame, *i.e.* along a trajectory, over the permanent subduction period the annual permanent subduction rate could be derived.

Speer & Tziperman (1992) examined surface buoyancy fluxes to estimate the implied transformation rate between water masses of different density classes. If the influence of mixing is ignored then the net rate of water mass production can be estimated by the divergence in the water mass flux in density space. This method has also been applied to model data (R.Marsh, personal communication).

The three methods described here rely on the accuracy of the surface buoyancy fluxes which renders them vulnerable to large errors. Tracer studies, however, offer a more direct means of assessing the rate of mode water formation. Tracers can be used as markers for water masses which were isolated from the mixed layer (therefore permanently subducted) at a particular time, *e.g.* through trace ratios. Sarmiento (1983a) studied the distribution of tritium and helium in the subtropical North Atlantic and used a simple isopycnic box model of the ocean to estimate the rates of water mass formation. The estimate derived from this study is probably the best available, while the study of CFC tracers in the North Atlantic offers the hope of future estimates to validate or amend the result of Sarmiento.

In the following sections the four methods of determining the permanent subduction and permanent entrainment rates noted above will be described and their results for the AIM model will be presented. Throughout this chapter it will be assumed that the ventilation tracer result is the most accurate and will therefore be taken as 'truth' when the other three methods are examined.

4.3 Permanent subduction rates in AIM derived from tracer studies

To establish the permanent subduction rate on to each isopycnic layer using tracers requires the identification of thermocline water that was detrained from the mixed layer

over the previous year. This can be done by setting the initial tracer concentration in the thermocline to zero and holding the mixed layer tracer concentration at 1.0 for the duration of the first year. All water detrained from the mixed layer bears the concentration 1.0 until it is diluted in the thermocline. The tracer 'concentration' is referred to loosely, the number is actually non-dimensional and represents the fraction of the water mass which was previously in the mixed layer. To ensure that the whole spring detrainment is caught, the model run is started before the winter maximum in mixed layer depth and continues over 360 days (one model year).

At the end of the first year the mixed layer concentration is re-set to zero and all tracer re-entering the mixed layer is removed from the system. The second re-stratification of the run introduces tracer-free water to the thermocline, further diluting the tracer. By the summer of the second year the tracer remaining in the thermocline can only have been subducted during the first year. The product of the tracer concentration and the layer volume at each grid point summed over the whole domain gives the volume of water permanently subducted on to that layer over the previous year.

Unlike the other methods of determining the permanent subduction rate, the tracer method allows the effects of sub-grid scale, diffusive processes to be included in the dispersion of the subducted water. This permits the role of diffusive processes to be evaluated. However, in a diffuse fluid the source of a particular body of tracer is not well-defined. This implies that the exact source regions of the tracer placed in the permanent thermocline cannot be established exactly.

The permanent entrainment rate can be established by reversing the procedure. At the start of the model run the thermocline tracer concentration is set to 1.0 at all grid-points in the thermocline. Over the run the volume of tracer entering the mixed layer from each isopycnic layer is calculated and a running total kept for each layer at each grid-point. The tracer is not returned to the thermocline from the mixed layer during detrainment. The model is then run for a period of 420 model days. The difference between the running total over a period of 360 days gives the annual permanent entrainment rate from each layer at each grid point which can then be summed to give the total permanent

entrainment rate, the permanent entrainment rates from each layer and maps of the local permanent entrainment rates.

It will be noted from the examination of figures 4.2a&b that the effect of vertical truncation is to increase the estimate of the permanent subduction and entrainment rates. Tracer placed on an isopycnic layer in the thermocline is instantaneously mixed throughout the thickness of that isopycnic layer. For a layer that lies at the base of the seasonal thermocline this will result in a flux into the permanent thermocline. While estimates made from this one-dimensional model imply a large potential error in the tracer flux (O(10)%), it is shown in Chapter Five that in practice the effects of vertical truncation are small.

The tracer method was used to establish the permanent subduction rate in AIM. The influence of isopycnic diffusion on permanent subduction was examined by conducting two runs, one where the tracer was diffused along isopycnic layers and another where it was not. The permanent entrainment rates in AIM were not derived using the tracer method. Experiments presented in Chapter Five will show that the difference between the permanent entrainment rate and the permanent subduction rates derived by the tracer method balance with the observed change in thermocline volume. The permanent entrainment rate can therefore be derived from the subduction rate and the change in the volume of the permanent thermocline.

4.3.1 Results of the tracer studies in the Atlantic Isopycnic Model

The annual permanent subduction rate for AIM derived from the tracer studies where isopycnic tracer diffusion is used to distribute the tracer in the thermocline is 66.7 Sv over the year. If isopycnic diffusion is not used to disperse tracer in the thermocline then the permanent subduction rate is 66.3 Sv. The permanent subduction rates on to each layer are shown in figure 4.3 for the run with isopycnic tracer diffusion. The only significant difference found in the ventilation of the two runs was the ventilation of layer σ=25.65, 6.4 Sv subducted by advection (both the mean flow and the mass flux associated with the thickness diffusion, Gent & McWilliams, 1990) and Ekman pumping, and a further 0.3 Sv by isopycnic diffusion. Layers σ=25.65 and 27.75 receive the largest

amount of permanently subducted water (17.5 Sv subducted on to σ=27.75), whilst layers σ=25.80-26.25 and σ=27.45-27.60 receive very little water (between 0.5 and 1.5 Sv). There is a secondary peak in permanent subduction rates for the layers σ=26.40-26.70 (between 3.1 and 4.7 Sv).

Figure 4.4 shows the tracer 'depth' distribution (layer thickness multiplied by tracer concentration) on layer σ=26.70 eighteen months after the tracer was introduced to the model and six months after the second winter has removed tracer from the seasonal thermocline. The tracer therefore represents water that has been permanently subducted. The position of the maximum of subducted tracer depth lies ~550km to the south-west of the permanent subduction zone for this layer indicated in figure 4.16.

4.3.2 Discussion of the tracer estimate of permanent subduction

The role of isopycnic tracer diffusion in the permanent subduction of mode waters in AIM appears to be insignificant, less than 0.6% of the total permanent subduction rate for the whole basin. The work of Jia & Richards (1994) would suggest that this is the result of an advection dominated flow regime in the thermocline. Later results will be presented to validate this inference.

The volume of the layers in the permanent thermocline remains stable for layers in the density range σ<26.25. However, for most of the density classes identified with the subtropical mode waters 26.40<σ<27.45 there is a net loss of volume at a total rate of 6.8 Sverdrups. In the subpolar gyre the permanent subduction rate dominates with a total rate of 6.3 Sverdrups subducted. This net conversion of waters in the model to the sub-polar mode waters suggests that the model has not yet reached a thermal equilibrium with its forcing. However, it is doubtful that a limited domain model could reach an equilibrium which faithfully represented the Atlantic basin, the southern boundary of the model prevents the export of deep water and the import of light surface water implied by Broecker's conveyor belt model (Broecker, 1991).

The permanent entrainment rates suggested by the change in permanent thermocline layer volumes and the permanent subduction rates are shown in figure 4.5. The overall

pattern is similar to that of the permanent subduction rate in figure 4.3, three peaks for the tropical σ=25.65 water, the subtropical ($26.40 \leq \sigma \leq 27.00$) mode waters, and the subpolar mode waters. The total permanent entrainment rate is 67.7 Sverdrups.

4.4 The particle method of determining permanent subduction and entrainment rates

The particle method described here examines the origin of water parcels whose trajectory defines the boundary between the seasonal and permanent thermoclines (see figure 4.6). In the equatorward flowing arm of a gyre, the depth of the seasonal thermocline rises along the trajectory of the particles placed in the thermocline in spring. Those particles placed deep enough in the thermocline are not re-entrained during the following winter and are therefore permanently subducted.

The particle method identifies the boundary between those particles that are too high in the water column to evade re-entrainment and those particles that enter the permanent thermocline by examining the limiting case, the particle which skims the base of the mixed layer during the following winter (see figure 4.6). By tracing the trajectory of this particle backwards to the point and time when it was detrained from the mixed layer during the previous winter, the end of the permanent subduction period can be found. The permanent subduction rate can then be estimated by integrating the instantaneous subduction rate at this interception point over the local permanent subduction period.

A particle is placed at the base of the mixed layer at each grid point at the time of the local maximum in mixed layer depth. The upstream trajectory of each particle is then calculated using the velocity field for the layer (k) immediately beneath the mixed layer at this time. The algorithm to calculate the horizontal advection of the particle is the Runge-Kutta scheme described in Chapter Three. The vertical position of the particle is easily determined when the layer is isolated from the mixed layer, the particle maintains a position that is a constant fraction of the layer thickness above the lower layer interface (see figure 4.7). However, where the mixed layer and layer k are in contact and can transfer water, the particle is assumed to maintain a constant distance from the lower

interface of layer k. The periods over which layer k is exposed to the mixed layer are short and so the errors introduced by this approximation are slight, with the notable exception of layer 2, the lightest isopycnic layer, which is not isolated from the mixed layer at any time. The velocities and layer depths and thickness are all derived by linear space and time interpolation. The data sets were available at six day intervals.

The upstream interception points for these particle are irregularly distributed, necessitating the interpolation of the times of interception (local end of permanent subduction) back on to the model grid. This is done using a Numerical Algorithms Group subroutine which uses nearest-neighbour triangulation to determine three data points which are then used to derive the time at the grid point the triangle contains. This produces a grid of times defining the end of local permanent subduction. Where grid points were not enclosed by three data points it is assumed that permanent subduction does not occur. The start of the permanent subduction period for each grid point is the time when the mixed layer begins to detrain water. The difference in the running integral of the instantaneous subduction rate (taken directly from AIM) between the start and end of the permanent subduction period is then used to determine the local permanent subduction rate per unit area. A basin-wide integral establishes the total permanent subduction rate.

The permanent subduction rate can be divided into the rate on to each isopycnic layer. This is done through examining the evolution of the mixed layer density over the permanent subduction period using linear interpolation and assuming that the water is placed on the first stable isopycnic layer.

A similar approach can be taken to determine the permanent entrainment period and rate through the downstream advection of particles to determine the start of the permanent entrainment period (figure 4.8). This permits the integration of the instantaneous subduction rate over the permanent entrainment period.

4.4.1 Results of the particle method for the Atlantic Isopycnic Model

The results for the Atlantic Isopycnic Model (AIM) show an ordered pattern of both permanent entrainment and permanent subduction. The region of permanent entrainment is found to extend from Cape Hatteras along the North Atlantic Current (NAC) and into the north-eastern Atlantic to the north of the British Isles and in the subpolar gyre (see figure 4.9). Other, less important entrainment areas are found in the tropics and in the Gulf of Mexico. The southern boundary of the permanent entrainment zone appears to follow a line running from Bermuda to the Bay of Biscay with a series of projections associated with isopycnic outcropping towards the eastern end. This southern boundary coincides with the zero net buoyancy flux line derived in Chapter Three. Over the Gulf Stream the entrainment period lasts for between 80 and 150 days with shorter entrainment periods near the southern edge of the zone and in meridional bands at 25°W and 50°W.

The permanent entrainment rate found by integrating the change in mixed layer depth over the permanent entrainment period is 44.3 Sverdrups (Sv). The integral of the instantaneous subduction rate is 59.4 Sv, indicating that the contribution of advection through the base of the mixed layer is important in the NAC. The contribution of Ekman pumping would be expected to be of minimal importance (see McWilliams, 1983). Permanent entrainment is concentrated at two points in the NAC (figure 4.10), one to the south-east of Cape Cod and the second further downstream to the south-east of Newfoundland where the depth of fluid permanently entrained is up to 350 metres per annum. These areas correspond to the longest permanent entrainment period. In the subpolar gyre permanent entrainment depths are far larger and appear to have a less ordered arrangement than in the NAC. The amount of fluid permanently entrained from each layer is shown in figure 4.11. This shows peaks in the permanent entrainment rate for layers σ=26.55 and 27.75 with a broad spectrum of subtropical mode waters entrained at rates in excess of 2 Sverdrups. The distribution of the permanent entrainment depth for layer σ=27.70 is shown in figure 4.12. This indicates that permanent entrainment from this layer occurs in a largely meridional band at rates of 250 metres per year with a broad area upstream where the permanent entrainment rates are

lower. The permanent entrainment regions for layers σ=26.40-27.30 are similarly arranged with the denser layers' entrainment regions placed further downstream in the NAC.

The region of subtropical permanent subduction lies to the south of the permanent entrainment zone with some overlap along the boundary (see figure 4.13). As with the entrainment zone, the boundary is found to coincide with the zero net buoyancy flux line found in Chapter Three. In the eastern basin, the boundary is composed of a series of projections. Permanent subduction is also found to occur in the subpolar gyre, the Gulf of Mexico, and in the tropics. The subduction period is short over most of the regions of permanent subduction, typically 10-20 days. Longer periods are found in the southern part of the subtropical gyre in the region of the return flow.

The permanent subduction rate found from the integral of the instantaneous subduction rate over the permanent subduction period is 58.8 Sverdrups. The permanent subduction is distributed as shown in figure 4.14. Along the northern edge of the subtropical permanent subduction region the permanent subduction rate can take values of up to 650 metres per annum. To the south of this narrow band the permanent subduction rate is 50-150 metres, while in the extreme south even lower rates are encountered.

The permanent subduction rate on to each layer is shown in figure 4.15. It will be seen that the peak subduction rates are found at densities σ=25.65, 26.70 and 27.75. The distribution of the permanent subduction on to layer σ=26.70 is shown in figure 4.16. This indicates that permanent subduction on to this layer occurs along its winter outcrop with most permanent subduction at the point where the winter outcrop intercepts the northern rim of the permanent subduction region.

4.4.2 Discussion of the particle method

The estimates of the permanent entrainment and subduction rates are in reasonable balance with each other, 59.4 Sv entrained against 58.8 Sv subducted. Both rates compare reasonably well with the tracer estimates, although it should be noted that they are higher than the advection-only component of the flow estimated by the kinematic

study of the following section. If the subtropical mode water masses in the range σ=25.80-27.30 are considered then the balance is slightly worse, 35.9 Sv entrained *vs.* 33.5 Sv subducted. This compares with permanent entrainment and subduction rates derived from the tracer method of 25.1 Sv and 29.4 Sv respectively.

Evidently the particle method over estimates both the permanent entrainment and permanent subduction rates in the subtropics. In the subpolar gyre both the permanent entrainment and subduction rates are under estimated, possibly because of the absence of thickness diffusion in the calculation of the particles' trajectories.

The over estimate of the rate of production of subtropical mode can be explained by the large instantaneous permanent subduction rate over the permanent subduction period. A small error in the length of the period is amplified by the large subduction rate to become a large error in the permanent subduction depth. In addition the use of linear time interpolation assumes that the changes in the mixed layer depth are well behaved; the results of Chapter Two, however, indicate that in the length of one model time step the mixed layer can detrain several hundred metres of water. This does not explain why the results should appear to be biased towards over-estimation.

4.5 The kinematic method

The kinematic method (Marshall, *et al.*, 1993) was described above in section 4.2 as the calculation of the water mass flux across the base of the seasonal thermocline. The calculation presented here determines $\overline{\mathbf{u}_H} \cdot \nabla H$, the lateral induction term in Eq.1.2, in an isopycnic framework. The vertical velocities which also appear in Eq.1.2 are included implicitly in this term since motion along sloping isopycnic surfaces necessarily includes a vertical component. The vertical motion of isopycnic surfaces themselves, 'heaving', is not included; the calculation of the integral of the isopycnic layer divergences in the seasonal thermocline is susceptible to large errors owing to the numerical truncation of the data generated by the model. It is assumed that after a sufficient spin-up time has elapsed the stratification of the permanent thermocline should be steady, and thus

'heaving' should make a small contribution to the mass flux into the permanent thermocline.

The contribution of lateral induction was further divided into the flux due to mean advection and that generated by the diffusion of isopycnic layer thickness. The mean velocities were derived from the model data sets which were produced at six day intervals during an AIM run of one year's duration. The velocity, $\mathbf{u}^*$, associated with the diffusion of layer thickness was generated from the model stratification at six day intervals. The two components of the velocity were then used to compute the two corresponding components of the mass flux at each velocity point in the model's C-grid. The flux across the base of the seasonal thermocline was then calculated;

$$S_{ijk} = \left(U_{ijk} + U^*_{ijk}\right)\left(f_{i+1jk} - f_{ijk}\right) + \left(V_{ijk} + V^*_{ijk}\right)\left(f_{ij+1k} - f_{ijk}\right) \qquad \text{Eq. 4.1}$$

where U_{ijk} and V_{ijk} are the x and y components of the mean mass flux and U^*_{ijk} and V^*_{ijk} are the x and y components of the thickness diffusion mass flux. The indices refer to the grid point (i,j) on the k-th layer with which the fluxes are associated. The variable f_{ijk} is the fraction of the layer k at grid point (i,j) lying within the permanent thermocline. The use of this fraction permits the vertical velocities to be included implicitly since a difference in f along an isopycnic surface could occur through the slope of the isopycnic surface or through variations in the depth of the seasonal thermocline.

The depth of the seasonal thermocline is calculated from the six-day data sets as the maximum depth of the mixed layer over the annual cycle and then smoothed with a 1-4-1 numerical filter. For each layer at each grid point S_{ijk} is divided out of (subduction, $S_{ijk}>0$) and into (entrainment, $S_{ijk}<0$) the seasonal thermocline and are added to the appropriate running time-integral to give a total annual permanent subduction depth and a permanent entrainment depth for each layer at grid point. By dividing the permanent entrainment and subduction rates regions where the mass flux across the base of the seasonal thermocline reverses over the annual cycle can be identified.

4.5.1 Results of the kinematic method in AIM

The results of the kinematic method described above are shown in figures 4.17 and 4.18. These show the permanent entrainment and permanent subduction rate for each model

grid point respectively. The total annual permanent entrainment rate on to all layers is found to be 129.4 Sverdrups and the permanent subduction rate is 127.8 Sverdrups. The imbalance of the two fluxes into and out of the seasonal thermocline is close to zero (1.3%), however, since this calculation does not include the fluxes due to vertical displacement of the isopycnic surfaces the imbalance cannot be entirely prescribed to the cumulative errors in the mass fluxes.

A comparison of the locations of permanent entrainment in fig.s 4.10 (particle method) and 4.17 shows that both methods indicate that permanent entrainment in the NAC is divided into two areas, although the areas indicated by the kinematic method are shifted slightly to the west relative to those in figure 4.10. This is due to the fast advection of particles in this region. Fig. 4.17 also indicates that the eastern area of subtropical permanent entrainment is divided into two sub-regions, a feature not seen in fig.4.10, whilst in the Gulf Stream fig.4.17 shows exceptionally strong permanent entrainment. Permanent entrainment in the subpolar gyre in the kinematic calculations is stronger and more widespread than found by the particle method.

Permanent subduction in fig. 4.18 occurs along the subduction front indicated by the particle method in fig. 4.14 with additional patches of strong permanent subduction in the Gulf Stream and NAC regions. It will be noted that the region of permanent subduction indicated in the NAC is coincident with the patch of low permanent entrainment observed in fig. 4.17.

A substantially improved estimate of the permanent entrainment and subduction rates is gained from the kinematic method if the calculation is constrained to certain areas. The method of Marsh & Roberts (1995) was to define the area over which to integrate the kinematic calculations as a simple parallelogram. Here the integration was constrained to only those regions where permanent entrainment/subduction had been found to occur by the particle method. This constraint results in a large reduction in the total permanent entrainment and permanent subduction rates; 58.8 Sverdrups and 58.1 Sverdrups respectively. The permanent entrainment rate from each isopycnic layer is given in fig. 4.19 and the permanent subduction rate on to each layer is given in fig. 4.20. It will be

noted that the magnitude and distribution of the subduction rates compare well with the rates estimated by the tracer method. The contributions of thickness diffusion to the permanent entrainment and subduction rates are 4.2 Sverdrups and 4.7 Sverdrups respectively, <10% of the total mass flux across the base of the seasonal thermocline.

4.5.2 Discussion of the kinematic method results

The kinematic estimate gives a permanent subduction rate of 58.1 Sverdrups which compares well with the tracer estimate, taken as 'truth'. This implies that the permanent subduction of mode waters in AIM is dominated by the advection of water by the mean velocity field, the contribution of thickness diffusion is of secondary importance, <10% of the advected flux. The close balance of the permanent entrainment and subduction rates implies that the estimate of 58.8 Sverdrups for the permanent entrainment rate is also accurate.

It will be noted that the result of the kinematic method is sensitive to the region over which the calculation is integrated. Marsh & Roberts used a kinematic method to derive a permanent subduction rate of 15.4 Sverdrups on to layers $25.80 \leq \sigma \leq 27.30$, this is far lower than the tracer estimate of 27.4 Sverdrups or the kinematic estimate presented here of 24.1 Sverdrups. The calculations of Marsh & Roberts (1995) include the contribution of the vertical displacement of isopycnic layers which would, in general add to the permanent subduction rate over the subtropical gyre. A possible cause of the lower values derived by Marsh & Roberts could be the integration over the annual cycle to find the net permanent entrainment/subduction rate at each grid point rather than the division of the kinematic fluxes into permanent entrainment and permanent subduction at each time step for each grid-point. This has not been confirmed, but should it prove to be the case it would suggest that there is variability in the model velocity fields over the annual cycle studied which is strong enough to reverse the sense of the mass flux.

4.6 The WSM method

The calculation of the permanent subduction rate by Williams, *et al.* (1995) was described in section 4.2. The three-dimensional trajectory of a particle in the model ocean basin is calculated over a one year period. The particle trajectory starts from a

point on the base of the mixed layer at the time of the mixed layer's maximum depth. Over the following winter the separation of the particle and the base of the mixed layer is monitored and the minimum separation is found. The minimum separation for each particle that is subducted is equated with the depth of the water permanently subducted up-stream at the particle's point of origin. It will be noted that implicit in the equation of the minimum separation and the subducted depth is the assumption of both limited vertical shear and limited divergence. Using a similar argument the permanent entrainment rate can be found by examining the minimum separation of a particle advected backwards, up-stream and the mixed layer base over the winter preceding the particle's entrainment.

The particle calculations described in section 4.3 also use the advection of particles in the thermocline to establish the permanent subduction and entrainment rates. The calculations described above were appended to the diagnostic code written to find the time at which the permanent entrainment period started and when the permanent subduction period ended.

4.6.1 Results of the WSM method

The permanent entrainment and permanent subduction rates derived by this method for the AIM basin are shown in figures 4.21 and 4.22 respectively. The total permanent entrainment rate was found to be 22.9 Sverdrups over all layers, while the permanent subduction rate was found to be 21.1 Sverdrups. While it is possible to divide these fluxes between the isopycnic layers no attempt was made to do so. It will be noted that while these mass fluxes balance reasonably well they are significantly lower than the other three estimates presented above. The permanent subduction rate along the northern rim of the subtropical gyre reaches peak values of 250 metres compared to the peak estimates of ~600 metres from the particle and kinematic methods. Similarly the estimates of the permanent entrainment rate are also less than the corresponding estimates by the particle and kinematic methods. This will be discussed below.

4.6.2 Discussion of the WSM method

The WSM method appears to under-estimate the permanent entrainment and subduction rates in AIM by approximately 50% when compared to the particle and kinematic estimates, and by approximately 67% when compared to the tracer estimates. The size of this discrepancy is possibly due to divergence in the mass flux on the ventilated layer, k in the notation of Chapter Three. The divergence would flatten and broaden the recently formed mode water mass thus reducing the minimum separation depth. However, while changes in the thickness of the k-th layer do not influence the buoyancy budget in Chapter Three (buoyancy was referred to the k-th layer) it is difficult to imagine that such a strong divergence could leave the buoyancy content of the upper k-1 layers unaffected. It is possible that the divergence is due to the quasi-geostrophic dynamics of the seasonal thermocline relaxation from the spring restratification, *e.g.* through the radiation of Rossby waves, however without more information this remains speculative.

4.7 Discussion of permanent entrainment and permanent subduction in AIM

In this section the description of permanent subduction in the AIM basin derived from the estimates given above will be compared with other models of the North Atlantic and values derived from field measurements.

The values of three estimates of permanent subduction in AIM (tracer, particle and kinematic methods) for each isopycnic layer are shown in figure 4.23. This figure shows that the three methods also demonstrate the production of a class of subtropical mode waters in the range $26.40 \leq \sigma \leq 27.00$ with the peak in the mode water production close to $\sigma=26.55$. The particle and tracer methods also indicate that the model produces large quantities of $\sigma=27.75$ water, the model equivalent of Labrador Sea Water.

The permanent subduction of subtropical mode water is balanced by permanent entrainment in the NAC, and to a lesser extent in the sub-polar gyre. This balance of the permanent entrainment and subduction rates shows that the model is not in thermal equilibrium with its forcing. The longer permanent entrainment period indicates the

asymmetry of the mixed layer cycle, a long descent of the mixed layer base in autumn and winter followed by rapid restratification in spring.

Through the use of the kinematic method and the parallel tracers runs with and without isopycnic tracer diffusion the permanent subduction rate for AIM can be divided into component fluxes due to mean advection, thickness diffusion, isopycnic diffusion and a residual composed of cumulative errors in the other three components and the vertical flux due to displacements of the isopycnic layers. The results of this budget are shown in figure 4.24. It is clear that on most layers mean advection is the single most important source of permanent thermocline waters with thickness diffusion playing a secondary role. The large negative residual for permanent subduction on to isopycnic layer σ=27.75 indicates that the kinematic estimate of 23.4 Sverdrups for the permanent subduction rate is far too high.

The relative unimportance of both isopycnic and thickness diffusion in the transport of thermocline waters in AIM can be further demonstrated by the high Péclet numbers (Pé=UL/κ) in the AIM thermocline, between 66 and 240 for the sub-tropical isopycnic layers σ=26.40-27.30. These values of the Péclet number are higher than the lower limit of the advection-dominated regime identified by Jia & Richards (1994) at Pé=20. The dominance of advection in AIM is thought to be due to the high velocities encountered in the model thermocline. Thus the absence of thickness diffusion in the Lagrangian particle method should not cause too great an error. It has already been shown that the diffusion of tracer along isopycnic surfaces is not of great relevance to permanent subduction in AIM.

4.7.1 Permanent entrainment and subduction period

Studies of the permanent subduction and entrainment periods in the subtropical North Atlantic have been undertaken by Marshall, *et al.* (1993) from climatological data sets and by Williams, *et al.* (1995) from the CME model. Both of these results produce a boundary between the permanent entrainment and permanent subduction zones which runs from Bermuda to Biscay, although the path of this line is rather convoluted to the south-east of Newfoundland in the result produced by Marshall, *et al.*. The convolution

could either arise through an inadequate sampling of the hydrography in a region of strong variability or through the implicit inclusion of phyical processes in the hydrography (*e.g.* eddy processes, see McWilliams, 1983) which are poorly represented in both the CME and AIM models.

The permanent entrainment period found by Williams, *et al.* over the Gulf Stream lies between 90 and 120 days with a small area west of Cape Cod where the duration rises to 150 days. This compares favourably with the estimates presented above for a permanent entrainment period of between 70 and 140 days. The result derived by Marshall, *et al.* (1993) gives a longer period, up to 240 days to the south of Newfoundland. Again, the difference is a possible result of the hydrographic sampling in the Gulf Stream and NAC or the poor representation of some physical processes in the ocean models.

The permanent subduction periods found by Marshall, *et al.* give a duration of between 30 and 60 days along the northern edge of the permanent subduction zone with longer durations found in the southern parts of the gyre. Williams, *et al.* find a shorter duration than Marshall, *et al.* over most of the gyre, and demonstrate a region of longer permanent subduction periods in the westward intensification. However, the result of Williams, *et al.* is longer than the results derived above from AIM, ~30 days in the CME model compared to ~15 days in AIM. It is not possible to state whether the differences between the CME model and AIM are a result of different model formulations or the differing surface boundary conditions. It has been noted that the mixed layer retreat in MICOM is much faster than observed (Bleck, *et al.*, 1989), but this was presumed by the authors to be from the lack of storm forcing in spring. The brevity of the permanent subduction period has been noted by both Marshall & Marshall (1994) and Williams, *et al.* (1995). The findings presented above for AIM concur with their results and suggest that the Ekman demon proposed by Stommel (1979) acts efficiently to censor the waters entering the permanent thermocline in AIM.

4.7.2 Geographical distribution of permanent entrainment and subduction

The permanent entrainment and subduction rates per unit area of the North Atlantic have been calculated by numerous authors using the kinematic method. Marsh & Roberts

(1995) calculated the permanent entrainment/subduction rates for AIM and the Hadley Centre ocean model, Marshall, *et al.* (1993) studied climatological data sets, and Williams, *et al.* (1995) examined the data produced by the CME model of the North Atlantic. In all four studies a band of strong subduction is observed to run between Bermuda and Biscay, similar to the band found above. In Marshall, *et al.* (1993) this band is found to be diffuse. This is probably the result of smoothing implicit in climatological data.

The results of Williams, *et al.*, Marsh & Roberts and sections 4.4 and 4.5 show the same distribution of permanent subduction, a band from Bermuda to Biscay. Over most of the subtropical permanent subduction zone the permanent subduction rate is ~50m yr^{-1}, comparable to the Ekman pumping rate. Along the northern edge of the subtropical zone rates of ~300m yr^{-1} are found by Williams, *et al.* and Marsh & Roberts with the highest subduction rates found to the south of Newfoundland. This is lower than the peak subduction rate of ~600m yr^{-1} found in sections 4.4 and 4.5. The band of high permanent subduction in the subtropical gyre is consistent with strong lateral induction. In all three models (AIM, CME and the Hadley Centre model) this band coincides with a steep gradient in the depth of the seasonal thermocline. As demonstrated in Chapter Three this also coincides with the zero net buoyancy flux line, as predicted by Woods & Barkmann (1986a).

Permanent entrainment is found to occur in the Gulf Stream in all three models, and it also occurs in the analysis of climatological data by Marshall, *et al.* (1993). One important difference is that in both of the analyses of Marsh & Roberts and in that of Marshall, *et al.* there is an area of permanent subduction in the Gulf Stream to the immediate south or south-east of Newfoundland whereas neither particle nor tracer studies indicate permanent subduction. The apparent subduction is a result of undulations in the base of the seasonal thermocline and it is most probable that the water 'subducted' here is re-entrained further down-stream over time scales much shorter than the seasonal. This undulation causes a reduction in the permanent entrainment rate derived in section 4.4 in this region, but it does not produce permanent subduction. No permanent subduction in the Gulf Stream is observed by Williams, *et al.*.

The permanent entrainment rates observed in the studies of Marsh & Roberts are of the order 300 m yr^{-1}, comparable to the result of Marshall, *et al.*. Williams, *et al.* derive a lower rate of ~200 m yr^{-1} over the Gulf Stream with higher values found to the north of 50 °N. The particle method of section 4.4 produces permanent entrainment rates of ~350 m yr^{-1} over the Gulf Stream.

4.7.3 Water mass renewal rates

The rate at which the water masses of the North Atlantic are produced has been studied by numerous authors (see section 4.2). The North Atlantic water masses can be divided into two main groups, the subtropical mode water masses (*e.g.* 18°C) and the subpolar mode water masses (*e.g.* Labrador Sea Water). Each of these groups is dealt with separately below and tabulated in Table 4.1.

Author(s)	Method	Water mass	Subd. rate	Comments
Tracer method, Section 4.5	Ventilation tracer	σ=25.8-27.0 σ=27.15-27.45 σ≥27.60	22.5 Sv 5.9 Sv 31.6 Sv	AIM
Woods & Barkmann, 1986a	Mixed layer model ensemble	Subtropical mode waters	14.3 Sv	errors of ±50Wm^{-2} in the heat fluxes
Speer & Tziperman, 1992	Divergence in mass transformations	σ=26.0-27.0 σ=27.2-28.0	14.1 Sv 16.7 Sv	Errors in surface fluxes ?
Marsh & Roberts, 1995	Kinematic method	σ=25.80-27.30	15.4 Sv 20.6 Sv	AIM Hadley Centre
McCartney & Talley, 1982	Volumetric survey	Subpolar mode water	10.5 Sv	
McCartney & Talley, 1984	Water mass conversion	Subpolar mode water	14.1 Sv	
Wright, 1972	Volumetric survey	Labrador Sea Water	3.2 Sv	
Clarke & Gascard, 1983	Tracer study	Labrador Sea Water	3.9 Sv 7.8 Sv	without diffusion with diffusion[1]
Sarmiento, 1983a	Tracer study	σ=26.2-27.4 σ=26.2-27.0	39.5 Sv 27.4 Sv	Best current estimate ?

Table 4.1: A comparison of various estimates of the permanent subduction rate in the North Atlantic

It will be noted that the AIM tracer result is closest to the permanent subduction rate derived by Sarmiento (1983a), although the result is still much lower than the rate derived for the North Atlantic subtropics.

[1] McCartney & Talley, 1984

The distribution of production among the subtropical water masses is found to be a bell-shaped curve by Speer & Tziperman (1992) with a peak subduction rate found at σ=26.55. The AIM result of Marsh & Roberts (1995) produce a similar curve with a peak at the same value of σ. However, the Hadley Centre model produces water masses in three distinct classes with little permanent subduction occurring in the other subtropical density classes. The AIM tracer result produces a bell-shaped curve with a peak at σ=26.55, and a second peak at σ=25.65. This second peak arises through the large area covered by the model in the Tropics where this layer, the lightest in the model, receives all detrained water.

The subduction rate derived by Sarmiento for the denser classes of subtropical mode water (σ>26.9) is much greater than those found in other models. In Marsh & Roberts and Speer & Tziperman little water is subducted in the range 26.9<σ<27.1. In this range AIM tracer results suggest that ~2 Sv are subducted over an interval $\Delta\sigma$=0.15 while Sarmiento finds ~3 Sv subducted over $\Delta\sigma$=0.1.

The production of subpolar mode water masses has been estimated as 16.7 Sv by Speer & Tziperman (1992) over the density range 27.1<σ<28.0. Their study inferred a peak production of ~6 Sv of σ=27.6 water, approximately the density of Labrador Sea Water. The production of mode waters is again distributed in a bell-shaped curve, as the same authors found for the subtropical mode waters. McCartney & Talley (1982) find a production rate of 10.5 Sv for water masses of densities greater than σ=27.5 while McCartney & Talley (1984) used a method similar to that of Speer & Tziperman to derive a total of 14.1 Sv of subpolar mode waters produced, of which 8.5 Sv are Labrador Sea Water. This value is much higher than the estimated 3.9 Sv by Clarke & Gascard (1983) from tritium studies. However, if mixing is included in the Clarke & Gascard result then the production rate of Labrador Sea Water is 7.8 Sv (McCartney & Talley, 1984).

The tracer studies of the AIM subpolar mode water masses indicate that unlike the AIM subtropics, waters produced in the AIM subpolar gyre are placed in a narrow density

class, σ=27.75, the model equivalent of Labrador Sea Water. This layer receives 17.5 Sv of subducted fluid over the year, far higher than any of the above estimates of Labrador Sea Water production and the model does not include the mixing of water masses in the thermocline. Furthermore the site of production is to the south-east of the Labrador basin. The errors in the AIM result may be, in part, due to the poor vertical resolution that all isopycnic models have in subpolar regions although vertical resolution in the subpolar gyre of Boxmix has been found to have only slight influence on the depth of winter mixing (M.M.Lam, personal communication). Also, the model does not include any parametrisation of deep convecting plumes, thought to be important in this region. It should be noted that the spin-up time used in the AIM model is not long enough for the thermohaline circulation to adjust to the model boundary conditions.

4.8 Summary

It has been demonstrated that the particle method described in Section 4.3 can reproduce the distribution of permanent entrainment and permanent subduction derived by the kinematic method. In addition, the particle method does not indicate regions of permanent subduction where none would be expected to occur and the permanent subduction/entrainment rates per unit area are similar to those of the kinematic method, although the permanent entrainment rates in the Gulf Stream are slightly higher. The duration of the permanent subduction period is short, ~15 days, while the permanent entrainment period is much longer, 70-140 days. This indicates the asymmetry of the annual mixed layer cycle and the efficiency of the Ekman demon.

The particle method, however, does not give an accurate estimate of the subtropical permanent subduction rate (where the tracer method is taken as 'truth'). This is possibly due to the brevity of the permanent subduction period. The particle method also over estimates the permanent entrainment rate in the subtropics by approximately 10 Sv.

The permanent entrainment/subduction rate and period in AIM compare favourably with the results of the CME and Hadley Centre models, both of which are traditional depth-coordinate models. Comparison of the AIM results with estimates derived from

climatological data sets and tritium studies show that AIM reproduces the water mass production well in the subtropics, but is an unrealistically prolific producer of Labrador Sea Water. This appears to be a problem inherent to the MICOM formulation (see Chapters Five and Six).

Comparison of the AIM tracer runs with the results of the kinematic methods shows that the permanent subduction of mode waters in AIM is dominated by the advection of water into the permanent thermocline by the mean velocity field. The contribution of the eddy mass flux, represented by thickness diffusion makes a smaller, but significant contribution. Isopycnic eddy diffusion makes only a slight contribution to the permanent subduction rate. The contribution of vertical velocities to the permanent subduction rate has not been calculated and is therefore included with the errors in the other estimates in the residual term. Assuming that the errors are small, the contribution of vertical displacement to the permanent subduction rate is small, 12.3% overall.

Of the methods examined, only the tracer method can include the fluxes due to tracer diffusion. In the study of AIM presented in this chapter and in Chapter Three it is apparent that the ventilation of the thermocline in AIM is dominated by advection, the fluxes due to diffusion are of slight importance. Consequently the estimates derived by the tracer, kinematic and particle methods are is reasonable agreement. However, as will be shown in the following chapter, the tracer diffusion flux into the permanent thermocline can make a substantial contribution to the permanent subduction rate. Thus the use of the kinematic and particle methods will produce substantially lower estimates of the permanent subduction rate.

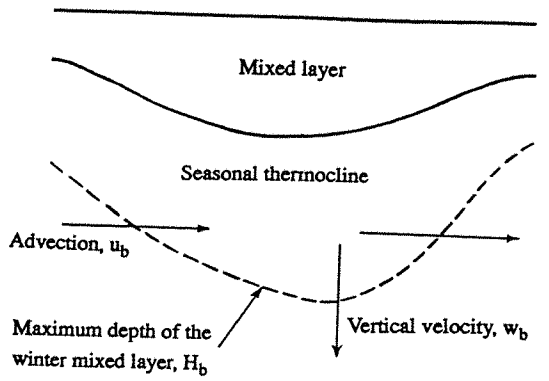

Figure 4.1: A schematic diagram of the kinematic method of determining the permanent subduction rates. The method calculates the flux through the base of the seasonal thermocline from its two components; u_b.grad $H_b + w_b$, where u_b is the horizontal velocity at the base of the seasonal thermocline, H_b is the depth of the seasonal thermocline and w_b is the vertical velocity at the base of the seasonal thermocline.

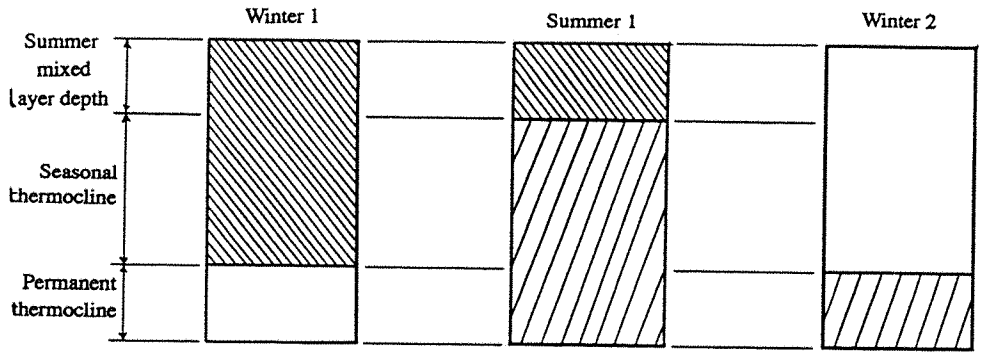

Figure 4.2a: A schematic diagram showing the seasonal cycle of mixed layer depth in a one-dimensional two layer isopycnic ocean. The shading shows the ventilation tracer concentration. The tracer is initially only found in the mixed layer until the Spring restratification, whereon tracer is deposited on the interior layer. It is immediately mixed (owing to the assumption of vertical homogeneity of all properties on isopycnic layers) and thus in the following winter some of the ventilation tracer remains below the mixed layer. This implies a permanent subduction rate.

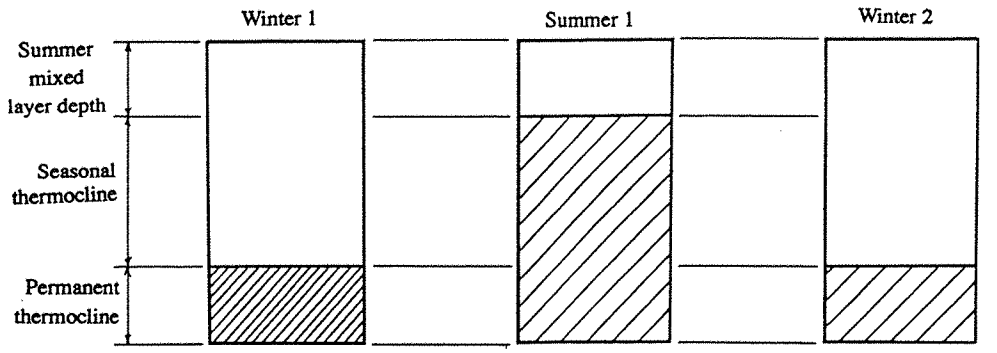

Figure 4.2b: A schematic diagram showing the seasonal cycle for the mixed layer in a one-dimensional two layer isopycnic ocean. The shading here shows the concentration of ventilation tracer. Initially the tracer is entirely contained by the permanent thermocline. However, after the Spring restratification the tracer is immediately diffused in the newly detrained water and so during the next winter tracer is entrained by the mixed layer. This gives an implied permanent entrainment rate.

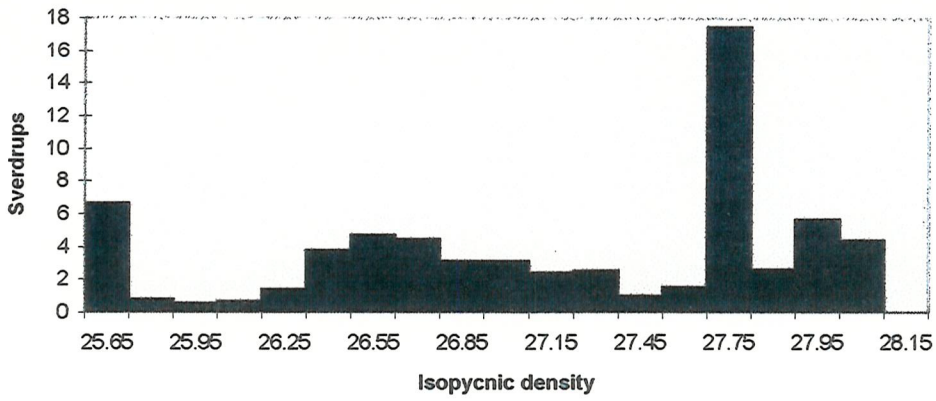

Figure 4.3: A bar graph of the annualised permanent subduction rate in AIM calculated from the volume of tracer remaining in the model thermocline after eighteen months of a model tracer run. The rates are given in Sverdrups. For the first twelve months the ventilation tracer concentration in the mixed layer was set to one and tracer was permitted to enter the thermocline through detrainment. In the following six months the mixed layer concentration of ventilation tracer was re-set to zero and the thermocline tracer left at its previous values and permitted to be advected and diffused for the remainder of the run. The results are shown for two model runs; the first with the tracer advected by both mean and 'thickness diffusion' mass fluxes and diffused by isopycnic tracer diffusion. In the second run the tracer was only advected, no isopycnic tracer diffusion was used to disperse the tracer.

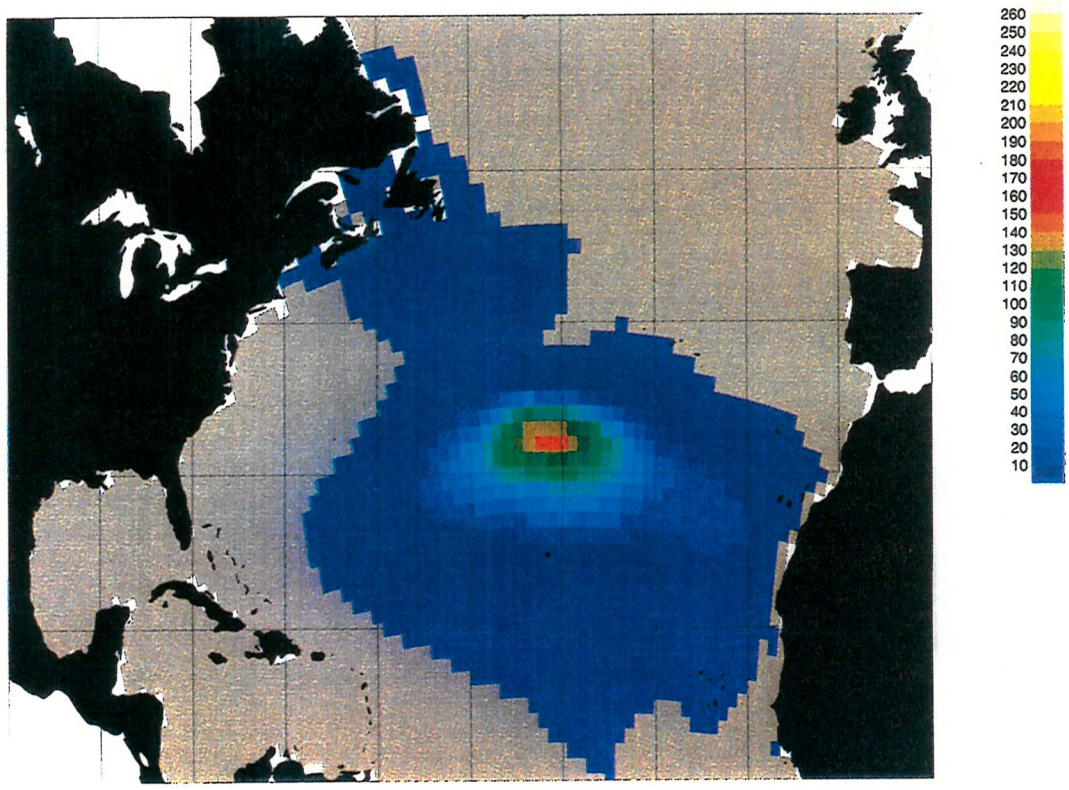

Figure 4.4: A plot showing the tracer 'depth' in metres (tracer concentration x layer thickness) for isopycnic layer σ=26.70 eighteen months after the tracer was first introduced to the model mixed layer and six months after the second Spring restratification of the run, The plot is constructed on the Mercator projection.

Figure 4.5: A bar graph of the annualised permanent entrainment rates calculated from the tracer estimates of the permanent subduction rates in Figure 4.14 and the observed change in the layer volumes between successive winters. The rates are given in Sverdrups.

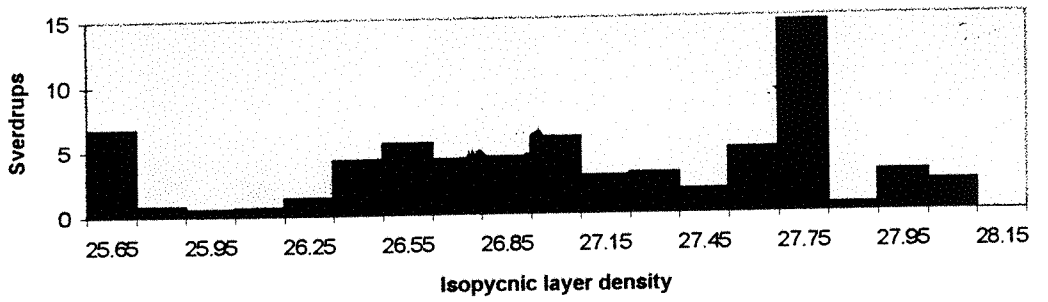

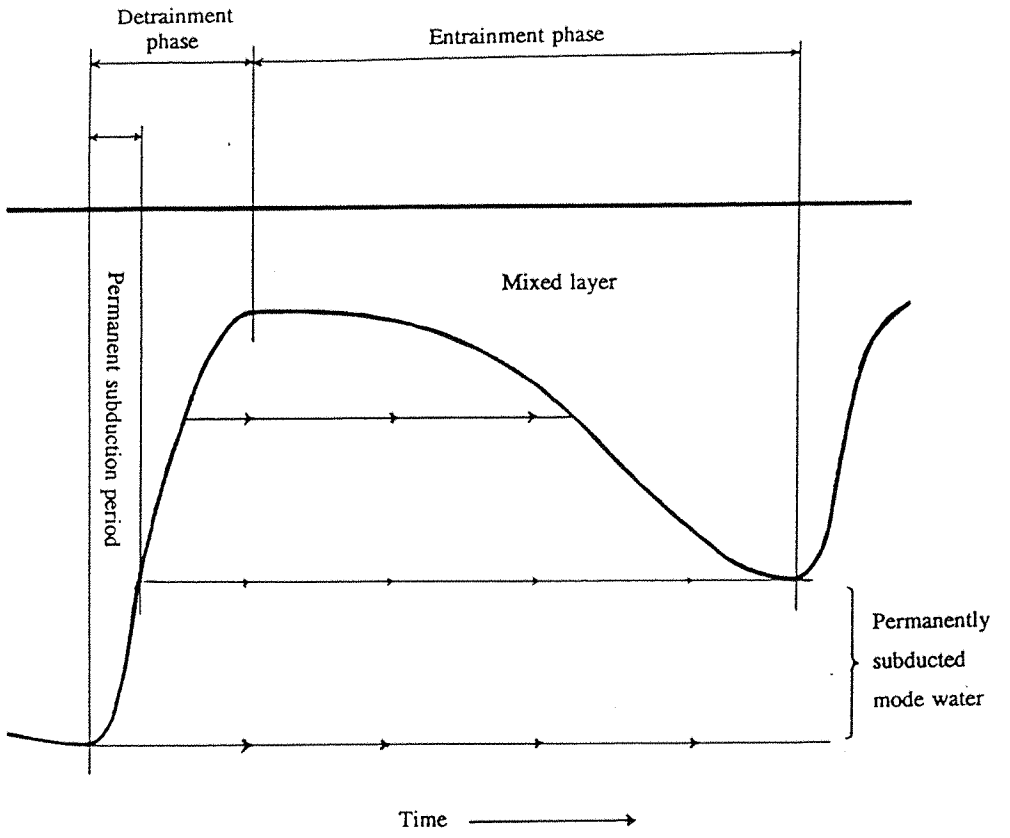

Figure 4.6: A schematic diagram showing permanent subduction by lateral induction in the equatorward flowing arm of an ocean gyre. The diagram shows the variation in the mixed layer depth over one annual cycle for a water column advected equatorward across the zero net surface buoyancy flux line. Time progresses toward the right. The trajectories of subducted water masses are shown.

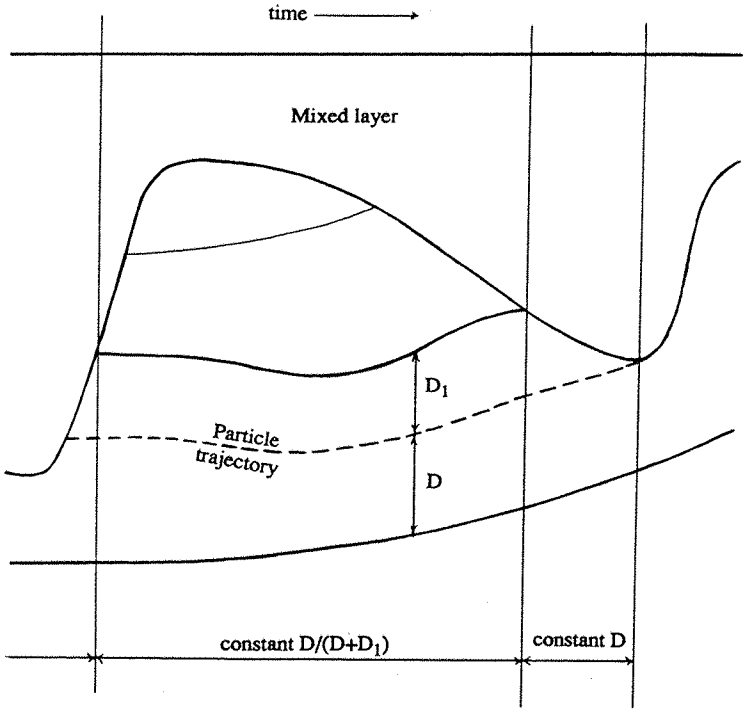

Figure 4.7: A schematic diagram showing the trajectory of a particle which skims the base of the seasonal thermocline during the second winter. The plot is shown in a Lagrangian framework with the particle in the equatorward flowing arm of a gyre. The depth of the particle in the water column is determined such that the particle maintains its position at a constant fraction $(D/(D+D_1))$of the layer thickness other than where the layer followed is exposed to the mixed layer where the particle maintains a constant distance (D) from the lower layer interface.

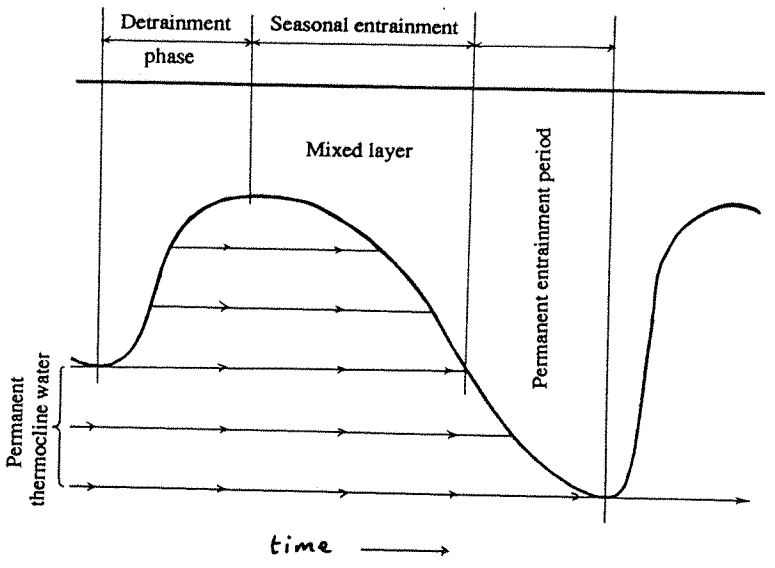

Figure 4.8: A schematic diagram of permanent entrainment in a poleward flowing arm of a gyre. The diagram shows the variation in mixed layer depth over one annual cycle for a water column in a Lagrangian framework. Time progresses to the right. The trajectories of particles in the thermocline are show to illustrate the processes of entrainment and permanent entrainment.

Figure 4.9: A plot of the permanent entrainment period calculated for the AIM basin between 10 and 60 degrees North by the particle method. The plot is constructed in the Mercator projection and shows the permanent entrainment period in days. The distortion of the grid arises from the use of a model grid that is regular in a rotated Mercator projection.

Figure 4.10: A plot of the permanent entrainment depth (rate per unit area) calculated for the AIM basin between 10 and 60 degrees North by the particle method. The plot is constructed in the Mercator projection and shows the permanent entrainment depth in metres. The distortion of the grid arises from the use of a model grid that is regular in a rotated Mercator projection.

Figure 4.9:

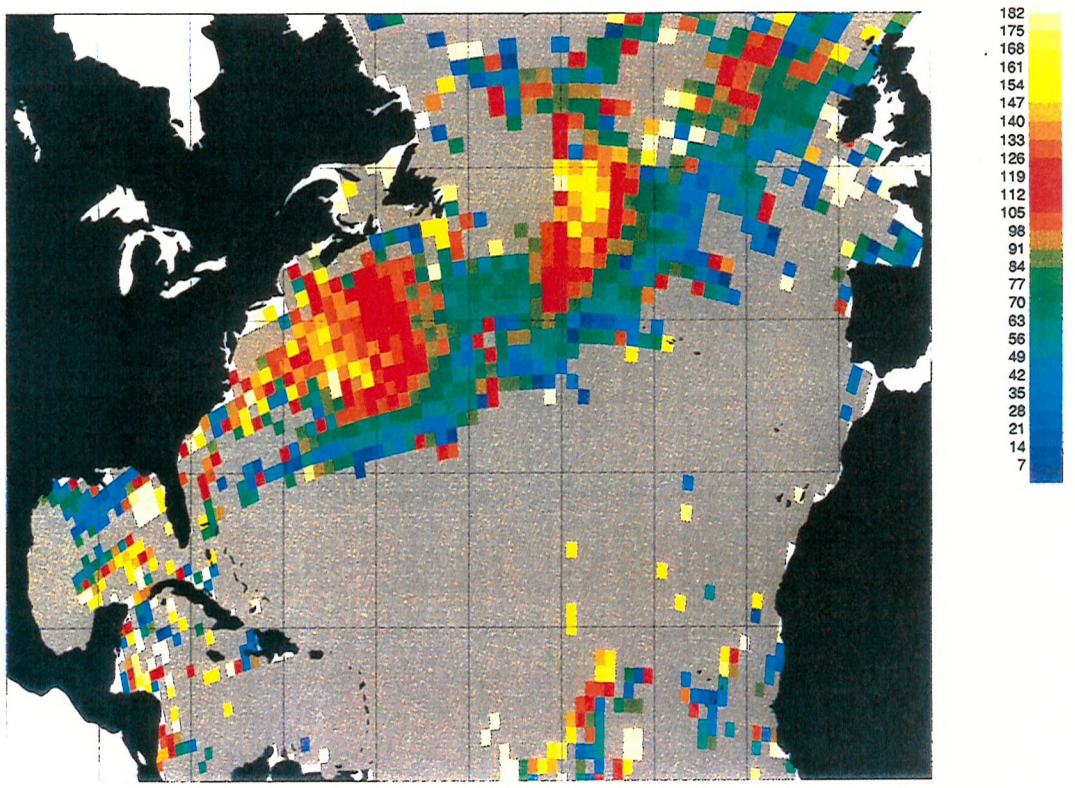

Figure 4.10:

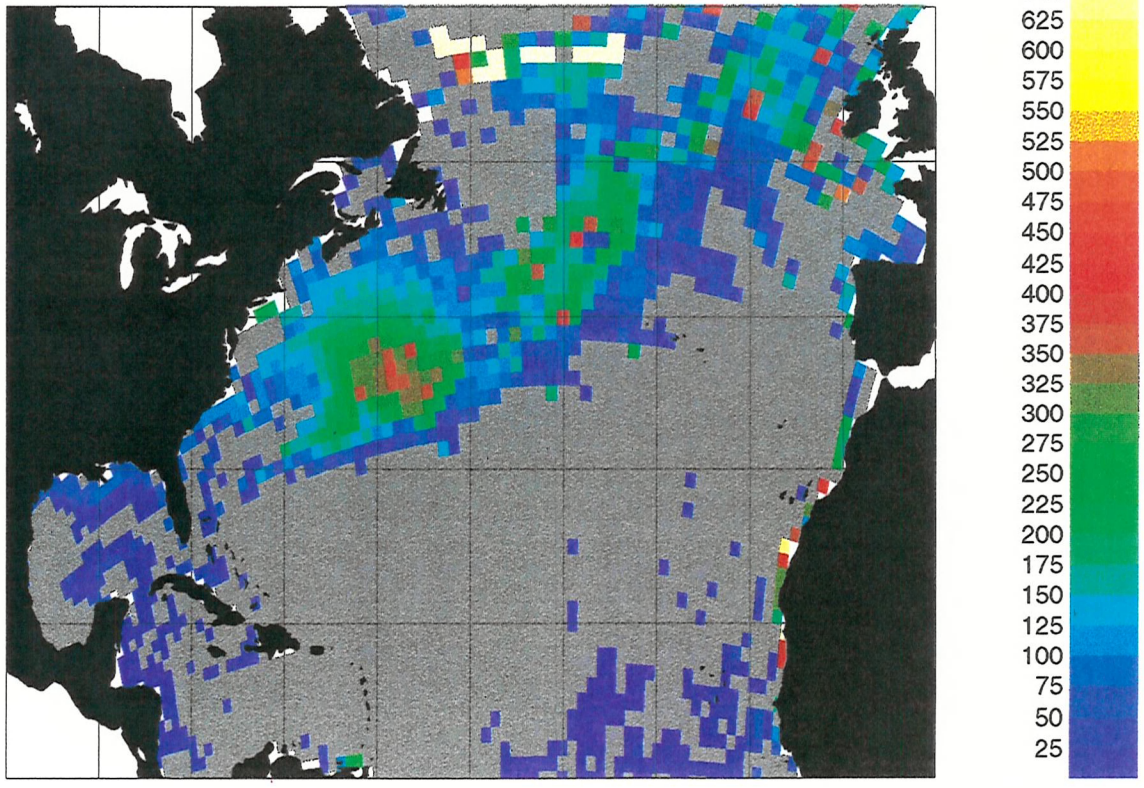

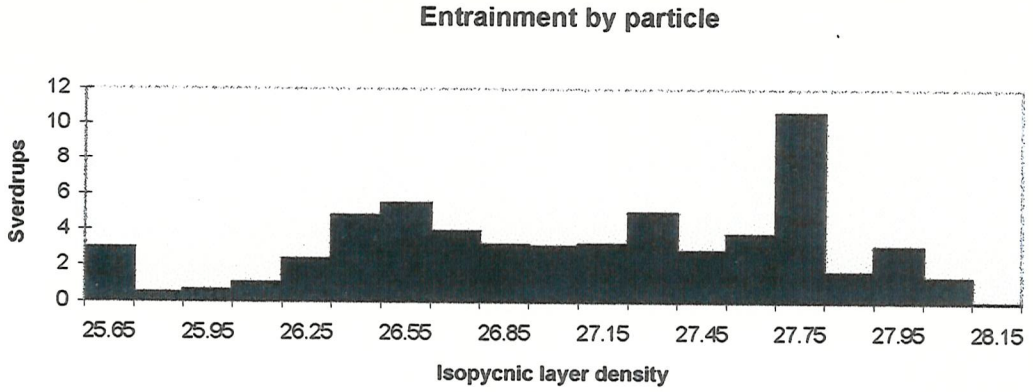

Figure 4.11: A bar graph of the annualised permanent entrainment rate from each of the isopycnic layers in AIM. The rates are given in Sverdrups ($10^6 m^3$) and the layer densities are given in σ-units.

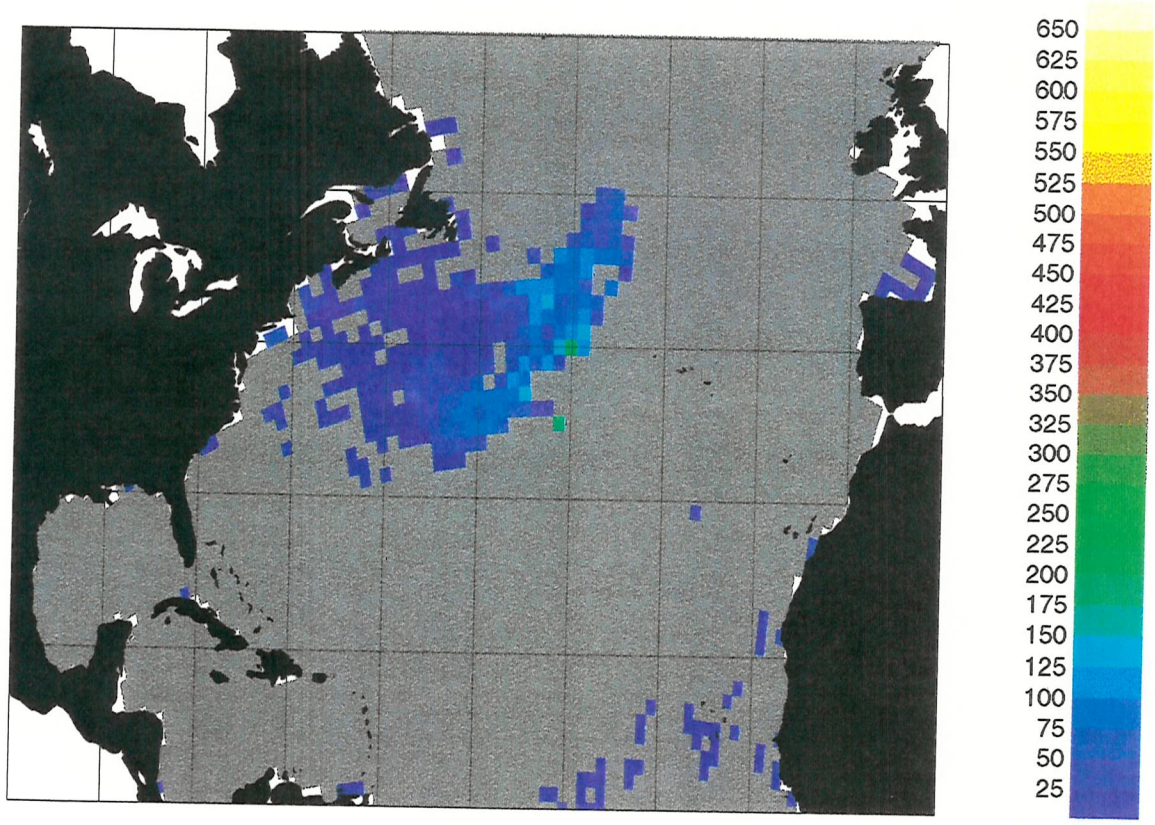

Figure 4.12: A plot of the depth of water permanently entrained from AIM isopycnic layer σ=26.70 between 10 and 60 degrees North. The plot is constructed on the Mercator projection and shows the permanent entrainment depth in metres. The distortion of the grid arises from the use of a model grid that is regular in a rotated Mercator projection.

Figure 4.13: A plot of the permanent subduction period calculated for the AIM basin between 10 and 60 degrees North calculated by the particle method. The plot is constructed on the Mercator projection with the permanent subduction period in days.

Figure 4.14: A plot of the permanent subduction depth (rate per unit area) for the Aim basin between 10 and 60 degrees North calculated by the particle method. The plot is constructed on the Mercator projection with the permanent subduction depth presented in metres.

Figure 4.13:

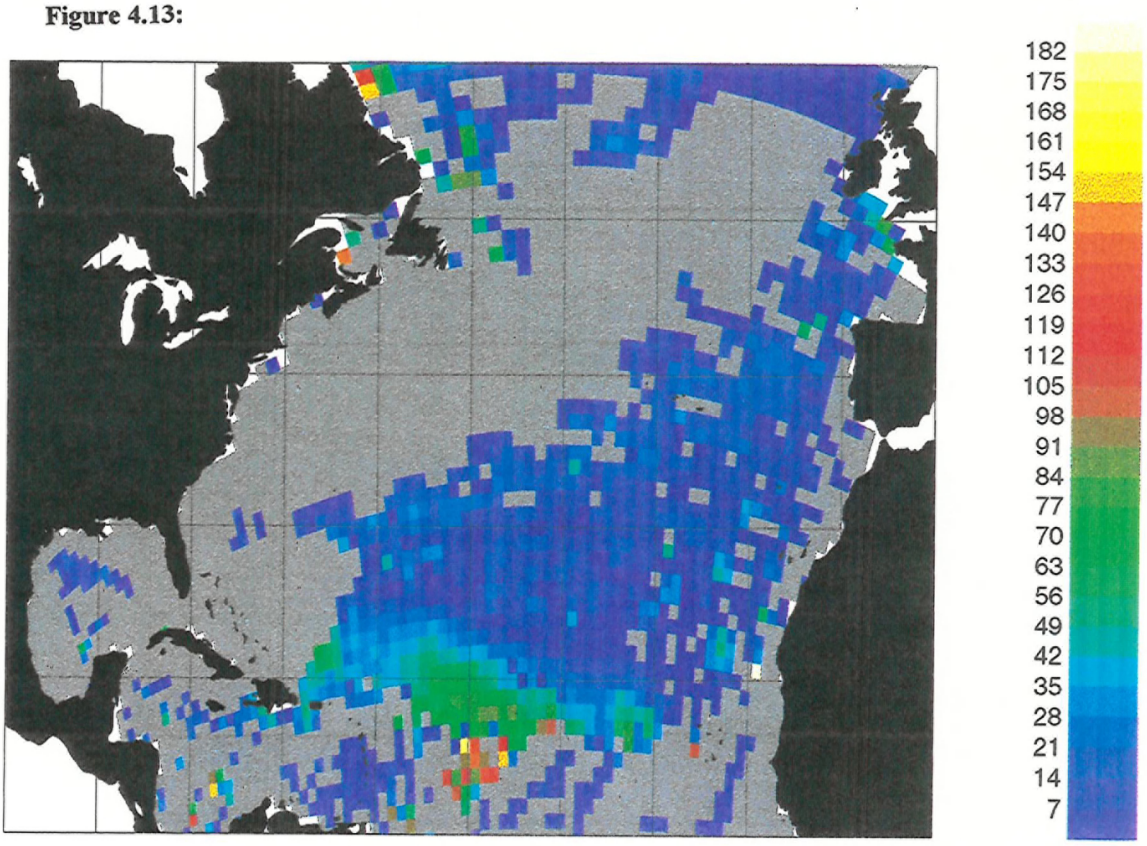

Figure 4.14:

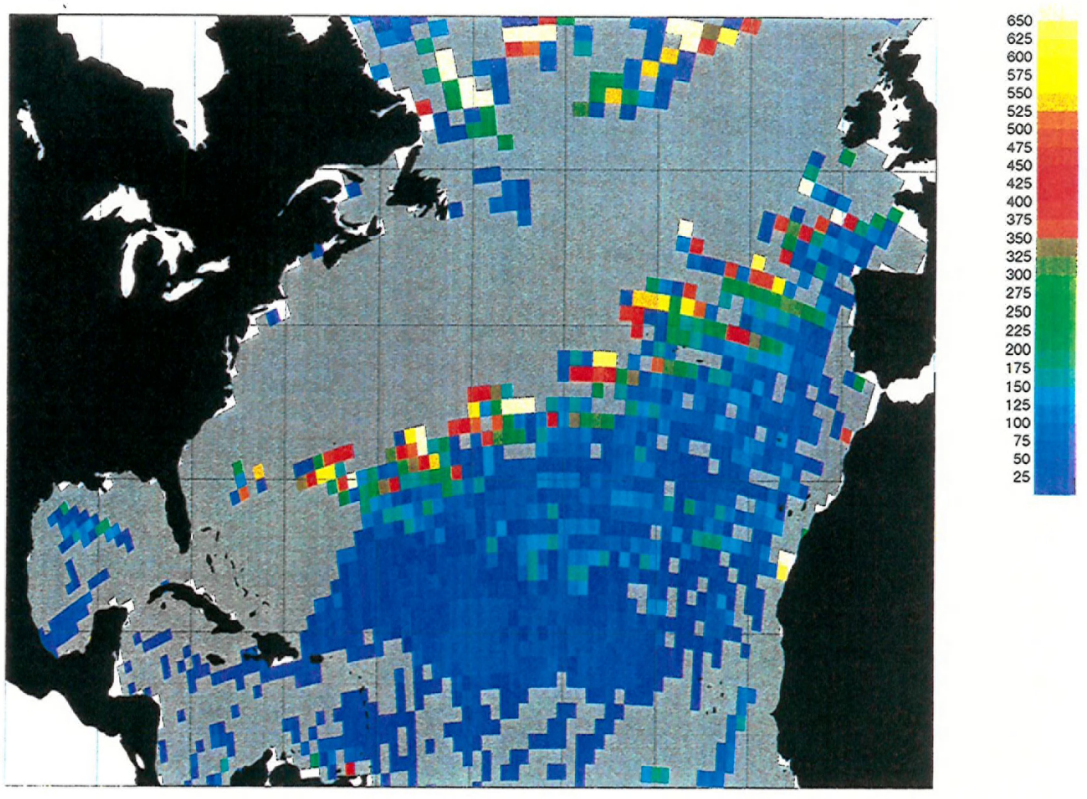

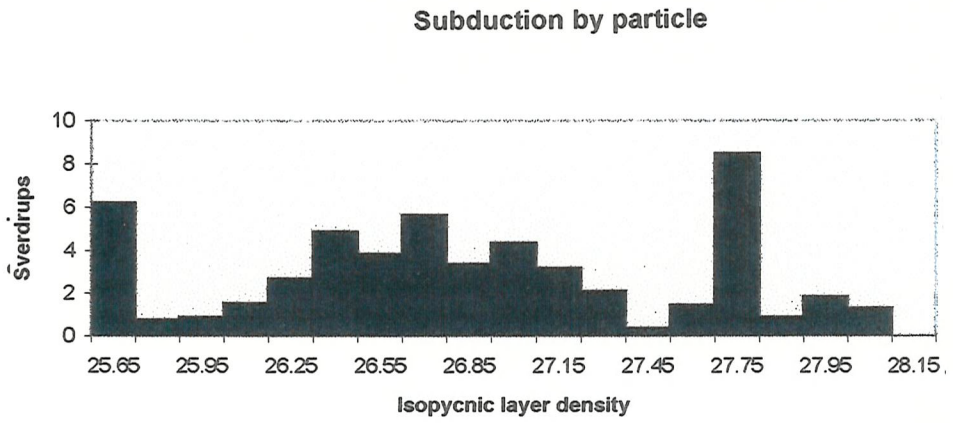

Figure 4.15: A bar graph of the annualised permanent subduction rate on to each of the isopycnic layers in AIM. The rates are given in Sverdrups ($10^6 m^3$) and the layer densities are given in σ-units.

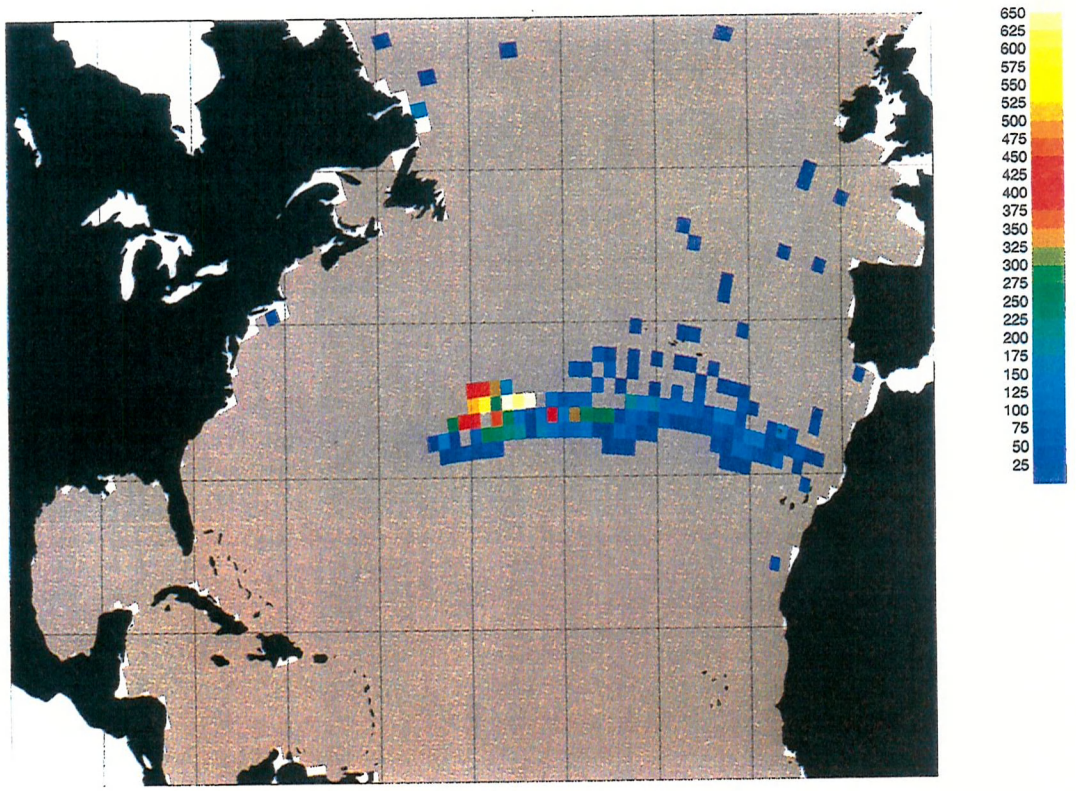

Figure 4.16: A plot of the depth of water permanently subducted on to the AIM isopycnic layer σ=26.70 between 10 and 60 degrees North. The plot is constructed on the Mercator projection and shows the permanent subduction depth in metres. The distortion of the grid arises from the use of a model grid that is regular in a rotated Mercator projection.

Figure 4.17: The permanent entrainment depth (rate per unit area) for the whole AIM domain calculated by the kinematic method. The permanent entrainment depth is given in units of metres. The plot is presented in the Mercator projection for the latitudes 10°-60°N.

Figure 4.18: The permanent subduction depth (rate per unit area) for the whole AIM domain calculated by the kinematic method. The permanent subduction depth is given in units of metres. The plot is presented in the Mercator projection for the latitudes 10°-60°N.

Figure 4.17

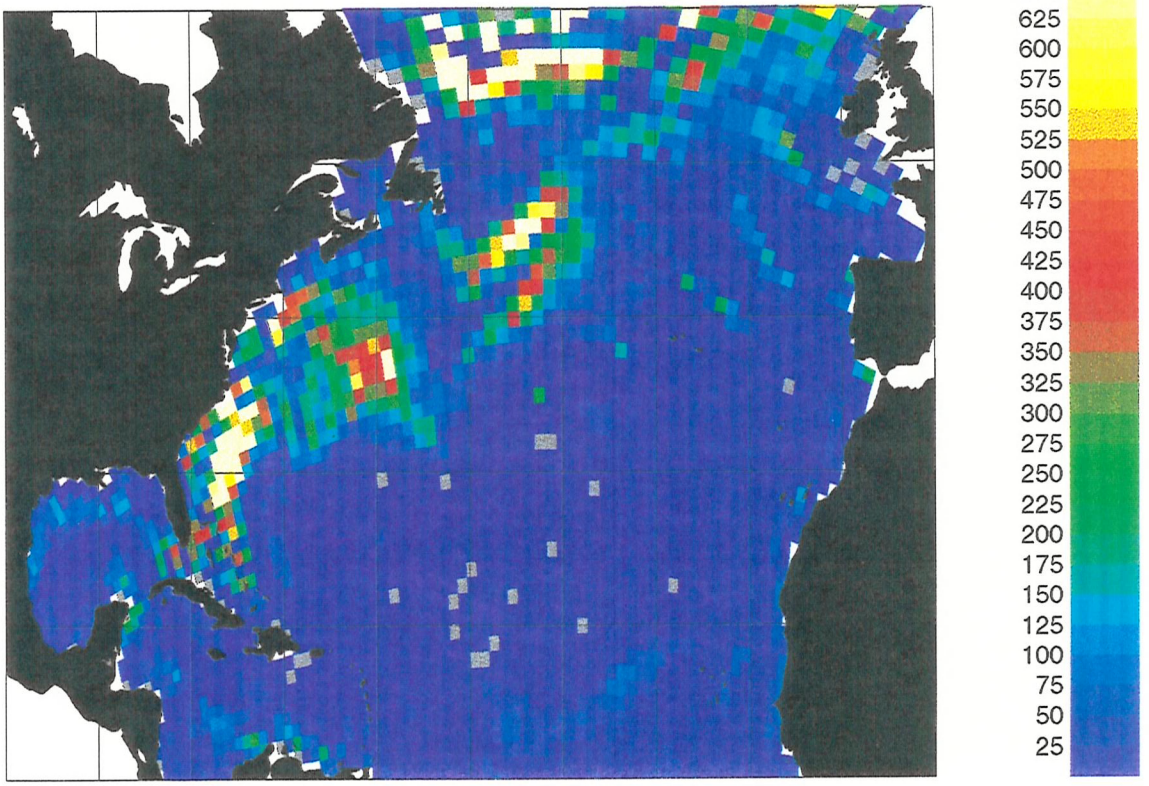

Figure 4.18

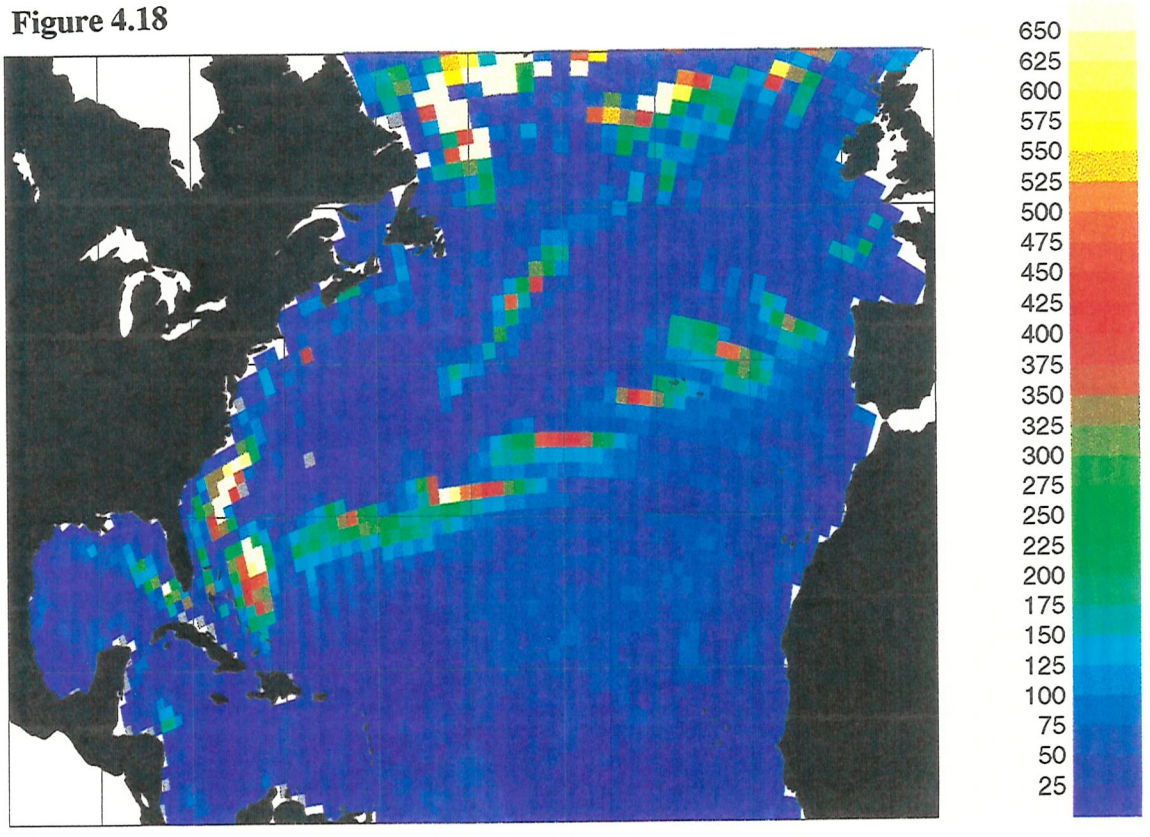

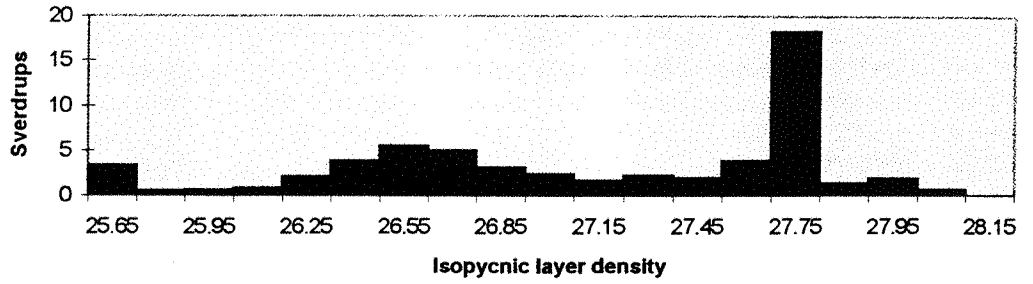

Figure 4.19: A bar graph showing the permanent entrainment rate for each isopycnic layer in AIM, calculated over the area where permanent entrainment was diagnosed by the particle method.

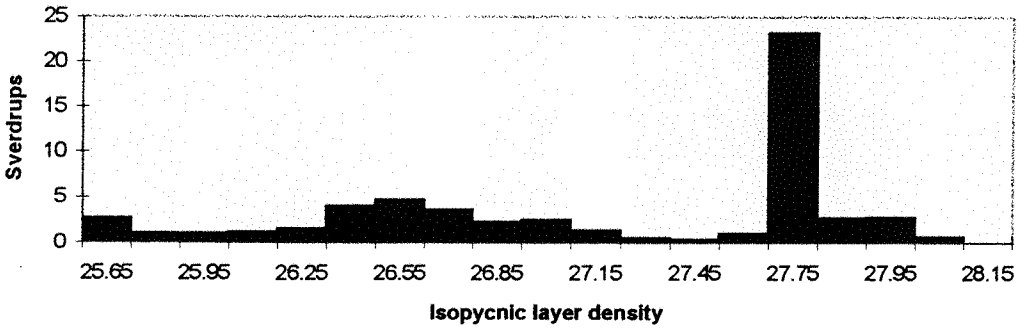

Figure 4.20: A bar graph of the permanent subduction rate for each isopycnic layer in AIM, calculated over the area where permanent subduction was diagnosed to occur by the particle method.

Figure 4.21: A plot of the permanent entrainment rate per unit area for the AIM basin calculated by the method of Williams, *et al.* (1994). The plot is presented in the Mercator projection between 10°N and 60°N with the permanent entrainment rate given in metres.

Figure 4.22: A plot of the permanent subduction rate per unit area for the AIM basin calculated by the method of Williams, *et al.* (1994). The plot is presented in the Mercator projection between 10°N and 60°N with the permanent subduction rate given in metres.

Figure 4.21

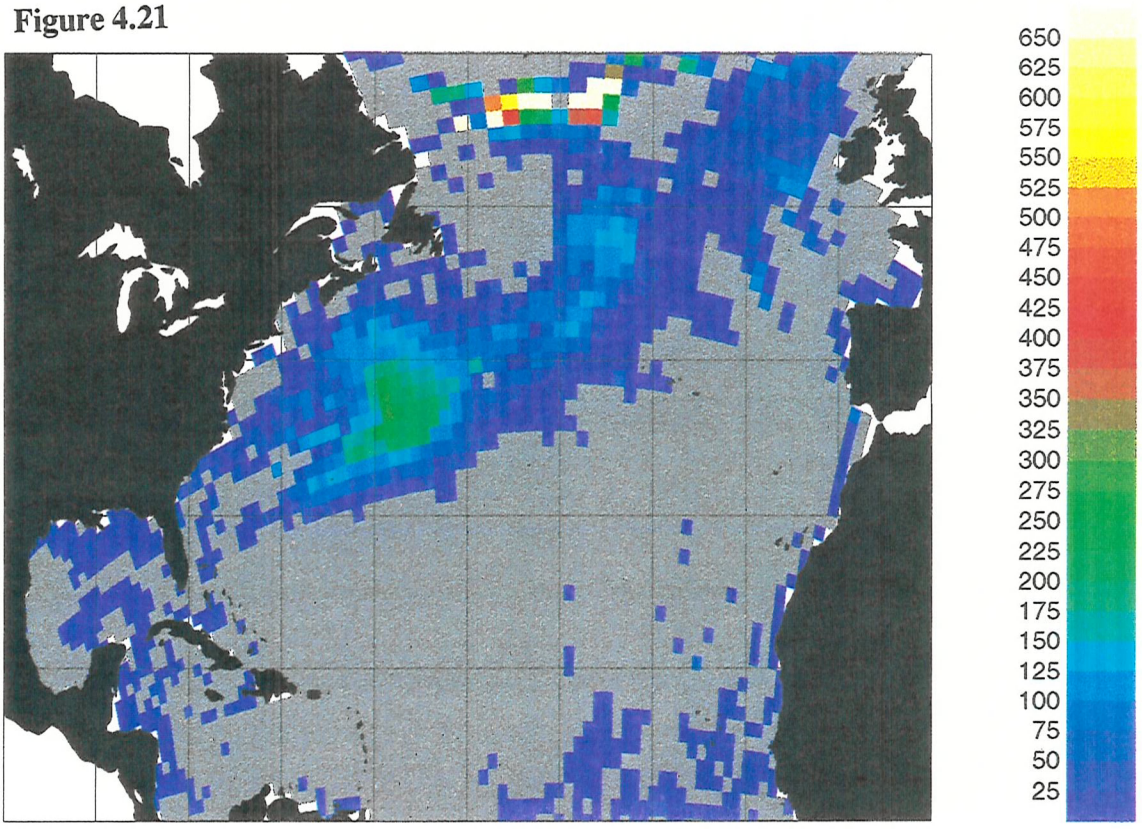

Figure 4.22

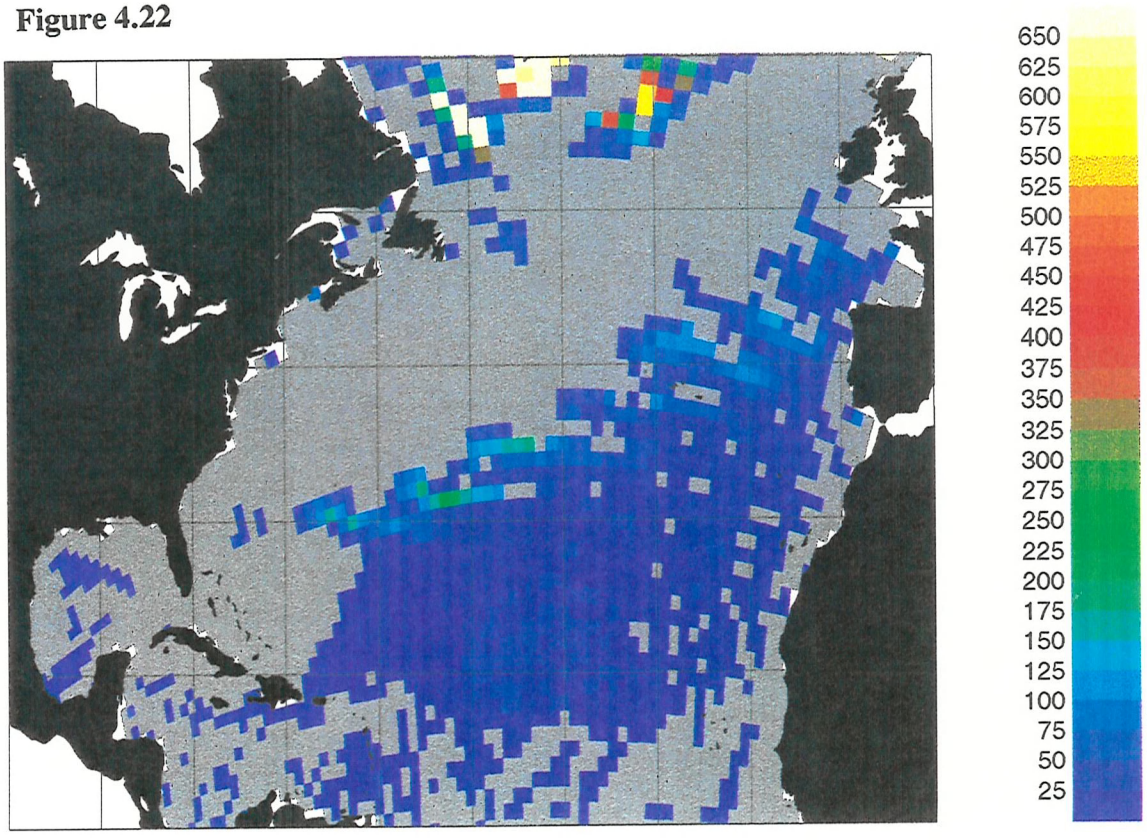

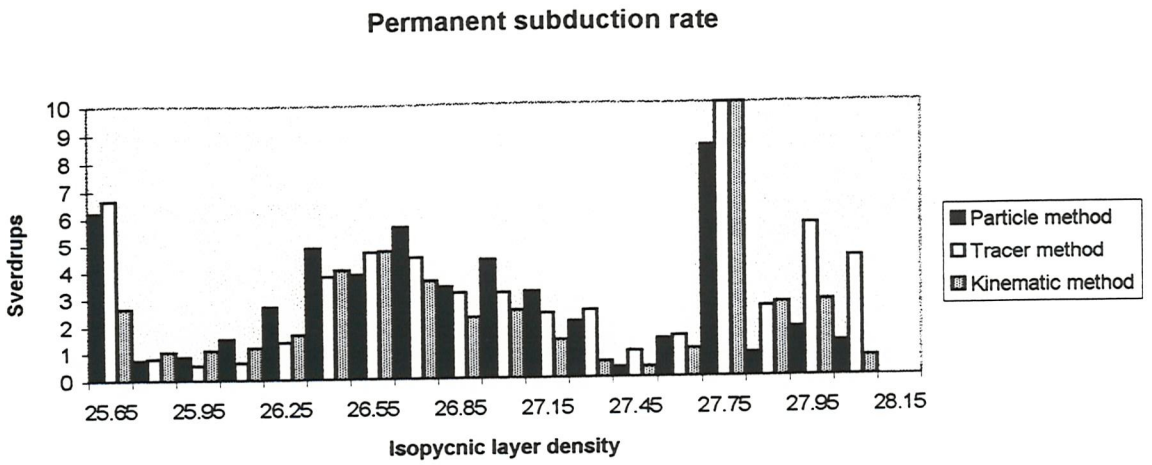

Figure 4.23: A bar graph showing the permanent subduction rate on to each of the isopycnic layers as estimated by three diagnostic methods; the ventilation tracer method of section 4.3, particle method of section 4.4 and the kinematic method of section 4.5.

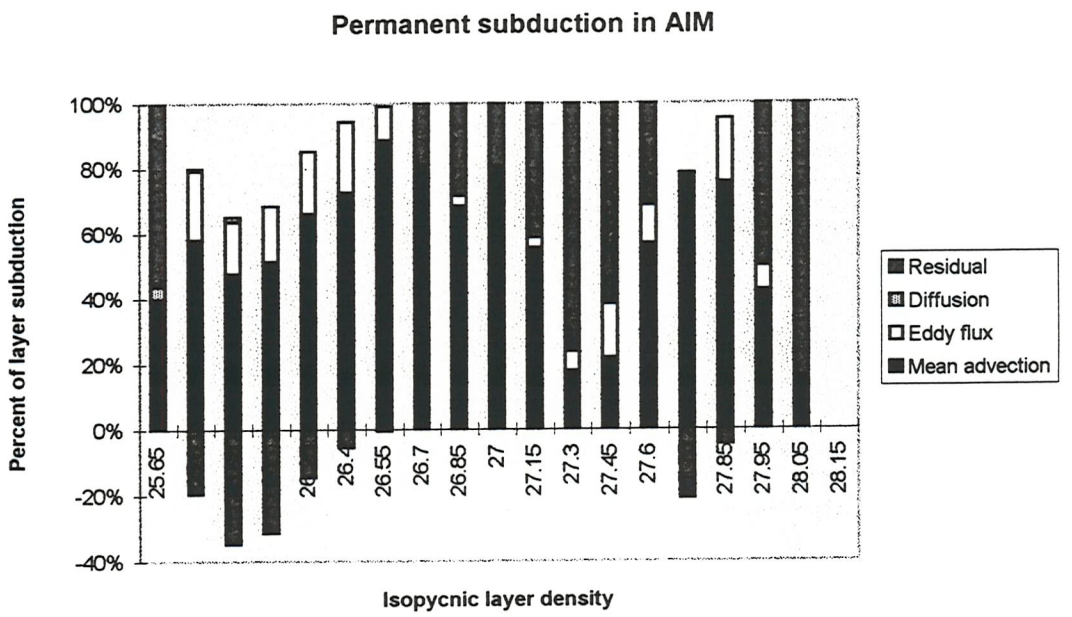

Figure 4.24: A bar graph showing the relative contribution of mean advection, eddy mass fluxes (represented by thickness diffusion), eddy tracer fluxes (represented by tracer diffusion) and the residual term, representing the cumulative errors of the three components and the contribution of vertical displacements in the isopycnic surfaces. The three components were found from the comparison of the two tracer runs with the kinematic estimates of the permanent subduction rate in AIM, with the tracer estimate from the run that included isopycnic tracer diffusion taken as truth.

CHAPTER FIVE

The influence of diffusion and vertical resolution on the permanent subduction rates in an isopycnic GCM

5.1 Introduction

The role of diffusive processes in the ocean was mentioned briefly in Chapter One. The mesoscale eddy field of the North Atlantic is more energetic than the mean flow, even in the Gulf Stream where the mean current is strong (Robinson, 1983). The eddies are therefore an important component of the ocean's dynamics. However, their characteristic length scale is less than the resolution of most ocean models, necessitating their parametrisation. The influence of eddies is generally represented as diffusive (either Laplacian or biharmonic in form), that is they spread properties, *e.g.* momentum and tracer concentration, down-gradient. The deficiencies of this representation are, however, widely acknowledged (Robinson, 1983). A role for diffusive processes in the process of permanent subduction has been suggested by Dewar (1986) and Musgrave (1990), and the influence of isopycnic diffusion on the ventilation of the thermocline has been explored in an idealised gyre by Jia & Richards (1994).

The aim of this chapter is to examine the part played by two of the diffusive processes that are represented in the MICOM GCM; first, the isopycnic tracer diffusion used to disperse temperature, salinity and other passive tracers along isopycnic surfaces, and secondly the isopycnic layer thickness diffusion which is introduced to simulate the influence of baroclinic eddies on the stratification of the ocean. Henceforward, these processes will be referred to as isopycnic and thickness diffusion respectively. The influence of these two processes is examined in three different configurations of the simple geometry version of MICOM, Boxmix (described in more detail in Appendix A).

In the following section of this chapter the control run is described, with sub-sections detailing the influence of isopycnic tracer diffusion on the dispersal of permanently

subducted water and on the ventilation of the thermocline. In the third section a parallel run of the model is described where the model is spun-up with a lower thickness diffusion coefficient. The differences in the dynamics of the thermocline circulation are observed and the influence of these differences on the permanent subduction rate are determined. In the fourth section a third configuration of Boxmix is used to examine the influence of the isopycnic model resolution on both dynamics and the permanent subduction rates observed in the model. A final section will give a summary of the findings of this chapter. The three configurations of Boxmix used in this chapter are summarised in Table 5.1. It will be noted that a diffusive velocity is used rather than a diffusivity; a diffusive velocity allows more structure to develop where the model resolution is higher.

Model	Run	Diffusive velocity for tracer	Diffusive velocity for thickness	Number of model layers	Duration of the run
Box1	**Run 1a**	2.0 cm/s	1.5 cm/s	10	20 years
do.	**Run 1b**	1.0 cm/s	1.5 cm/s	10	18 months[1]
do.	**Run 1c**	0.0 cm/s	1.5 cm/s	10	18 months[1]
Box2	**Run 2a**	2.0 cm/s	0.45 cm/s	10	15 years
do.	**Run 2b**	0.0 cm/s	0.45 cm/s	10	18 months[2]
Box3	**Run 3**	2.0 cm/s	1.5 cm/s	18	30 years

Table 5.1: The duration and parameters used in the runs presented in this chapter

5.2 The standard version, Box1

The model version Box1 is configured as described in Table 5.1, noting that the isopycnic diffusivity has no influence on the dynamics of the model. The stratification was initialised with zonally averaged data taken from Levitus (1982) and with the salinity of the model set to a fixed value of 34.5°/$_{oo}$ on all layers, rendering the isopycnic layers isothermal. The analytic forcing described in Appendix A was used to spin the model up from a state where the velocity field is in geostrophic balance. The results of the standard version of the model are presented in five sub-sections: the first sub-section describes the dynamical aspects of the model spin-up, the second examines the permanent subduction rate with the control value of the isopycnic tracer diffusion (Run 1a), the third sub-

[1] Runs 1b and 1c were initialised from the end of model year 15 (beginning of March) of Run 1a and were run until September, year 17.
[2] Run 2b was initialised from the end of model year 15 (beginning of March) of Run 2a and was run until September, year 17.

section describes a similar run where a lower isopycnic diffusion velocity is used (Run 1b) and in the fourth sub-section the permanent subduction rate for a model run without isopycnic tracer diffusion (Run 1c). The final sub-section contains a discussion of the experiments presented in the previous sub-sections. It should be noted that the three runs, 1a, 1b and 1c, are dynamically identical; thus when the dynamics of these runs are referred to the model version name, Box1, is used.

5.2.1 The dynamics of the standard version

The model was run for a total of twenty years. The total model kinetic energy of the model as it evolved over this period is shown in figure 5.1 with measurements taken in January of each year. This graph shows that by the fifteenth year the wind-driven circulation of Box1 has spun-up, although there is a continued drift in the model kinetic energy after this year. This downward drift is observed in longer runs (*e.g.* those described in Chapter Six) and it probably arises from the continuing adjustment of the thermohaline circulation to the imposed forcing, as evidenced by the longer time constant of the decay curve after year 15. In the fifteenth year the kinetic energy is $4.2 \times 10^{15}\,\mathrm{kgm^2s^{-2}}$ with a seasonal cycle of $0.4 \times 10^{15}\,\mathrm{kgm^2s^{-2}}$ in amplitude. The total kinetic energy of the model is found to be lower in winter, this is because the deepening of the mixed layer distributes the momentum of the surface layers over a greater depth, thus reducing the speed of the surface wind-driven circulation and hence the kinetic energy.

Bleck, *et al.* (1989) used the distribution of water between the isopycnic layers as the criterion for the equilibration of their version of Boxmix. This criterion is not used here since this final state is not representative of the North Atlantic, where there is a net conversion of water to the denser classes, estimated at ~11 Sverdrups (McCartney & Talley, 1984). Over the first fifteen years of the run the volume of layer σ=25.50 reaches an equilibrium, while layers σ=25.95-27.45 gradually deflate. Layer σ=27.60 gains volume over the first ten years of the run and thereafter deflates. Layer σ=27.70 inflates throughout the run, although the rate at which volume is gained increases after year 10. It will be shown later that the net permanent subduction rates, *i.e.* the difference between

the permanent subduction and permanent entrainment rates, implies a net conversion of water lighter than σ=27.45 to denser classes at a rate of 11.2 Sverdrups.

The subtropical western boundary current of the model transports 28.0 Sverdrups northward in January, year 15. Figure 5.2 shows a cross-section of the stratification in the upper 600 metres at the latitude of the subtropical gyre. It will be seen that there is a steep shoaling of the isopycnic layers in the western gyre, indicating a strong northward geostrophic velocity in the boundary current. In the eastern basin the isopycnic layers rise towards the surface, indicating a southward geostrophic flow. It will be noted that for successively deeper isopycnic layers the longitude of the strongest implied southward geostrophic velocity moves eastward. On layer σ=26.70 this southward geostrophic velocity is of the order of ~1.0 cm/s, with typical values of 0.6 cm/s to either side of the 'jet'. The mass flux associated with this southward flow is ~2.7 Sverdrups.

The barotropic streamfunction of the three gyres in the model basin, the subpolar, subtropical and tropical gyres, is shown in figure 5.3. The isolines are transport with a separation of 2.5 Sverdrups. This illustrates that the circulation of the model ocean is the same as that of Bleck, *et al.* (1989). The tropical gyre has a transport of 16.6 Sverdrups in March. However, the tropical gyre has little physical relevance since it acts as a buffer between the subtropical gyre and the southern boundary while in the North Atlantic this region is dynamically more complex through the intervention of the equatorial and tropical circulations. The subpolar gyre has a transport of 17.3 Sverdrups in January, year 16.

Although the transport of the western boundary current is in phase with the annual cycle of the wind stress, the magnitude is found to be higher than predicted by the Sverdrup relation, 28 Sverdrups in January rather than the 22 Sverdrups predicted. This is due to the continuing evolution of the thermohaline circulation. It has been demonstrated by Stommel & Veronis (1980) that the cooling of a rotating fluid can produce a barotropic response, and it has been observed that the Gulf Stream transport during an anomalously cool winter is stronger (Worthington, 1977).

A meridional cross-section of the upper 600 metres of the control run in September of the fifteenth year is shown in figure 5.4. This clearly shows the outcropping of isopycnic layers in the region of the separated western boundary current. To the south, in the heart of the subtropical gyre, the characteristic 'bowl' of the thermocline is visible. The position of these isopycnic outcrops varies over the annual cycle. In spring, immediately after the restratification of the seasonal thermocline, these isopycnic layers rise steeply to the surface. Over the rest of the year, thickness diffusion results in a net shift in these outcrop lines northward. The northward shift in the outcrop lines is most rapid immediately after restratification, but remains strong until the following winter when the descent of the mixed layer removes the stratification produced by thickness diffusion and closes the annual cycle of the stratification of the seasonal thermocline.

Figure 5.5 shows the thickness of layer σ=26.70, an isopycnic layer that outcrops in the northern subtropics, in September, year 17. There is clear evidence of a bolus of water lying in the centre of the plot with a thickness of 220 metres. It will be noted that the bolus displays a trefoil distribution with two axes aligned parallel to the outcrop and the third roughly perpendicular to the outcrop. This bolus lies within the seasonal thermocline and so is removed every year by the descending mixed layer.

The March mixed layer density was found to the most important determinant in the production of mode waters in Chapter Two; it is, therefore, plotted for Box1 in figure 5.6a. The isopycnals are distorted northward in the western basin through the advection of the western boundary current. The figure shows that the production of σ=27.70 water occurs in the north-west corner of the subpolar gyre while water in the range $25.50<\sigma\leq27.45$ is subducted in the subtropics. Production of σ=25.50 water is restricted to the tropical gyre and the southern-most regions of the subtropical gyre.

The mixed layer depth in March is shown in figure 5.6b. This plot shows that there are two regions where the gradient in the depth of the base of the winter mixed layer is large. The most notable coincides with the σ=27.60 isoline in figure 5.6a. To the north of this contour the isopycnic layer σ=27.60 is not hydrostatically stable and so the full thickness of this layer is eroded by the winter mixed layer which results in an exceptionally deep

winter mixed layer (>2200m). Experiments undertaken by M.M.Lam (personal communication) indicate that the depth of the winter mixed layer in this range of region is only weakly dependent on the density resolution of the isopycnic layers for σ>27.60. A second region of strong mixed layer depth gradients is found in the eastern subpolar gyre associated with the σ=26.40 isoline in figure 5.6a. To the south, in the northern subtropics there is a shoaling of the base of the winter mixed layer, indicating a region of potential permanent subduction (see Eq.1.2).

5.2.2 Permanent subduction in Run 1a

The permanent subduction rates on to layers σ=27.60 and 27.75 (not shown) are 37.3 and 19.9 Sverdrups respectively. The tracer diffusion velocity used in this run is 2.0 cm/s (Table 5.1) which gives a diffusivity of $3.7 \times 10^7\ cm^2 s^{-1}$ at 34°N. The permanent subduction rates calculated from Run 1a using the tracer method of Chapter Four are shown in figure 5.7. The permanent subduction rate over layers σ=25.65-27.45 is 29.5 Sverdrups with the greatest rates on to the denser layers. The distribution of tracer in the permanent thermocline is shown in figure 5.8 for layer σ=26.70 in September of year 17. It will be noted that by this time the volume of tracer in the thermocline has been spread over a large area. The approximate radial symmetry indicates that this dispersion is dominated by diffusion. The maximum in tracer 'depth' (tracer concentration multiplied by layer thickness) is 40 metres with the maximum lying at the centre of the gyre. To the east there is also significant permanent subduction (~15 metres).

Examination of the concentration of tracer on the same layer in September, year 17 (not shown) indicates a maximum in concentration of 25% along the subduction front, with a peak of 30% at the eastern boundary. Thus the variations in the tracer 'depth' with longitude shown in figure 5.8 are entirely the result of variations in layer thickness, shown in figure 5.5. The higher concentration located at the eastern boundary indicates that the dispersion is more advective here and that the implied renewal rate is higher, *i.e.* water here was more recently in the mixed layer. This conclusion is supported by meridional velocity measurements made across the basin.

5.2.3 Permanent subduction in Run 1b

The permanent subduction rate on all isopycnic layers was found to be 73.4 Sverdrups, of which 24.1 Sverdrups was deposited on to layers σ=25.65-27.45. This is 18% lower than the result of Run 1a. The annual mean permanent subduction rate on to each of the layers in the range σ=25.65-27.45 is shown in figure 5.7. The diffusion velocity used in Run 1b is 1.0 cm/s, equivalent to 1.8×10^7 cm^2s^{-1} at 34°N.

5.2.4 Permanent subduction in Run 1c

The permanent subduction rate on to all isopycnic layers is 52.0 Sverdrups, of which 15.2 Sverdrups were deposited on layers σ=25.65-27.45. The permanent subduction rate on to each isopycnic layer is given in figure 5.7. The diffusion velocity was set to zero in Run 1c, thus there is no diffusion of tracer in this run.

Figure 5.9 shows the 'depth' of tracer on layer σ=26.70 in September of year 17. The maximum in the tracer 'depth' lies in the same position as the maximum in figure 5.8, however the maximum is in excess of 60 metres compared to the maximum value of 40 metres found in Run 1a. In addition, the tracer is far more localised with the 5 metres contour of tracer 'depth' lying within 4° latitude of the maximum. To the east, the maximum in tracer 'depth' is ~20 metres and is displaced southward relative to the tracer distribution in the centre of the gyre. This further illustrates the eastern boundary current mentioned above.

The tracer concentration in September of year 17 on layer σ=26.70 (not shown) indicates a maximum in tracer concentration running zonally along the subduction front with a concentration of ~40%. At the eastern boundary the concentration is slightly higher with a value of 45%. It should be noted that almost no tracer has moved northward in to the seasonal thermocline over the six months since the mixed layer removed all of the tracer in the seasonal thermocline, whereas in Run 1a diffusion has carried the tracer northward, back in to the seasonal thermocline.

5.2.5 Discussion of the role of isopycnic tracer diffusion in permanent subduction and ventilation

From the above results it is clear that the isopycnic diffusion of tracer in the thermocline has a significant influence on the quantity of tracer remaining in the thermocline for more than one year. It would appear that the model proposed by Musgrave (1990) for the eddy transport of tracer from the seasonal thermocline to the permanent thermocline holds for Boxmix as configured here. A comparison of the results for Run 1a and Run 1c show that for layers σ=25.65-27.45 some 14.3 Sverdrups are permanently subducted by isopycnic diffusion for a diffusion velocity of 2.0cm/s (48% of total). For the intermediate diffusion velocity of 1.0cm/s, the permanent subduction rate due to isopycnic diffusion on to layers σ=25.65-27.45 is 8.9 Sverdrups (37% of total). From this it can be seen that the relation between tracer diffusion and permanent subduction due to isopycnic diffusion is not linear, the permanent subduction rate is slightly more sensitive to the value of the isopycnic diffusion velocity for smaller values.

The non-linear dependence of permanent subduction rate on diffusion velocity can be illustrated by an analogy with two fluids separated by a boundary, which is removed. If a simple diffusion-only dispersion is considered, it will be seen that the timescale over which the tracer is dispersed is entirely controlled by the diffusivity, or in this case, by the diffusion 'velocity' of the fluid. Thus, a change in the diffusion velocity changes the time taken for the distribution to reach a particular stage of its evolution. If the time at which the tracer is measured remains constant while the diffusion velocity is changed, then the net flux of fluid across a boundary, such as that between the seasonal and permanent thermoclines, will change. Given that the evolution of the distribution by the diffusion equation implies that the greatest instantaneous flux across this boundary will be in the initial phases, an increase in diffusivity will produce progressively smaller increases in the net flux across this boundary for progressively larger diffusion velocities. The appropriateness of this analogy depends on the relative importance of advective and diffusive processes in the dispersion of tracer in thermocline.

The dependence of permanent subduction rates in Boxmix on the isopycnic diffusion velocity is entirely counter to the lack of any dependence found in the Atlantic Isopycnic

Model (AIM) in Chapter Four. The isopycnic diffusion velocity used was 1.0 cm/s with a grid-resolution of 1°, giving a diffusivity one quarter of that used in Run 1a. This could be due to either of the other two diffusive processes used in MICOM. First, the isopycnic thickness diffusion coefficient used in AIM is lower than that used here. Secondly, the eddy viscosity used in AIM is lower. The influence of thickness diffusion on the circulation of the MICOM thermocline and the influence this has on the permanent subduction rates will be examined in the following section.

The Péclet number (Pé=UL/κ, where U=scale velocity, L=scale length, κ=diffusivity) determines the relative importance of diffusive processes over advection in the gyre-scale dispersion of tracers and particles. Jia & Richards (1994) have shown for a series of idealised basins that the threshold above which advection dominates is Pé=20. Below this value the role of diffusion in the dispersion of tracer becomes important. The Péclet number in AIM was found to be ~60-240 by Jia & Richards, indicating that diffusion is of little relevance to the dispersion of tracer in the thermocline. This confirms the findings of Chapter Four. The Péclet number for Box1 lies in the range 6-75, with Pé<20 for layers σ>26.35. The differences between AIM and Box1 stem from the faster thermocline circulation found in AIM. The AIM circulation has been found to be too vigorous in comparison with atlas data, and eddy-resolving models generate Péclet numbers of the order 2-3 (Böning & Cox, 1987). A comparison of isopycnic diffusivities with estimates made from field studies give values in the same range as those used here[1], although those generated by eddy-resolving models are higher (~8×10^7 cm^2s^{-1} for Böning & Cox).

5.3 The low thickness diffusion version, Box2

Isopycnic layer thickness diffusion (called 'thickness diffusion' for brevity in the rest of this section) is a necessary feature of the model to prevent numerical instability, through the smoothing of sharp changes in the model stratification. Thus the thickness diffusion coefficient cannot be set to zero. In addition, thickness diffusion has been used to represent the action of baroclinic instabilities on the stratification through the removal of

[1] *e.g.* Olbers, *et. al.* (1985), $\kappa=1.0\times10^7 cm^2s^{-1}$; Jenkins (1991), $\kappa=1.8\times10^7 cm^2s^{-1}$; Thiele, *et al.*(1986), $\kappa=2.5\times10^7 cm^2s^{-1}$, Schäfer & Krauss (1995), $\kappa=10.2\text{-}2.1\times10^7$ cm^2s^{-1}.

available potential energy (Gent & McWilliams, 1990). This section examines a version of Boxmix, denoted Box2, which used the same initial conditions and surface forcing conditions as Box1, but where the thickness diffusion velocity has been lowered to 0.45 cm/s, giving a thickness diffusion coefficient of the same order as that used by AIM. This section is divided into three parts, the first described the spin-up and dynamics of Box2 while the second examines the influence the change in thickness diffusion has on permanent subduction in Boxmix. A third section will examine the influence of isopycnic tracer diffusion on the permanent subduction rate through a parallel run where the isopycnic diffusion velocity is set to zero.

5.3.1 The dynamics of Box2

The model was run for seventeen years in total. Figure 5.1 shows the total model kinetic energy measured in January of successive years. Throughout this period the total kinetic energy of the model remained higher than that of the parallel Box1 run, and it appears to be in a steady state by the fifteenth year of the run with a mean kinetic energy of 9.8×10^{15} kgm^{2}s^{-2} and a seasonal cycle of amplitude 0.7×10^{15} kgm^{2}s^{-2}.

The higher model kinetic energy in Box2 is mirrored by a larger mass flux through the western boundary current in January, year 15, some 34.3 Sverdrups compared to the 28.0 Sverdrups in Box1. Figure 5.10 shows a zonal section through the subtropical gyre in Box2. The outcropping of the isopycnic layers in the western boundary current is steeper in Box2 than in Box1, resulting in the stronger northward flow. In the eastern basin the isopycnic layers shoal over much shorter longitudinal distances with higher, more localised gradients. This produces swifter southward geostrophic velocities in the permanent thermocline, ~3 cm/s, than those found in Box1 and these stronger velocities are concentrated into a 'jet' coincident with the steep shoaling. The total southward mass flux on layer σ=26.70 is 6.9 Sverdrups compared to 2.7 Sverdrups in Box1.

The circulation pattern of Box2 is shown by the barotropic streamfunction shown in figure 5.11. A comparison of this figure with the streamfunction for Box1 shows that the circulation of the tropical gyre has not changed greatly. The circulation of the subtropical and subpolar gyres has been influenced by the reduced thickness diffusivity.

The barotropic transport of the subtropical gyre in Box2 is enhanced when compared to Box1 (see above). Most of the enhanced circulation is restricted to a narrow band adjacent to the western boundary current which has a longitudinal extent of ~4°. This recirculation is visible in zonal cross-sections of the subtropical gyre (figure 5.10) which show a slight shoaling of the isopycnic layers next to the steep gradients of the western boundary current. The recirculation in this region is most probably a spurious result of the Smagorinsky eddy viscosity parametrisation (D.Webb, personal communication). It will also be noted that the strength of the separated boundary current in Box2 is greater than in Box1, as indicated by the closer spacing of the barotropic streamlines in figure 5.11, which gives a flow speed of 1-2 cm/s higher in Box2 than Box1. This is related to the steeper meridional outcropping of the isopycnic surfaces in Box2 (see figure 5.12). Figure 5.12 also shows a clear mode water bolus in the subtropical thermocline. An examination of the layer thickness for σ=26.70 (figure 5.13) shows that the water mass left by the spring detrainment is thick (360 metres) and in the permanent thermocline there is a well-defined tongue leading from the southern edge of the bolus into the westward current intensification. An examination of the currents on this isopycnic layer show that the strongest currents are found on the eastern flank of the bolus and a slower flow on the western flank. This implies an anticyclonic circulation around the bolus with a background southward drift of ~0.5 cm/s.

The winter mixed layer conditions are also influenced by the thickness diffusion. The March mixed layer density is shown in figure 5.14a. The σ=27.60 contour extends further east in Box2 than in Box1 while in the subtropics the mixed layer isolines of density show greater meridional variation across the basin than observed in Box1. In the western basin the isolines of density are markedly meridional.

The mixed layer depth for Box2 in March is shown in figure 5.14b. This shows that there is a steeper southward shoaling of the base of the seasonal thermocline in the subtropics in Box2. The mixed layer in the northern half of the subtropical gyre is also deeper with strongly meridional depth contours. The depth of the seasonal thermocline in the southern subtropics and tropics is not influenced by the change in thickness diffusion.

5.3.2 Permanent subduction in Run 2a

The tracer velocity used in this run is 2.0 cm/s which gives a diffusion coefficient of 3.7×10^7 cm^2s^{-1} at 34°N. The mean annual volume flux into the permanent thermocline is given in figure 5.15 for isopycnic layers σ=25.65-27.45 with a flux of 34.6 Sverdrups over this range (17% more than Run 1a) and 95.3 Sverdrups over all isopycnic layers. It will be noted that the simple monotonic increase of permanent subduction rate with increasing layer density observed in Runs 1a, 1b and 1c is not observed here. The maximum permanent subduction rate in the range shown is on to layer σ=27.00.

The distribution of tracer 'depth' on layer σ=26.70 is given in figure 5.16 for September, year 17. It will be noted that the distribution of tracer is approximately radially symmetric with a 'tail' leading eastward. The maximum in tracer 'depth' is >80 metres while the 'tail' has a value of only 10 metres. Studies of the tracer concentration on the same isopycnic layer indicate that there are two maxima in tracer concentration; one at the eastern boundary and the other lying in the mid-basin, to the east of the maximum in tracer 'depth'. Both of these maxima have concentrations of ~30%. The distribution of the tracer 'depth' would therefore appear to be more strongly influenced by the distribution of layer thickness than by the distribution of tracer concentration.

5.3.3 Permanent subduction in Run 2b

The diffusion velocity in this run was set to zero, giving no isopycnic tracer diffusion in the model. The permanent subduction rate in year 16 of this run was derived by the tracer method and was found to be 60.4 Sverdrups over all layers of which 21.9 Sverdrups were subducted on to layers σ=25.50-27.45. The permanent subduction rates on to layers σ=25.50-27.45 are shown in figure 5.15. It will be noted that the greatest permanent subduction rate is on to layer σ=26.70.

The distribution of tracer 'depth' is shown in figure 5.17 for September, year 17. This shows that there is a clear, localised maximum in tracer 'depth' in the mid-basin with a 'depth' of 170 metres. To the east, some 20 metres of tracer are permanently subducted on to layer σ=26.70. This is the same tracer 'depth' as is permanently subducted on to

layer σ=26.70 in Run 1c although a comparison of the layer thicknesses for this layer in Box1 and Box2 shows that the layer is thinner in this region in Box2. This implies that the tracer concentration is greater in this region in Box2 and hence that the water mass properties are renewed more quickly. This is confirmed by the tracer concentration on layer σ=26.70 in September, year 17 (not shown). The tracer concentration at the site of the maximum in tracer 'depth' is ~60% while to the east there is a narrow band of permanently subducted tracer with a concentration of ~55%, far higher than the concentration found in Run 1c.

5.3.4 Discussion of the influence of isopycnic diffusion on permanent subduction in version Box2

The results presented above illustrate that the permanent subduction rate is significantly enhanced by the inclusion of an isopycnic diffusivity. For Box2 the use of an isopycnic tracer diffusivity of 3.7×10^7 cm^2s^{-1} produces an enhanced permanent subduction rate of 12.7 Sverdrups for layers σ=25.50-27.45, some 37% of the total permanent subduction rate over these layers in Run 2a. This is slightly less than the enhanced permanent subduction rate due to isopycnic diffusion observed in section 5.2, run1a. In Box1 an isopycnic diffusivity of 3.7×10^7 cm^2s^{-1} produces a further 14.3 Sverdrup or 48.0% greater permanent subduction on to layers σ=25.50-27.45. The weaker influence of isopycnic diffusion on permanent subduction rates in runs 2a and 2b compared to runs 1a, 1b and 1c is the result of the faster thermocline circulation in Box2 compared to Box1. As noted above, the faster flow in Box2 arises through a southward 'jet' on the eastern flank of the mode water bolus. The higher thickness diffusion in Box1 moderates the geostrophic velocity of this jet by partially removing the steep slope of the isopycnic layers, rendering the 'jet' slower and less localised.

5.4 Discussion of the role of thickness diffusion

The comparison of the dynamics of Box1 and Box2 shows that thickness diffusion exerts a strong influence over the circulation of the thermocline. Its most notable role appears to be in the suppression of the ventilation tongues and their associated 'jets' that otherwise develop. A second influence appears to be on the northward heat transport in

the model. It was noted in section 5.2 that thickness diffusion played an important role in the annual cycle of the seasonal thermocline stratification in the separated western boundary current. In this region, after the spring re-stratification, thickness diffusion moves the isopycnic outcrops northward, thus transporting water into the subpolar gyre. The reduction in this eddy-transport in Box2 compared to Box1 results in a larger area where σ>27.60 in the March subpolar gyre, implying a cooler gyre. A comparison of the meridional mass fluxes due to thickness diffusion in Box1 with those due to advection shows that the northward thickness diffusion mass flux in the seasonal thermocline is up to five times greater than the southward gyral mass flux. On the boundary between the permanent and seasonal thermocline the influence of thickness diffusion is much less pronounced.

A comparison of the permanent subduction rates of Run 1c and Run 2b, both of which do not include the dispersion of tracer due to isopycnic diffusion, shows that an increased thickness diffusion 'velocity' decreases the permanent subduction rate for layers σ=25.5-27.25. There are two possible contributors to the increase in permanent subduction rate with the decrease in thickness diffusion. The first is the reduction in the northward thickness diffusion mass flux observed in the seasonal thermocline, the second is the increased southward velocity in the thermocline 'jet'. The northward mass flux arising from thickness diffusion in Box1 is some 5 times greater than the southward geostrophic mass flux over most of the seasonal thermocline, thus, all other things being equal, the northward thickness diffusion mass flux in Box2 should be 1.5 times greater than the southward geostrophic flux. However, the southward flux on layer σ=26.70 is 6.9 Sverdrups in Box2 whereas in Box1 it is 2.7 Sverdrups. It is clear that the primary cause of the increased permanent subduction rate in runs 2a and 2b compared to runs 1a and 1c is the thermocline 'jet'.

The thickness diffusion coefficient implied by the North Atlantic eddy-field is, as yet, unmeasured. The authors who have included thickness diffusion in their models (*e.g.* Bleck, *et al.*, 1992; Danabasoglu, *et al.*, 1994; Gent, *et al.*, 1995) have generally used values in the same range as those currently used for isopycnic tracer diffusion ($\sim 1-3\times10^{7}\ cm^{2}s^{-1}$). The choice of the thickness diffusion used in Box1 appears to

generate an ocean stratification closer to that seen from hydrographic surveys, although it should be borne in mind that this value may be necessary to suppress model imperfections rather than being representative of the implied thickness diffusion prevalent in the North Atlantic.

5.5 The balance of permanent subduction and permanent entrainment

The balance of permanent entrainment and permanent subduction is a re-statement of the conservation of volume and so it would be expected to hold for an ideal measurement. In Chapter Four it was assumed that the tracer measurements of the permanent subduction rate were exact and that the conservation of volume could be assumed, thus allowing the derivation of the permanent entrainment rates in AIM. A simple tracer experiment was conducted to test this assumption in Boxmix.

The tracer method was altered to give a concentration of 1.0 in the thermocline at all points at the start of the model run. As the model run progressed, tracer entrained by the mixed layer was removed from the model and the volume of tracer entrained at each grid point from each layer was monitored. At the end of the run the running total of the entrained tracer can be examined and the change in the running total over a twelve month period gives the permanent entrainment rate. Water detrained from the mixed layer was given the tracer concentration 0.0. The model was then run over thirteen months starting from the end of year fifteen of Box1 (the beginning of March). Over the run tracer was diffused with an isopycnic diffusion 'velocity' of 2.0 cm/s. Thus the permanent entrainment rates produced by this run are comparable to the permanent subduction rates produced by Run 1a.

The permanent entrainment rate found by this method was 88.9 Sverdrups over all isopycnic layers, of which 40.7 Sverdrups were permanently entrained from layers σ=25.5-27.45. The permanent subduction rate in Run 1a is 86.7 Sverdrups over all layers with 29.5 Sverdrups on to σ=25.5-27.45. This implies a net entrainment of 2.2 Sverdrups by the mixed layer over year 15, an increase of 6.8×10^4 km^3 in the volume of

the seasonal thermocline. The increased volume is entirely through the deepening of the winter mixed layer in the subpolar gyre.

The imbalance in the permanent subduction rates for layers σ=25.5-27.45 implies a thermohaline circulation of 11.2 Sverdrups, comparable to estimates of the thermohaline circulation of the North Atlantic (*e.g.* Walin, 1982).

From the change in the late March volumes of the isopycnic layers the actual net entrainment rate over this density interval is 10.5 Sverdrups. The difference between the imbalance in the tracer estimates and the observed change in permanent thermocline volume implies an error of 2.3% in a flux of 29.5 Sverdrups. Most of the error occurs in the change in volume of the lightest isopycnic layer which receives most of the spring detrainment water in the tropical and southern subtropical gyres. In these regions the spring restratification begins earlier and so the errors in the above calculation are possibly due to the use of a uniform census date for water mass volumes, rather than an error in the tracer estimate.

5.6 The high vertical resolution version, Box3

The influence of the density resolution of the isopycnic model is examined in this section. An eighteen layer version of Boxmix (Box3 in Table 5.1) was spun-up and its permanent subduction rate was examined in year 16, in parallel with the permanent subduction rate measured in Run 1a. The dynamics of the model are described in the following sub-section. In the second section a comparison is made between the permanent subduction rate derived here and that derived in Run 1a.

5.6.1 Dynamics of an eighteen layer isopycnic model

The model was initialised using the Levitus (1982) data set of zonally averaged density for the North Atlantic. The initial velocities were set in geostrophic balance with this stratification and the model was forced for fifteen years using the analytic forcing functions given in Appendix A. After the permanent subduction rate was measured in

year 16 the model run was continued until year 30. It will be noted that the parameters used in the model are identical to those used in Run 1a.

Figure 5.1 shows the total model kinetic energy measured in January over the 29 years of the run. The kinetic energy of the run drops from $9.3 \times 10^{15}\ \mathrm{kgm^2 s^{-2}}$ in year 1 to $3.6 \times 10^{15}\ \mathrm{kgm^2 s^{-2}}$ in year 29. A comparison of this with the kinetic energy of Box1 shows that the spin-up times for the two models are similar. This would be expected since the models indicate a similar group velocity for the first baroclinic Rossby wave. The continued downward drift in the model kinetic energy arises from the thermal adjustment to surface forcing.

A comparison of barotropic streamfunctions for successive years after year 15 shows that there is a negligible change in the barotropic circulation. The maximum subtropical gyre transport is 29.0 Sverdrups in January, year 15 with a seasonal cycle of amplitude 2.5 Sverdrups. The maximum gyre transport is 1.0 Sverdrups greater than observed in Box1. Over the remainder of the run the subtropical gyre transport drops slightly, giving a maximum transport of 28.1 Sverdrups in January, year 29.

The meridional cross-section of the upper kilometre of Box1 and Box3 are shown in figures 5.4 and 5.18 respectively. Although the density intervals differ, it can be seen the meridional slope of the isopycnic outcrops are similar in the two runs, implying a similar eastward geostrophic flow on the northern rim of the subtropical gyre. The March mixed layer density fields for Box1 and Box3 indicate that the isolines of density lie at the same latitude in the eastern basin. In the central and western basin the latitudes of the density isolines differ; in the western basin the isolines lie slightly further north in Box1 than in Box3 while in the central basin the isolines lie slightly further south in Box1 than in Box3. The differences in the March mixed layer depth arise from the finer resolution of the thermocline density structure in Box3. A comparison of March mixed layer depths shows that the mixed layer is marginally shallower in the northern subtropics in Box3 compared to Box1.

The permanent subduction rate in Box3 was measured at five year intervals using the tracer method of Chapter Four. The sequence of permanent subduction rates on to each isopycnic layer is show in figure 5.25. The permanent subduction rate on to all isopycnic layers is found to be 73.5 Sverdrups in year 6 rising to 81.5 Sverdrups in year 11. From year 16 onwards the total permanent subduction rate is ~84.0 Sverdrups. From figure 5.19 it is clear that the permanent subduction rate on to layers σ=25.65-27.45 decreases as the basin cools; the isopycnic layer outcrops move southward into regions where the seasonal thermocline is shallower. The two densest layers receive most of the permanently subducted water, although the distribution of the permanent subduction rate between these two layers changes as the March mixed layer temperature of the subpolar gyre drops over the run. After year 11 the permanent subduction rate on to layer σ=27.60 is seen to drop while the permanent subduction rate on to layer σ=27.75 is seen to rise.

5.6.2 Permanent subduction in year 16

The permanent subduction rate on to all layers in year 16 for Run 3 is 84.0 Sverdrups, compared to 86.7 Sverdrups in Run 1a for the same year (a difference of 3.1% from Run 1a). For layers σ=25.65-27.45 the total permanent subduction rate is 28.8 Sverdrups which compares favourably with the 29.5 Sverdrups found in Run 1a, a difference of 2.4% from the result of Run 1a. Thus it can be concluded that the vertical truncation resulting from the finite number of isopycnic layers has little influence on the permanent subduction rate observed.

In Chapter Four it was noted that the upper limit of the errors arising from vertical truncation are large, however it was also noted that this upper limit is set by purely one-dimensional considerations and that the influence of advection and diffusion would produce a much smaller truncation error. The upper limit of the truncation errors calculated for $\sigma \leq 27.45$ in Box1 and Box3 are 15.5 Sverdrups and 10.6 Sverdrups respectively, which implies that the expected difference in the permanent subduction rate, assuming that any differences are purely the result of improved resolution, would be 4.9 Sverdrups. The observed difference is 0.7 Sverdrups, some 15% of the predicted value.

This implies that vertical truncation is of little relevance to the permanent subduction rates on to layers $\sigma \leq 27.45$.

This configuration (Box3) of Boxmix is used in Chapter Six for studies of the influence of buoyancy fluxes on the permanent subduction rate.

5.7 Summary

The permanent subduction rates observed in the experiments presented above are summarised here in Table 5.2.

Run	Isopycnic diffusive velocity	Thickness diffusive velocity	Number of model layers	Total permanent subduction	Permanent subduction $\sigma \leq 27.45$
Run 1a	2.0	1.5	10	86.7	29.5
Run 1b	1.0	1.5	10	73.4	24.1
Run 1c	0.0	1.5	10	52.0	15.2
Run 2a	2.0	0.45	10	95.3	34.6
Run 2b	0.0	0.45	10	60.4	21.9
Run 3	2.0	1.5	18	84.0	28.8
UNITS	cm/s	cm/s	-	Sverdrups	Sverdrups

Table 5.2: Summary of the permanent subduction rates for year 15.

It will be noted that the total permanent subduction rate is dominated in all runs by the densest layers, σ=27.60 and 27.70 in Runs 1a, 1b, 1c, 2a and 2b, and σ=27.60 and 27.75 in Run 3. The permanent subduction rate on to the densest layer in all runs is found to be uninfluenced by the isopycnic diffusion velocity; in runs 1a, 1b and 1c the permanent subduction rate remains at 19.9 Sverdrups on to σ=27.70. This occurs because the density of this layer is too great to be lifted by the mixed layer during the winter, thus the permanent entrainment rate from layer σ=27.70 is only 5.5 Sverdrups. During Run 3 and its continuation in Chapter Six to year 40, the depth of the seasonal thermocline in the subpolar gyre is seen to rise primarily through the inflation of layer σ=27.70.

The permanent subduction rate on to the isopycnic layer outcropping in the subpolar gyres is not of primary interest in this study. The timescale for the spin-up of these layers is much longer than of the wind-driven gyre (O(100 years) compared to O(20 years)). In

addition, the creation of dense water masses is thought to occur through deep convecting chimneys, which this model is not capable of resolving and the physics of these small-scale features is beyond the capacity of this model. Thus the results of primary interest are those concerning the lighter layers, outcropping in the subtropics.

The potential role of isopycnic diffusion in Boxmix, and, by inference, in the North Atlantic, is large. For an isopycnic diffusion 'velocity' of 1.0 cm/s ($1.8 \times 10^7 \, cm^2 s^{-1}$ at 34°N) the permanent subduction rate due to isopycnic diffusion is ~8 Sverdrups, 37% of the total permanent subduction rate on to layers σ=25.50-27.45. However, from the distribution of tracers after 18 months it would appear that much of this tracer is re-entrained within two years of its detrainment. No extended runs have been performed to examine the amount of tracer placed in the thermocline in one spring remains in the thermocline after a number of years.

The role of thickness diffusion in the model is to moderate the size of the mode water boluses in the permanent thermocline. A decreased thickness diffusion velocity appears to increase the permanent subduction rate through the intensifying of the southward geostrophic 'jet'. An appropriate value of the thickness diffusion velocity for the North Atlantic is not yet clear, nor is it clear to what extent thickness diffusion in MICOM is necessary to suppress the noise in the potential vorticity field generated by the mixed layer detrainment algorithm. Comparisons of AIM with the Hadley Centre Bryan-Cox model (Marsh & Roberts, 1995) suggest that, although the potential vorticity field in AIM is slightly more noisy, the two models both produce noisy potential vorticity fields and the ventilation tongues associated with them. It should be noted, however, that the Hadley Centre model did not include the Gent & McWilliams scheme for isopycnic mixing.

Within the constraints of the idealised geometry and the parametrisation of eddy processes, it would appear that the eddy fluxes in the North Atlantic play an important role in the dispersion of tracers and mode waters.

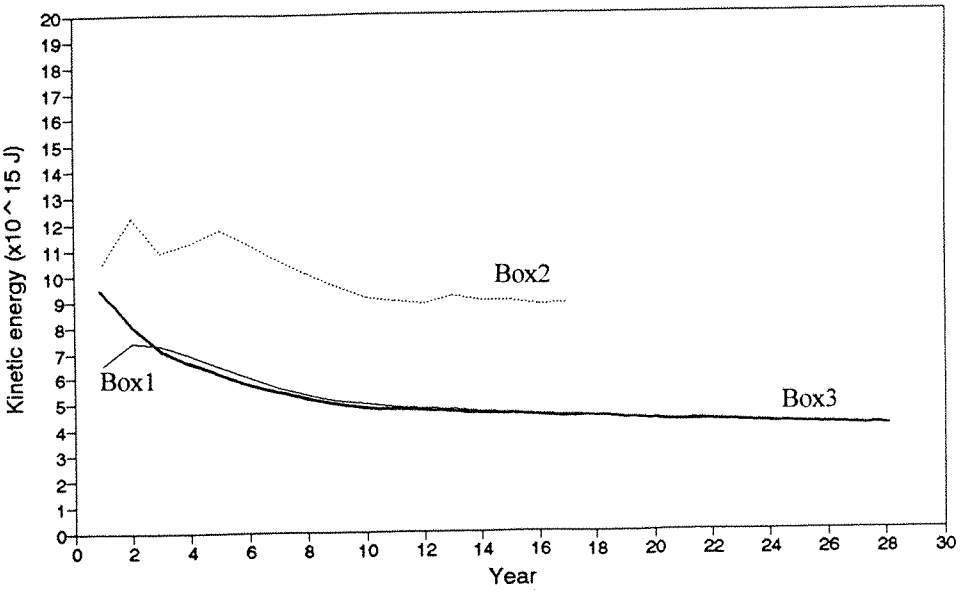

Figure 5.1: A graph of the total model kinetic energy of the model versions Box1, Box2 and Box3 during spin-up. The total kinetic energy for each model was measured at the peak of the annual cycle in January of each year. The results are presented in SI units.

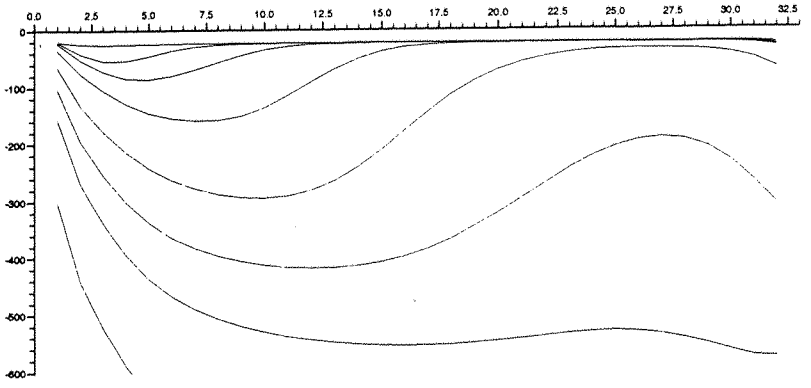

Figure 5.2: A zonal cross section of the upper 600 metres of the Box1 basin at index j=15 (34°N) in the subtropics in September, year 16. The plot shows the variation of the depth of the isopycnic surfaces. The scale across the top of the plot gives the model i-index with each gradation marking one degree longitude.

Figure 5.3: A plot of the barotropic stream function of the Box1 basin during September, year 16. The function is plottted in units of Sverdrups with contours at 2.5 Sverdrup intervals. The scales show the mode grid indices. Negative values imply anticyclonic circulation.

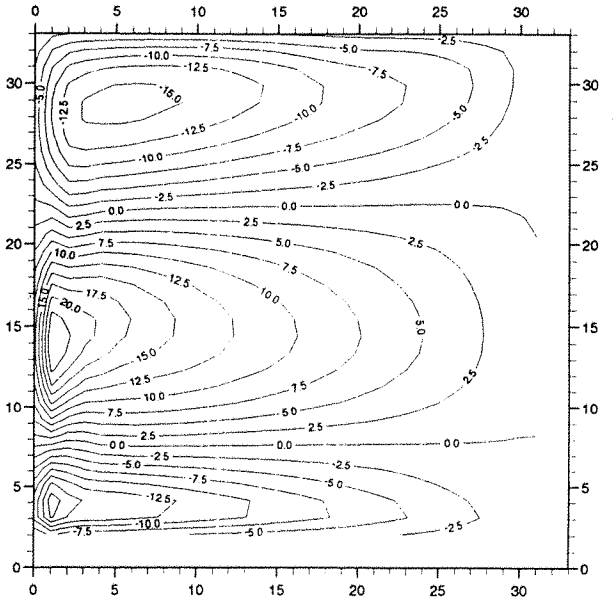

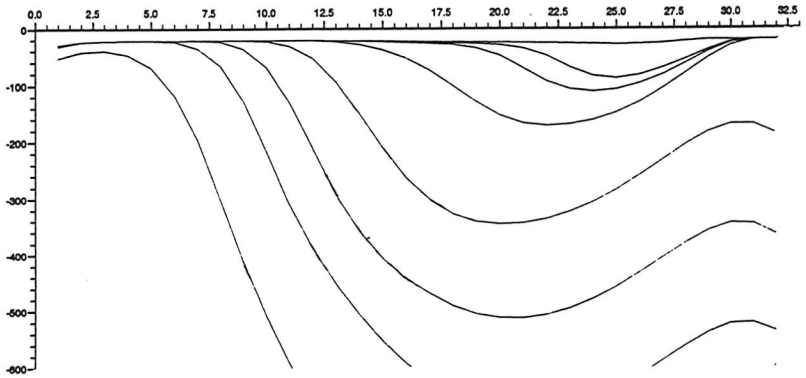

figure 5.4: A meridional cross section of the upper 600 metres of Box1 basin at index i=15 through the interior of the ocean in September, year 16. The plot shows the outdropping of isopycnic surfaces with latitude. The scale along the top of the plot shows the model grid j-index.

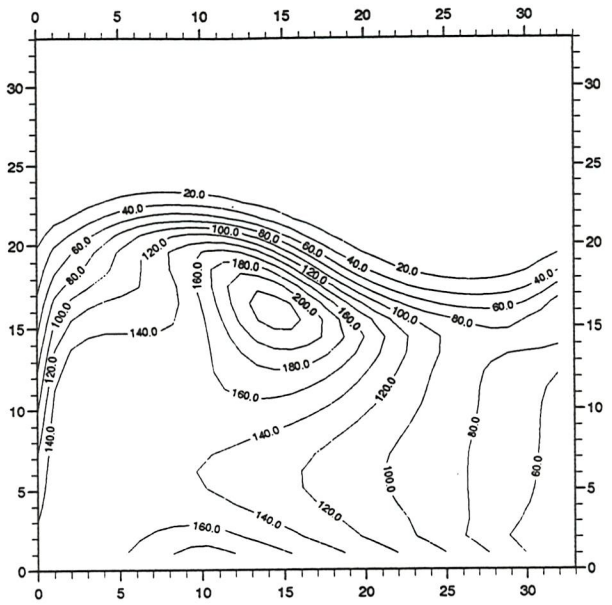

Figure 5.5: A plot of the isopycnic layer thickness in metres of sigma = 26.70 in September, year 16 of Box1. The plot is presented on the model grid with the scales showing the model grid indices.

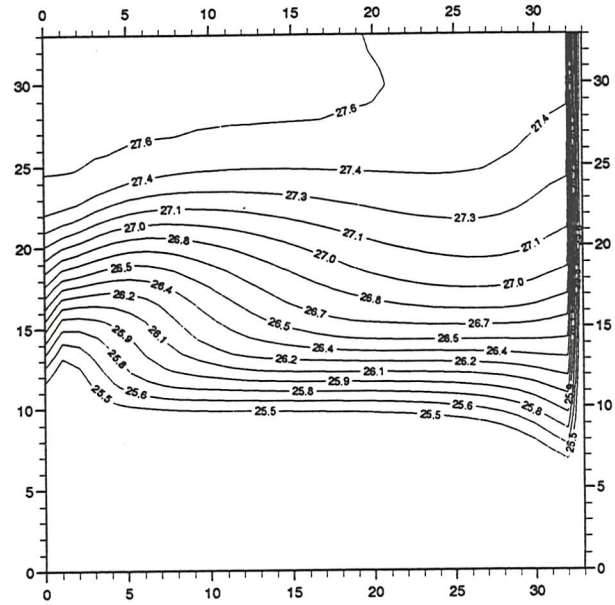

Figure 5.6a: A plot of the mixed layer density (sigma units) in March, year 16 of Box1. The plot is presented on the model grid with the scales showing the model grid indices.

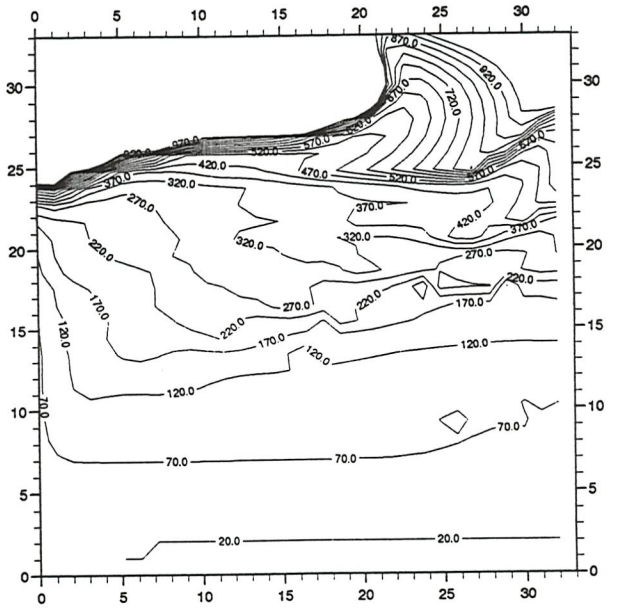

Figure 5.6b: A plot of the mixed layer depth in metres in March, year 16 of Box1 The plot is presented on the model grid with the scales showing the model grid indices

Figure 5.7: A bar graph of the permanent subduction rates on to each isopycnic layer sigma= 25.50-27.45 in spring, year 16 of Box1 for three values of the isopycnic tracer diffusion velocity (2, 1 and 0 cm/s). The rates are presented as annualised rates in Sverdrups.

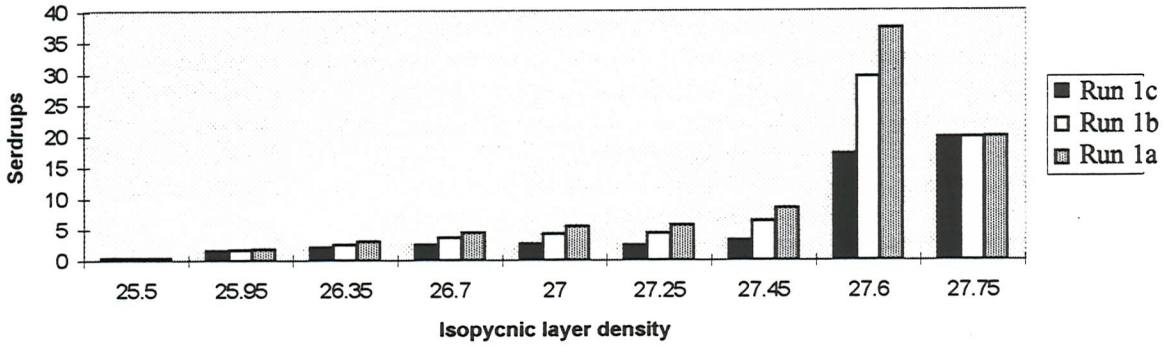

Figure 5.8: A plot of the tracer 'depth' (tracer concentration multiplied by layer thickness) in metres- for layer sigma = 26.70 in September, year 17 of Run 1a of Box1 (using an isopycnic tracer diffusion velocity of 2 cm/s). The 'depth' is plotted on the model grid with the scales giving the model grid indices.

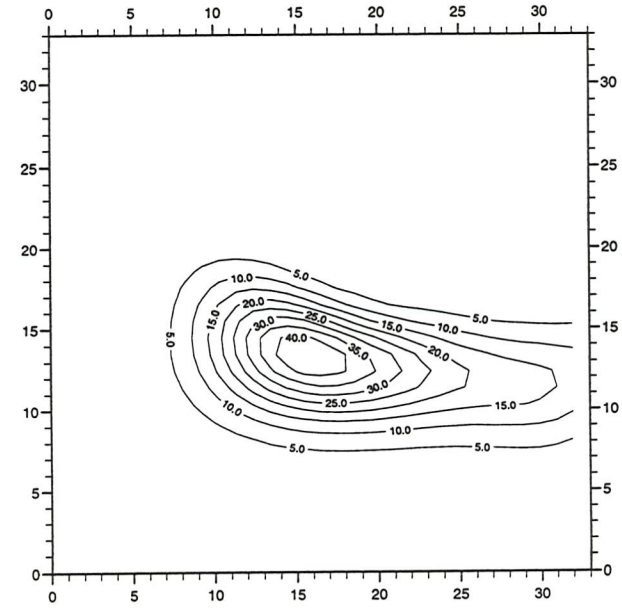

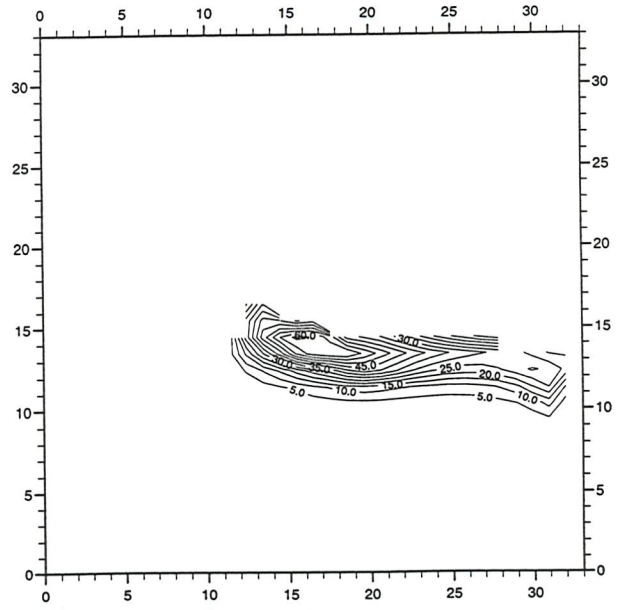

Figure 5.9: A plot of the tracer 'depth' (tracer concentration multiplied by layer thickness) in metres for layer sigma = 26.70 in September, year 17 of Run 1c of Box1 (using an isopycnic tracer diffusion velocity of 0 cm/s). The 'depth' is plotted on the model grid with the scales giving the model grid indices.

Figure 5.10: A zonal cross section of the upper 600 metres of the Box2 basin at index j=15 (34°N) in the subtropics in September, year 16. The plot shows the variation of the depth of the isopycnic surfaces. The scale across the top of the plot gives the model i-index with each gradation marking one degree longitude.

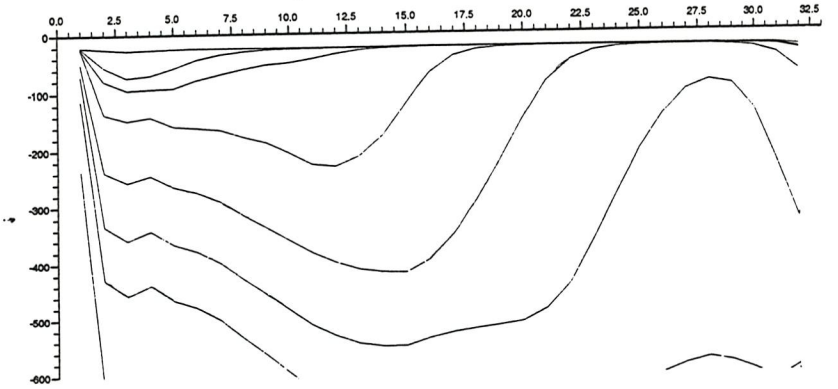

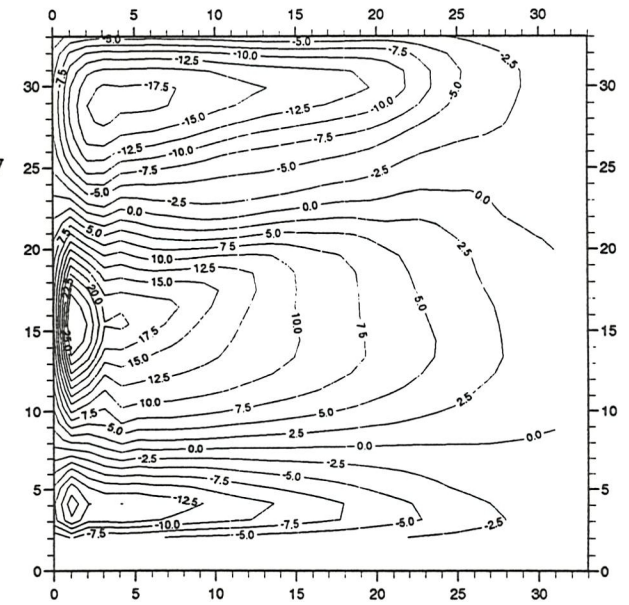

Figure 5.11: A plot of the barotropic stream function of the Box2 basin during September, year 16. The function is plottted in units of Sverdrups with contours at 2.5 Sverdrup intervals. The scales show the mode grid indices. Negative values imply anticyclonic circulation.

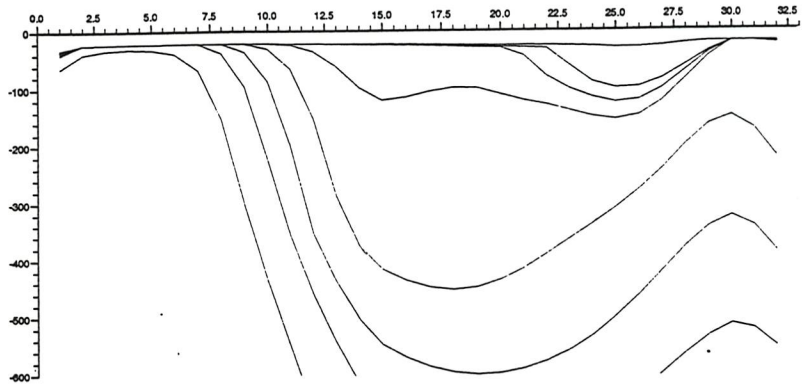

Figure 5.12: A meridional cross section of the upper 600 metres of Box2 basin at index i=15 through the interior of the ocean in September, year 16. The plot shows the outdropping of isopycnic surfaces with latitude. The scale along the top of the plot shows the model grid j-index.

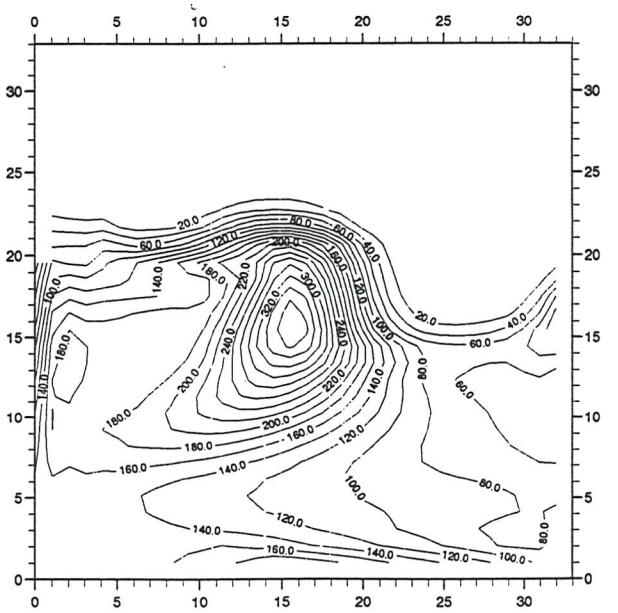

Figure 5.13: A plot of the isopycnic layer thickness in metres of sigma = 26.70 in September, year 16 of Box2. The plot is presented on the model grid with the scales showing the model grid indices.

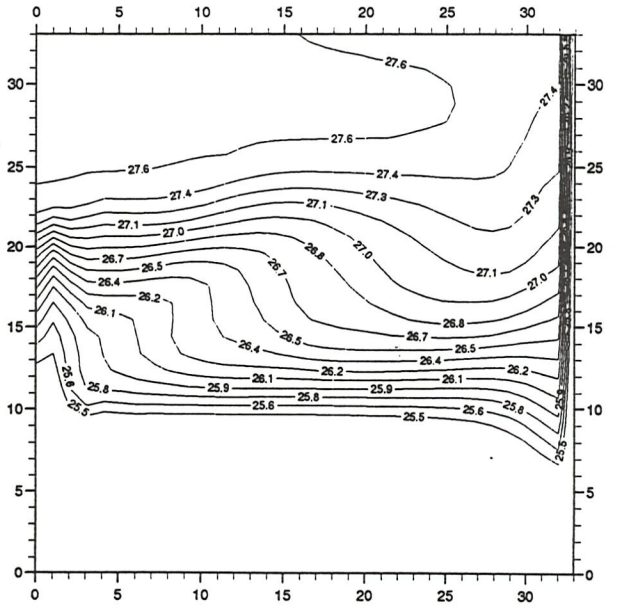

Figure 5.14a: A plot of the mixed layer density (sigma units) in March, year 16 of Box2. The plot is presented on the model grid with the scales showing the model grid indices.

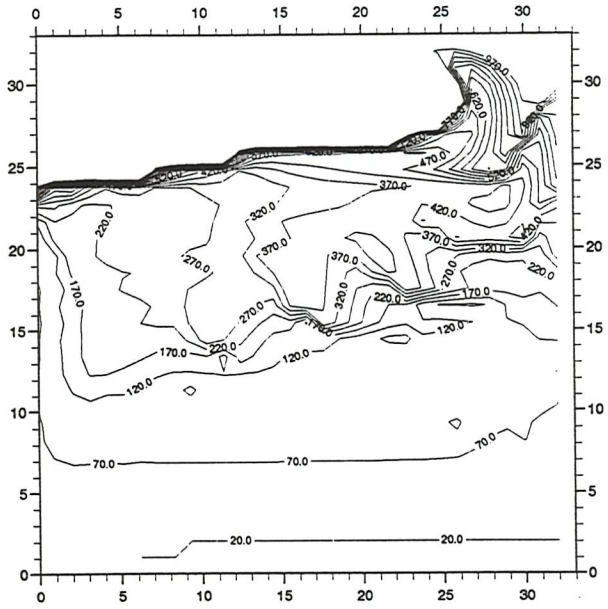

Figure 5.14b: A plot of the mixed layer depth in metres in March, year 16 of Box2. The plot is presented on the model grid with the scales showing the model grid indices

Figure 5.15: A bar graph of the permanent subduction rates on to each isopycnic layer sigma= 25.50-27.45 in spring, year 16 of Box2 for two values of the isopycnic tracer diffusion velocity (2 and 0 cm/s). The rates are presented as annualised rates in Sverdrups.

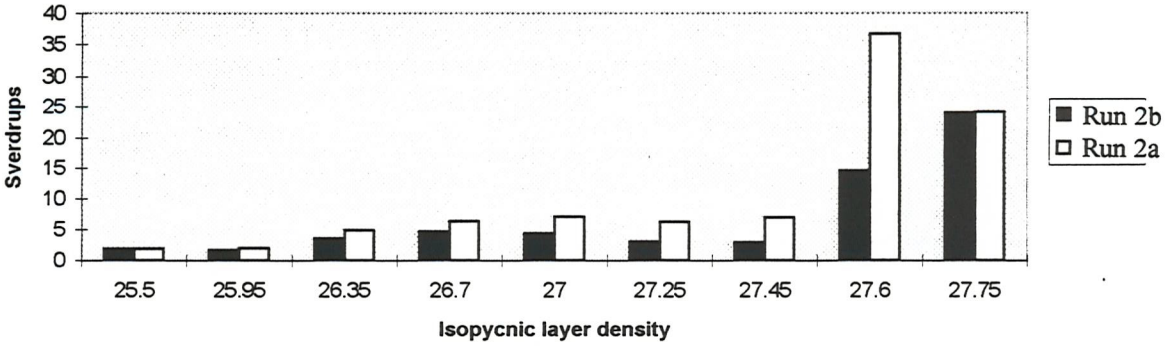

Figure 5.16: A plot of the tracer 'depth' (tracer concentration multiplied by layer thickness) in metres-for layer sigma = 26.70 in September, year 17 of Run2a of Box2 (using an isopycnic tracer diffusion velocity of 2 cm/s). The 'depth' is plotted on the model grid with the scales giving the model grid indices.

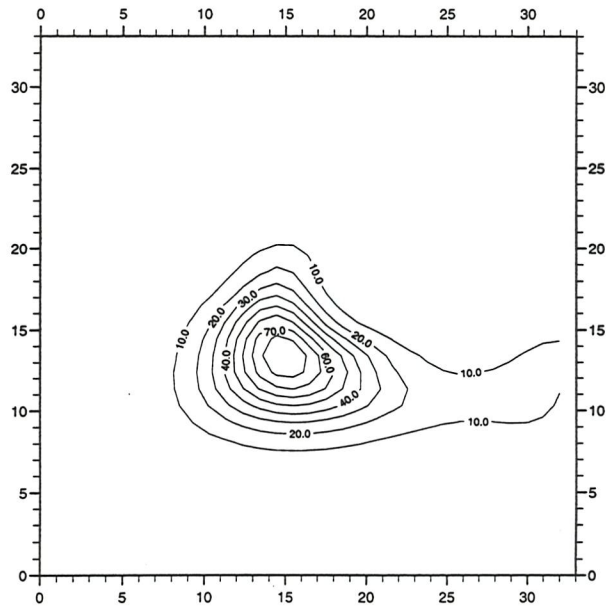

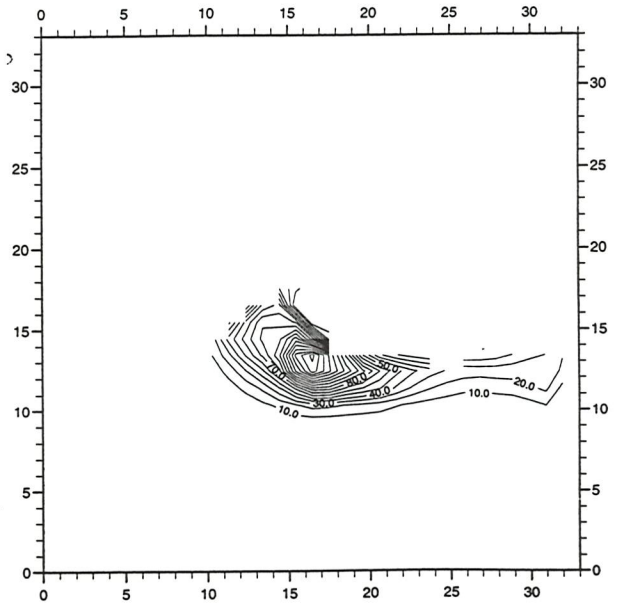

Figure 5.17: A plot of the tracer 'depth' (tracer concentration multiplied by layer thickness) in metres-for layer sigma = 26.70 in September, year 17 of Run2b of Box2 (using an isopycnic tracer diffusion velocity of 0 cm/s). The 'depth' is plotted on the model grid with the scales giving the model grid indices.

Figure 5.18: A meridional cross section of the upper 600 metres of Box3 basin at index i=15 through the interior of the ocean in September, year 16. The plot shows the outdropping of isopycnic surfaces with latitude. The scale along the top of the plot shows the model grid j-index.

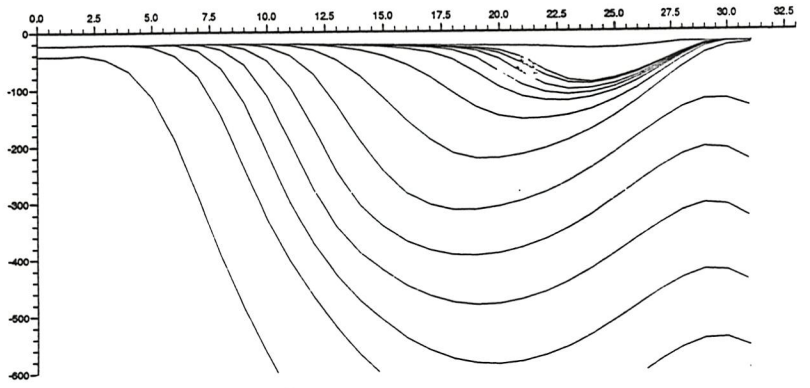

Figure 5.19: A bar graph showing the annualised permanent subduction rates in Sverdrups on to isopycnic layers sigma = 25.50-27.45 for Box3. For each layer the permanent subduction rate was measured in the spring of five years of the Box3 spin-up, years 6, 11, 16, 21 and 26. The permanent subduction rates are presnented such that the left-hand bar corresponds to the subduction rate in the sixth year and the left-hand bar to the permanent subduction rate in year 26.

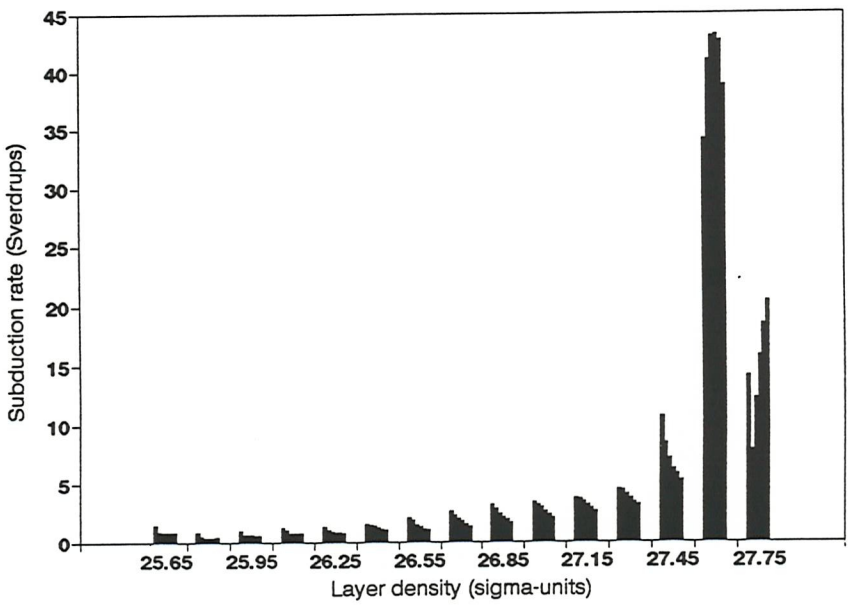

CHAPTER SIX

The influence of buoyancy forcing on permanent subduction rates in an isopycnic GCM

6.1 Introduction

The role of the surface buoyancy forcing in permanent subduction has been emphasised by a number of authors. Woods & Barkmann (1986a) associated the front along which permanent subduction by lateral induction occurs in the subtropics with the region of zero net buoyancy flux. Water columns advected through the zero net buoyancy flux region experience a shallowing seasonal thermocline, through the base of which lateral induction occurs. The mathematical treatment of Nurser & Marshall (1991) gives a clearer relation between the observed subduction rate and the surface buoyancy flux, associating the shallowing of the seasonal thermocline with the increasing buoyancy content and stratification of the water column.

The surface buoyancy flux, together with the surface wind stress, is also thought to control the circulation of the permanent thermocline. Williams (1991) has shown that the potential vorticity of the water entering the thermocline is set at the time of the spring detrainment. The potential vorticity of detrained water is governed by the ratio of the rate at which the mixed layer density decreases to the rate of detrainment, both which are determined by the surface forcing through the response of the mixed layer. It was established in Chapter Two that this relationship does not hold for the Kraus-Turner mixed layer model used in MICOM. However, the surface buoyancy flux does determine the winter mixed layer density field and through this the position of the low potential vorticity mode waters.

General circulation models (GCMs) use repeating annual cycles of wind stress and buoyancy fluxes to drive the circulation and the mixed layer, thus establishing a steady state cycle which is intended to represent some mean ocean cycle. In actuality, the

surface forcing of the ocean is subject to inter-annual variations which are potentially large. It would, therefore, be natural to assume that the permanent subduction of thermocline water in the North Atlantic is subject to strong variations over inter-annual time-scales, and that, through the potential vorticity generated in spring, this causes a variability in the circulation of the permanent thermocline.

The influence of inter-annual variation has been found to have a strong influence on transport through the Florida Straits (Worthington, 1977) and on the position of water masses along the Gulf Stream (McCartney, *et al.*, 1980). However, studies of the properties of the mode waters found within the Sargasso Sea over a period of 85 years found the temperature properties to be largely invariant on inter-annual time-scales (Schroeder, *et al.*, 1959, Warren, 1972) while on decadal and mesoscale time scales significant variability is observed (Frankignoul, 1981, Jenkins, 1982). Variability on the time scale of mesoscale eddies would imply that these eddies are significant in the Sargasso Sea circulation. The reported decadal variability is largely concerned with a change in the ventilation rates which occurred between the late 1960's and early 1970's; it is possible that this was connected to the Great Salinity Anomaly which occurred over the same period.

The variability of the circulation of the permanent thermocline has been studied in an idealised thermocline model by Liu (1993a&b) and by Liu & Pedlosky (1994). These authors found that the circulation of the ventilated thermocline was not strongly influenced by changes in the wind stress pattern, the oceanic repsonse was largely barotropic in this region. Liu & Pedlosky examined the influence of variability in the surface buoyancy flux and found that this induced variability in the potential vorticity field for a forcing function of sufficient amplitude. The authors also found a strong dependence of the mode water variability forced by surface buoyancy fluxes on the period of the forcing buoyancy flux, with a peak thermocline response at decadal time scales. This is in accord with the observations from '*Panulirus*' cited above.

The aim of this chapter is to examine the response of both subduction and ventilation to inter-annual variations in buoyancy forcing in the eighteen layer version of the Boxmix

implementation of MICOM. In the following section a control run will be examined; this uses a repeating cycle of surface buoyancy fluxes to drive the mixed layer cycle and the ocean circulation. In the third section a perturbation experiment will be described where the surface buoyancy fluxes are doubled for the course of one year, starting in spring. Thereafter the surface buoyancy fluxes are returned to the standard values. The evolution of the model in the wake of this perturbation is studied. In a fourth section a discussion of the result will be given. A final section will summarise the conclusions drawn in this chapter.

6.2 The control run

For the study of the surface buoyancy flux it is important that the flux should remain under direct control throughout the experiment. In the original formulation of Boxmix version Box3 (see Appendix A) the buoyancy flux comprises two components; an imposed radiative heat flux and a total turbulent heat flux generated by a Haney-term. This last uses the difference between the model sea surface temperature and an imposed pseudo-air temperature to generate a heat flux. The pseudo-air temperature used is lower than that observed over the North Atlantic, this offset is designed to include the contribution of the latent heat of evaporation to the cooling of the ocean surface. If the radiative heat flux is increased then the sea surface temperature of the model will rise and will increase the heat loss by the turbulent fluxes, thereby partially compensating for the increased radiative heat flux. It is, therefore, necessary to modify the model's formulation to ensure that the imposed changes in the surface heat flux are as intended.

The most appropriate way of doing this is to set the Haney term to the values used during the later stages of spin-up. To do this the Haney term was used to produce the turbulent heat flux from the imposed pseudo-air temperature and historical values of the model sea surface temperature. The twenty-sixth year of the spin-up of Boxmix was chosen as the year from which the model sea surface temperatures were extracted; data for this year is available at six day intervals, a higher temporal resolution than for other comparable years. Sea surface temperatures (SSTs) were linearly interpolated over the six day intervals. These historical SSTs are then substituted for the model's current SST

in the calculation of the Haney term. This gives a repeatable set of surface heat fluxes. The mean annual surface heat flux used is given in figure 6.1, positive values of the surface heat flux indicate heat loss by the ocean, negative values indicate heat gain. The GCM is initialised using the Box3 data for the end of year 26 (Chapter Five) and is run for thirteen and a half years, that is until the summer of year 40.

6.2.1 General description of the model circulation

The general circulation of the model over the first four years of the control run is essentially the same as the comparable years in the spin-up of Boxmix version Box3 in Chapter Five. The transport of the western boundary current in the two parallel runs are similar (~0.01% difference) and both exhibit the same downward drift (0.9% over four years). Over the rest of the control run the transport by the western boundary current continued to drop slightly. The total kinetic energy of the model over the same period remains stable with only a slight decrease over the thirteen years of the run. Thus the repeating fluxes used in this chapter give a circulation that is close to that found during run of Box3 in Chapter Five during the model years 26-30.

The volume tendencies of the isopycnic layers are largely the same as those of version Box3 in Chapter Five during years 26-30. The mean layer thicknesses of layers σ=25.65-26.70 remain stable throughout the run, while layers σ=26.85 and 27.00 rapidly deflate at a combined rate of 6.9 Sverdrups. The denser layers σ=27.15-27.60 deflate over the run by much larger annual rates than for layers σ=26.85 and 27.00, but much smaller when compared to the far larger bulk of these denser layers. The densest ventilated layer, σ=27.75, grows steadily throughout the thirteen years of the run. In conclusion, the subtropical thermocline is largely in thermal equilibrium with the surface forcing from year 26 onwards, with a net growth rate of 0.45 Sverdrups by the seasonal thermocline. Thermal equilibrium of the denser layers outcropping in the subpolar gyre has not occurred and would not occur until significantly longer model time had elapsed. This should not unduly influence the results of the following experiments.

6.2.2 Permanent subduction rates

The permanent subduction rate in the control run was measured using the tracer method at intervals over the period of the control run: in years 31, 32, 34, 35 and 39. The results of measurements made in years 31 and 39 are shown in figures 6.2a&b for the layers σ=25.65-27.45. It will be seen that variations in the permanent subduction rate for these layers are relatively slight, a drop from 22.0 Sverdrups to 19.9 Sverdrups in total (10% over the interval year 31-39, implying an exponential decay time scale of 76 years). The total permanent subduction rate on to the two densest ventilated layers (not shown) remains at ~59.0 Sverdrups throughout the run although the distribution of this flux between the layers shifts in favour of the σ=27.75 layer as the model evolves. This is in keeping with the general cooling of the sub-polar gyre that the surface fluxes for year 26 imply.

6.2.3 Permanent entrainment rates

The permanent entrainment calculated from the permanent subduction rate and the observed change in the permanent thermocline volume for years 31 and 39 is shown in figures 6.3a&b. This shows that there is more permanent entrainment than subduction on all layers shown; net entrainment occurs on layers σ=25.65-27.60, while layer σ=27.75 shows a large net subduction rate. This further illustrates the general cooling of the basin. The net entrainment of the lighter layers is slight for layers σ=25.65-26.70 throughout the model run and the total net entrainment rate for these layers drops from 1.0 Sverdrups in year 31 to 0.5 Sverdrups in year 39. The net entrainment rate of layers σ=26.85-27.45 drops slightly over the same period from 6.9 Sverdrups to 6.5 Sverdrups.

6.2.4 Renewal period

Figures 6.4a&b shows the renewal period of the water in each of the isopycnic layers σ=25.65-27.45, figure 6.4a shows the renewal period for year 31 and figure 6.4b the same quantities for year 39. The renewal period is found from the ratio of the mean annual permanent subduction rate for each layer to the volume of that isopycnic layer lying in the permanent thermocline. This is held to give an approximate estimate of the longevity of features in the permanent thermocline and the time over which the water in each isopycnic layer is renewed. It will be noted that the lightest layer, σ=25.65, has a

longer ventilation period than the layers σ=25.80 and 25.95, with a renewal period of 3.03 years in year 31, rising to 4.01 years in year 39. This is a result of the large volume of σ=25.65 water lying underneath the permanent thermocline in the extreme south of the model basin. In this region there is Ekman suction and the shallowness of the seasonal thermocline gives only weak lateral induction.

For the denser layers the larger permanent thermocline volume increases the renewal period. In figure 6.3a it will be seen that layers σ=25.65-26.25 are ventilated over a time scale of less than five years while layers σ=26.40-26.70 are renewed over periods of between five and ten years. For the denser layers the time scale for renewal increases rapidly with a renewal period of 15 years for σ=26.85 and 37 years for σ=27.45. For the densest ventilated layers the renewal period is 31 years for σ=27.60 and 61 years for σ=27.75. It should be noted however that these denser layers are not in thermal equilibrium so the measured renewal periods for these layers will be shorter than those of the eventual ocean state. In addition, the model does not include the export of deep water from the basin, the results for these deeper layers cannot, therefore, be used to estimate the renewal period of the deep water masses of the North Atlantic.

By year 39 (see figure 6.4b) the estimates of the renewal periods of the isopycnic layers have fallen for all of the layers σ=26.25-27.00 through the smaller permanent thermocline volumes of these layers. For the layers σ=25.65-26.10 the renewal period increased through the dropping permanent subduction rates while the volume of water ventilated remained stable. For the layers σ=27.15-27.45 the renewal period increased through the lower permanent subduction rates.

6.2.5 Tracer distribution in the thermocline

The distribution of tracer on layer σ=26.55 is shown in figure 6.5a for March (month 1), year 33. The tracer shown was detrained into the model thermocline in the previous spring (year 32) and the tracer is contained entirely within the permanent thermocline, entrainment has eroded the seasonal thermocline. The maximum in subducted tracer 'depth' (tracer concentration multiplied by layer thickness) is slightly to the west of the centre of the basin at a latitude of 34°N with a long ridge in the depth of subducted

tracer lying to the east of this maximum. By the following September the tracer has been diffused into a more radially-symmetric cloud with a maximum tracer depth of 12 metres (figure 6.5b). The maximum lies at the same longitude as it did in winter but is displaced southwards by 180 km by advection.

6.3 The perturbation run

The perturbation run began in March of year 31 (month 1) and lasted until March of year 32 (month 1). Over this period the surface heat fluxes due to both radiative and turbulent heat transports were doubled. The strength of this forcing is undoubtedly much higher than that observed but the aim of this experiment is not to simulate the exact response of an ocean but to examine the manner in which the processes that govern permanent subduction respond to changes in the surface forcing. From March, year 32 onwards the surfaces fluxes used in the perturbation run are the same as those used in the control run.

6.3.1 General description of the model circulation

The kinetic energy of the model during the first six years of the perturbation run remains higher than that for the control run. During the period of the perturbation the kinetic energy rises but after the re-stratification of year 32 the difference becomes more pronounced, rising to 8.6% higher than the control run by the autumn of year 33. The kinetic energy of the model decays slowly once the surface fluxes are returned to their control values; by the end of the run in the summer of year 40 the kinetic energy of the perturbation run remains 3.2% higher than the control run. Most of the increase in the kinetic energy lies in the deeper layers which through their bulk dominate the kinetic energy calculations.

The western boundary current transport in the sub-tropical gyre increases only slightly in the perturbation run and this increase is delayed until the spring of year 33, one year after the end of the perturbation period. By the summer of year 40 the western boundary transports of the two runs have converged. The response in the sub-polar gyre is more marked. The gyre transport (given by the extremum in the streamfunction) in the perturbation run, given by the extremum in the streamfunction in that gyre, is far higher

than that for the control run, 19.0 Sverdrups in the summer of year 33 rather than 17.5 Sverdrups. This strong response to the change in surface forcing disappears by the summer of year 37 (0.25 Sverdrups difference). There is no appreciable response by the tropical gyre transports.

6.3.2 Permanent subduction rates

The permanent subduction rate for each isopycnic layer was found by the tracer method for years 31-35 and 39. The results of the measurements for layers σ=25.65-27.45 are shown in figure 6.6a-c for year 31, 32 and 39. These results should be compared to the results of figure 6.2a&b. It will be noted that the initial response to the perturbation surface forcing is a reduction in the permanent subduction rate on all layers in year 31, although the permanent subduction rate for layer σ=27.75 remains largely unaffected by the change in surface forcing. In year 32, however, the permanent subduction rate on all layers is far higher than is found in the control run, with a total permanent subduction rate of 30.8 Sverdrups for layers σ=25.65-27.45 compared to 21.8 Sverdrups for the control run. The increase in the permanent subduction rates on layers σ=27.60 and 27.75 is greater still, from 60.2 Sverdrups in the control run to 105.6 in the perturbation run.

The difference between the results for years 31 and 32 of the perturbation run arises from the deeper mixed layer that the stronger winter forcing produces. Mode waters produced in the spring of year 31 must move from the seasonal thermocline into the permanent thermocline to be permanently subducted. However, the boundary between the seasonal thermocline and the permanent thermocline moves southward during the course of the year as the mixed layer reaches deeper into the thermocline in the winter at the end of year 31. Thus water must move further south from the place in which it was produced to ensure that it is permanently subducted. The mode waters produced in the spring of year 32, however, are advected southward as a northward shift in the boundary between the seasonal and permanent thermocline occurs, thus the distance over which water must travel to enter the permanent thermocline is less than in the control run and the permanent subduction rate for that year is higher than for the control run.

The change in the mixed layer depth resulting from the perturbation can be seen in figures 6.7a&b which shows the mixed layer depth at its winter maximum in (a) the control run and (b) the perturbation run. It will be noted that the strong gradient in the depth of the base of the seasonal thermocline moves further south in the perturbation run, especially in the eastern basin. This region is associated with the σ=27.60 isopycnal in the winter mixed layer; to the north of this line convective adjustment removes this isopycnic layer, resulting in an exceptionally deep mixed layer. In the sub-tropical gyre it will be noted that significant deepening of the seasonal thermocline is restricted to the northern half of the gyre, the area in which most permanent subduction occurs.

In years 33-35 (not shown) the permanent subduction rates on to layers σ=25.65-27.45 are lower in year 33 than in year 32, as would be expected from the shallower mixed layer depth produced by the return to standard forcing. The mixed layer depth in the winter at the beginning of year 33 is largely the same as for the same year in the control run. The differences are largely restricted to the sub-polar gyre where the increased production of σ=27.75 water the previous winter has raised the base of the seasonal thermocline, while the southward migration of the σ=27.60 mixed layer isopycnal has increased the depth of the seasonal thermocline in the eastern sub-polar gyre. By the winter at the beginning of year 34 the position of the σ=27.60 isopycnal is largely the same in the control and perturbation runs.

The permanent subduction rates for year 39 are shown in figure 6.6c. This figure should be compared to the results for the same year in the control run in figure 6.2b. The total permanent subduction rate on to layers σ=25.65-27-45 is 18.9 Sverdrups, 1.0 Sverdrups less than the same measure from the control run in the same year. The position of the mixed layer isopycnals at the time of the mixed layer's maximum depth (not shown) is identical in the control and perturbation runs in year 39. The depth of the mixed layer at this time is slightly greater in the control run in the centre of the basin at the latitude of the western boundary current separation. This greater depth results in a slightly higher subduction rate through the larger ∇h_1 term in equation 1.2. The shallower depth of the seasonal thermocline in the later stages of the perturbation run arises through the denser

waters laid down during the winter of the perturbation which arrest the descent of the mixed layer in subsequent years.

6.3.3 Permanent entrainment rates

The permanent entrainment rates in the perturbation run are calculated as in section 6.2.3 from the permanent subduction rates and the observed change in the volume of the layer in the permanent thermocline. This gives a large permanent entrainment rate in year 31, a natural consequence of the deeper mixed layer that the stronger heat fluxes generated in the winter of years 31-32. In total 39.0 Sverdrups are entrained from layers σ=25.65-27.45 in the permanent thermocline in year 31, 10.0 Sverdrups greater than the permanent entrainment rate for the control run. The permanent entrainment rate falls to 29.9 Sverdrups in year 33 and to 28.8 Sverdrups in year 34. This compares well with the control run measurement of 28.7 Sverdrups in year 34. The permanent entrainment rate continues to drop for the rest of the run, reaching 26.4 Sverdrups in year 39.

6.3.4 Renewal period

The renewal period of water in the thermocline was found to vary a great deal between years 31 and 32 (see figures 6.8a&b). The differences in the renewal periods on each of the isopycnic layers is most marked on the denser layers, where the value for layer σ=27.60 rises to 60.5 years in year 31 and then drops to 22.5 years in year 32. This sudden change occurs because of the reciprocal relationship between renewal period and permanent subduction rate, a three-fold increase in permanent subduction reduces the renewal period to one third its value. In year 33 it returns to a value of 28.6 years, rising to 31.2 years in year 34. In the same year for the control run the renewal period for that isopycnic layer is 31.8 years. For the less dense layers the magnitude of the change in the renewal periods is slight, as would be expected from the reciprocal relationship between renewal period and subduction rate. By year 34 the renewal periods for layers σ=27.00-27.45 have returned to close to their control run values, while those for σ=25.65-26.85 remain longer in the perturbation run. This largely due to the lower permanent subduction rates in the perturbation run, the volumes of these isopycnic layers in the perturbation run are less.

6.3.5 The distribution of tracer in the thermocline

The distribution of tracer on layer σ=26.55 is shown in figure 6.9a for March (month 1), year 33, this plot should be compared with figure 6.5a. The tracer shown here was detrained from the mixed layer in the spring at the beginning of year 32 and so this plot shows the tracer that has been introduced to the permanent thermocline. The distribution of the tracer is similar to that observed in fig. 6.5a, however the maximum in the tracer depth of the subducted tracer lies approximately 3° to the west and 2° to the south of the same maximum in the control run. In addition the maximum depth of subducted tracer is 25.5 metres, greater than the maximum of 21 metres for the control run. By the following September the tracer on this isopycnic layer has assumed a more diffusive distribution (figure 6.9b), similar to that in figure 6.5b although the maximum in the tracer depth still lies further west than in the control and the maximum in the tracer depth is greater, 15 metres rather than 12 metres.

6.3.6 Comparison of the permanent thermocline circulation with the control run

The circulation of the control and perturbation runs are illustrated by figures 6.10a&b. These plots show the advection of particles on layer σ=26.55 over a two year period running from the summer of year 31 to the summer of year 33. It will be noted that there is some change in the trajectory of particles advected along the northern edge of the layer outcrop as a result of the perturbation to the surface heat fluxes. This is due to the shift in the outcrop of the layer to the south and the steepening of the isopycnic layer outcrops in this region in year 32. Of more interest is the lack of any response in the more southerly parts of the gyre. The trajectories of particles advected through this region during this period are largely identical and there does not appear to be any influence of the circulation of the permanent thermocline away from the outcrop regions at this time.

The lack of an observable response may be the result of the slow propagation of the signal into the thermocline. However, an examination of the Montgomery potential on layer σ=26.55 from year 31 to year 40 (not shown) indicates that away from the outcrop region the geostrophic velocity, of which the Montgomery potential is the

streamfunction, is not greatly influenced by the changes made to the surface forcing. The ventilation period for this layer is estimated as between 5.9 and 6.4 years. Thus over a period of nine years the signal generated from the change in surface buoyancy forcing would be expected to have propagated throughout the ventilated basin.

Evidently the signal generated by the perturbation buoyancy forcing does not reach the interior of the ventilated thermocline. The lack of an observed signal can be explained by a number of mechanisms. The first possible mechanism is that the strong changes in the surface forcing elicit only a slight response in the thermocline structure and, therefore, do not change the potential vorticity field greatly. A second explanation is that thickness diffusion in the thermocline removes the perturbation induced by the change in the surface forcing and thus prevents the transmission of the perturbation signal through the thermocline. An alternative explanation is that the advection time scale is too long for the signal to reach the permanent thermocline before the onset of the following autumn when the water mass anomaly and its associated potential vorticity anomaly are re-entrained.

The Rossby waves generated by an anomaly introduced into the seasonal thermocline would also be expected to re-establish mean conditions. However, the time scales over which Rossby waves act in the mid-latitudes is far longer than the limit imposed by the annual cycle.

The diffusion time scale of the potential vorticity anomaly can be gauged from the half-width of the anomaly (L) and the diffusion coefficient (κ); this gives a thickness diffusion time scale ($L^2/2\kappa$) of 1.8 years. This time scale is longer than the seasonal, which implies that thickness diffusion cannot directly arrest the propagation of the thermocline anomaly into the permanent thermocline over the period imposed by the annual mixed layer cycle. However, the North-South extent of the outcrop zone is approximately 1100 km and the mean meridional velocity is of the order of 1.4 cm/s giving an advection time scale of 2.5 years, significantly longer than the seasonal time scale. Thus the lack of an observable signal in the permanent thermocline could arise from the slow advection of thermocline waters.

Figures 6.11a&b show the potential vorticity fields on layer σ=26.55 in April, year 32 in the (a) control run and (b) perturbation run, one month after the end of the perturbation period and after the re-stratification of the seasonal thermocline. This shows that the potential vorticity fields of the two runs differ in the region of the outcrop. In the perturbation run the 0.5×10^{-12} $cm^{-1}s^{-1}$ contour is more zonal; it extends further east than the same contour in the control run and covers a greater area in the western part of the outcrop, however it does not extend as far south as the same contour in the control run. The potential vorticity fields on the same layer for the control and perturbation runs in September, year 32 are shown in figures 6.14c&d. The perturbation run gives a lower potential vorticity in the eastern parts of the outcrop and the area enclosed by the 0.5×10^{-12} $cm^{-1}s^{-1}$ contour is greater and extends slightly further south than in the control run, indicating that low potential vorticity water is penetrating further into the thermocline.

It can be concluded that the potential vorticity anomaly that is generated by the perturbation does not propagate into the permanent thermocline. It would appear that in this implementation of MICOM the influence of individual anomalous years on the circulation of the permanent thermocline is slight, the advection of the layer thickness anomaly into the permanent thermocline takes longer than the time scale imposed by the seasonal cycle.

6.4 Discussion of the results of the perturbation to the surface heat flux

The results of the previous experiment show that for an isopycnal ocean model an enhanced basin-wide cooling reduces the permanent subduction rate of the previous year through the increase in the volume of the seasonal thermocline. Under severe conditions it also possible that the seasonal thermocline would deepen to the extent that mode waters which were permanently subducted in previous winters would become partially re-entrained. During the spring following a severe winter the deeper winter mixed layer introduces much larger quantities of mode water to the permanent thermocline. In

subsequent years the permanent subduction rate drops to the control value; the time-scale of this relaxation is of the order of two years.

It would appear from this experiment that the "Ekman demon" proposed by Stommel (1979) serves not only to control the season of the year during which the mixed layer introduces water to the permanent thermocline, but also partially controls which winters dominate the water mass properties of the permanent thermocline. Colder winters will be favoured over warmer through two mechanisms; the first is the greater volume of fluid transferred between the seasonal and permanent thermoclines, while the second is the removal of water from previous, warmer years as a result of the deepening seasonal thermocline.

A second result of this study, and one of potentially greater interest, is the invariance of the circulation of the permanent thermocline during the years following the perturbation to the surface forcing. Both particle trajectories and the Montgomery potential in the permanent thermocline remain unaffected by the extreme changes in the surface heat flux. This arises from the slight response of the model potential vorticity field to the surface forcing and from the inability of the model circulation to advect the layer thickness anomaly into the permanent thermocline over the seasonal time scale.

The response of the potential vorticity field to the surface forcing arises from the reciprocal relationship of potential vorticity to the layer thickness. In the regions of the mode water boluses the ventilated layers are thick, giving a low potential vorticity. An increase in the layer thickness in these regions will produce only a small decrease in the potential vorticity. Thus the greatest change in the potential vorticity field will occur in regions away from the mode water boluses, such as in the eastern basin and in the separated western boundary current. However, the ventilation of the thermocline predominantly occurs at the mode water boluses where the change in the potential vorticity field is suppressed by the thickness of the ventilated layer, thus changes in the surface forcing will produce a slight change in the potential vorticity entering the permanent thermocline.

In addition to the slight response of the potential vorticity field to the surface forcing, the velocities encountered in the ventilated thermocline are not fast enough to advect a potential vorticity anomaly into the permanent thermocline during the period imposed by the seasonal cycle. Thus even the slight anomaly produced in the above experiment did not enter the permanent thermocline before the onset of the autumn entrainment phase.

It was noted in Chapter Five that the southward jet associated with the ventilation of the permanent thermocline was faster when a lower thickness diffusion coefficient was used. For Boxmix version Box2 the southward velocity was found to be approximately twice than of version Box1. This increase in the southward velocity would halve the advection time scale to 1.2 years, only slightly longer than the annual cycle. The decrease in the thickness diffusion coefficient would also double the diffusion time scale for the anomaly to 3.6 years. Only a slightly faster thermocline flow would be necessary for the anomaly to enter the permanent thermocline over the annual time scale. This could be accomplished through a smaller thickness diffusion coefficient than used in Box2 or a lower eddy viscosity. The presence of low potential vorticity ventilation tongues in Box2 indicates the greater potential sensitivity of the thermocline circulation to potential vorticity anomalies in a low thickness diffusion regime. The presence of circulating/radiating potential vorticity anomalies in the eddy-resolving model of Cox (1987) suggests that this model was in a low thickness diffusion regime.

The problem of conserving heat content during the detrainment phase of the mixed layer evolution in an isopycnic model has been discussed in Chapter Two. This constraint on the detrainment phase prevents the mechanism proposed by Williams (1991) from operating, the stratification and therefore the potential vorticity field produced by the mixed layer are insensitive to the surface forcing during detrainment. The changes observed in the potential vorticity field arise from the deepening of the seasonal thermocline and from the south-western shift in the sites of mode water production, indicated by a shift in the late winter mixed layer isopycnals.

If the above result is taken to be representative of the North Atlantic then we would expect the circulation pattern of the permanent thermocline to be largely invariant to

inter-annual changes in the surface heat flux. However, it is not clear that the thickness diffusion coefficient used in this model is appropriate, nor is it clear what an appropriate value for the North Atlantic would be, disregarding the problems associated with the use of a simple diffusion scheme to represent sub-gridscale processes. Although the potential vorticity fields found in the permanent thermocline appear to be similar to the maps of McDowell, *et al.* (1982), the mixed layer detrainment algorithm may require a thickness diffusion coefficient much greater than that which could be derived from observations of the North Atlantic. Alternatively, the intensity of the eddy field in the North Atlantic may be great enough to allow the use of a thickness diffusion coefficient large enough to smooth out the anomalies inherent in a coupled isopycnic-mixed layer model.

If an appropriate value for the thickness diffusion coefficient in the North Atlantic is much lower then it is possible that there could be some dynamical feedback as a result of perturbations to the surface heat flux. Studies of a mid-latitude eddy-resolving model by Cox (1987) indicate that a potential vorticity anomaly was circulating the model gyre. If such a mechanism were at work in the North Atlantic then anomalies introduced to the potential vorticity field in winter would continue to influence the circulation and ventilation of the thermocline for some years. It has been suggested that a similar circulating anomaly can occur in the North Pacific, induced by the El Niño cycle (Jacobs, *et al.*, 1994). There is, however, little evidence that such circulating anomalies occur in either the North Atlantic or the Pacific. The Cox result could be a result of weak dissipation at the mesoscale, resulting in 'spectral blocking'.

6.5 Summary

In this chapter a perturbation to the surface buoyancy forcing has been applied to an isopycnic ocean model. This demonstrated that the potential vorticity anomaly generated by inter-annual variability in the meteorological forcing may not necessarily produce a change in the circulation pattern of the permanent thermocline, the signal is weak through the reciprocal relation between layer thickness and potential vorticity. In addition, the signal is not advected into the permanent thermocline before the onset of the entrainment phase of the mixed layer cycle. A perturbation of several years duration

to the surface forcing would therefore be necessary to induce a change in the permanent thermocline circulation. Over this time scale the diffusion of layer thickness in the permanent thermocline and Rossby dynamics would become would become important. This finding is in accord with the study of the ideal thermocline equations made by Liu & Pedlosky (1994).

It has also been demonstrated that the 'Ekman demon' proposed by Stommel (1979) also works on an inter-annual time scale through the variation of the depth of the seasonal thermocline. The mode waters produced by colder winters will make a greater contribution to the water properties of the permanent thermocline compared to those generated in other years. For water subducted in the preceding years, the deepening of the seasonal thermocline will increase the entrainment rate from the seasonal thermocline, whilst in subsequent years the denser waters laid down in the spring following an anomalously cold winter will prevent the creation of deep winter mixed layers.

Figure 6.1: The annual mean heat flux in Box3 year 26. The flux is plotted in units of W/m^2 on the model grid with positive fluxes indicating heat loss by the ocean. The contours are set at intervals of 10 W/m^2. The axes show the model grid indices.

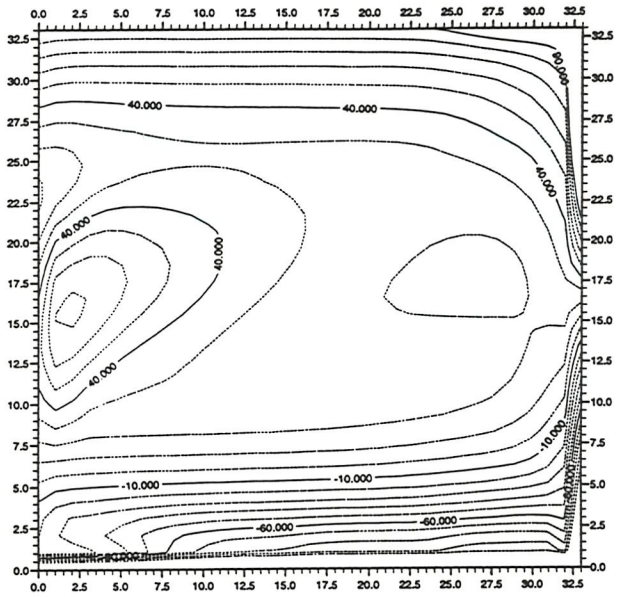

Figure 6.2a: A bar graph of the annualised permanent subduction rates in Sverdrups on to layers sigma 25.65-27.45 in year 31 of the standard run

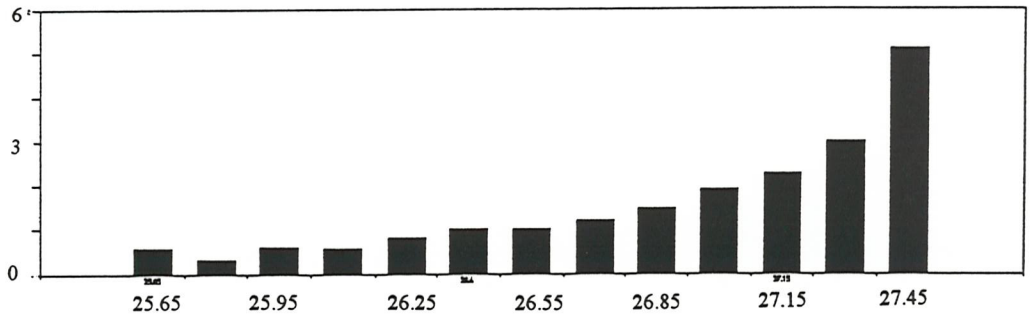

Figure 6.2b: A bar graph of the annualised permanent subduction rates in Sverdrups on to layers sigma 25.65-27.45 in year 39 of the standard run

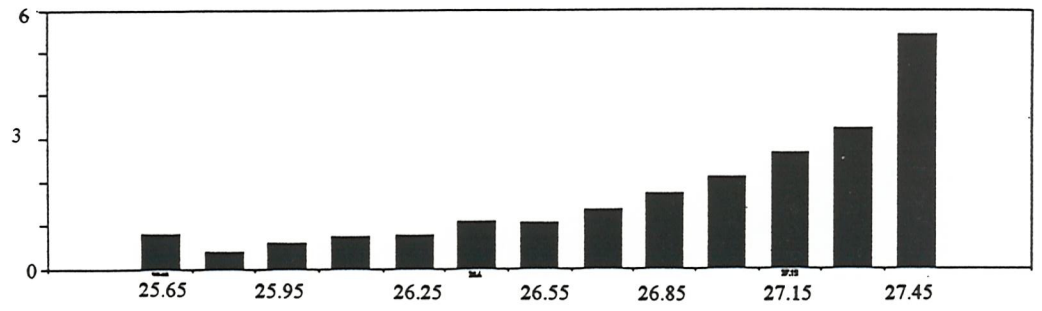

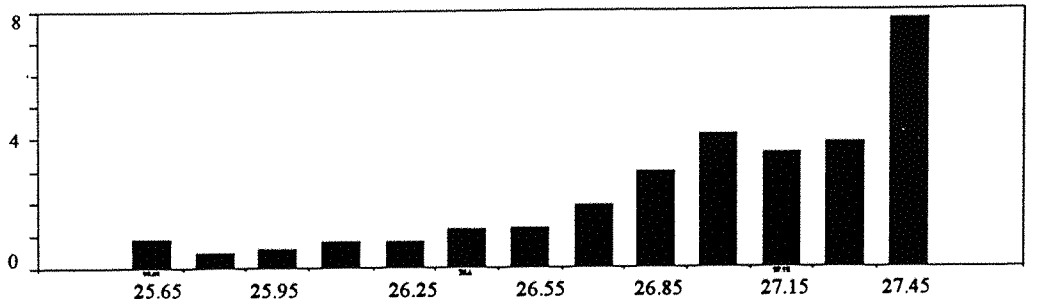

Figure 6.3a: A bar graph of the annualised permanent entrainment rates in Sverdrups on to isopycnic layers σ=25.65-27.45 in year 31 of the standard run.

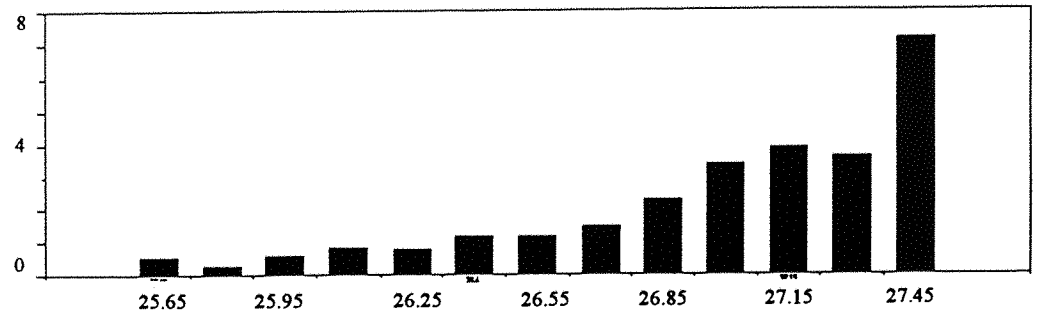

Figure 6.3b: A bar graph of the annualised permanent entrainment rates in Sverdrups on to isopycnic layers σ=25.65-27.45 in year 39 of the standard run.

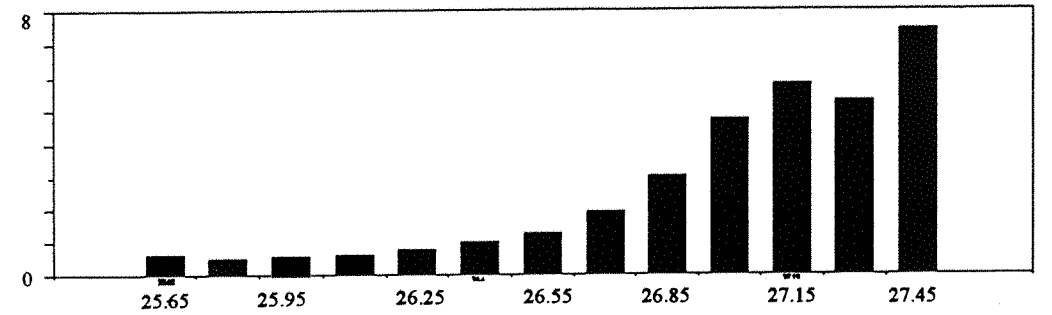

Figure 6.4a: A bar graph of the renewal period in years for isopycnic layers σ=25.65-27.45 in year 31 of the standard run.

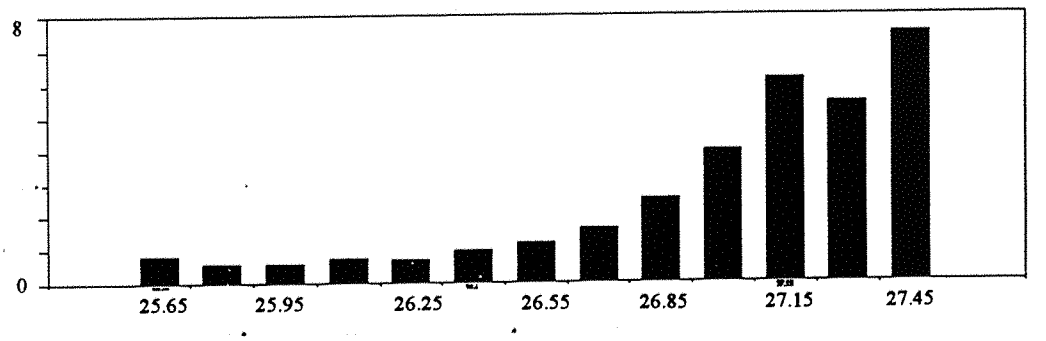

Figure 6.4b: A bar graph of the renewal period in years for isopycnic layers σ=25.65-27.45 in year 39 of the standard run.

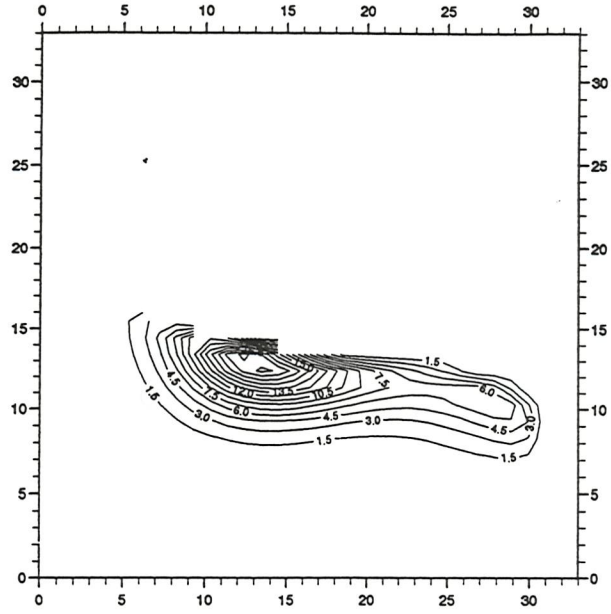

Figure 6.5a: A plot of the tracer 'depth' (tracer concentration multiplied by layer thickness) in metres on layer 26.70 in March, year 33 of the standard run.

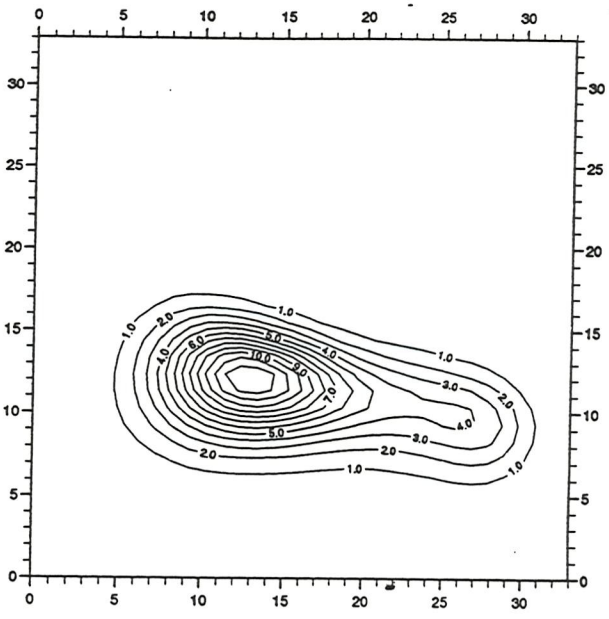

Figure 6.5b: A plot of the tracer 'depth' (tracer concentration multiplied by layer thickness) in metres on layer 26.70 in September, year 33 of the standard run.

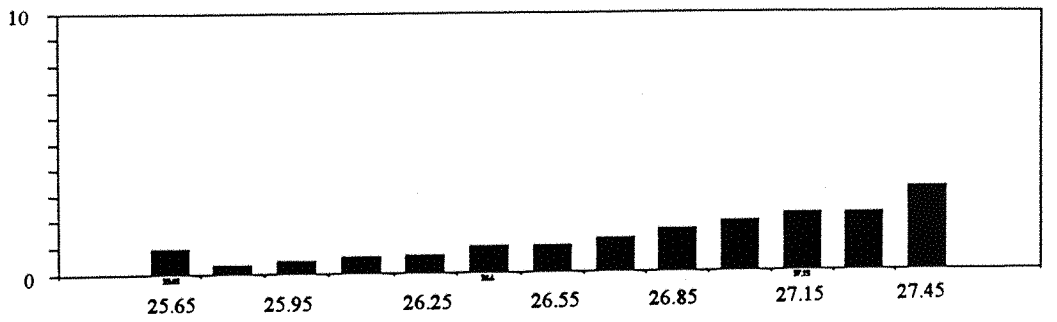

Figure 6.6a: A bar graph of the permanent subduction rates in Sverdrups on to layer sigma 25.65-27.45 in year 31 of the perturbation run.

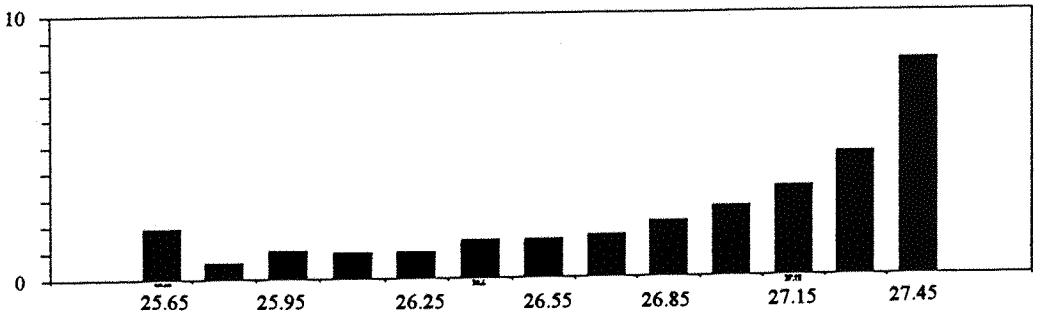

Figure 6.6b: A bar graph of the annualised permanent subduction rate in Sverdrups on to layers sigma=25.65-27.45 in year 32 of the perurbation run.

Figure 6.6c: A bar graph of the annualised permanent subduction rate in Sverdrups on to layers sigma=25.65-27.45 in year 39 of the perurbation run.

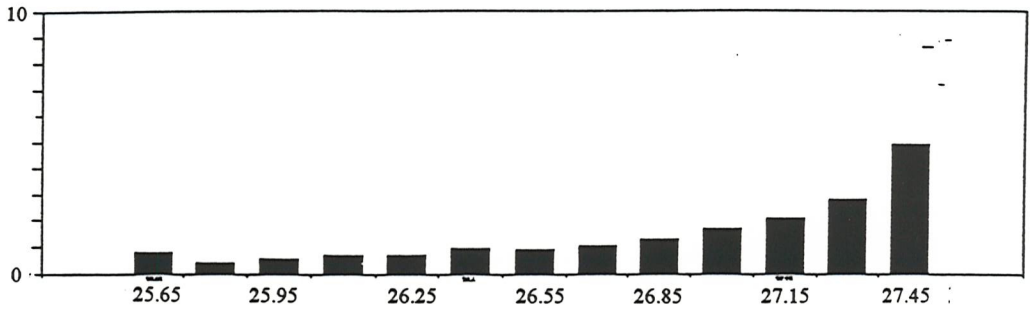

Figure 6.7a: A plot of the mixed layer depth in March of year 32 for the control run. The depth is given in metres and is plotted on the model grid with the scales giving the mode grid indices.

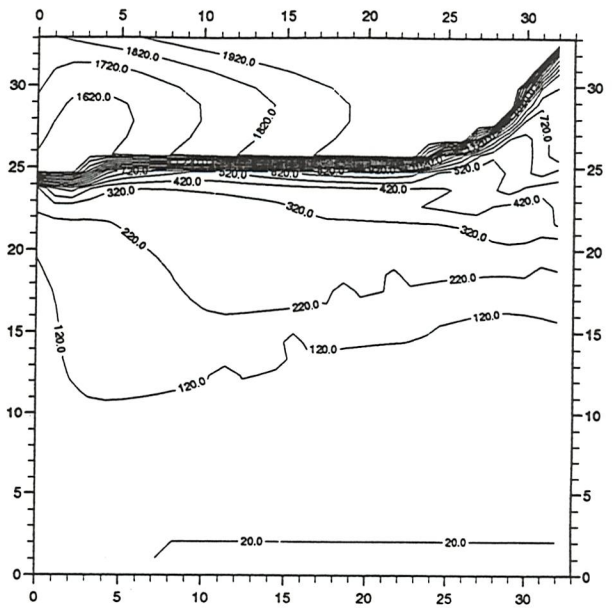

Figure 6.7b: A plot of the mixed layer depth in March of year 32 for the perturbation run. The depth is given in metres and is plotted on the model grid with the scales giving the mode grid indices.

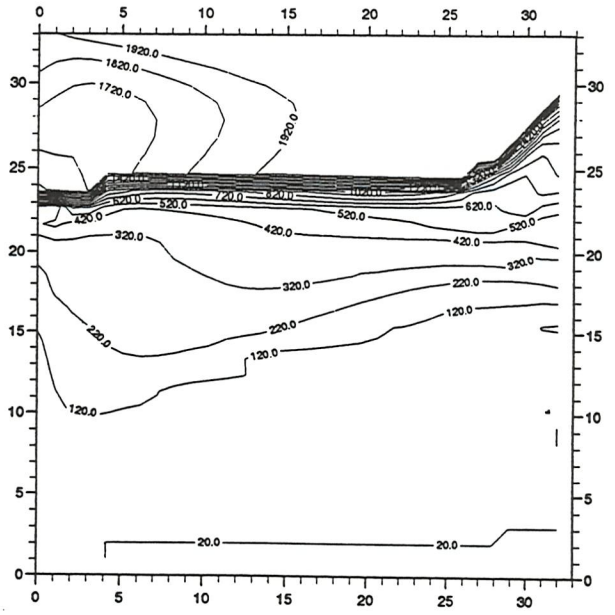

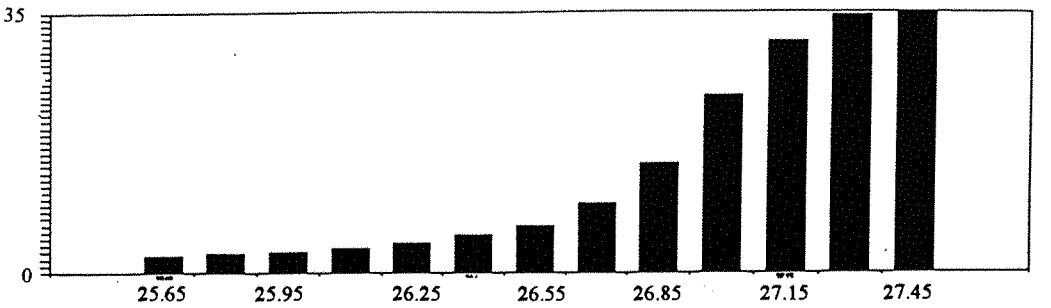

Figure 6.8a: A bar graph of the renewal period in years for isopycnic layers σ=25.65-27.45 in year 31 of the perturbation run.

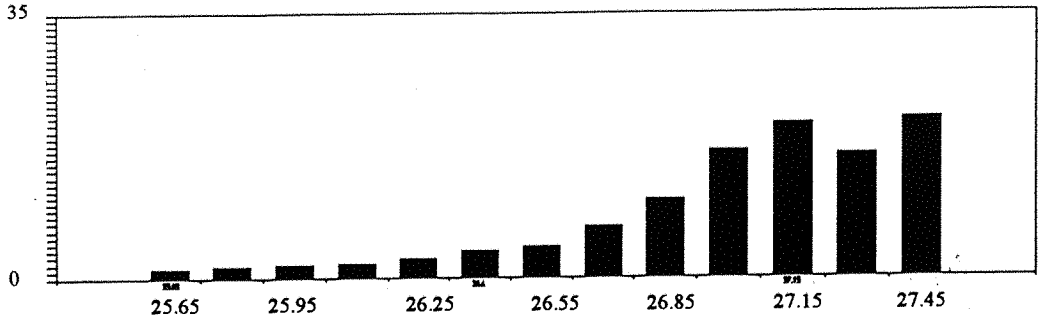

Figure 6.8b: A bar graph of the renewal period in years for isopycnic layers σ=25.65-27.45 in year 32 of the perturbation run.

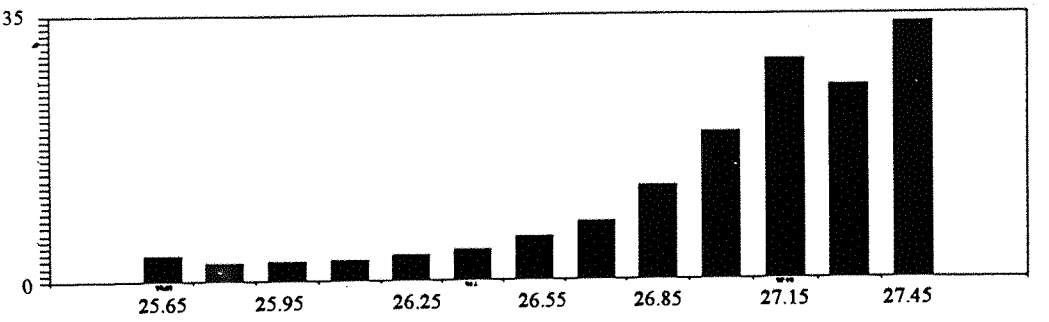

Figure 6.8c: A bar graph of the renewal period in years for isopycnic layers σ=25.65-27.45 in year 39 of the perturbation run.

Figure 6.9a: A plot of the tracer 'depth' (tracer concentration multiplied by layer thickness) in metres on layer sigma 26.70 in March, year 33 of the perturbation run.

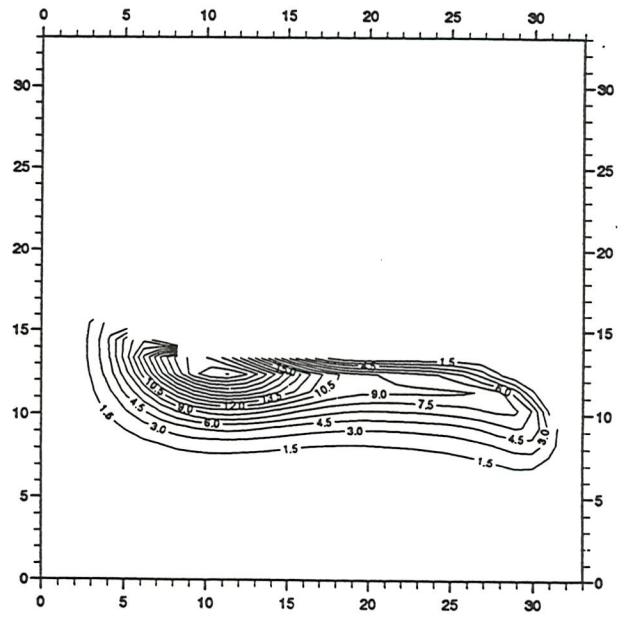

Figure 6.9a: A plot of the tracer 'depth' (tracer concentration multiplied by layer thickness) in metres on layer sigma 26.70 in September, year 33 of the perturbation run.

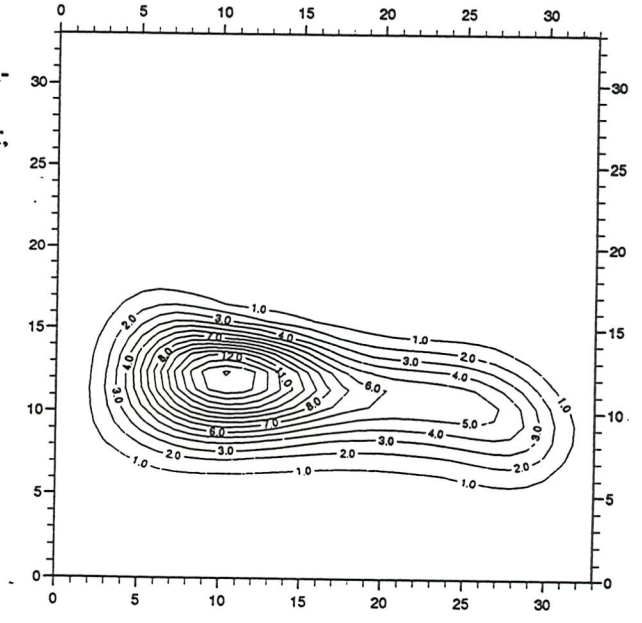

Figure 6.10a: A plot showing the trajectories of particle placed on isopycnic layer sigma 26.70 in March of year 31 of the control run and advected for two years. The plot is presented on the model grid with the scales showing the model grid indices. (Overleaf)

Figure 6.10b: A plot showing the trajectories of particle placed on isopycnic layer sigma 26.70 in March of year 31 of the perturbation run and advected for two years. The plot is presented on the model grid with the scales showing the model grid indices. (Overleaf)

Figure 6.10a:

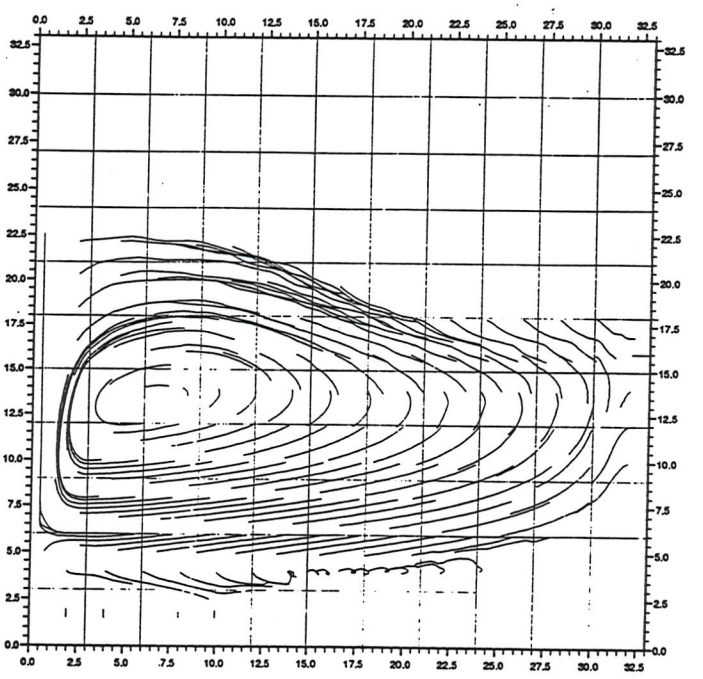

Figure 6.10b:

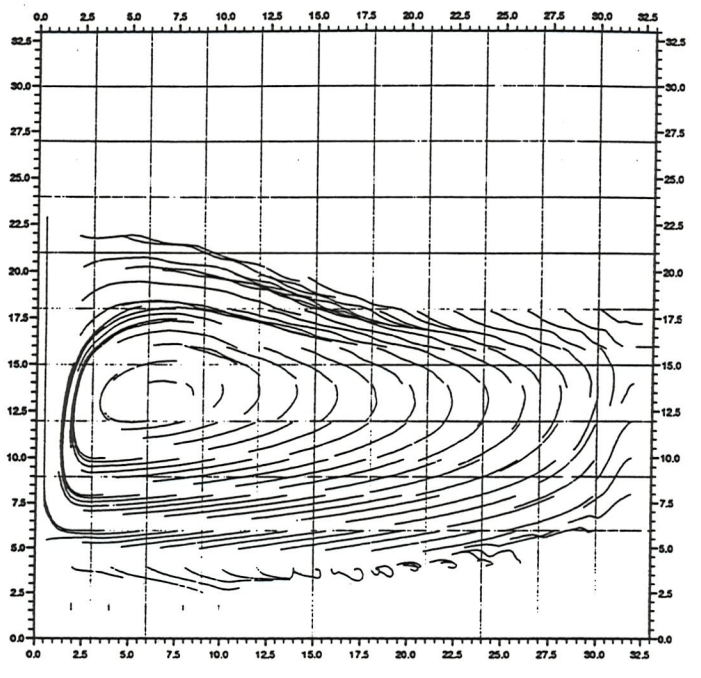

Figure 6.11a: A plot of the potential vorticity in units of $10^{-12}cm^{-1}s$ on layer sigma 26.70 in April of year 32 in the control run. The plot is presented on the model grid with the scales showing the model grid indices.

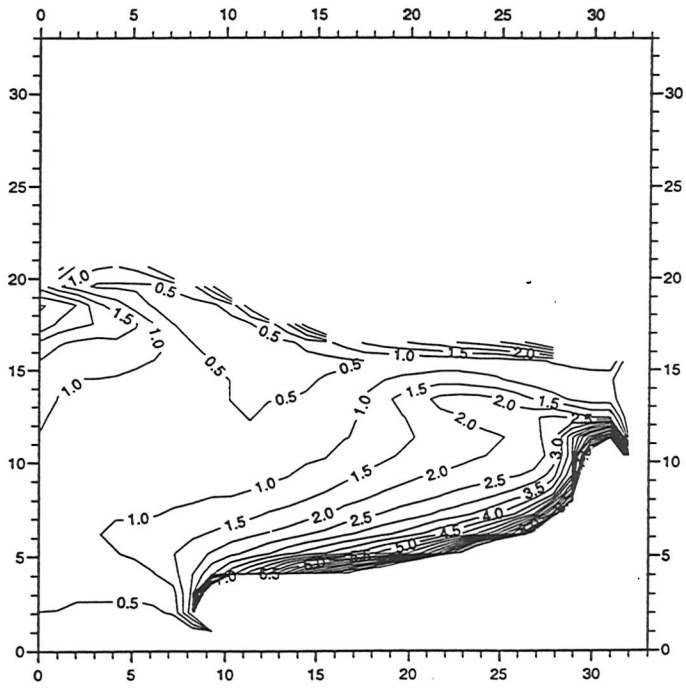

Figure 6.11b: A plot of the potential vorticity in units of $10^{-12}cm^{-1}s$ on layer sigma 26.70 in April of year 32 in the perturbation run. The plot is presented on the model grid with the scales showing the model grid indices.

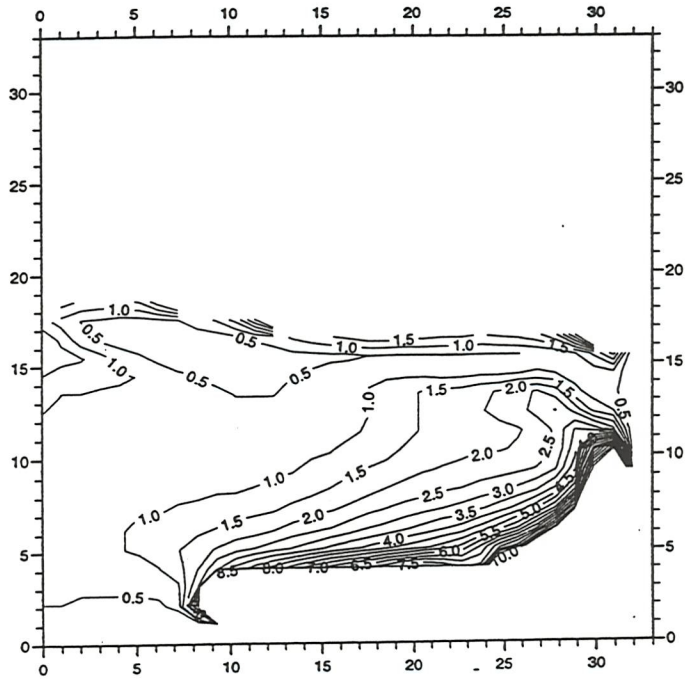

Figure 6.11c: A plot of the potential vorticity in units of $10^{-12}cm^{-1}s$ on layer sigma 26.70 in September of year 32 in the control run. The plot is presented on the model grid with the scales showing the model grid indices.

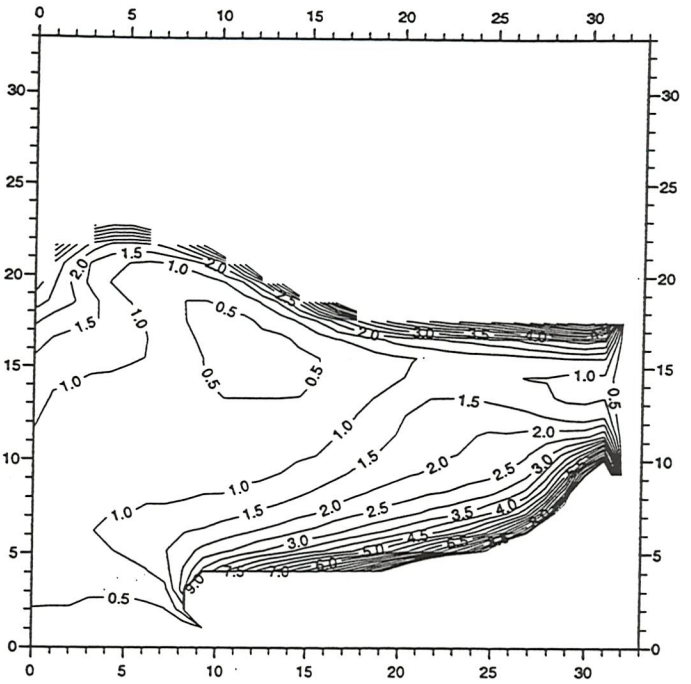

Figure 6.11d: A plot of the potential vorticity in units of $10^{-12}cm^{-1}s$ on layer sigma 26.70 in September of year 32 in the perturbation run. The plot is presented on the model grid with the scales showing the model grid indices.

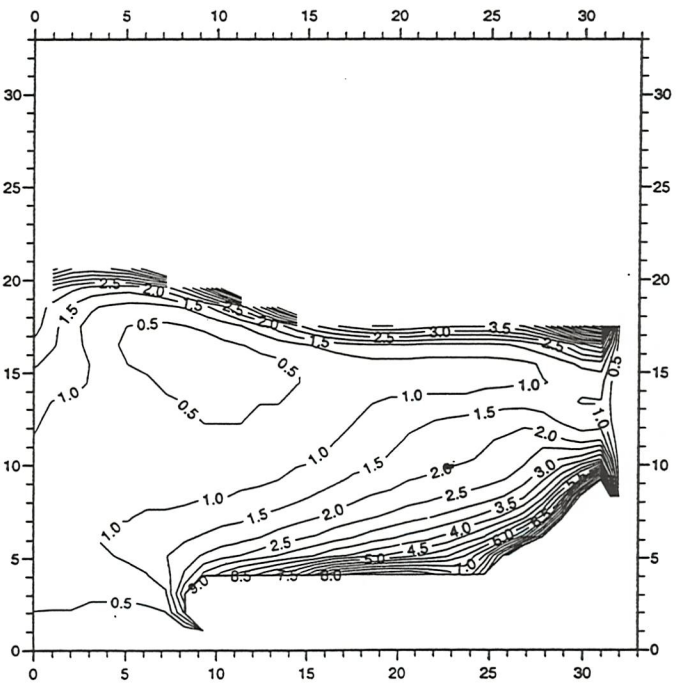

CHAPTER SEVEN

Discussion and conclusion

"Look not for whales in the Euxine Sea, or expect great matters where they are not to be found. Seek not for Profundity in Shallowness, or Fertility in a Wilderness. Place not the expectation of great Happiness here below, or think to find Heaven on Earth."

Sir Thomas Brown (1605-1687),
"On Happiness" from "Christian Morals"

7.1 Preliminary remarks

The aims of this thesis are to examine the processes of permanent subduction and ventilation as they are represented in an isopycnic GCM and to use the insight gained through this study to infer the nature of the processes as they occur in the North Atlantic. The focus of this thesis is on the formation of the subtropical mode waters rather than the denser classes of mode water produced in the subpolar gyre.

A number of diagnostic techniques are applied to the AIM model in order to fully diagnose the permanent subduction rate in that model. The influence of the parametrised eddy tracer and thickness diffusion fluxes on the permanent subduction rate and on the nature of the permanent thermocline circulation are also examined. The influence of inter-annual variability in the surface boundary conditions on the permanent subduction rate and thermocline circulation are also considered.

The processes of permanent subduction and ventilation are important for two main reasons. First, the generation of mode waters and their transfer to the permanent thermocline controls the structure of the permanent thermocline and hence the circulation in the ocean interior. Secondly, the transfer of water from the seasonal to the permanent thermocline also transfers heat and dissolved gases, which remain stored for up to decadal time scales in the subtropics. The study of the processes that govern the formation and life cycle of the subtropical mode waters are therefore of interest in the study of climate over these time scales.

The ability of a GCM to form water masses of the correct density, in the correct quantities and to reproduce the structure of the North Atlantic is a good test of the model's correct representation of the inter-action of the circulation and the surface boundary conditions. In addition, through the use of GCMs the process can be studied in more detail than is permitted from observational data. The influences of the parametrised eddy processes are under direct control which permits their role to be examined. A number of diagnostic methods have been developed to estimate the production rate of mode waters. These methods are to an extent complementary; they measure different components of the permanent subduction rate.

In the following section of this chapter the experiments undertaken in the previous five chapters are summarised in turn and a brief account of their main conclusions are given. In the third section of this chapter a discussion of the processes of permanent subduction and ventilation of the thermocline in the North Atlantic will be presented. This will be followed by a description of further work that could be undertaken to clarify some of the issues raised by these findings.

7.2 Description of the experiments

The coupling of the mixed layer to the isopycnic thermocline is examined in a comprehensive series of sensitivity studies in Chapter Two. In recognition of the asymmetry of the processes of entrainment and detrainment these processes are examined separately. For each parameter, surface boundary condition and initial condition a series of model runs are conducted using various values of the parameter or condition under examination; the values are chosen to span a broad range of possible values. The influence of each parameter or condition on the model's evolution is evaluated by the variation in one of the model variables. For experiments in the entrainment phase the late winter mixed layer temperature and depth are chosen, while for the detrainment phase experiments the thicknesses of the isopycnic layers after spring restratification are chosen.

It is found that the mixed layer is sensitive to all parameters and boundary conditions imposed during the entrainment phase. This behaviour can be understood through the

energy balance equation B.12 in Appendix B. The sensitivity of the mixed layer entrainment to the parametrisation offers a wide scope for tuning the model to reproduce the observed mixed layer entrainment phase. In contrast, the detrainment phase is found to be insensitive to all parameters used. The stratification of the thermocline after spring depends only on the isopycnic layers available and the initial density of the mixed layer at the start of the detrainment phase. This dependence indicates that the detrainment algorithm is constrained by the requirement of placing detrained water on isopycnic layers whilst conserving heat content.

Through the use of Lagrangian mixed layer models and their comparison with the stratification of a GCM in Chapter Three it is shown that the structure of the thermocline in the GCM cannot be reproduced by a mixed layer ensemble. The sensitivity of the spring thermocline to the late winter conditions and the strong sensitivity of the late winter mixed layer conditions on all aspects of the model parameters and forcing produce a rapid divergence between the mixed layer model and GCM at the first spring.

The influence of a number of GCM processes on the evolution of the upper thermocline can be examined through a buoyancy budget of an ensemble of Lagrangian water columns. In AIM it is found that the change in the water column buoyancy content for a water column advected in the subtropical gyre over one annual cycle is dominated by the net surface flux of buoyancy (including surface heat and fresh water fluxes and the fluxes due to Ekman drift). In contrast, the divergence in the shear-advected buoyancy flux (Eq.s 3.4 & 3.5) makes a large contribution to the buoyancy content change in the subtropical gyre of Box1. This difference indicates a qualitative difference in the circulations of the two models which is assumed to be the result of differences in the values of eddy parameters, particularly thickness diffusion.

The rate of production of mode waters in AIM is examined in Chapter Four. Four methods of determining the permanent subduction rate are used; a ventilation tracer method, the kinematic method (Marshall, *et al.* 1993), the method used by Williams, *et al.* (1995) and a Lagrangian particle method (described in section 4.4). The permanent subduction rate in AIM is found to be of the order of 67 Sverdrups with 22.5 Sverdrups

of the subtropical mode waters produced (σ=26.80-27.00). This flux into the thermocline is found to be dominated by advection by the mean currents, with the eddy transport (represented by thickness diffusion) representing 7% of the total flux. The diffusion of seasonal thermocline water into the permanent thermocline is found to be insignificant. A large residual (12%) includes the contribution of diplacements of the isopycnic layers through the base of the seasonal thermcline and cumulative errors from the estimates of other fluxes.

Subtropical permanent subduction is found to occur on the southern flank of the North Atlantic Current, coincident with the zero net buoyancy flux contour of Chapter Three. Permanent subduction rates per unit area of up to 600 metres per annum are found in this region, with this transfer occuring over ~20 days in April of each year. Away from the northern rim of the gyre the permanent subduction rates are lower and are spread over slightly shorter periods with the exception of the westward intensification where the subduction period is long yet the permanent subduction rate per unit area is low.

The production of subtropical mode waters is balanced by permanent entrainment in the Gulf Stream and North Atlantic Current centred on two regions; the first to the south-east of Newfoundland and the second to the south-east of Cape Cod. The permanent entrainment period here is long (order 100-150 days) with large permanent entrainment rates (up to 350 metres per annum).

AIM is found to produce excessive amounts of Labrador Sea Water and other dense water masses. This probably arises from the short spin-up time of the model (30 years in this study) and the poor vertical resolution of the model in the poleward basins.

In contrast to AIM, the permanent subduction rate of the Boxmix GCM version Box1 is found to be sensitive to the value of the tracer diffusion coefficient. A tracer diffusion coefficient of $\sim 2 \times 10^7 \, cm^2 s^{-1}$ contributes 37% of the total permanent subduction rate. The contrast in the results of AIM and Box1 arise from the different regions of parameter space the models occupy. While AIM has low eddy parameters, representing a weakly eddying ocean, Box1 has much larger values of the eddy parameters,

representing a more active eddy field and more linear flow. The greater diffusivity and consequently slower circulation in Box1 typically gives lower Péclet numbers than AIM (a factor of 2.8 between the two model circulations).

The role of thickness diffusion , and by inference the baroclinic eddies they represent, is examined through comparisons of two parallel runs of the Boxmix model (Box1 and Box2) with differing values of the thickness diffusion coefficient. It is shown that a lower thickness diffusion coefficient permits the formation of a ventilation tongue in the permanent thermocline with an associated southward jet. The increased speed of the thermocline circulation increases the Péclet number, indicating a reduced importance of tracer diffusion to the permanent subduction rate. It is suggested that the strongly advective regime of the AIM thermocline arises through the low eddy coefficients, in particular the eddy viscosity and thickness diffusion coefficients, which permit fast flows and their associated thermocline structures.

The role of advection also appears to be important in maintaining the circulation of the thermocline under fluctuating forcing in the strongly diffusive thermocline regime. The circulation of the permanent thermocline is governed by the potential vorticity of the water masses that ventilate the interior. A change in the surface buoyancy forcing induces changes in the injected potential vorticity through the lateral shift in mode water production sites and through the process identified by Williams (1991), although the second process cannot manifest itself in MICOM because of the mixed layer model's heat conservation condition during detrainment.

In Chapter Six a spun-up isopycnic model is subjected to an anomalous annual forcing cycle and then returned to the spin-up annual forcing cycle. For the duration of the perturbation year the total surface heat fluxes is doubled. The permanent subduction rate for the anomalous year is far higher than that of a parallel control run. The permanent subduction rate is found to return to the control values over a period of 2-3 years.

The circulation of the permanent thermocline is found to be largely unaffected by the extreme change in the surface boundary conditions. This is found to arise partly through

the weak response of the potential vorticity field but also through the long advection time scale in the seasonal thermoline. It will be noted that the model used was in a strongly diffusive regime with the same parameters as used in Box1, Run 1a. It is suggested that a strong thermocline response would be observed for an ocean with a faster thermocline circulation (therefore shorter advection time scale), which the results of Chapter Five suggest would occur for lower values of the thickness diffusion coefficient.

7.3 General discussion

The potential role of eddies in the permanent subduction of mode waters into the permanent thermocline and the subsequent ventilation of the ocean interior has been demonstrated in Chapter Five. In models of the coarse resolutions used here, the eddy processes are necessarily represented by diffusive parametrisations (a Laplacian scheme is used here). Eddy viscosity is used to represent the transport of momentum $\left(\overline{\mathbf{u}'\mathbf{u}'}\right)$, eddy tracer diffusivity is used to represent the transport of tracer quantities $\left(\overline{\mathbf{u}'\tau'}\right)$ and layer thickness diffusion is used to represent the transport of water masses $\left(\overline{\mathbf{u}'\mathrm{h}'}\right)$. Although MICOM does not include an explicit interfacial friction parametrisation of the vertical penetration of mesoscale eddies, it has been shown that the influence of thickness diffusion is to maintain ageostrophic currents which bring about the vertical redistribution of momentum (Gent & McWilliams, 1990). The inadequacies of the diffusive parametrisation scheme are acknowledged. However, the use of such a parametrisation is a necessity of computational economy and aids insight into the role of each process through the reduction of their efficacy to a small set of parameter values.

The circulations of Aim and Box1 represent different ocean states; the weakly diffusive circulation represented by AIM produces fast thermocline flows, the dominance of advection in permanent subduction, higher Péclet numbers and ventilation tongue structures in the thermocline. In addition, the eddy parameter values are probably responsible for the dominance of the net surface buoyancy flux in the evolution of the upper thermocline buoyancy content in a Lagrangian frame.

In contrast, the strongly diffusive circulation represented by Box1 produces broad, slow thermocline flows, low Péclet numbers and results in an enhancement of the contribution of tracer diffusion to pemanent subduction. This flow regime may also result in the significant contribution of vertical shear in the evolution of the buoyancy content of the upper thermocline in a Lagrangian frame.

The values of the eddy tracer diffusivities which are pertinent to the North Atlantic are open to dispute. The range of values taken from oceanographic tracer data and eddy-resolving GCMs indicates values as high as $8 \times 10^7\ cm^2 s^{-1}$ (Böning & Cox, 1988). The values taken from field studies span a range of values including the values used in AIM and Box1 (*e.g.* Olbers, *et al.* 1985; $1.0 \times 10^7 cm^2 s^{-1}$, Thiele, *et al.* 1986; $2.5 \times 10^7 cm^2 s^{-1}$, Schäfer & Krauss 1995; $10.2 \times 10^7 cm^2 s^{-1}$). The problem is further complicated by the probable spatial non-uniformity and anisotropy of the North Atlantic eddy field and thus non-uniformity and anisotropy of the implied diffusivity.

Estimates of the thickness diffusivity implied by the eddy field of the North Atlantic are not currently available. The parameters used by Danasbasoglu, *et al.*(1994) and Bleck, *et al.* (1992) have assumed values of the same order as the tracer diffusivities. The potential for the generation of baroclinic eddies exists throughout the North Atlantic subtropical gyre. McDowell, *et al.* (1982) found a reversed potential vorticity gradient with depth over most of the gyre. It would be expected that the spring seasonal thermocline would be unstable to pertubations and that this would result in substantial mixing soon after detrainment.

Some further circumstantial evidence of the nature of the subtropical North Atlantic's flow regime can be inferred from hydrographic data. The survey of potential vorticity by McDowell, *et al.* (1982) indicates that the thermocline potential vorticity field is largely uniform, especially in the deeper subtropical thermocline. On lighter isopycnic layers there is some evidence of inhomogeneity, however, it is not clear whether this is the signature of a ventilation tongue. The examination of zonal hydrographic sections through the subtropical gyre do not show the steep eastward shoaling of isopycnic

surface observed in AIM or Box2 which are associated with the ventilation tongues of a weakly eddying ocean. The tracer distributions of Sarmiento (1983b) do not indicate that bomb tritium is advected into the permanent thermocline along ventilation jets, rather the process appears more diffusive.

The weight of evidence appears to suggest that the North Atlantic is in a low Péclet regime; a strongly diffusive ocean with a slow mean thermocline circulation and with the eddies making a large contribution to the coupling of the seasonal and permanent thermoclines. It should be emphasised that further evidence needs to be gathered before this description can be accepted completely.

Assuming that the description given in the previous paragraph holds for the North Atlantic, it is suggested that the permanent subduction rate of the North Atlantic is higher still than the tracer estimate of AIM, closer to the tracer estimate of Sarmiento (1983a). A number of studies have attempted to diagnose the permanent subduction rate in the North Atlantic (summarised in Table 4.1). The estimate of Sarmiento (1983a) using bomb tritium data gives the largest permanent subduction rate, indicating a permanent subduction rate of 39.5 Sverdrups for water masses in the range σ=26.20-27.40. The method employed by Sarmiento (1983a) is the most direct means of estimating the permanent subduction rate in the North Atlantic; in future this tracer estimate should be augmented by others using CFC tracer ratios.

Estimates of the permanent subduction rate in the North Atlantic have been derived from observational data by a number of authors. The methods employed have been diverse while methods previously applied to ocean models could conceivably be applied to ocean data. Of all these methods, the most reliable is the study of tracer distribution, *e.g.* tritium and CFCs. Tracers are effective markers of the mode water masses and the distribution of tracer mirrors the mode water distribution. The tracer distribution implicitly includes diffusive processes and the vertical transport of tracers whereas many of the other methods estimate only the advective component of the permanent subduction rate or idealise the mechanism of permanent subduction. However, tracer studies are far more difficult in the ocean than in a GCM. The distribution of tracer is

examined through tracer ratios from which an age can be derived for the water mass. The ratio (and therefore the age estimate) are influenced by the mixing of water masses and by the de-gassing of 'elastic' tracers such as helium. This problem could be removed if a stable tracer introduced to the environment for only a short period could be found. The distribution of such a tracer would give a reliable estimate of the mean permanent subduction rate during the period of its presence in the atmosphere.

The response of the North Atlantic to variability in the surface forcing conditions would appear to be slight if the ocean is assumed to be strongly eddying. This weak response arises from the slower thermocline circulation and through the dissipation of the anomaly signal in the permanent thermocline. The ocean eddy field has previously been invoked to explain the invariance of 18°C mode water properties on inter-annual time scales through the communication of the ventilated thermocline and the pool zone (Dewar, 1986). It is possible that the dynamical invariance of the permanent thermocline may also depend on the eddy field.

7.4 Future work

The use of a diffusive representation of eddy processes is a necessary weakness of the experiments presented here; necessitated by both economy and by the ease with which the model's parameters can be controlled. In order to extend the conclusions of this thesis to the North Atlantic with more confidence it is necessary that the broad properties of weakly and strongly diffusive oceans are examined more directly. This would require the use of a far higher model resolution than either those of AIM or Boxmix. The three diffusive processes, eddy viscosity, eddy mass transport and eddy tracer transport, would then be partly represented by resolved dynamics and would, therefore, be related to one another. A change from a weakly diffusive ocean to one with stronger diffusive fluxes would not only alter the implied thickness diffusion and isopycnic tracer diffusion, but would also vary the eddy viscosity. The influence of the eddy viscosity on the permanent subduction rate and on the circulation of the model was not investigated in this thesis. It would therefore be necessary to undertake studies of the influence of eddy viscosity in a low resolution run on the permanent subduction rate and circulation before proceeding with a fully eddy-resolving simulation.

For ease of comparison, an eddy-resolving comparison is best carried out using the same model code as the low-resolution model with the model grid and eddy coefficients adjusted to suit the higher spatial resolution. The eddy field of the high-resolution model can be controlled through the eddy viscosity and thickness diffusion coefficients used to parametrise the processes remaining below the grid scale. A high value of the coefficients would remove energy from the circulation and produce a weakly eddying ocean simulation. A lower value of the coefficients would permit the creation of a strongly eddying circulation. The comparison of the two high resolution runs would indicate whether there is a shift in the nature of the dynamics of the ocean thermocline with the strength of the eddy field and through the use of tracer studies, particle trajectories and kinematic studies the permanent subduction rate in the model could be fully diagnosed. This method is essentially the same as that applied by Krauss & Böning (1988) to the study of horizontal diffusivities in a Bryan-Cox model.

A second area of uncertainty lies in the role of Rossby waves in the ocean thermocline. In the eddy-resolving model of Cox (1987) and in the idealised study of Dewar (1990) Rossby waves are seen to have a strong influence on the circulation of the permanent thermocline. In addition, recent theories concerning the variability of the climate in the northern hemisphere have been advanced where the ocean Rossby wave dynamics control the ocean part of the feedback (Latif & Barnett, 1995). In part, the role of Rossby waves is suppressed by the annual mixed layer cycle, radiating Rossby waves are set up by the retreating mixed layer and propagate westwards in the seasonal thermocline, producing the strong southward current on the eastern flank of the mode water boluses seen in the Box2 version of Boxmix and in Dewar (1990). These waves are however removed by the descending mixed layer in autumn/winter erasing the structure of the seasonal thermocline and with it the signature of the Rossby waves. The influence these waves have on the circulation of the seasonal thermocline, their influence on the permanent subduction of mode waters over seasonal timescales and their influence on the closure of the mixed layer annual cycle are of interest.

In Chapter Three a buoyancy budget for AIM and for the high thickness diffusion run, Box1, were presented. It was asserted that the qualitative difference in the balance of the terms in the buoyancy budget resulted from the differing dynamics of the thermocline between the two models. In order to confirm this finding a buoyancy budget of a low thickness diffusion run would be necessary. If the conjecture of Chapter Three is correct the buoyancy budget for an ensemble of Lagrangian columns in the Box2 subtropical gyre should be dominated by the net surface buoyancy flux (sum of the surface buoyancy fluxes and those due to Ekman drift).

The influence of inter-annual perturbations on the circulation of the permanent thermocline was found to be slight in a high thickness diffusion version of Boxmix (Box3). It was found that the advection timescale for a potential vorticity anomaly was too long for the influence of the change to the surface forcing to propagate beyond the seasonal thermocline. An increase in the thermocline velocities through a decrease in the thickness diffusion coefficient would result in an increase in the southward thermocline velocities and, if the mechanism described in Chapter Six is correct, anomalies generated by changes to the surface forcing of the model would be advected into the permanent thermocline. In order to have full confidence in this explanation it is necessary that the prediction for the low thickness diffusion run is confirmed.

"Procopius mentions that ... a great sea monster was captured in the neighbouring Propontis ... he must have been whale; and I am strongly inclined to believe a sperm whale."

Herman Melville (1819-1891),
"Moby Dick"

APPENDIX A

The Miami Isopycnic Coordinate Ocean Model

A.1 Introduction

The Miami isopycnic coordinate ocean model (MICOM) has been developed over a number of years at the Rosenthiel School of Marine and Atmospheric Sciences, Miami. The development of the model has been reported in numerous papers by Bleck, *et al.*, but the papers of greatest relevance to this study are Bleck & Boudra, 1986 (covering the first version of MICOM, 'Boxmix'), Bleck, Hanson, Hu & Kraus, 1989 (describing the coupling of the mixed layer model to the ocean model), Bleck & Smith, 1990 (describing the version of MICOM implemented as AIM) and Bleck, Rooth, Hu & Smith, 1992 (giving a general review of the properties of MICOM). This appendix is intended to give a brief description of MICOM, for a fuller description the reader is referred to the above papers and their antecedents.

The model was initially developed from an atmospheric isentropic coordinate model, however the coordinate scheme is more suited to adiabatic flows, to which atmospheric conditions do not generally conform. The depths of the ocean, away from surface forcing, are largely adiabatic as evidenced by the coherence of water masses properties, and confirmed by studies of tracer distributions; consequently flow and mixing in the ocean occur predominantly along surfaces of constant density. Isopycnic coordinates appear, therefore, to be the natural coordinate system to use when studying the ocean interior. Isopycnic coordinate models are a more recent development than the standard Bryan-Cox model (Bryan, 1969 and Cox & Bryan, 1984), which use Cartesian coordinate grids at set depths to solve the prognostic equations. Comparisons between the UKMO Hadley Centre Bryan-Cox model and MICOM are the subject of two papers by Roberts, New, Wood & Marsh (1995) and Marsh & Roberts(1995), while further comparisons are taking place with the Kiel Bryan-Cox model, the Grenoble semi-spectral model and the OPYC isopycnic model (Oberhuber, 1993a,b).

This appendix is structured as follows. A general overview of the two MICOM implementations (AIM and Boxmix) is given in the following section. In section three the models are described in more detail with a separate sub-section on each of the major processes/properties represented in the model; the grid arrays, time differencing, barotropic divergence, the continuity equation, the momentum equations, the diffusion of isopycnic layer thickness, isopycnic tracer diffusion, diapycnic mixing, tracer advection, surface forcing, the mixed layer model and equation of state. In a final section the merits and defects of the MICOM model, and of isopycnic schemes generally, will be discussed.

A.2 Model description

The isopycnic scheme uses layers of constant density but variable depth to represent the structure of the thermocline whereas the standard Bryan-Cox model uses constant depth but variable density. To permit the evolution of the stratification these layers must deform and so are semi-Lagrangian, capable of moving through the water column. The layers lie between impermeable interfaces and so the shallow water equations are solved on each layer with the pressure forces being used to couple the dynamics of the layers. The generation of metric terms in this inherently curvi-linear coordinate system is avoided by referring 'horizontal' derivatives (*e.g.* velocity) to the Cartesian horizontal (Bleck, 1978). Thus (u,v) in the isopycnic coordinate scheme is the identical to (u,v) in the Cartesian coordinate scheme.

The two versions of MICOM examined in this thesis are the Atlantic Isopycnic Model (AIM) and Boxmix (various versions; Box1, Box2 and Box3).

AIM is a 1°-resolution model of the northern and equatorial Atlantic from approximately 20°S to 80°N, but not including the northern European shelf seas or the Mediterranean basin or outflow and with solid boundaries at the northern and southern extremes. The model uses a C-grid (Arakawa & Lamb, 1977) on a rotated Mercator projection with the axis of the rotation passing through 40°W on the equator. This rotation gives less variation in grid size over the Atlantic basin. The model has twenty layers of which the upper-most is a Kraus-Turner mixed layer of the type described in Appendix B. Beneath

the mixed layer lie nineteen isopycnic layers with densities of σ=25.65-27.75 at intervals of 0.15 σ-units and σ=27.85-28.15 at intervals of 0.1 σ-units. The topography used in the model is taken directly from the Scripps 1° data set.

Boxmix has a simple basin geometry; straight zonal and meridional boundaries enclosing an area spanning 64° longitude and from approximately 10°N to 60°N. The model uses a B-grid (Arakawa & Lamb, 1977) with 2°-resolution on a standard Mercator projection. In the ten layer configurations (Box1 and Box2) there are nine isopycnic layers with densities of σ=25.50, 25.95, 26.35, 26.70, 27.00, 27.25, 27.45, 27.60 and 27.70 and a Kraus-Turner mixed layer identical to that of AIM. For the eighteen layer version (Box3) there are seventeen isopycnic layers with densities equal to those of the upper seventeen isopycnic layers of AIM (σ=25.65-27.95). The basin depth is 5km with a 5 metres hyperbolic cosine variation across its width.

The dynamics of the two models are similar but there are some notable differences. AIM used a split-explicit scheme to resolve the barotropic gravity wave whereas Boxmix uses a rigid lid to remove them. Comparisons have shown that the split-explicit method is computationally more efficient. Both models are able to advect both salt and heat, however only AIM does so; Boxmix has its salinity set to 34.5‰ in the experiments presented in this thesis and no freshwater fluxes are imposed to change this initial value. This allows greater computational efficiency by removing the need to advect either temperature or salinity in the isopycnic interior.

A.3 Governing equations

In the interior there are three prognostic equations, the momentum equation A.1, the continuity equation A.2 and the hydrostatic equation A.3;

$$\frac{\partial}{\partial t}\mathbf{v} + \nabla\frac{\mathbf{v}^2}{2} + (\zeta + f)\mathbf{k}\times\mathbf{v} + \nabla M = \frac{1}{\Delta p}\nabla\cdot(\upsilon\Delta p\nabla\mathbf{v}) \qquad \text{Eq. A.1}$$

$$\frac{\partial}{\partial t}\Delta p + \nabla\cdot(\mathbf{v}\Delta p) = 0 \qquad \text{Eq. A.2}$$

$$\frac{\partial}{\partial \alpha} M = p \qquad \text{Eq. A.3}$$

where M is the Montgomery potential, given by $M = gz + p\alpha$, Δp is the layer thickness in pressure units, and α is the reciprocal of the reference density.

In the mixed layer these equations must be altered; the momentum equation must account for the non-isopycnic character of the mixed layer in the pressure term, *i.e.* $\nabla M \rightarrow \nabla M - p\nabla\alpha$, and for the additional momentum input from the wind stress; $\frac{g\overline{\tau_0}}{\Delta p_1}$ on the left-hand side of A.1. The continuity equation also requires an additional term to allow for mass transfer to and from the mixed layer. In MICOM this transfer occurs solely in the mixed layer model and so the continuity equation solved for the mixed layer is identical to that solved on all other layers.

The surface buoyancy flux also requires a heat conservation equation for the mixed layer;

$$\frac{\partial}{\partial t} T + \mathbf{v} \cdot \nabla T = -g \frac{H + R}{\Delta p_1 c_w} \qquad \text{Eq. A.4}$$

where H is the turbulent heat flux and R the radiative heat flux at the surface.

A.3.1 Horizontal and vertical grid arrays

Boxmix uses a B-grid with mass and velocity points distributed as figure A.1a. Mass fluxes are calculated half-way along the appropriate grid side , between velocity points. All quantities referring to the bulk properties of the layer (temperature, velocity, thickness, potential vorticity, etc.) are calculated at the mid-thickness of the layer, surface interface pressure is calculated on the interfaces (see figure A.1b).

AIM uses a C-grid with mass and velocity points distributed as in figure A.2. As above the bulk layer properties are calculated at the centre of the grid-square, while the velocities and calculated at the boundaries of the grid. The u-component of the velocity is found on the eastern flank of the grid box and the v-component of the velocity is found on the southern flank of the gridbox. The potential vorticity of the fluid is therefore placed at the vertices of the grid squares.

The use of the B-grid is suited to models which do not resolve the Rossby radius; this grid arrangement is less susceptible to the growth of computational modes at low resolution than the otherwise superior C-grid (Arakawa & Lamb, 1977). The problem of computational noise in the C-grid versions of MICOM have yet to be resolved (R.Bleck, personal communication).

A.3.2 Time differencing

The model uses a leapfrog scheme to integrate the prognostic equations. To remove the high frequency computational modes associated with the decoupling of the two time levels a time filter is used (Asselin, 1972) for the tracer and velocity fields. This filter takes a weighted average of the n+1 and n time levels for the n+1 value with a strong weighting towards the current n+1 time level value. Even for small weights the computational model is suppressed.

A.3.3 The barotropic component of the velocity

Barotropic gravity waves have a significantly higher frequency than any other wave found in an ocean model. Consequently to resolve all modes the time step used in a model must be short, with obvious implications for the computational load involved in integrating the model. This load can be reduced in one of two ways. The first is to explicitly integrate the barotropic mode separately with a smaller time step than the baroclinic modes. This is the split-explicit scheme used in AIM. The second alternative is to filter out the gravity waves as is done in Boxmix. This is called the rigid lid approximation since the method filters out the divergent part of the barotropic mass flux. To do this fast Fourier transforms are used to solve the Poisson equation in the rectangular model basin. This allows a time step of $^{1}/_{15}$th of a day. The split-explicit scheme has been found to be faster than the rigid lid scheme.

A.3.4 Continuity equation

The problem of zero thickness isopycnic layers requires a complex advection scheme to prevent the creation of negative layer thickness. The flux corrected transport (FCT) algorithm of Zalesak (1979) is used to overcome this problem. In MICOM this algorithm has four steps. The first step is to use a low order, diffusive advection scheme (forward

up-stream) to advance the depth field. This scheme cannot create negative layer thicknesses. A higher order advection scheme (2nd order time and space centred) is then used to calculate the advection of water mass and this is compared to the mass fluxes generated by the low-order scheme. The differences between the two fluxes are the "anti-diffusive" fluxes. These fluxes are then compared to the layer thicknesses and where the anti-diffusive flux would generate a negative layer thickness the flux is reduced or "clipped". However, the barotropic mass flux must remain unchanged so the "clipped" mass fluxes are re-distributed between the rest of the layers. The use of the FCT algorithm allows strong isopycnic gradients removed which are otherwise removed by lower order schemes and the FCT algorithm suppresses the ripples associated with higher order schemes.

The metric terms associated with the earth's spherical surface are avoided by the use of line integrals around the grid squares. This renders the continuity equation in flux form. This ensures the conservation of potential vorticity and potential enstrophy at massive grid points.

A.3.5 Momentum equations

The momentum equation described above is solved at all grid-points in the model. This removes the problem of defining the velocity field at the edges of massless layer regions for the calculation of eddy viscosity. At massless grid-points the velocity is derived from a vertical average over 10 cm. The eddy viscosity in the model is derived by a deformation dependent term (Smagorinsky, 1963). This gives a shear dependent eddy viscosity in the western boundary current and other strong current systems. However, the use of Smagorinsky's viscosity formulation has been found to introduce spurious systems of counter currents parallel to western boundary currents (D.J.Webb, personal communication). In the ocean interior a constant background viscous velocity is used 2 cms^{-1} (Boxmix), when multiplied by the grid spacing this gives an eddy viscosity of $3.7 \times 10^7 cm^2 s^{-1}$ at 34°N (Δx=185km). The use of an viscous velocity rather than the more familiar viscosity is to allow for the variation in the grid resolution across the basin; a constant eddy viscosity would remove resolvable features in those parts of the basin where the grid mesh was relatively fine.

The input of momentum through the surface is balanced by dissipation at the lateral boundaries and through the bottom. The lateral boundaries of the model are defined along velocity points with a no-slip condition, that is the velocity at these points is set to zero. Layers within 10 metres of the ocean floor are influenced by the bottom friction. The layer is assumed to have a linear stress profile with the stress determined by,

$$\tau_H = -\rho c_D |\mathbf{v}| \mathbf{v}$$

where c_D=0.003.

A.3.6 Isopycnic layer depth diffusion

Isopycnic layer depth diffusion is required by the model to remove the checked-pattern noise generated on the B-grid and to suppress the noise inherent in the mixed layer detrainment algorithm. In its formulation it integrates,

$$\frac{\partial}{\partial t} p - \nabla \cdot (\upsilon \nabla p) = 0 \qquad \text{Eq.A.5}$$

The diffusion of p (interface 'depth') rather than Δp (layer 'thickness') avoids the problem of vanishing layer thicknesses. In its action the diffusion of layer depth results in a mass flux which resembles the action of eddy mass transports. This has been the formulation adopted by Gent & McWilliams (1990) in developing an isopycnic eddy mass flux for Bryan-Cox models. In practice a constant diffusion 'velocity' is used (1.0 cm/s in AIM and 1.5 cm/s in Boxmix) which is multiplied by the local grid length scale to produce a diffusion coefficient. Through the use of diffusive velocity the variable resolution of the model grid can be accomodated. It is intended to use a biharmonic thickness diffusion term in future developments of MICOM to make the diffusion scheme more scale-selective.

A.3.7 Isopycnic mixing

Isopycnic mixing is done using a constant mixing velocity: this forms an isopycnic diffusivity when multiplied by the grid scale, thus allowing for a variable grid. Various values of the isopycnic diffusion velocity are used in Boxmix in this thesis (0, 1.0 and 2.0 cm/s giving diffusivities of 0, 1.85 and 3.7 $\times 10^7 cm^2 s^{-1}$ at 34°N). In AIM the standard

isopycnic tracer diffusion velocity is 1.0 cm/s giving an isopycnic diffusivity of $1.1\times10^{7}cm^{2}s^{-1}$ for the main body of the North Atlantic.

A.3.8 Diapycnic mixing

The diapycnic diffusion algorithm was not available when AIM was set up and for comparisons with AIM the diapycnic mixing scheme was not implemented in Boxmix. However, for completeness the scheme is described here.

The algorithm takes an average of the density above and below the layer mid-depth. The depth-range (h_0) over which this average is taken varies linearly from a value of 10 metres at the surface to 5 metres at 1000m depth. Below this depth the range is held at 5 metres. The difference in the two average densities is used to calculate a downward buoyancy flux using set values for the diapycnic diffusivity and the Brunt-Vaisala frequency. The divergence of this flux is calculated at the layer interface and is used to displace the interface. Evidently the diapycnic flux algorithm will only generate a diapycnic flux for layers thinner than 20 metres, which restricts its operation to the near surface layers.

A.3.9 Tracer transport

The transport of tracer quantities in the interior of the model is done by a variant of the FCT scheme used for the continuity equation, described in Smolarkiewicz (1984). The scheme is third order, conservative and monotony-preserving. The advection scheme is used to advect tracer quantities for both the mean advection field and for the eddy mass fluxes implied by the layer depth diffusion.

A.3.10 Surface forcing

The surface forcing used in Boxmix and its derivation are described fully in Bleck, Hanson, Hu & Kraus (1989). Boxmix uses four functions to force the model each zonally uniform; a radiative heat flux, a pseudo air temperature, a surface wind stress and a wind speed at 10 metres.

The pseudo air temperature is used to simulate the turbulent heat fluxes at the surface, the sensible and latent heat fluxes. These fluxes depend on the difference between the sea surface and air temperatures, the air humidity and the wind speed. The flux is calculated as a Haney term (Haney, 1971) using a wind speed-dependent exchange coefficient. The pseudo air temperature was derived from data in Woodruff, et al. (1981) using zonal averages of North Atlantic data and is much lower than the observed air temperature to generate the correct heat flux.

Measurement of the radiative heat flux over the North Atlantic are prone to large errors on the seasonal timescale and so, for consistency, the radiative component was derived from the Lamb & Bunker heat budget of the North Atlantic as a residual. This function therefore includes the influence of cloud cover and other modulators implicitly.

The surface wind stress is derived from the Comprehensive Ocean-Atmosphere Data Set by regression techniques. The resulting data set includes the mid-latitude westerlies with the strongest forcing in winter, and less seasonal trade winds. The wind speed is derived from Woodruff, et al. (1981).

The form of all four forcing functions is $c_1\left[f_1(\phi)+f_2(\phi)\sin\left(\frac{2\pi t}{360}-\gamma\right)\right]$ where the coeffients of this function for each of the forcing functions are given in Table A.1. These forcing functions are shown as functions of latitude and time in figures A.3-A.6.

The surface forcing used in AIM is taken from a set of climatological atlases. The model is driven by heat fluxes (turbulent and radiative) taken from Ebensen & Kushnir (1981) and the wind speed and surface wind stresses are taken from Hellerman & Rosenstein (1983). The salinity forcing in the model is taken from two sources; the evaporation rates are taken from Ebensen & Kushnir (1981) while the precipitation rates are taken from Jaeger (1976). In addition to the imposed surface forcing the ocean surface is relaxed through a Haney-term (Haney, 1971) to the climatological sea surface temperatures and salinities given by the Levitus atlas (Levitus, 1982).

	c_1	γ	f_1	f_2	Units
τ_x	$39.6 c_D \rho_a$	3.55	$\sin\left(2\pi\left(\frac{\phi_N - \phi_i}{\phi_N - \phi_S}\right)\right)$	-0.24(1.0-3.78ϕ)	dyn/cm^2
T*	16.2	-1.87	1.0-0.11ϕ-0.76ϕ^2	0.13(1.0-7.91ϕ+4.6ϕ^2)	°C
U_{10}	4.43	0.53	1.0+1.15ϕ	0.21(1.0-4.35ϕ)	cm/s
R	-185.6	0.67	1.0+0.91ϕ	0.13(1.0+3.91ϕ)	W/cm^2

Table A.1: The coefficients of the surface forcing functions for Boxmix

A.3.11 Mixed layer

The mixed layer model is described fully in Appendix B of this thesis, here only a brief overview will be given. A Kraus-Turner mixed layer is used which considers the mixed layer to be a slab of homogenous water with uniform temperature, salinity and momentum properties throughout its depth. The turbulent kinetic energy is calculated from the wind stress at the ocean surface and the amount of cooling. During periods of deepening, that is when there is a net input of TKE into the ocean the depth of the mixed layer is determined by the available TKE, this energy is converted into potential energy through the lifting of the underlying water mass.

A.3.12 Equation of state

The equation of state used in all MICOM implementations is the third-order Friedrich-Levitus equation (Friedrich & Levitus, 1972). This has the form,

$$\rho(\mathrm{T,S}) = \left[\ c_1 + c_3\,\mathrm{S} + \mathrm{T}\left(c_2 + c_5\,\mathrm{S} + \mathrm{T}\left[c_4 + c_7 S + c_6\,\mathrm{T}\right]\right)\ \right] \times 10^{-3}\ \mathrm{gcm}^{-3}$$

Where the values of c_i are constants. It will be noted that this approximation to the equation of state does not include a pressure term. This means that the equation become less accurate at depth. If soundings taken from the South Atlantic are examined using this equation of state then it is found that the North Atlantic Deep Water and the Antarctic Bottom Water are hydrostatically unstable, whereas the full UNESCO equation of state indicates that they are not. This is not of great relevance in this study which concentrates on the upper kilometre of the ocean.

The use of a non-linear equation of state introduces the problem of conserving constant density on isopycnic layers in model that include both heat and salt as tracer quantities.

The mixing of different water masses results in a deviation of the implied density from that of the layer. This requires (in AIM) the transfer of water between interior layers to re-distribute mass and heat in the interior. This does not occur in Boxmix since the absence of salt renders the isopycnic layers isothermal, thus the mixing of water masses along isopycnic surfaces cannot alter the density of water on that layer. It is intended to advect only salinity in the ocean interior in future developments of MICOM, thus dispensing with the computational expense of advecting two tracers and of maintaining the isopycnic character of the interior.

A.4 The merits and defects of isopycnic coordinate models

Comparisons of the Bleck isopycnic model with the Hadley Centre Bryan-Cox model and Oberhuber's OPYC isopycnic model have been undertaken and further comparisons are currently underway to compare AIM with the Kiel Bryan-Cox model and the Grenoble semi-spectral model. From these studies the relative merits and defects of the isopycnic scheme have been distinguished. The notes given below cover the main points brought up by these comparisons.

A.4.1 Mixing and flow

The division of mixing, of both momentum and tracer quantities, into isopycnic and diapycnic components is explicit in isopycnic models. In standard Bryan-Cox models isopycnic mixing of tracer quantities is represented by vertical and horizontal diffusivities which results in strong diapycnal fluxes near the western boundary current. A rotated diffusion tensor has been introduced to the Bryan-Cox model (Redi, 1982, Cox, 1987) but this method is only successful if the slope of the isopycnic surface considered is moderate, otherwise a strong diapycnic component results. This is particularly important at sill overflows (Roberts, *et al.*, 1995). Bryan-Cox models still require a slight horizontal diffusivity for tracer quantities to prevent instabilities.

A second source of diapycnic mixing in Bryan-Cox models arises from strong internal wave fields, again this does not result in diapycnic fluxes in MICOM.

Potential vorticity in the isopycnic interior is more naturally conserved in an isopycnic model than in a Bryan-Cox model.

The diffusion of momentum, that is the eddy viscosity, is purely isopycnic in MICOM with momentum transferred vertically only through a pressure torque resulting from isopycnic surface deformation. In Bryan-Cox models eddy viscosity is represented by vertical and horizontal components.

A.4.2 Quasi-Lagrangian coordinates

The isopycnic coordinate scheme is quasi-Lagrangian, that is the isopycnic surfaces move vertically to conform to the ocean's stratification. This gives isopycnic coordinate models much better vertical truncation properties than standard Bryan-Cox models, improving the resolution of baroclinic structures, fronts and instabilities.

This property also allows the model to use un-smoothed topography. Bryan-Cox models must first have their topography smoothed to prevent numerical instabilities and following this the topography must discretised to conform to the depth spacing of the model grid. Even after such preparations, Bryan-Cox models produce anomalous flows along topography (Roberts, *et al.*, 1995). Evidently this is undesirable, especially in regions were the flow is strongly influenced by the topography.

A.4.3 Boundaries

The greatest problem is how the isopycnic coordinate scheme approaches boundaries. In parts of the ocean water of a particular density may not be present which implies that the thickness of the corresponding isopycnic layer must be set to zero. This, however, introduces the possibility of numerical advection schemes generating negative layer thicknesses if mass fluxes are not carefully managed. Flux-corrected transport (FCT) algorithms have been developed which manage mass fluxes to prevent this occurring but they require more computation than standard algorithms. The time taken for MICOM to complete one year's integration for its implementation in AIM requires 6 hours CPU-time on an eight-processor Cray YMP, this compares with 12 hours for the OPYC isopycnic model, 12 hours for the Hadley Centre Bryan-Cox model and 3 hours for the

Kiel Bryan-Cox model for the same domain and number of layers (A.New, personal communication).

A.4.4 Resolution

Isopycnic models must necessarily span a wide range of densities if they are to resolve the water masses present in the world ocean. However, at northern latitudes many of these layers will be defunct, their outcrop lines lying to the south, and so they are massless. This means that the poleward oceans will always be more poorly resolved than tropical and sub-tropical oceans. This can be overcome by increasing the density resolution of the model for the higher values of σ, but this cannot be done without a corresponding increase in the computational load.

A.4.5 Mixed layer

The use of surface buoyancy forcing in isopycnic models requires the introduction of a mixed layer which can alter its density both spatially and temporally. This mixed layer must also interact with the isopycnic layers beneath it by exchanging water. During entrainment this is a straight-forward process but when water is being passed from the mixed layer to the isopycnic interior the variable density of the mixed layer must be reconciled with the fixed density values of the isopycnic layers. To conserve heat the detrained water is divided between isopycnic layers but this results in an un-realistic potential vorticity field in the seasonal thermocline (Chapter Two). The problem of truncation errors in the potential vorticity is field is also encountered in Bryan-Cox models (Bleck, *et al.*, 1989), but the magnitude of the problem is less (R.Marsh, personal communication).

A further problem with the mixed layer is that it is a slab layer and it assumed that all of its properties are homogenous, including momentum. This means that a separate Ekman layer cannot develop, unlike Bryan-Cox models where the mixed layer is resolved by a number of grid-points allowing the use of depth-varying functions for momentum, salinity and temperature.

Similarly the mixed layer in MICOM cannot be allowed to shallow too far, otherwise the surfaces fluxes would generate delta-function profiles for momentum, temperature and salinity. A minimum depth of 20 metres is introduced therefore.

Insolation, the heating of the ocean at depth, is not permitted in MICOM since this would violate the isopycnic condition of the interior. It is assumed that all of the heat flux is drawn from or enters the mixed layer. This condition makes the model unsuited to studies of the tropics where insolation is important in the heat balance over annual time scales (Woods, *et al.*, 1984).

A.4.6 Equation of state

The non-linearity of the equation of state means that the mixing of water masses with the same density but different temperatures and salinities will result in a slightly denser water mass. On isopycnic layers this requires some house-keeping to be done to maintain the isopycnic nature of the layer. In MICOM this is done by re-distributing the heat in an isopycnic layer vertically to restore the correct density in part of the layer and give the remainder of the layer the density of an adjacent isopycnic layer. This water is then transferred.

The equation of state used in MICOM does not included a pressure dependent term. This means that at depth the equation of state will be in error. As a result, the relative positions of North Atlantic Deep Water and Antarctic Bottom Water in the column are predicted incorrectly in MICOM. The isopycnic ocean model of Oberhuber (1993a,b) uses a pressure-varying reference level when calculating hydrostatic stability, it is planned to use this scheme in future versions of MICOM.

A.4.6 Problems specific to MICOM

The implementations of MICOM presented in this thesis have additional problems not intrinsic to the isopycnic coordinate scheme.

Diapycnic mixing is not included in either AIM or Boxmix. This should not be of great concern for the study of the sub-tropical and sub-polar regions over time-scales shorter

than that of the thermohaline circulation. The value of the diapycnic diffusion coefficient implies that the time scale over which this process works is longer than that studied in these models. This may not be true for the equatorial dynamics of AIM where strong upwelling implies that diapycnic fluxes will have a greater influence. A diapycnic diffusion scheme for MICOM has since been developed at Miami.

The interior layers are coupled through the hydrostatic equation and the deformation of the isopycnic interfaces. MICOM does not include interfacial stresses generated by the meso-scale eddy field, although these could be computed with a suitable parameterisation scheme. Such a scheme has been developed for OPYC (Oberhuber, 1993a).

APPENDIX B

The Kraus-Turner mixed layer model

B.1 The surface mixed layer

The upper layers of the ocean are characterised by low vertical gradients of tracer properties and by the intensity of turbulent mixing, hence the denomination 'mixed layer'. The turbulence in the mixed layer has numerous sources, most notably convection and breaking surface waves, but also including Langmuir circulation, shear instabilities and breaking internal waves. Explicit modelling of all of these processes through the solution of the Navier-Stokes equation is beyond the capacity of computers, either cuurent of foreseeable. Research into the mixed layer has focused on the development of simpler mixed layer models. These models are usually one-dimensional since the variation of properties in the vertical is usually greater than variations in the horizontal. The range of model currently available is large (see the review by Large, *et al.* (1994)), and these models can be divided into four broad classes (Kraus, 1988).

Turbulence closure models solve the Reynolds flux equations for a water column by expressing the turbulent fluxes in terms of other, higher order turbulent fluxes with some set of closure conditions at the highest order. This gives a hierachy of turbulent closure models, as outlined by Mellor & Yamada (1982). The most commonly used versions are the second and 2.5 order schemes. Third order schemes have been used but they are computationally demanding.

Transilient turbulence models invoke the matrix relation $T_i(t+\Delta t) = \mathbf{C}_{ij}.T_j(t)$ to determine the evolution of the mixed layer. The elements of $\mathbf{C}_{ij}$ are functions of the local Richardson number. See Stull (1984) for an example.

Eddy coefficient and mixing length hypothesis assume that the turbulent transfer of properties can be parametrised as a diffusion of properties through the water column. The method is widely used, *e.g.* Pacanowski & Philander (1981), although the deficiencies of a diffusive represnentation of eddy processes is acknowledged.

Slab mixed layer models are the simplest mixed layer models currently used. These models *a priori* the presence of a well-mixed surface layer and integrate the

equations governing the evolution of that layer over its depth. The most common type of this model is that of Kraus & Turner (1967), while that of Price, *et al.* (1986) is also commonly used in GCMs.

The model used in MICOM is the Kraus-Turner model with certain alterations made to couple the mixed layer to the isopycnic thermocline. A detailed description of the model is given in the next section.

B.2 The Kraus-Turner mixed layer model

The Kraus-Turner mixed layer was derived from Ball's (1960) atmospheric boundary layer model by Kraus and Turner (1967) and has been subsequently developed by a number of authors. The thorough review of the developments of the Kraus-Turner model is given in Niiler & Kraus (1977) is precised below. The details of the variant of the Kraus-Turner model used in MICOM are given in Bleck, Hanson, Hu & Kraus (1989).

The conservation equations for the mixed layer are;

$$\frac{dT_1}{dt} + \frac{w_e \Delta T_1}{h_1} = \frac{-H_0}{\rho c_p h_1} \qquad \text{Eq. B.1}$$

and

$$\frac{dS_1}{dt} + \frac{w_e \Delta S_1}{h_1} = \frac{Q_0 S_1}{\rho h_1} \qquad \text{Eq. B.2}$$

where the entrainment velocity, w_e, is given by,

$$w_e = \frac{dh_1}{dt} \Lambda\left(\frac{dh_1}{dt}\right) \qquad \text{Eq. B.3}$$

where Λ is the Heaviside function ($\Lambda(x)=1$ if $x>0$, else $=0$).

To close these equations it is necessary that the a prognostic equation for the mixed layer depth is added. This is derived from considerations of the layer-integrated turbulent kinetic energy equation.

$$\underset{1}{\int_h^0 -\overline{w'v'}\frac{\partial \bar{v}}{\partial z}dz} + \underset{2}{\int_h^0 \overline{w'b'}\,dz} + \underset{3}{\int_h^0 -\tfrac{1}{2}\overline{w'\left(w'^2+v'^2\right)}} + \underset{4}{\frac{\overline{w'p'}}{\rho}dz} + \underset{5}{\int_h^0 \varepsilon\,dz} = 0$$

Eq. B.4

These terms represent, in order, the shear-generation of TKE, the flux of buoyancy into the layer, the turbulent flux of TKE into the layer, the generation of TKE through fluctuations in the pressure field and dissipation.

The shear generation of TKE (term 1) only makes a contribution at the base of the mixed layer and so this integral can be replaced by the limit;

$$\lim_{h' \to h} \int_{h'}^{h} -\overline{w'v'} \frac{\partial \bar{v}}{\partial z} dz = \tfrac{1}{2} w_e \overline{v^2} - \tfrac{1}{3} C |\bar{v}|^3 \qquad \text{Eq. B.5}$$

Where the two terms on the right-hand side represent the energy taken to accelerate the underlying fluid to match the mixed layer and the generation of internal waves. Note, C is the drag coefficient.

Term 2 in Eq. B.4 is the change in the mixed layers buoyancy. This can be determined through the buoyancy conservation equation by eliminating the time-dependent terms. On integrating this produces,

$$\int_{-h}^{0} \overline{w'b'} dz = \frac{h_1 B_0}{2} - \tfrac{1}{2} w_e \Delta b_1 h_1 + \frac{g \alpha I_0}{\rho c_p} \left(\frac{h_1}{2} - \frac{1}{\gamma} \right) \qquad \text{Eq. B.6}$$

where the buoyancy flux (B_0) is,

$$B_0 = g \left[\frac{\partial \sigma}{\partial S} S Q_0 - \frac{\partial \sigma}{\partial T} \frac{H_0}{c_P \bar{\rho}} \right] \qquad \text{Eq. B.7}$$

The three terms on the right-hand side represent the changes due to bulk mixed layer buoyancy gain through surface fluxes, the entrainment of less buoyancy fluid and the buoyancy gain from penetration of surface radiation through the depth of the mixed layer.

Term 3 in Eq. B.4 represents the mechanical turbulent energy flux. The sites of mechanical input into the mixed layer are at the surface and the base of the mixed layer and so can be expressed as the sum of the generation terms at the two boundaries.

$$\int_{-h}^{0} \tfrac{1}{2} \overline{w' \left(w'^2 + v'^2 \right)} + \frac{\overline{w'p'}}{\rho} dz = m_1 u_*^3 - \frac{w_e u_{rms}^2}{2} \qquad \text{Eq. B.8}$$

The two terms on the RHS represent the input from the wind-waves at the surface and the energy required to raise the TKE of entrained water.

The above expression can be combined to give,

$$\tfrac{1}{2} w_e\left(u_{rms}^2 + \Delta b_1 h_1 - \bar{v}^2\right) = m_1 u_*^3 + \frac{h_1 B_0}{2} - \frac{g\alpha I_0}{\rho c_p}\left(\frac{h_1}{2} - \frac{1}{\gamma}\right) - C|\bar{v}|^3 - \int_h^0 \varepsilon \, dz$$

Eq. B.9

This expression can be further simplified. The u_{rms} term is ~1/1000th of $\Delta b_1 h_1$ term and can be ignored. It is also usual to neglect the radiation term $C|\bar{v}|^3$, although this is not always a valid approxmiation (Pollard, *et al.* ,1973), and in this model the energy necessary to accelerate the underlying fluid ($\frac{1}{2}\bar{v}^2$) and the influence of penetrating radiation is also neglected.

The final term (5) in Eq. B.4 and Eq. B.8 is the layer-integarted dissipation term. This is generally assumed to occur locally, and is assumed to be proportional to the generation of TKE. This allows the use of simple factors (m,n,s) to,

$$\tfrac{1}{2} w_e \Delta b_1 h_1 = m u_*^3 + \frac{h_1}{4}\left[(1+n)B_0 + (1-n)|B_0|\right] \qquad \text{Eq. B.10}$$

Thus the rate at which the mixed layer potential energy changes is equal to the net input of TKE into the mixed layer.

Wind-driven turbulent eddies have a characteristic eddy length-scale which is proportional to the amplitude of the breaking waves generating them (Phillips, 1966). Thus the effects of wind-mixing will be reduced below a depth equal to this length scale. To allow for this, the model uses two wind-mixing parameters (m_2 and H_w); m_2 is the proportion of the wind-driven turbulence available to erode the underlying strata, and H_w is an exponential scale depth; the deeper the mixed layer is, the less wind-generated TKE reaches the mixed layer base. Thus,

$$m = m_2 \exp\left\{\frac{-h_1}{H_w}\right\} \qquad \text{Eq.B.11}$$

The exponential form of the parameter is a crude approximation to the decrease in the efficiency of the wind-driven mixing with depth.

At each time step the model balances this input of TKE with a change in the potential energy of the water column; erosion of the thermocline requires the lifting of the mass of the underlying water and the distribution of this mass through out the new mixed layer depth. A simple consideration of the potential energy change for a two layer system (Fig.2.1) gives the energy required (E) as,

$$E = \tfrac{1}{2}\left[h_1'\left(\rho_2 h_1 - \rho_1 h_1\right) - \rho_2 h_1^2 - \rho_1 h_1^2\right] \qquad \text{Eq.B.12}$$

The term h_1 is the original mixed layer depth, ρ_1 is the original mixed layer density, ρ_2 is the density of the underlying layer, and h_1' is the new mixed layer depth. This equation can easily be inverted to derive the new mixed layer depth. The mixed layer model used in MICOM iterates this calculation over each isopycnic layer in turn until the available TKE has been exhausted.

During periods of surface heating or surface fresh water input the buoyancy flux acts to suppress the wind-driven turbulence. The suppression of turbulence cannot involve dissipation, thus (1-n)=0.0 for conditions of net buoyancy gain. Under the influence of surface heating the mixed layer depth to which the model attempts to shallow is given by the Monin-Obukhov length scale (H_{MO}). This length scale is the depth at which the action of wind-mixing to deepen the mixed layer is balanced by the tendency of the buoyancy flux to re-stratify. For the above parametrisation this depth is approximately given by,

$$H_{MO} = \frac{-2\,mg\,\tau^{3/2}}{B_0\sqrt{\rho}} \qquad \text{Eq.B.13}$$

The neglect of the exponential in the wind-mixing parametrisation is of little importance to the model operation and simplifies the calculation. In the version of the Kraus-Turner model developed for MICOM this expression for the mixed layer depth is not attained during most of the detrainment period because of the requirement to conserve heat in an isopycnic thermocline. The requirement that water leaving the mixed layer is deposited in an isopycnic layer implies that the detrained water possesses one of a limited range of densities. During detrainment heat is transferred to the remainder of the mixed layer from

the detrained water to lower the density of the detrained water to the value of the first hydrostatically stable isopycnic layer.

However, to prevent the mixed layer temperature rising too fast during the Spring detrainment, an upper limit is set on the rate of increase of the mixed layer temperature and, consequently, on the rate at which water can be detrained. The limit is set by the surface heat fluxes; the temperature must not rise faster than the rate at which a mixed layer of the depth of the Monin-Obukhov length would rise given the same heat flux. For most of the Spring the magnitude of the detrainment rate is lower than the rate at which the Monin-Obukhov length scale shallows. Consequently, the Spring re-stratification takes longer in the version of the Kraus-Turner model developed for MICOM than for a Kraus-Turner model with a continuous thermocline structure.

The ocean mixed layer can disappear under conditions of strong heating and light winds, however the Kraus Turner model cannot simulate the mixed layer response under such conditions. In the Kraus-Turner mixed layer model the surface heat flux is concentrated in the mixed layer, whereas in the ocean the heat input is distributed over a depth that depends on a number of upper ocean properties. The depth that is heated in the real ocean will always be non-zero and this will act to moderate the sea surface temperature rise. In the Kraus-Turner model this is done artificially by limiting the mixed layer depth to a minimum depth of 20m.

The mixed layer temperature is calculated using two sources: the net surface heat flux H_o (latent, sensible and radiant heat fluxes combined) and the heat flux arising from mass entering the mixed layer, either through Ekman suction or mixed layer deepening. A downward Ekman pumping velocity or the detrainment of mixed layer water should not affect the mixed layer temperature, although the lateral mass fluxes associated with the Ekman drift would imply some heat transport under most conditions. However, the isopycnic nature of the thermocline requires the transfer of heat through the water column to allow detrainment. The temperature of the mixed layer is limited to equal that of the Monin-Obukhov depth, as described above, but the heat content of the mixed layer is higher than the Monin-Obukhov mixed layer through its greater depth.

Appendix C

Tables of permanent subduction and entrainment rates

Table C.1: Permanent subduction rates for year 31 in AIM (rates given in Sverdrups).

Density[1]	Tracer[2]	Mean flow[3]	Thickness diffusion[4]	Tracer diffusion[5]	Residual[6]	Marsh & Roberts[7]	Particle[8]
25.65	6.65	2.66	-0.01	0.25	3.75	-	6.21
25.80	0.79	0.76	0.28	0.01	-0.26	0.73	0.74
25.95	0.53	0.83	0.28	0.03	-0.61	0.72	0.87
26.10	0.64	0.89	0.30	0.00	-0.55	1.02	1.53
26.25	1.38	1.29	0.38	0.00	-0.29	1.91	2.69
26.40	3.78	3.09	0.92	0.01	-0.24	2.8	4.86
26.55	4.68	4.21	0.50	0.01	-0.04	2.19	3.86
26.70	4.45	3.57	0.03	0.01	0.84	2.05	5.64
26.85	3.15	2.15	0.10	0.01	0.89	1.23	3.37
27.00	3.14	2.5	0.02	0.01	0.61	1.55	4.31
27.15	2.39	1.32	0.08	0.00	0.99	0.82	3.2
27.30	2.5	0.44	0.15	0.01	1.9	0.40	2.1
27.45	0.97	0.21	0.16	0.00	0.60	-	.37
27.60	1.52	0.86	0.18	0.01	0.47	-	1.43
27.75	17.5	23.44	0.30	0.03	-6.27	-	8.47
27.85	2.59	2.17	0.56	0.00	-0.14	-	0.88
27.95	5.65	2.38	0.42	0.02	2.83	-	1.81
28.05	4.38	0.67	0.03	0.00	3.68	-	1.29
28.15	0.00	0.00	0.00	0.00	0.00	-	0.00
Total	**66.7**	**53.40**	**4.69**	**0.40**	**8.21**	**15.42**	**58.8**

Notes

1. Isopycnic layer density given in dimensionless sigma units.
2. Total permanent subduction rates (in Sverdrups) derived by the tracer method (section 4.3) using isopycnic diffusion.
3. Permanent subduction rates due to mean advection derived from the kinematic method (section 4.5) using the mean (*i.e.* not including parametrised eddy velocities) thermocline velocities only.
4. Permanent subduction rates due to thickness diffusion derived from the difference in the estimates kinematic method (section 4.5) for advection by the mean plus thickness diffusion velocities and advection by mean velocities only.
5. Permanent subduction rates due to isopycnic tracer diffusion derived from a comparison of tracer results (section 4.3) with and without isopycnic tracer diffusion.
6. Residual permanent subduction rates, *i.e.* the difference between the total permanent subduction rate derived from the tracer estimate and the sum of the permanent subduction rates due to mean

advection, layer thickness diffusion and isopycnic tracer diffusion. This term includes errors in the other estimates and the contribution of Ekman pumping.

7. The permanent subduction rates as derived by Marsh & Roberts (1995) for the AIM subtropical gyre.
8. Permanent subduction rates derived from the particle method (section 4.4).

Table C.2: Permanent entrainment in year 31 of AIM (rates given in Sverdrups).

Density[1]	Tracer[2]	Mean flow[3]	Thickness diffusion[4]	Particle[5]
25.65	6.70	3.24	0.19	2.93
25.80	0.79	0.43	0.07	0.46
25.95	0.53	0.47	0.08	0.60
26.10	0.65	0.67	0.09	1.00
26.25	1.35	2.00	0.11	2.35
26.40	4.23	3.79	0.05	4.77
26.55	5.47	5.14	0.35	5.48
26.70	4.20	4.32	0.63	3.90
26.85	4.36	2.39	0.68	3.19
27.00	5.86	1.99	0.41	3.09
27.15	2.84	1.46	0.17	3.22
27.30	3.04	2.19	0.03	5.00
27.45	1.80	1.96	-0.02	2.83
27.60	4.88	3.89	-0.09	3.76
27.75	14.58	16.94	1.32	10.65
27.85	0.51	1.24	0.03	1.66
27.95	3.08	1.78	0.11	3.09
28.05	2.27	0.75	-0.08	1.38
28.15	0.00	0.00	0.00	0.03
Total	**67.14**	**54.65**	**4.13**	**59.39**

Notes

1. Isopycnic layer density given in dimensionless sigma units.
2. Total permanent entrainment rates (in Sverdrups) derived by the tracer method (section 4.3) using isopycnic diffusion.
3. Permanent entrainment rates due to mean advection derived from the kinematic method (section 4.5) using the mean (*i.e.* not including parametrised eddy velocities) thermocline velocities only.
4. Permanent entrainment rates due to thickness diffusion derived from the difference in the estimates kinematic method (section 4.5) for advection by the mean plus thickness diffusion velocities and advection by mean velocities only.
5. Permanent entrainment rates as estimated by the particle method (section 4.4).

Table C.3: Permanent subduction rates in year 16 of Boxmix versions Box1 and Box2 (rates given in Sverdrups).

Density	Box1[1]			Box2[2]	
	Run1c[3]	Run1b[4]	Run1a[5]	Run2c[6]	Run2a[7]
25.50	0.455	0.460	0.460	1.809	1.875
25.95	1.593	1.703	1.825	1.698	1.972
26.35	2.176	2.615	3.030	3.516	4.875
26.70	2.604	3.651	4.521	4.623	6.278
27.00	2.652	4.265	5.489	4.293	7.075
27.25	2.453	4.412	5.787	3.032	6.242
27.45	3.301	6.320	8.416	2.895	6.943
27.60	17.012	29.493	37.273	14.539	36.653
27.75	19.766	19.832	19.880	24.008	24.125
Total	**52.013**	**73.394**	**86.684**	**60.400**	**95.331**

Notes

1. Boxmix version Box1 had a layer thickness diffusion velocity of 1.5 cm/s, giving a layer thickness diffusion coefficient of $2.8 \times 10^7 cm^2 s^{-1}$ at 34°N on the Boxmix grid.
2. Boxmix version Box2 had a layer thickness diffusion velocity of 0.45 cm/s, giving a layer thickness diffusion coefficient of $0.8 \times 10^7 cm^2 s^{-1}$ at 34°N on the Boxmix grid.
3. Run1c of Boxmix version Box1 had an isopycnic tracer diffusion velocity of 0 cm/s, *i.e.* the tracer was distributed by mean advection and thickness diffusion only.
4. Run1b of Boxmix version Box1 had an isopycnic tracer diffusion velocity of 1.0 cm/s, giving an isopycnic tracer diffusion coefficient of 1.9×10^7cm/s at 34°N.
5. Run1a of Boxmix version Box1 had an isopycnic tracer diffusion velocity of 2.0 cm/s, giving an isopycnic tracer diffusion coefficient of 3.7×10^7cm/s at 34°N.
6. Run2b of Boxmix version Box2 had an isopycnic tracer diffusion velocity of 0.0 cm/s, *i.e.* the tracer was distributed by mean advection and thickness diffusion only.
7. Run2a of Boxmix version Box2 had an isopycnic tracer diffusion velocity of 2.0 cm/s, giving an isopycnic tracer duffusion coefficient of 3.7×10^7cm/s at 34°N.

REFERENCES

Arakawa, A., and V.R.Lamb, 1977: Computational design of the basic dynamical processes of the UCLA GCM, *Methods.Comp.Phys.*, ***17***, 174-265.

Armi, L., 1979:, Effects of variations in eddy diffusivity on property distributions in the oceans, *J.Mar.Res.*, ***37***, 515-530.

Armi, L., and H.Stommel, 1983: Four views of a portion of the North Atlantic subtropical gyre, *J. Phys.Oceanogr.*, ***13***, 828-857.

Asselin, R., 1972: Frequency time filter for time integrations, *Mon.Wea.Rev.*, ***100***, 487-490.

Ball, F.K., 1960: Control of inversion height by surface heating, *Q.J.R.Met.Soc.*, ***86***, 483-494.

Batchelor, G.K., 1956: Steady laminar flow with closed streamlines at large Reynolds numbers, *J.Fluid Mech.*, ***1***, 177-190.

Bleck, R., 1978: Finite difference equations in generalised vertical coordinates, *Beitrage fur Physik der Atmosphäre,* ***51***, 360-372.

Bleck, R., and D.Boudra, 1981: Initial testing of a numerical ocean circulation model using hybrid vertical coordinates, *J.Phys.Oceanogr.*, ***11***, 755-770.

Bleck, R., and D.Boudra, 1986: Wind-driven spin-up in eddy-resolving ocean models formulated in hybrid and isopycnic coordinates, *J.Geophys.Res.*, ***91***, 7611-7621.

Bleck, R., H.P.Hanson, D.Hu and E.B.Kraus, 1989: Mixed layer thermocline interaction in a three-dimensional isopycnic coordinate model, *J.Phys.Oceanogr.*, ***19***, 1417-1439.

Bleck, R., and L.T.Smith, 1990: A wind-driven isopycnic coordinate model of the North and Equatorial Atlantic Oceans: I) Model development and supporting experiments, *J.Geophys.Res.*, ***95***, 3273-3285.

Bleck, R., C.Rooth, D.Hu and E.B.Kraus, 1992: Salinity-driven thermocline transients in a wind and thermohaline driven isopycnic coordinate model of the North Atlantic Ocean, *J.Phys.Oceanogr.*, ***22***, 1486-1505.

Böning, C.W., and M.D.Cox, 1988: Particle dispersion and mixing of conservative properties in an eddy-resolving model, *J.Phys.Oceanogr.*, ***18***, 320-337.

Broecker, W.A., 1991: The great ocean conveyor, *Oceanography,* ***4***,79-89.

Broecker, W.A., T.Takahashi and H.J.Simpson, 1979: Fate of fossil fuel carbon dioxide and the global carbon budget, *Science,* ***206***, 409-418.

Bryan, K., 1969: A numerical method for the study of the circulation of the world ocean, *J.Comp.Phys.*, ***4***, 347-376.

Bryden, H., and Hall, 1980: Heat transport by currents across 25°N in the North

Atlantic Ocean, *Science, **207***, 884.

Cane, M.A., 1993: Near-surface mixing and the ocean's role in climate, Ch.22, pp.489-509 from *Large-scale eddy simulations of complex engineering and geophysical flows*, ed. B.Galperin and S.A.Orszag, C.U.P.

Cessi, P., 1992: Ventilation of the eastern subtropical gyre, *J.Phys.Oceanogr., **22***, 683-685.

Chen, D., L.M.Rothstein and A.J.Busalacchi, 1994: A hybrid vertical mixing scheme and its application to tropicl models, *J.Phys.Oceanogr., **24***, 2156-2179.

Clarke,J-C, and R.A.Gascard, 1983: The formation of Labrador Sea Water i) Large scale processes, *J.Phys.Oceanogr., **13***, 1779-1797.

Cox, M.D., 1985: An eddy-resolving model of the ventilated thermocline, *J.Phys.Oceanogr., **15***, 1312-1324.

Cox, M.D., 1987: An eddy-resiolving primitive equation model of the ventilated thermocline: time dependence, *J.Phys.Oceanogr., **17***, 1044-1056.

Cox, M.D., and K.Bryan, 1984: A numerical model of the ventilated thermocline, *J.Phys.Oceanogr., **14***, 674-687.

Csanady, G.T., 1984: Warm water mass formation, *J.Phys.Oceanogr., **14***, 264-275.

Cushman-Roisin, B., 1987: Subduction, p.181-196 from *'Dynamics of the ocean mixed layer'*, ed. P.Muller & D.Henderson, Hawaii Institute of Geophysics Special Publication.

Danabasoglu, G., J.C.McWilliams and P.R.Gent, 1994: The role of mesoscale tracer transports in the global ocean circulation, *Science, **264***, 1123-1126.

Dewar, W.K., 1986: On the potential vorticity structure of weakly ventilated isopycnals: a theory of subtropical mode water maintenance, *J.Phys.Oceanogr., **16***, 1204-1216.

Dewar, W.K., 1990: Connected thermal and transport anomalies in the general circulation, *J.Phys.Oceanogr., **20***, 534-550.

Dickson, R.R., J.Meincke, S.A.Malmberg and A.J.Lee, 1989: The Great Salinity Anomaly in the northern North Atlantic, 1968-82, *Prog.Oceanogr., **20***, 103-151.

Doney, S.C., and W.J.Jenkins, 1988: The effects of boundary conditions on tracer estimates of thermocline ventilation, *J.Mar.Res., **46***, 947-965.

Ebensen, S.K., and Y.Kushnir, 1981: Heat budget of the global ocean: estimates from surface marine observations, Report no.29, Climatic Reasearch Institute, Oregon State Univ., Corvallis, Oregon, 27pp.

Fischer, J., H.Leach and J.D.Woods, 1989: A synoptic map of isopycnic potential vorticity in the seasonal thermocline, *J.Phys.Oceanogr.*, ***19***, 519-531.

Fofonoff, N.P., 1954: Steady flow in a frictionless homogeneous ocean, *J.Mar.Res.*, ***13***, 254-262.

Frankignoul,C., 1981: Low frequency temperature variations off Bermuda, *J.Geophys.Res.*, ***84***, 6522-6528.

Freeland, H.J., P.B.Rhines and H.T.Rossby, 1975: Statistical observations of trajectories of neutrally buoyant floats in the North Atlantic, *J.Mar.Res.*, ***33***, 384-404.

Friedrich, H.J., and S.Levitus, 1972: An approximation to the equation of state for sea water, suitable for numerical ocean models, *J.Phys.Oceanogr.*, ***2***, 514-517.

Fugilister, F.C., 1960: Gulf Stream '60, *Prog.Oceanogr.*, ***1***, 265-383.

Gent, P.R., anc J.C.McWilliams, 1990: Isopycnal mixing in ocean circulation models, *J.Phys.Oceanogr.*, ***20***, 150-155.

Gent, P.R., J.Willebrand, T.J.McDougal and J.C.McWilliams, 1995: Parametrising eddy-induced tracer transports in ocean circulation models, *J.Phys.Oceanogr.*, ***25***, 463-474.

Gill, A.E., 1982: *Atmosphere-Ocean Dynamics*, Academic Press, 662pp.

Gough, W.A., and W.J.Welch, 1994: Parameter-space exploration of an ocean general circulation model using isopycnic mixing parameterisation, *J.Mar.Res.*, ***52***, 773-796.

Haney, R.L., 1971: Surface thermal boundary conditions for ocean circulation models, *J.Phys.Oceanogr.*, ***1***, 241-248.

Hellerman, S., and M.Rothenstein, 1983: Normal monthly windstress over the world ocean with error estimates, *J.Phys.Oceanogr.*, ***13***, 1093-1104.

Hogg, N.G., and H.Stommel, 1985: On the relation between the deep circulation and the Gulf Stream, *Deep Sea Res.*, ***32***, 1181-1193.

Holland, W.R., T.Keffer and P.B.Rhines, 1984: Dynamics of the oceanic general circulation: the potential vorticity field, *Nature*, ***308***, 698-705.

Huang, R.X., 1987: Two-layer models for the thrmocline and current structure in the subtropical/subpolar gyres, *J.Phys.Oceanogr.*, ***17***, 872-884.

Huang, R.X., 1991: The three-dimensional structure of wind-driven gyres - ventilation and subduction, *Rev.Geophys.(suppl.)*, 590-609.

Huang, R.X., and K.Bryan, 1987: A multilayer model of the thermocline and wind-driven ocean circulation, *J.Phys.Oceanogr.*, ***17***, 1909-1924.

Huang, R.X., and B.Qui, 1994: Three-dimensional structure of the wind-driven circluation in the subtropical North Pacific, *J.Phys.Oceanogr.*, ***24***, 1608-1622.

Ierley, G.R., 1990: Boundary layers in the general ocean circulation, *Ann.Rev.Fluid Mech., **22**,* 111-142.

Ierley, G.R., and W.R.Young, 1983: Can the western boundary current affect the potential vorticity distribution in the Sverdrup interior of a gyre, *J.Phys.Oceanogr., **13**,* 1753-1763.

Iselin, C.O'D., 1939: The influence of vertical and lateral turbulence on the characteristics of the ocean at mid-depths, *Trans.Am.Geo.U., **20**,* 414-417.

Jacobs, G.A., H.E.Hurlbert, J.C.Kindle, E.J.Metzger, J.L.Mitchell, W.J.Teague, and A.J.Wallcroft, 1994: Decade-scale trans-Pacific propagation and warming effects of an El Niño anomaly, *Nature, **370**,* 360-370.

Jaeger, L., 1976: Monatskarten des Niederschlags fur die ganze Erde, *Berichte des Deutschen Wetterdienstes, **18**,* no.139, Offenbach, FRG.

Jenkins, W.J., 1980: Tritium and ^{3}He in the Sargasso Sea, *J.Mar.Res., **38**,* 533-569.

Jenkins, W.J., 1982: On the climate of a subtropical gyre: Decadal timescale variations in water mass renewal in the Sargasso Sea, *J.Mar.Res., **40 (suppl.)**,* 265-290.

Jenkins, W.J., 1987: ^{3}H and ^{3}He in the beta-triangle: observations of gyre ventilation and oxygen utilisation rates, *J.Phys.Oceanogr., **17**,* 763-783.

Jenkins, W.J., 1991: Determination of isopycnic diffusivities in the Sargasso Sea, *J.Phys.Oceanogr., **21**,* 1058-1061.

Jia, Y., and K.J.Richards, 1995: Tritium distributions in an isopycnic model of the North Atlantic, submitted to *J.Phys.Oceanogr.*.

Keffer, T., 1985: The ventilation of the world's oceans: maps of potential vorticity field, *J.Phys.Oceanogr., **15**,* 509-523.

Kraus, E.B., 1988: Merits and defects of different approaches to mixed layer modelling, 37-50 from *Small-scale turbulence in the ocean*, ed. C.J.Nihoul, Elsevier.

Kraus, E.B., and J.S.Turner, 1967: A one-dimensional model of the seasonal thermocline ii) General theory and its consequencies, *Tellus, **19**,* 98-105.

Kraus, E.B., R.Bleck and H.P.Hanson, 1988: The inclusion of a surface mixed layer model in a large scale circulation model, from *Small-scale turbulence in the ocean*, ed. C.J.Nihoul, Elsevier.

Krauss, W., and C.W.Böning, 1987: Lagrangian properties of eddy fields in the northern North Atlantic Ocean as deduced by satellite-tracked buoys, *J.Mar.Res., **45**,* 259-291.

Large, W.G., J.C.McWilliams, and S.C.Doney, 1994: Oceanic vertical mixing: a review and a model with nonlocal boundary layer parameterization,

Rev.Geophys., ***32***, 363-403.

Latif, M., and T.P.Barnett, 1995: Causes of decadal climate variability over the North Pacific and North America, *Science,* ***266***, 634-637.

Lazier, A., 1988: Temperature and salinity changes in the deep Labrador Sea, 1962-1986, *Deep Sea Res.*, ***35***, 1247-1253.

Leetmaa, A., 1997: Effects of the winter '76-'77 on the northwestern Sargasso Sea, *Science,* ***198***, 188-189.

Leetmaa, A., P.P.Niiler, and H.Stommel, 1977: Does the Sverdrup relation account for the mid-Atlantic circulation?, *J.Mar.Res.*, ***35***, 1-10.

Levitus, S., 1982: Climatological atlas of the world ocean, NOAA Professional Paper 13, 173pp., U.S. Dept. of Commerce.

Liu, Z., 1993a: Thermocline forced by varying Ekman pumping - i) spin-up and spin-down, *J.Phys.Oceanogr.*, ***23***, 2505-2522.

Liu, Z., 1993b: Thermocline forced by varying Ekman pumping - ii) annual and decadal Ekman pumping, *J.Phys.Oceanogr.*, ***23***, 2523-2540.

Liu, Z., J.Pedlosky, D.Marshall and T.Warnecke, 1993: On the feedback of the Rhines and Young pool on the ventilated thermocline, *J.Phys.Oceanogr.*, ***23***, 1592-1596.

Liu, Z., and J.Pedlosky, 1995: Thermocline forced by annual and decadal surface temperature variation, *J.Phys.Oceanogr.*, ***25***, 587-608.

Lutyen,J., J.Pedlosky and H.Stommel, 1983: The ventilated thermocline, *J.Phys.Oceanogr.*, ***13***, 292-309.

McCartney, M.S., 1982: The subtropical recirculation of mode waters, *J.Mar.Res.*, ***40*** *(Suppl.)*, 427-464.

McCartney, M.S., and L.V.Worthington, and M.E.Raymer, 1980: Anomalous water mass distributions at 55°W in the North Atlantic Ocean, 1977, *J.Mar.Res.*, ***38***, 147-172,1980.

McCartney, M.S., and L.D.Talley, 1982: The subpolar mode waters of the North Atlantic Ocean, *J.Phys.Oceanogr.*, ***12***, 1169-1188.

McCartney, M.S., and L.D.Talley, 1984: Warm to cold water conversion in the northern North Atlantic Ocean, *J.Phys.Oceanogr.*, ***14***, 922-935,.

McDougall, T.J., and J.A.Church, 1986: Pitfalls with the numerical representation of isopycnal and diapycnal mixing, *J.Phys.Oceanogr.*, ***16***, 196-199.

McDowell, S., P.Rhines and T.Keffer, 1982: North Atlantic potential vorticity and its relation to general circulation, *J.Phys.Oceanogr.*, ***12***, 1417-1436.

McWilliams, J.C., 1983: On the mean dynamical balances of the Gulf Stream recirculation zone, *J.Mar.Res.*, ***41***, 427-460.

Marsh, R., and M.J.Roberts, 1995: An intercomparison of a Bryan-Cox type ocean

model and an isopycnic ocean model, ii) the subtropical gyre and heat balances, *submitted to J.Phys.Oceanogr.*

Marshall, D., and J.Marshall, 1995: Subduction in a time dependent thermocline model, *J.Phys.Oceanogr.*, ***25***, 138-151.

Marshall, J.C., and A.J.G.Nurser, 1991: A continuously stratified thermocline model incorporating a mixed layer of variable thickness and density, *J.Phys.Oceanogr.*, ***21***, 1780-1792.

Marshall, J.C., A.J.G.Nurser and R.G.Williams, 1993: Inferring the subduction rate and period over the North Atlantic, *J.Phys.Oceanogr.*, ***23***, 1315-1329.

Masuzawa, J., 1969: Subtropical mode water, *Deep Sea Res.*, ***16***, 463-472.

Mellor, G.L., and T.Yamada, 1982: Development of a turbulence closure model for geophysical flows, *Rev.Geophys.*, ***20***, 851-875.

Montgomery, R.B., 1938: Circulation in the upper layers of the southern North Atlantic deduced with the use of isentropic coordinates, *Pap.Phys.Oceanogr.Meteor.*, ***6(2)***, pp55.

Musgrave, D.L., 1990: Numerical studies of ^{3}H and ^{3}He in the thermocline, *J.Phys.Oceanogr.*, ***20***, 344-373.

New, A.L., R.Bleck, Y.Jia, R.Marsh, M.Huddleston and S.Barnard, 1995: An isopycnic model study of the North Atlantic i) Model experiments and water mass formation, *submitted to J.Phys.Oceanogr.*

New, A.L., and R.Bleck, 1995: An isopycnic model study of the North Atlantic ii) Interdecadal variability of the subtropical gyre, *J.Phys.Oceanogr.*

Niiler, P.B., 1992: The ocean circulation, Ch.4 from *Climate systems modelling,* ed. K.Trenberth, C.U.P.

Niiler, P.P., and E.B.Kraus, 1977: One dimensional models of the upper ocean, from *Modelling and prediction of the upper layers of the ocean*, ed. E.B.Kraus.

Nurser, A.J.G., and J.Marshall, 1991: On the relationship between subduction rates and diabatic forcing of the mixed layer, *J.Phys.Oceanogr.*, ***21***, 1793-1802.

Oberhuber, J.M., 1993a: Simlutions of the Atlantic circulation with a coupled sea-ice-mixed layer-isopycnal GCM i) Model description, *J.Phys.Oceanogr.*, ***23***, 808-829.

Oberhuber, J.M., 1993b: Simlutions of the Atlantic circulation with a coupled sea-ice-mixed layer-isopycnal GCM ii) Model experiments, *J.Phys.Oceanogr.*, ***23***, 829-845.

Olbers, D.J., M.Wenzel and J.Willebrand, 1985: The inference of North Atlantic circulation patterns from climatological hydrographic data, *Rev.Geophys.*, ***23***, 313-356.

Pacanowski, R.C., and S.G.H.Philander, 1981: Parameterization of vertical mixing in numerical models of the tropical oceans, *J.Phys.Oceanogr., **11***, 1443-1451.

Parsons, A.T., 1969: A two layer model of Gulf Stream separation, *J.Fluid Mech., **39***, 511-528.

Pedlosky, J., 1983: Eastern boundary ventilation and the structure of the thermocline, *J.Phys.Oceanogr., **13***, 2038-2044.

Pedlosky, J., and W.R.Young, 1983: Ventilation, potential vorticity homogenisation and the structure of ocean circulation, *J.Phys.Oceanogr., **13***, 2020-2037.

Phillips, O.M., 1966: *The dynamics of the upper ocean,* C.U.P.

Pocklington, R., 1972: Secular changes in the ocean off Bermuda, *J.Geophys.Rev., 77*, 6604-6607.

Pollard, R.T., and L.Regier, 1990: Large variations in potential vorticity at small spatial scales in the uper ocean, *Nature, **348***, 227-229.

Pollard, R.T, P.B.Rhines and R.O.R.Y.Thompson, 1973: The deepening of the wind-mixed layer, *Geophys.Fluid Dyn., **3***, 381-404.

Price, J.F., R.A.Weller and R.Pinkel, 1986: Diurnal cycling: observations and models of the upper ocean response to diurnal heating, cooling and wind-mixing, *J.Geophys.Rev., **91***, 8411-8427.

Redi, M.H., 1982: Oceanic isopycnal mixing by coordinate rotation, *J.Phys.Oceanogr., **12***, 87-94.

Rhines, P.B., and W.R.Young, 1982: Homogenisation of potential vorticity in planetary gyres, *J.Fluid Mech., **122***, 347-367.

Roberts, M.J., A.L.New, R.A.Wood and R.Marsh, 1995: An intercomparison of a Bryan-Cox type ocean model and an isopycnic ocean model, I) the subpolar gyre and high latitude processes, *submitted J.Phys.Oceanogr.*

Robinson, A.R., 1983: Eddies in marine science, Springer-Verlag.

Rooth, C.G., and H.G.Ostlund, 1972: Penetration of tritium into the North Atlantic thermocline, *Deep Sea Res., **19***, 481-492.

Sarmiento, J.L., 1983a: A simulation of bomb tritium entry into the Atlantic Ocean, *J.Phys.Oceanogr., **13***, 1924-1939.

Sarmiento, J.L., 1983b: A tritium box model of the North Atlantic thermocline, *J.Phys.Oceanogr., **13***, 1969-1274.

Sarmiento, J.L., and J.R.Toggweiler, 1984: A new model for the role of the oceans in

determining atmospheric pCO_2, *Nature, **308***, 621-624.

Sarmiento, J.L., J.C.Orr and U.Seigenthaler, 1992: A perturbation simulation of carbon dioxide uptake in an OGCM, *J.Geophys.Res., **97***, 3621-3645.

Sawdey, A., M.O'Keefe and R.Bleck, 1995: The design, implementation and performance of a parallel ocean circulation model, to appear in *Proceedings of the sixth ECMWF workshop on parallel processing in meteorology.*

Schäfer,A., and B.Krauss, 1995: Eddy statistics in the South Atlantic as derived from drifters drogued to 100m, *J.Mar.Res., **53***, 403-431.

Schopp, R., and M.Arhan, 1986: A ventilated mid-depth circuation model for the eastern North Atlantic, *J.Phys.Oceanogr., **16***, 344-357.

Schroeder, E., H.Stommel, D.Menzel and W.Sutcliffe, 1959: Climatic stability of 18°C water at Bermuda, *J.Geophys.Res., **64***, 363-366.

Smagorinsky, J.S., 1963: General circulation experiments with the primitive equations, i) the basic experiment, *Mon.Wea.Rev., **91***, 99-164.

Smolarkiewicz, P.K., 1984: A fully multi-dimensional positive definite advection transport algorithm with small implicit diffusion, *J.Comp.Phys., **54***, 325-362.

Speer, K., and E.Tziperman, 1992: Rates of water mass formation in the North Atlantic Ocean, *J.Phys.Oceanogr., **22***, 93-104.

Stommel, H., 1979: Determination of water mass properties of water pumped down from the Ekman layer to the geostrophic flow below, *Proc.Natl.Acad.Sci.USA, **76***, 3051-3055.

Stommel, H., and G.Veronis, 1980: Barotropic response to cooling, *J.Geophys.Res., **85***, 6661-6666.

Stull, R.B., 1984: Transilient turbulence theory: i)the concept of eddy mixing across finite differences, *J.Atmos.Sci., **41***, 3351-3367.

Talley, L.D., and M.S.McCartney, 1982: Distribution and circulation of Labrador Sea Water, *J.Phys.Oceanogr., **12***, 1189-1205.

Talley, L.D., and M.E.Raymer, 1982: Eighteen degree water variability, *J.Mar.Res., **40** (suppl.)*, 757-775.

Thiele, G., *et al., 1986:* Baroclinic flow and transient-tracer fields in the Canary-Cape Verde Basin, *J.Phys.Oceanogr., **16***, 814-826.

Walin, G., 1982: On the relation between sea surface heatflow and thermal circulation in the oceans, *Tellus, **34***, 187-195.

Warren, B.A., 1972: Insensitivity of subtropical mode water characteristics to meteorological fluctuations, *Deep Sea Res., **19***, 1-19.

Warren, B.A., 1983: Why is no deep water formed in the North Pacific?, *J.Mar.Res.*

41, 327-347.

Williams, R.G., 1989: The influence of air-sea interaction on the ventilated thermocline, *J.Phys.Oceanogr.*, ***19***, 1255-1267.

Williams, R.G., 1991: The role of the mixed layer in setting the potential vorticity of the main thermocline, *J.Phys.Oceanogr.*, ***21***, 1803-1814.

Williams, R.G., M.A.Spall and J.C.Marshall, 1995: Does Stommel's Ekman demon work?, *submitted to J.Phys.Oceanogr.*

Woods, J.D., 1980: Diurnal and seasonal variation of convection in the wind-mixed layer of the ocean, *Quart.J.Roy.Meteor.Soc.*, ***106***, 379-394.

Woods, J.D., 1985: The physics of thermocline ventilation, p543-590 from *Coupled Ocean-Atmosphere models*, ed.C.J.Nihoul, Elsevier.

Woods, J.D., W.Barkmann, and A.Horsch, 1984: Solar heating of the oceans - diurnal, seasonal and meridional variations, *Quart.J.Roy.Meteor.Soc.*, ***110***, 633-656.

Woods, J.D., and W.Barkmann, 1986a: A Lagrangian mixed layer model of Atlantic 18°C water formation, *Nature*, ***319***, 574-576.

Woods, J.D., and W.Barkmann, 1986b: The response of the upper ocean to solar heating i) the mixed layer, *Quart.J.Roy.Meteor.Soc.*, ***112***, 1-27.

Worthington, L.V., 1959: The eighteen degree water in the Sargasso Sea, *Deep Sea Res.*, ***5***, 297-305.

Worthington, L.V., 1972: Negative oceanic heat flux as a cause of water mass formation, *J.Phys.Oceanogr.*, ***2***, 205-211.

Worthington, L.V., 1976: *On the North Atlantic circulation,* John Hopkins Oceanographic Studies No.6, Baltimore.

Worthington, L.V., 1977: Intensification of the Gulf Stream after the winter of 1976-'77, *Nature*, ***270***, 415-417.

Wright, W.R., 1972: Northern sources of energy for the deep Atlantic, *Deep Sea Res.*, ***19***, 865-877.

Young, W.R., 1984: The role of western boundary layers in gyre-scale ocean mixing, *J.Phys.Oceanogr.*, ***14***, 478-483.

Young, W.R., and P.B.Rhines, 1982: A theory of the wind-driven circulation ii) gyres with western boundary layers, *J.Mar.Res.*, ***40***, 849-872.

Young, W.R., and G.R.Ierley, 1986: Eastern boundary conditions and weak solutions of the ideal thermocline equations, *J.Phys.Oceanogr.*, ***16***, 1884-1900.

Zalesak, S.T., 1979: Fully multi-dimensional flux-corrected transport algorithms for fluids, *J.Comp.Phys.*, ***31***, 335-362.